

# Open Research Online

---

The Open University's repository of research publications and other research outputs

## Development of a tissue engineered implantable device for the surgical repair of the peripheral nervous system

### Thesis

How to cite:

Georgiou, Melanie (2013). Development of a tissue engineered implantable device for the surgical repair of the peripheral nervous system. PhD thesis The Open University.

For guidance on citations see [FAQs](#).

© 2013 The Author

Version: Version of Record

---

Copyright and Moral Rights for the articles on this site are retained by the individual authors and/or other copyright owners. For more information on Open Research Online's data [policy](#) on reuse of materials please consult the policies page.

---

[oro.open.ac.uk](http://oro.open.ac.uk)

# Development of a tissue engineered implantable device for the surgical repair of the peripheral nervous system

Melanie Georgiou, M.Eng

A thesis submitted to The Open University, UK, for the degree of  
Doctorate of Philosophy.



**The Open  
University**

Department of Life, Health and Chemical Sciences

June 2013

Supervised by:

Dr James B Phillips

Dr Jon P Golding

Dr Jane A Loughlin

Department of Life, Health and Chemical Sciences,  
The Open University, Milton Keynes, UK.

DATE OF SUBMISSION: 23 July 2013

DATE OF AWARD: 9 DECEMBER 2013

## **Declaration**

The work contained in this thesis is entirely my own and is the result of my own academic and experimental enquiry. Contributions to the work by colleagues are fully acknowledged in the text. This work has not been, and is not currently being submitted for candidature for any other degree.

## Acknowledgments

I would like to express my great appreciation to my primary supervisor, James Phillips. Without his guidance and support this thesis would not have been possible. His willingness to give his time so generously has been very much appreciated. He has been a true mentor and I will always be grateful. I am also deeply thankful for all the help, encouragement and useful critiques of this research work from my second supervisors, Jane Loughlin and Jon Golding.

I am particularly grateful for the assistance given by Heather Davies, Francis Colyer and Gordon Imlach in the Electron Microscopy Suite; and to the Biomedical Research Unit staff, Steve Walters, Karen Evans, Sophie Brooks and especially Agata Stramek, who all made the *in vivo* work possible. Furthermore, I would like to thank Steve Bunting for training me in the techniques required for the *in vivo* model; and a special thank you to Paul Kingham for his expertise and providing the differentiated adipose-derived stem cells. I would also like to thank Stan Hiller and Darren Burke for their help with the tensile testing experiment.

I would like to thank all my colleagues, especially David Male for his expertise and advice, and Julia Barkans for keeping the lab in order. I would like to especially thank Camilla, Prasanna, Pratima, Radka for all their encouragement throughout this journey; and Emma, Caitriona, Alex, Abraham and Jake for their contributions to this research project.

Last, but not least, I would like to thank my family and friends who have been there for me throughout this challenging journey. A big thank you to my boyfriend for his unconditional support. Finally, and most importantly, I would like to thank my grandparents. Without them, none of this would have been possible. I dedicate this thesis to my γαγιά and παππού.

Thank you!

## **Publications**

### Papers

**Georgiou M**, Bunting SCJ, Davies HA, Loughlin AJ, Golding JP, Phillips JB (2013). Engineered neural tissue for peripheral nerve repair. *Biomaterials*, 34:7335-7343.

### Conference proceedings

**Georgiou M**, Loughlin AJ, Golding JP, Phillips JB (2013). Comparing Engineered Neural Tissue formats within a peripheral nerve repair conduit. *In: Annual meeting of the Tissue and Cell Engineering Society (TCES), 23-25 July 2013, Cardiff, Wales.*

Sanen, Kathleen; Martens, Wendy; **Georgiou, Melanie**; Phillips, James; Lambrichts, Ivo and Ameloot, Marcel (2013). Aligned Schwann cells derived from human dental pulp stem cells direct neurite growth in a tissue engineered collagen construct. *In: XI European Meeting on Glial Cells in Health and Disease, 3-6 July 2013, Berlin, Germany.*

**Georgiou, Melanie**; Golding, Jon; Loughlin, Jane and Phillips, James (2013). Fabrication of an endoneurium using engineered neural tissue within a peripheral nerve repair conduit. *In: Tissue Engineering and Regenerative Medicine International Society - EU Meeting, 17-20 June 2013, Istanbul, Turkey.*

**Georgiou, Melanie**; Bunting, Stephen; Golding, Jon; Loughlin, Jane and Phillips, James (2012). A living replacement tissue for peripheral nerve that can enhance

regeneration in vitro and in vivo. *In: Tissue Engineering and Regenerative Medicine International Society - World Congress 2012, 5 - 8 September 2012, Vienna, Austria.*

**Georgiou, Melanie;** Kingham, Paul; Bunting, Stephen; Golding, Jon; Loughlin, Jane and Phillips, James (2012). A nerve repair conduit containing differentiated adipose-derived stem cells within engineered neural tissue can support and guide neuronal growth in vitro and in vivo. *In: Tissue Engineering and Regenerative Medicine International Society - World Congress 2012, 5 - 8 September 2012, Vienna, Austria.*

**Georgiou, M.;** Loughlin, J.; Golding, J. P.; Kingham, P. J. and Phillips, J. B. (2012). Engineered neural tissue with aligned Schwann cells supports neuronal regeneration in vivo and can be assembled using differentiated adipose-derived stem cells. *In: Annual meeting of the Tissue and Cell Engineering Society (TCES), 4-6 July 2012, Liverpool, UK.*

**Georgiou, Melanie;** Kingham, Paul; Golding, Jon; Loughlin, Jane and Phillips, James (2012). Engineered neural tissue with columns of aligned Schwann cell-like cells from differentiated adipose-derived stem cells can support and guide neuronal growth in vitro. *In: 3rd International Conference on Stem Cell Engineering "Designing Cellular Therapies", 29 April - 02 May 2012, Seattle, US.*

**Georgiou, M.;** East, E.; Loughlin, J.; Golding, J. and Phillips, J. (2011). Aligned Schwann cells within 3D tissue-like gels provide guidance to regenerating neurites. *In: 10th European Meeting on Glial Cells in Health and Disease, 13-17 September 2011, Prague, Czech Republic.*

**Georgiou, Melanie;** Loughlin, Jane; Golding, Jon and Phillips, James (2011). Aligned cellular and acellular collagen guidance substrates for peripheral nerve repair. *In: Tissue and Cell Engineering Society, 19 - 21 July 2011, Leeds.*

Karamsadkar, S.; Alekseeva, T.; Bunting, S.; Stomati, K.; Cheema, U.; **Georgiou, M.;** Phillips, J.; Brown, R. A. and Priestley, J. V (2011). 3d micro-structured collagen conduits for nerve repair. *In: Tissue Engineering & Regenerative Medicine International Society, 7-10 June 2011, Granada, Spain.*

**Georgiou, M.;** East, E.; Loughlin, A. J.; Golding, J. P. and Phillips, J. B. (2011). A tissue engineered collagen conduit containing columns of aligned Schwann cells supports neuronal regeneration in vitro. *In: 2011 PNS Biennial Meeting of the Peripheral Nerve Society, 25-29 June 2011, Potomac, Maryland, US.*

**Georgiou, M.;** East, E.; Loughlin, J.; Golding, J.P. and Phillips, J.B. (2010). Schwann cells in collagen gels survive plastic compression and maintain their alignment: development of a cellular biomaterial for peripheral nerve repair. *In: Tissue and Cell Engineering Society, 28-30th July, Manchester, U.K.*

East, E.; **Georgiou, M.;** Loughlin, A.J.; Golding, J.P. and Phillips, J.B. (2010). Plastic compression of aligned cellular collagen gels for nervous system repair. *In: Tissue Engineering and Regenerative Medicine International Society - EU Meeting, 13-17th June, Galway, Ireland*

## Abstract

Peripheral nerve injury as a result of trauma affects approximately 1 million people in Europe and America annually. The current clinical gold standard treatment for repairing long gaps is the nerve autograft, in which only ~50% of cases result in satisfactory functional recovery. Tissue-engineered cellular bridging devices for surgical implantation into peripheral nerve injury sites could provide an attractive alternative to the autograft. This project reports the development of a robust, anisotropic biomaterial with highly aligned cells that can form the basis of a peripheral nerve repair device.

Engineered neural tissue (EngNT), which is formed from columns of Schwann cells or stem cells within a 3D aligned collagen matrix, can promote directed neurite outgrowth *in vitro*. This study demonstrates that sheets of EngNT can be arranged to form the 'endoneurium' of a peripheral nerve repair device within a NeuraWrap™ outer tube, and can be used for the repair of critical sized defects in rat.

Schwann cells are the preferred cell type for peripheral nerve repair because of their ability to enhance axon migration and secrete factors that further increase regeneration. However the use of autologous Schwann cells has a number of disadvantages, including the sacrifice of host nerve tissue for their extraction and slow expansion times *in vitro*. Various therapeutic cell types and a bovine collagen source that can potentially be used to make EngNT to form the device core were investigated. EngNT devices containing Schwann cell-like cells from adipose-derived stem cells (dADSC) or human neural progenitor cells differentiated to glial cells (dCX) were tested in a critical sized gap in the rat sciatic nerve model. The *in vivo* experiments demonstrated that there is potential



for the dADSCs to be used for peripheral nerve repair. The results from the dCX repairs were less clear.

The technology reported here offers a simple, rapid and effective method for the manufacture of an aligned cellular biomaterial, and could be applied to a range of tissue engineering applications. This study demonstrates that there is potential for EngNT to be used in the construction of nerve repair conduits.

## **Contents**

Declaration	2
Acknowledgments	3
Publications	4
Papers	4
Conference proceedings	4
Abstract	7
Contents	9
Index of figures	14
Index of tables	18
Abbreviations	19
1.0 Introduction	23
1.1 The nervous system	23
1.2 Peripheral nerve damage	26
1.3 Current treatments for peripheral nerve injury	31
1.3.1 Primary repair	31
1.3.2 Clinically available devices for peripheral nerve repair	32
1.3.2.1 Conduit repair devices	32
1.3.2.2 Decellularised repair devices	35
1.3.3 Nerve autograft	35
1.4 Neural tissue engineering	37
1.4.1 Neural scaffolds	39
1.4.1.1 Natural biomaterials	39
1.4.1.2 Synthetic materials	43
1.4.2 Growth factors	44
1.4.3 Support cells	46
1.4.3.1 Schwann cells	46

1.4.3.2 Stem cells	47
1.4.3.3 Considerations for translation of cell therapies to the clinic	51
1.4.4 Guidance structures within tissue engineered scaffolds	52
1.5 Aims and objectives	57
2.0 Materials and methods	58
2.1 Materials	58
2.2 Cell culture	63
2.2.1 Schwann cells (F7 cell line)	63
2.2.2 Primary adult rat neurons	63
2.2.3 Primary rat bone-marrow mesenchymal stem cells	64
2.2.4 Primary rat Schwann cell-like cells derived from adipose stem cells	65
2.2.5 Human neural progenitor cells (ReNcell CX cell line)	66
2.3 3D hydrogels	68
2.3.1 Collagen type I	68
2.3.2 Fibrin	69
2.4 Engineered neural tissue protocol	70
2.4.1 Tethered cellular gels	71
2.4.2 Plastic compression	72
2.5 <i>In vitro</i> co-culture of EngNT with neurons	73
2.6 Tensile testing	74
2.7 <i>In vivo</i> testing in the rat sciatic nerve model	74
2.7.1 Device assembly	74
2.7.2 Surgery	74
2.7.3 Device harvest	76
2.7.4 Gastrocnemius muscle dissection	76
2.8 Sectioning	76

2.8.1 Vibratome sections	76
2.8.2 Cryo-sections	76
2.9 Staining	77
2.9.1 Immunofluorescence labelling protocol	77
2.9.2 Flow cytometry	78
2.9.3 CellTracker™ staining	78
2.10 Electron microscopy	79
2.10.1 Scanning electron microscopy	79
2.10.2 Transmission electron microscopy	79
2.11 Analyses	80
2.11.1 Cell death quantification	80
2.11.2 Assessment of cellular alignment	80
2.11.3 Assessment of neurite growth <i>in vitro</i>	81
2.11.4 Assessment of neuronal regeneration <i>in vivo</i>	82
2.11.5 Analysis of myelin <i>in vivo</i>	82
3.0 Development and optimisation of Engineered Neural Tissue (EngNT)	83
3.1 Introduction	83
3.2 Results	90
3.2.1 Schwann cell characterisation	90
3.2.2 The effect of plastic compression on Schwann cell death	91
3.2.3 The effect of plastic compression on Schwann cell alignment	92
3.2.4 Neuronal growth on the surface of collagen EngNT-Schwann cell	97
3.2.5 Exploring the use of fibrin to engineer EngNT-Schwann cell	100
3.2.6 Exploring the use of decellurised collagen EngNT-Schwann cell	106

3.3 Discussion	109
4.0 Investigating ways to deliver EngNT within a nerve repair conduit	113
4.1 Introduction	113
4.2 Results	120
4.2.1 Investigating the contribution of cells and alignment to neuronal regeneration through EngNT rods <i>in vivo</i>	120
4.2.2 Optimisation of the device core design using EngNT-Schwann cell	126
4.2.2.1 Device core assembly	126
4.2.2.2 Investigating the effect of different EngNT arrangements on neuronal regeneration <i>in vivo</i>	128
4.2.2.3 Investigating how different amounts of EngNT-Schwann cell affects regeneration using the rod-based device design <i>in vivo</i>	132
4.2.3 <i>In vivo</i> proof-of-principle testing in the rat sciatic nerve	134
4.2.3.1 Mid-point analysis	136
4.2.3.2 Neurite regeneration analysis	142
4.2.4 Preliminary investigation into whether sheets of plastic compressed collagen would have the appropriate mechanical properties for use as an outer sheath for a nerve repair device	147
4.3 Discussion	149
5.0 Investigating the feasibility of making an EngNT nerve repair device using clinically relevant cells and materials	159
5.1 Introduction	159
5.2 Results	168
5.2.1 Investigating the use of bovine collagen for the production of EngNT	168
5.2.2 Cell characterisation of the different clinically relevant cell types investigated for peripheral nerve repair	170
5.2.3 Assessing the capacity of (rat collagen) EngNT containing different cell types to support and guide	176

neurite outgrowth <i>in vitro</i>	
5.2.3.1 Primary rat BM-MSCs	176
5.2.3.2 Schwann cell-like cells differentiated from rat ADSCs	178
5.2.3.3 Human neural progenitor cells (ReNcell)	182
5.2.3.4 Cell type comparison	184
5.2.4 Initial <i>in vivo</i> testing in rat sciatic nerve	185
5.2.4.1 EngNT-dADSC devices	185
5.2.4.2 EngNT-dCX devices	188
5.3 Discussion	192
6.0 Discussion	198
7.0 References	207

## Index of figures

	Page
<b>Chapter 1</b>	
Figure 1.1 The nervous system	23
Figure 1.2 Anatomical overview of a PNS nerve	25
Figure 1.3 Schematic of the events after a peripheral nerve has been cut, shown at the level of a single axon.	29
Figure 1.4 Schematic of epineurial repair	32
<b>Chapter 2</b>	
Figure 2.1 Production of EngNT	70
Figure 2.2 Tethered gel preparation	71
Figure 2.3 Stabilisation of cellular alignment by plastic compression	72
Figure 2.4 Automated 3D analysis of cell alignment in EngNT using Volocity™	81
Figure 2.5 Example measurements to assess myelination from an electron micrograph using Image J	82
<b>Chapter 3</b>	
Figure 3.1 Schwann cells on coverslips stained to detect S100	90
Figure 3.2 Contraction profile for Schwann cells in collagen gels	91
Figure 3.3 The effect of plastic compression on Schwann cell viability	92
Figure 3.4 Self-aligned Schwann cells in fully hydrated and plastic compressed gels	94
Figure 3.5 Schwann cell elongation and orientation pre- or post-plastic compression	95
Figure 3.6 Scanning electron micrographs of plastic compressed collagen with aligned cells and without cells	96
Figure 3.7 Neuronal growth on EngNT-Schwann cell	96
Figure 3.8 Orientation of neuronal growth on EngNT-Schwann cell	99
	14

Figure 3.9 Fibrin gel disruption in wells after attempting to free the edges	100
Figure 3.10 Schwann cells in tethered hydrated or plastic compressed fibrin gels	102
Figure 3.11 Schwann cell elongation and orientation pre- or post-plastic compression of fibrin gels	103
Figure 3.12 Scanning electron micrographs of fibrin gels in fully hydrated acellular fibrin and fibrin EngNT-Schwann cell	104
Figure 3.13 Neuronal growth on fibrin EngNT-Schwann cell	105
Figure 3.14 Neuronal growth on EngNT-Schwann cell, EngNT-acellular and EngNT-freeze-killed	108

## Chapter 4

Figure 4.1 The rod-based device design	120
Figure 4.2 Assembly of a nerve repair device with an EngNT core within a silicone tube	121
Figure 4.3 EngNT-Schwann cell within a silicone outer tube after 2 weeks <i>in vivo</i>	121
Figure 4.4 Comparison of neurite alignment between devices containing EngNT with aligned Schwann cells, unaligned Schwann cells or acellular collagen <i>in vivo</i>	123
Figure 4.5 The location of regenerating axons in the proximal part of the devices containing EngNT with aligned Schwann cells, unaligned Schwann cells or acellular collagen <i>in vivo</i>	125
Figure 4.6 The sheet-based device design	127
Figure 4.7 Implantation of rod- and sheet-based devices within a NeuraWrap™ outer tube	127
Figure 4.8 The different zones within cross-sections from the rod- and sheet-based devices	129
Figure 4.9 The number and location of axons within cross-sections from the proximal parts of the rod- and sheet-based EngNT devices	131
Figure 4.10 Frequency distribution showing the angle of deviation of axon growth from the long axis of the devices, in longitudinal sections from the proximal part of each device	133
Figure 4.11 The number of neurites in the cross-sections from the distal part of each device	134



Figure 4.12 Scanning electron microscopy images of the mid-point of the different device groups after 8 weeks <i>in vivo</i>	136
Figure 4.13 Schematic of harvested device/graft with stumps, showing the 5 sampling positions for analysis	136
Figure 4.14 Light micrographs of semi-thin transverse sections from the mid-point of each repair after 8 weeks <i>in vivo</i> , stained with toluidine blue	137
Figure 4.15 Transmission electron micrographs of transverse sections through regenerated nerve at the mid-point of the repair site after 8 weeks <i>in vivo</i>	138
Figure 4.16 Morphological analyses of regenerated nerve fibres at the mid-point of the repair site after 8 weeks <i>in vivo</i>	139
Figure 4.17 Distribution of myelinated and unmyelinated fibres by diameter at the mid-point of the repair site after 8 weeks <i>in vivo</i>	141
Figure 4.18 The number of regenerated axons in 10 $\mu\text{m}$ thick cross-sections from different parts of each device from each experimental group	143
Figure 4.19 Histological overview of axons (neurofilament-positive) in the different parts of the device	144
Figure 4.20 Relative gastrocnemius muscle weight ratios after the 8 week recovery period for each experimental group	146
Figure 4.21 Tensile strength testing of nerves and selected sheath elements	148
 <b>Chapter 5</b>	
Figure 5.1 Contraction profile for Schwann cells in bovine and rat collagen gels	168
Figure 5.2 Schwann cell orientation in EngNT made with bovine collagen	170
Figure 5.3 Identification of Sox 10 in neural crest stem cells	171
Figure 5.4 Characterisation of dADSCs on coverslips	172
Figure 5.5 Characterisation of BM-MSCs by flow cytometry	173
Figure 5.6 Characterisation of undifferentiated (A, B) and differentiated (C, D) CX ReNcells by supplier, Millipore (reproduced from data sheet, Millipore, Cat. No. SCC007)	174
Figure 5.7 Neurite outgrowth on the surface of EngNT-BM-MSCs after 3 days in culture	177
Figure 5.8 Contraction profile for rat collagen gels with Schwann cells or dADSCs	178
	16

Figure 5.9 Cell elongation within EngNT-dADSC	179
Figure 5.10 dADSC orientation in EngNT-dADSC	180
Figure 5.11 Neurite outgrowth on EngNT-dADSC	181
Figure 5.12 Neuronal growth on the surface of EngNT-uCX and EngNT-dCX	183
Figure 5.13 Neurite outgrowth per mm <sup>2</sup> quantification on aligned cellular EngNT	184
Figure 5.14 Micrographs of transverse sections from the mid-point of the EngNT-dADSC devices after 8 weeks <i>in vivo</i>	186
Figure 5.15 Fluorescent micrographs of transverse sections through the different parts of the repair site after repair with EngNT-dADSC devices after 8 weeks <i>in vivo</i>	188
Figure 5.16 Micrographs of transverse sections from the mid-point of the EngNT-dCX devices after 8 weeks <i>in vivo</i>	190
Figure 5.17 Confocal micrographs of transvers sections from the proximal part of the EngNT-dCX devices after 8 weeks <i>in vivo</i>	191

## **Index of tables**

	Page
<b>Chapter 1</b>	
Table 1.1 Clinically approved conduits for peripheral nerve repair	34
Table 1.2 Summary table for cells that have been used in peripheral nerve repair	49
Table 1.3 Some of the current techniques and materials used to fabricate anisotropic neural scaffolds	54
<b>Chapter 2</b>	
Table 2.1 Cell lines used in this project	58
Table 2.2 Consumables used in this project	59
Table 2.3 Antibodies used in this project	62
<b>Chapter 5</b>	
Table 5.1 Therapeutic cells currently in clinical trials for nervous system repair/regeneration	165
Table 5.2 Summary table for cell characterisation	174
Table 5.3 Cell death in compressed gels in rat collagen I gels	175

## Abbreviations

± SEM	± standard error of the mean
2D	two-dimensional
3D	three-dimensional
3Rs	replacement, refinement and reduction
ADSC	adipose-derived stem cells
ANOVA	analysis of variance
Ara-C	cytosine arabinoside
ASC	adult stem cells
ATMP	advanced therapy medicinal product
BDNF	brain-derived neurotrophic factor
bFGF	basic fibroblast growth factor
BM-MSC	bone-marrow mesenchymal stem cells
CE approval	The mark placed on products that meet safety standards that apply to all the countries of the European Union
CMAP	compound muscle action potential
CNS	central nervous system
CNTF	ciliary neurotrophic factor
CO <sub>2</sub>	carbon dioxide
CsA	cyclosporine A
CTX	human neural progenitor cells currently in clinical trials at ReNeuron
dADSC	differentiated adipose-derived stem cells
dCX	differentiated human neural progenitor cells (research grade)
DD	distal part of the device

DMEM	Dulbecco's Modified Eagle's Medium
DMSO	dimethyl sulfoxide
DRG	dorsal root ganglia
DS	distal stump
E-ACA	$\epsilon$ -amino Caproic acid
ECM	extracellular matrix
EGF	epithelial growth factor
EM	electron microscopy
EMA	European Medicines Agency
EngNT	Engineered Neural Tissue
ESC	embryonic stem cell
Fb	fibrinogen
FBS	fetal bovine serum
FCS	fetal calf serum
FDA	Food and Drug Administration
FEGSEM	field emission gun scanning electron microscopy
FGF	fibroblast growth factor
GDNF	glial derived neurotrophic factor
GFAP	glial fibrillary acidic protein
GFP	green fluorescent protein
GGF	glial growth factor
GMP	good manufacturing practice
IGF	insulin-like growth factor
iPS cell	induced pluripotent stem cell
MEM	minimum essential media
MSC	mesenchymal stem cell

NaOH	sodium hydroxide
NCSC	neural crest stem cell
NGF	nerve growth factor
NRG	neuregulin
NSC	neural stem cell
NT	neurotrophin
NTF	neurotrophic factor
P/S	penicillin/streptomycin
PB	phosphate buffer
PBS	phosphate buffered saline
PCL	polycaprolactone
PD	proximal part of the device
PDGF	platelet-derived growth factor
PDL	poly-D-lysine
PFA	paraformaldehyde
PGA	poly(glycolic acid)
PHB	poly-3-hydroxybutyrate
PI	propidium iodide
PLA	poly(lactic acid)
PLGA	poly(lactide-co-glycolide)
PLL	poly-L-lysine
PNI	peripheral nerve injury
PNS	peripheral nervous system
PS	proximal stump
PVA	polyvinyl alcohol
SD	Sprague-Dawley

SEM	scanning electron microscopy (see also ± SEM)
SIC	small intestine submucosa
TAP	The Automation Partnership
TEM	transmission electron microscopy
Th	thrombin
uCX	undifferentiated human neural progenitors (research grade)
UK	United Kingdom
US	United States

## 1.0 Introduction

### 1.1 The nervous system

The nervous system can be divided into two parts: the central nervous system (CNS) and the peripheral nervous system (PNS) (figure 1.1). The CNS consists of the brain, spinal cord, optic, olfactory and auditory systems. The PNS consists of all the sensory and motor nerves that carry information into and from the spinal cord and the brain. This research will focus on the PNS, in particular nerve damage and regeneration.

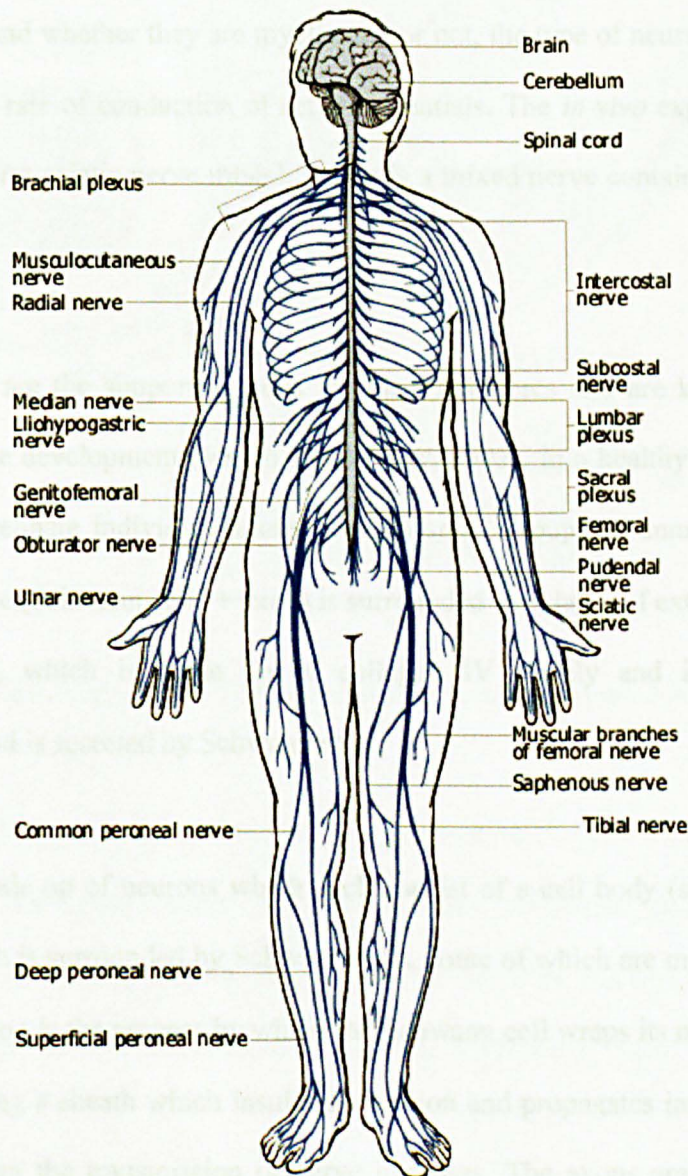


**Figure 1.1 The nervous system**

The peripheral nervous system is shown in blue (A.M.A., 1998).



There are three types of peripheral nerve, described below.

- Motor: send impulses from the brain and spinal cord to all of the skeletal muscles in the body.
- Sensory: send impulses from muscles, sensors (pain, temperature etc.) in the skin and within the body to the spinal cord and brain.
- Autonomic nerves: control involuntary and semi-involuntary functions i.e. heart rate, digestion, sweating etc.

Within these, there are different types of nerve fibres, which are classified according to their diameter and whether they are myelinated or not, the type of neurotransmitter they release and the rate of conduction of action potentials. The *in vivo* experiments in this project use the rat sciatic nerve model, which is a mixed nerve containing sensory and motor neurons.

Schwann cells are the supporting cells for the PNS fibres and are key regulators of peripheral nerve development (Jessen and Mirsky, 1997). In a healthy nerve, Schwann cells either myelinate individual axons or wrap small groups of unmyelinated axons. Each nerve fibre (Schwann cells + axon) is surrounded by a layer of extracellular matrix (basal lamina), which is made up of collagen IV mainly and includes laminin components, and is secreted by Schwann cells.

The PNS is made up of neurons which each consist of a cell body (soma) and a long thin axon which is surrounded by Schwann cells, some of which are myelinating. In the PNS, myelination is the process by which the Schwann cell wraps its membrane around an axon, creating a sheath which insulates the axon and propagates impulses along the axon, facilitating the transmission of nerve impulses. The axons are packed into the endoneurium. These are enclosed by the perineurium to form fascicles, which are

grouped together by the epineurium to form the nerve itself (figure 1.2). The epineurium is the strongest component of the nerve trunk and is a major contributor to nerve tensile strength (Topp and Boyd, 2006).

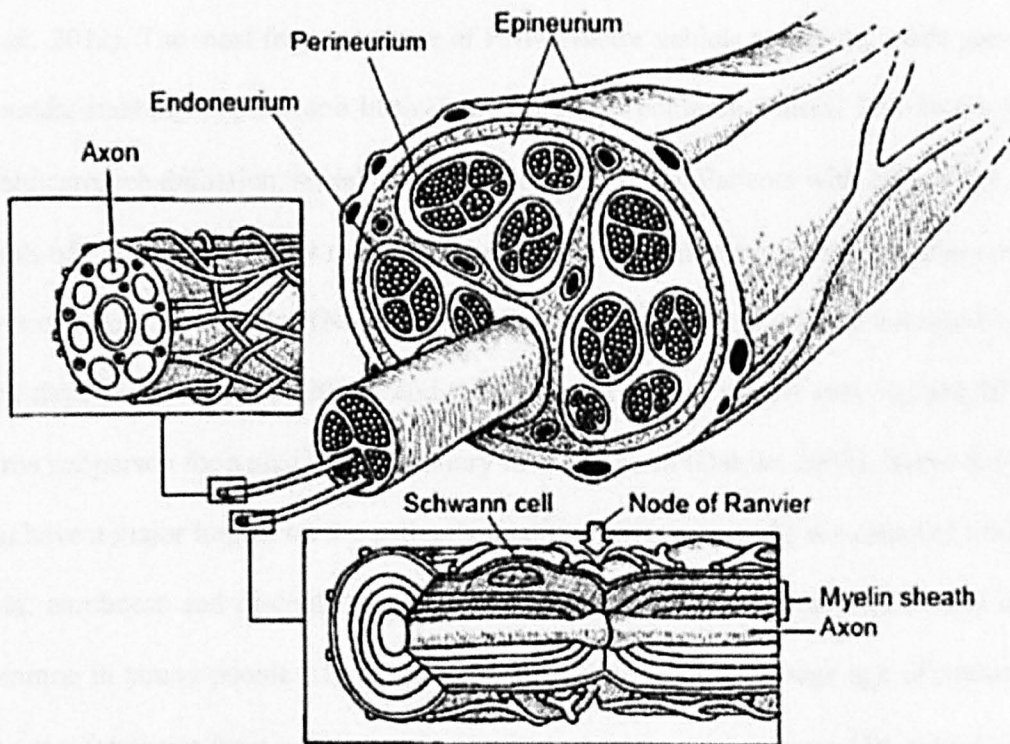


**Fig. 1.2 Anatomical overview of a PNS nerve (Stroncek and Reichert, 2008)**

After a peripheral nerve has been damaged, Schwann cells play a crucial role in the repair process, due to their ability to de-differentiate, proliferate, phagocytose debris, express growth promoting factors, guide regenerating axons and myelinate new axons (Hall, 2005). This is explained in more detail in the next section (1.2).

## 1.2 Peripheral nerve damage

In this research the focus was peripheral nerve injury as a result of trauma. It has been reported that 5% of all open wounds of the limbs are complicated by peripheral nerve trauma (Mumenthaler and Mattle, 2001). Each year approximately 300,000 people of working age in Europe are affected by peripheral nerve injury (PNI) (Ruijs *et al.*, 2005); of these less than 50% regain full function after treatment (Ichihara *et al.*, 2008; Kehoe *et al.*, 2012). The most frequent cause of PNI is motor vehicle accidents, while gunshot wounds, stabbings, sports and birth trauma are also common causes. PNI incurs high healthcare, rehabilitation, social and unemployment costs. Patients with disabilities as a result of PNIs can be costly to the healthcare system, with average hospital stays of 28 days each year in America (Noble, 1998). Forearm PNI patients take an average of 273 sick days (Rosburg *et al.*, 2005), and the estimated cost to society may exceed 50,000 euros per person for a median nerve injury in the forearm (Dahlin, 2008). Nerve damage can have a major impact on the patient's quality of life and can be the cause of lifelong pain, numbness and discomfort; often leading to a permanent disability. PNI is more common in young people within the working generation, the average age of patients is 33 years (statistics from a retrospective study in America that reviewed 96 patients with various kinds of PNI) (Wangenstein and Kalliainen, 2010), so a successful therapy would have a great impact on lifetime productivity.

Injury to a peripheral nerve induces a series of cellular and molecular changes in the injured neurons and their microenvironment (Fu and Gordon, 1997). After a nerve is severed, there are cellular and molecular changes that occur in the neuron body, known as retrograde reaction and chromatolysis. In these changes, neurons switch from their adult phenotype (the transmission state) to a growth state where there are changes in the expression of genes that encode for transcription factors (Leah *et al.*, 1991), which

regulate the expression of genes involved in cell survival and neurite outgrowth (Raivich and Makwana, 2007).

In the segment of the axon distal to the injury, which is no longer connected to the cell body, Wallerian degeneration begins (Dahlin and Brandt, 2004). Wallerian degeneration is an active process controlled by specific genes (*Wld<sup>f</sup>*) and signals (Aldalbert *et al.*, 2005). During Wallerian degeneration, macrophages penetrate the basal lamina and invade the Schwann cell tube, where they degrade the myelin sheaths and phagocytose debris (Glass, 2004, Dailey *et al.*, 1998). Schwann cells de-differentiate into their “survivor” phenotype, resembling immature Schwann cells, changing the expression of genes to promote cell proliferation. This switch in phenotype in the denervated Schwann cells is associated with the up-regulation of several growth associated genes including those coding for the proteins GFAP and p75, and neurotrophic factors such as NT-3, NGF, BDNF, NT-4, GDNF and IGF-1 (Gillen *et al.*, 1997; Fawcett and Keynes, 1990). The Schwann cells then proliferate by mitosis and align themselves into columns inside the basal lamina and form the “bands of Bungner” – these longitudinal structures are crucial in the repair process and they lie within the endoneurial tubes and form continuous chains of cells (Hall, 2005).

In the PNS, nerves can successfully regenerate and spontaneously repair two (class I and II) out of the three types of PNS injuries which are possible: class I (neuropraxia) involves temporary disruption of conduction without loss of axonal continuity; class II (axonotmesis) involve loss of continuity of the axons and myelin with preservation of connective tissue frame work; and class III is where there is a complete cut through the nerve (epineurium and endoneurium) (as classified by Sedden, 1943). Axon sprouts will begin to emerge from the proximal end of the nerve and elongate along the Schwann

cell columns, which provide a pathway that serves as a guide for sprouts of regenerating axons to follow (figure 1.3). The regeneration of an axon that has been cut (class II and III injuries) involves the transformation of a stable axonal segment into a highly motile tip, called the growth cone. Each regenerating axon can initially give rise to about 10 axonal sprouts (Witzel *et al.*, 2005), but the branches that do not make peripheral connections (innervate muscle or skin) undergo atrophy and disappear with time. The growth cones can sense their environment and are guided by neurotrophic (e.g. NGF, GDNF, BDNF, NT-3) and neurotropic (e.g. laminin, collagen) factors produced mainly by Schwann cells. Once the regenerating axons make contact with the Schwann cells, the Schwann cells differentiate and re-myelinate the re-growing axon, however, the newly formed myelin is thinner than normal and the newly formed internodes (portion of nerve fibre between two Nodes of Ranvier, see figure 1.2) are shorter than normal (Hall, 2005). However, axons are not necessarily functional immediately; the fibre diameter (axon + myelin sheath) and motor conduction velocities are a better indication of functional recovery and have been shown to increase with time (Ikeda and Oka, 2012). Although this spontaneous axonal regeneration occurs naturally *in vivo* after class I and II peripheral nerve injuries, complete recovery is rare and so surgical intervention is often required. Surgical intervention is also required when there is a complete cut in the nerve (class III injury).

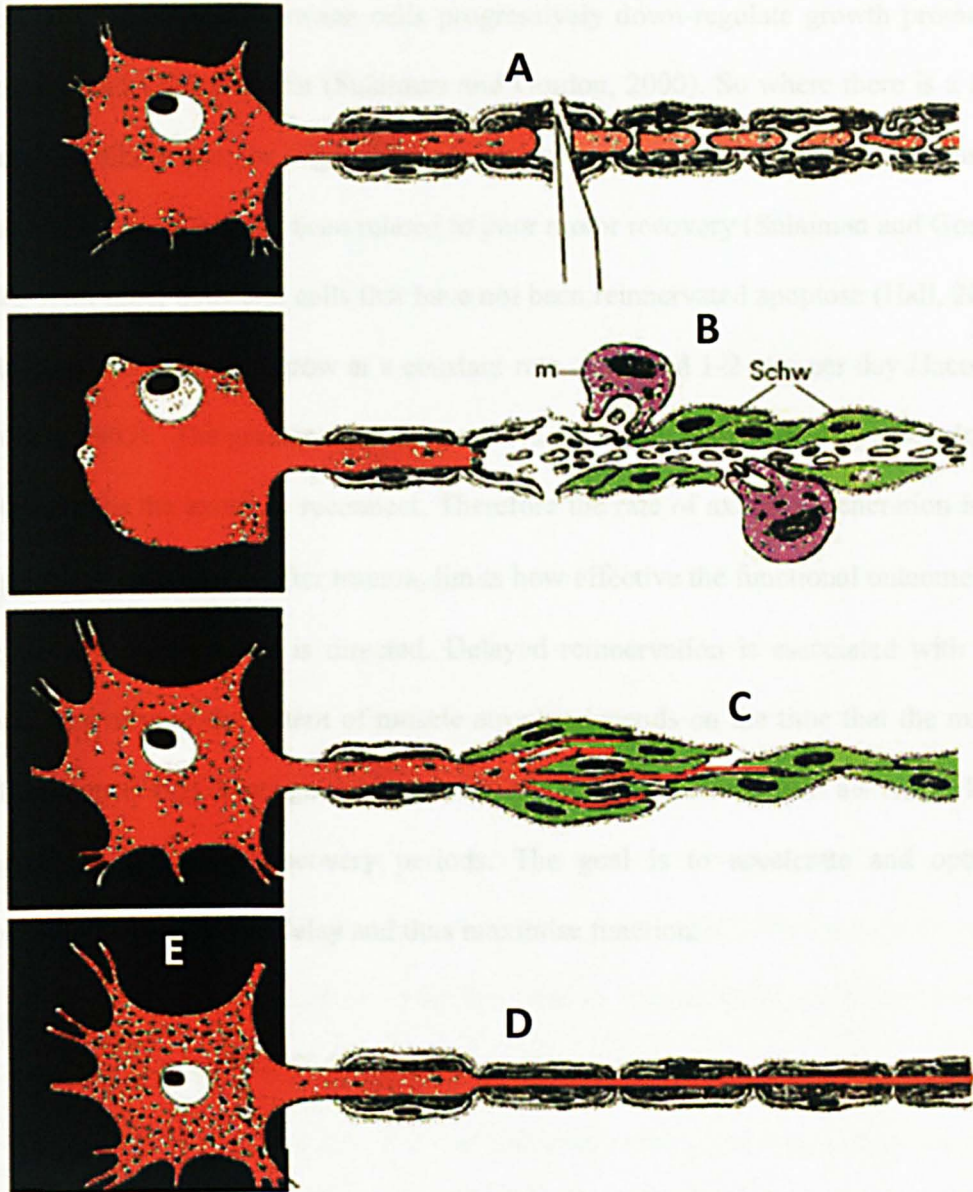


**Figure 1.3 Schematic of the events after a peripheral nerve has been cut, shown at the level of a single axon**

Neuron in red, Schwann cells (Schw) in green, myelin in black, macrophages (m) in pink. After a peripheral nerve has been cut, the proximal part seals (A) and Wallerian degeneration begins in the axon distal to the injury. The Schwann cells de-differentiate to their survivor phenotype; macrophages clear away debris (B), and the Schwann cells align to form the Bands of Büngner to guide regenerating axons (C). Schwann cells differentiate back to their myelinating phenotype and remyelinate the new axon (D). Changes, known as chromatolysis, also occur in the cell body, where the chromatin and cell nucleus are displaced to the cell periphery (E). Adapted from Hall, 2005.

Chronically denervated Schwann cells progressively down-regulate growth promoting molecules such as neuregulin (Sulaiman and Gordon, 2000). So where there is a large defect, it is likely that the regenerating axons will eventually reach “non-responsive” Schwann cells, and this has been related to poor motor recovery (Sulaiman and Gordon, 2000). With time, Schwann cells that have not been reinnervated apoptose (Hall, 2005). In ideal conditions, axons grow at a constant rate of around 1-2 mm per day (Jacobson and Guth, 1965). The greater the distance the nerve injury is from the target, the longer it will take for the axons to reconnect. Therefore the rate of axonal regeneration in the complicated environment after trauma, limits how effective the functional outcome may be even when the growth is directed. Delayed reinnervation is associated with poor muscle recovery, as the extent of muscle atrophy depends on the time that the muscle has been denervated. Damage to extremities due to lack of sensation is also more likely to occur during longer recovery periods. The goal is to accelerate and optimise regeneration to reduce the delay and thus maximise function.

## **1.3 Current treatments for peripheral nerve injury**

### **1.3.1 Primary repair**

If there is a small clean cut (creating a gap of usually no more than a few millimetres) in the nerve the surgeon can bring the ends together and perform end-to-end surgical reconnection of the damaged nerve ends by suturing (figure 1.4). In 1973 Hueter achieved end-to-end repair by an epineurial suturing technique, which became the standard method of short gap repair (Millesi, 1973). This particular therapy carries a risk of causing fibrosis; however it can be very effective when the nerve ends are directly adjacent and can be brought together without introducing any tension (Schmidt and Leach, 2003). Localised tension could cause fibroid adhesions in repaired nerves. During normal daily activities, peripheral nerves bend and stretch as limbs move, exposing the nerves to various mechanical stresses (Topp and Boyd, 2006; Mason and Phillips, 2011). This is also accompanied by ‘intranural’ movement, of the internal structures to accommodate this stress (Abrams *et al.*, 1998). Peripheral nerves can withstand a certain degree of stress and deformation without adverse effects. However, failure to restore the biomechanical integrity of peripheral nerves after injury can compromise the repair, as a result of the localised tension causing damage to neural elements (Topp and Boyd, 2006). The use of conduits or grafts to bridge longer gaps (more than a few millimetres) can alleviate tension and is therefore used to improve repair.



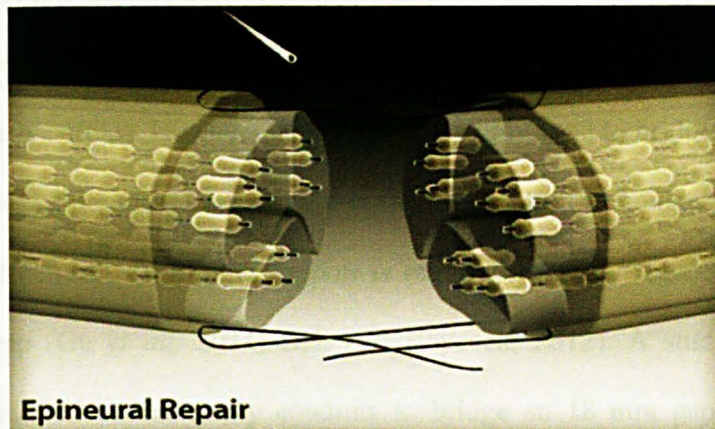


**Figure 1.4 Schematic of epineurial repair**

End-to-end repair of a severed nerve by suturing the epineurium of the two stumps, drawing the two ends together. (<http://www.vet.purdue.edu/cpr/essays1.html>)

### 1.3.2 Clinically available devices for peripheral nerve repair

#### 1.3.2.1 Conduit repair devices

For lesions more than a few millimetres in length, where a tension-free repair is not possible, empty silicone or bioresorbable tubes can be used to bridge the gap at the injury site. In 1997 Lundborg *et al.* used silicone conduits to repair 3-4 mm defects in the ulnar and median nerves in the human forearm (Lundborg *et al.*, 1997). A five year follow-up study showed no significant difference in sensory and motor function between repair using the silicone conduits and standard microsurgical repair, except that cold intolerance was significantly less severe with the tubular technique (Lundborg *et al.*, 2004). Silicone is not biodegradable and, in 8 out of 17 cases in the Lundborg study, the tubes were removed because they caused discomfort. Ideally a tube used for peripheral nerve repair should be biodegradable and not cause any discomfort or an inflammatory response during degradation. Only 4 absorbable synthetic conduits, involving 3 materials (*collagen, polycaprolactone and polyglycolic acid*) have obtained the US Food and Drug Administration (FDA) and the European approval (CE) for

clinical use (these have been summarised in table 1.1) (Kehoe *et al.*, 2012; Bell and Haycock, 2012). These devices function by providing a conduit to concentrate factors and offer overall tissue guidance/containment, with reduced fibrosis/adhesion (Danielsen *et al.*, 1993). However empty tubes are only used to bridge gaps of less than 3 cm in damaged peripheral nerves, the critical gap length in humans, because beyond this length structural and trophic support is required to allow regenerating neurites to bridge the gap (Gu *et al.*, 2011; Bell and Haycock, 2012). A study by Maeda and colleagues in 1993 tested empty conduits to bridge an 18 mm gap using a 20 mm silicone conduit in rat sciatic nerve, which is beyond the critical gap length in a rat (Bellamkonda, 2006). During a 16 week observation period no axons were found in any of the conduits (Maeda *et al.*, 1993). This could be due to the lack of an intraluminal guidance structure and the absence of living cells (Daly *et al.*, 2012; Bellamkonda, 2006).

Company	Name	Material
SaluMedica	Salubridge	polyvinal alcohol (PVA)
SaluMedica	Salutunnel Nerve Protector	PVA
Integra NeuraGen Nerve Guide	Neuragen Nerve Guide	Bovine type I collagen
Integra NeuraWrap Nerve Protector	Neurawrap Nerve Protector	Bovine type I collagen
Synovis Micro companies Alliance Inc.	Neurotube	Polyglycolic acid (PGA)
Collagen Matrix Inc.	Neuroflex	Bovine type I collagen
Collagen Matrix Inc.	Neuro Matrix	Bovine type I collagen
Collagen Matrix Inc.	Neuromend	Bovine type I collagen
Cook Biotech Products	Axo Guard Nerve Connector	Porcine small intestine submucosa (SIC)
Cook Biotech Products	Axo Guard Nerve Protector	Porcine SIC
Polyganics	Neurolac	lactide caprolactone co-polyesters (PCL)

**Table 1.1 Clinically approved conduits for peripheral nerve repair**

Decellularised allografts are also available for peripheral nerve repair. These are typically prepared by processing harvested nerves with detergent to selectively remove cellular components and debris, and they are then terminally sterilized (Brooks *et al.*, 2011). Decellularised allografts preserve the correct three-dimensional architecture for cell migration and nerve fibre elongation and provide the appropriate biomechanical properties to the repair site. However these grafts do not contain any living cells, limiting their application to the repair of gaps less than 5cm (Brooks *et al.*, 2012; Karabekmez *et al.*, 2009). This is discussed in more detail in the next section (1.3.2.2).

### 1.3.2.2 Decellularised repair devices

AxoGen are the first company to develop a product, Avance<sup>®</sup> Nerve Graft, for repair of gaps > 3 cm in peripheral nerves. Avance<sup>®</sup> Nerve Graft is a processed nerve allograft which is a decellularised, sterile extracellular matrix from donor human peripheral nerve tissue (Brooks *et al.*, 2012; Karabekmez *et al.*, 2009). Avance<sup>®</sup> functions include all those mentioned above for conduit repairs, and in addition it provides the inherent and relevant structural characteristics of peripheral nerve, the structure can be remodelled by the host cells and has similar handling properties to the nerve autograft. Additionally, chemically decellularised nerve grafts maintain the laminin component within the collagen matrix (Karabekmez *et al.*, 2009), which is known to enhance axon regeneration (Hall, 1986).

### 1.3.3 Nerve autograft

The current 'gold standard' to bridge larger gaps (> 3 cm) is to use a live nerve autograft (Bhandari *et al.*, 2007). Philipeaux and Vulpian first showed that nerve regeneration was possible with autografts in a dog model (Philipeaux and Vulpian, 1870). Later in 1878, Albert Verhandlungen described the first clinical experience of nerve grafting (Verhandlungen, 1878). The nerve autograft is typically harvested from a cutaneous sensory nerve from the patient, most commonly the sural nerve, and is connected to the proximal and distal stumps with micro-sutures.

A nerve autograft does not provide neurons, as the axons in the nerve grafts degenerate leaving the endoneurial tubes and Schwann cells (autologous, denervated). It provides a cell-rich environment with the correct tissue architecture (Schwann cell basal laminae) to promote cell adhesion and migration, biomechanical properties and guidance cues, which promote axon regeneration from the proximal nerve stump. Disadvantages of the

nerve autograft therapy include the requirement for an additional surgery, limited nerve availability and donor site morbidity, which can include a loss of sensation within the harvest area, neuroma formation, pain and scarring (Rappaport *et al.*, 1993; Staniforth and Fisher, 1978).

The success of the nerve autograft depends on the age of the patient, timing of surgery, the size of the defect, altered fascicular architecture causing axons to scatter during regeneration, the type of nerve injured, the amount of scarring in the surrounding tissue, and the distance to the denervated end-organ (Wolford and Stevao, 2003; Matejcik, 2002). The extent of vascularisation at the site of injury also has an effect on outcome. Free-vascularised nerve grafts (where vasculature in the graft is connected to recipient vasculature) have a better outcome than non-vascularised nerve grafts (standard autograft repair) (Koshima *et al.*, 1981, Restrepo *et al.*, 1985). Free-vascularised grafts can be used if the wound bed is heavily scarred or poorly vascularised, and when long and large calibre grafts are necessary. Harvesting free-vascularised grafts is time-consuming and requires great clinical expertise.

Nerve allografts have been used previously, which give similar regeneration to that observed in the autograft; however the requirement for immunosuppression and the risk of rejection are a major drawback (Rustemeyer and Dicke, 2010; Mackinnon *et al.*, 2001). Other biological materials have also been used as a nerve guidance conduit, such as vein (Walton *et al.*, 1989; Risitano *et al.*, 2002), muscle (Battiston *et al.*, 2000) and small intestine submucosa (Badylak *et al.*, 1998).

After peripheral nerve repair, patients are advised to perform physical and occupational therapy to aid the cortical remodelling process. Only 50% of patients treated with an

autograft regained the function they had prior to their nerve injury (Kehoe *et al.*, 2012; Ichihara *et al.*, 2008). In addition, 20% of autograft repairs do not achieve any functional recovery (Chiu, 1995). Without being able to guarantee success, most surgeons would prefer to avoid a second operation, and in turn, avoid permanent loss of function at the donor site. As a result, extensive research efforts have focussed on developing an alternative to the nerve autograft or allograft therapy.

#### **1.4 Neural tissue engineering**

Tissue engineering is a multi-disciplinary field where biology, material science, theoretical modelling and engineering combine towards the development of tissue replacements that restore or establish normal function (Langer and Vacanti, 1993). Conventionally, tissue engineering has relied on the use of scaffolds as temporary structures to facilitate cell migration into the repair site and then eventually be replaced with native extracellular matrix (ECM). More recently scaffolds have been developed that can also confer bio-functionality, and this need is reflected in recent reviews which describe how the addition of cells and combination of molecular and mechanical signals can enhance the repair and regeneration process (Bell and Haycock, 2012; Bellamkonda, 2006). In addition to this, other implant properties that are critical to function include the scaffold structure and biomechanical properties (Brown and Phillips, 2007). It is not essential for a tissue-engineered implant to exactly reproduce every feature of the native tissue; the success of tissue engineering is dependent on the restoration of adequate function. For some tissues, function must be restored immediately, for example covering a skin wound. For peripheral nerve, function is restored in time through regenerative processes including the elongation of neurites, reconnection of neurons to target organs and subsequent cortical remodelling. The initial design requirement for a peripheral nerve repair device therefore is for it to be

able to facilitate the repair process, providing an environment for nerve structure and function to be restored.

Recent academic reviews agree that the optimal solution for peripheral nerve repair would be an aligned cellular conduit that can (1) mimic the nerve graft to provide guidance and growth-promoting factors (secreted by the cells) to enhance regeneration; (2) provide adequate mechanical support for the regenerating axons; and (3) prevent the infiltration of fibroblasts that inhibit the repair process. However for cell-containing conduits, there are hurdles to be overcome regarding the source and availability of suitable cells before this can become a viable clinical option (Bell and Haycock, 2013; Nectow *et al.*, 2012; Gu *et al.*, 2011).

Recent approaches for making guidance conduits include the use of aligned fibres or channels, patterned surfaces, electrical and magnetic fields, mechanical loading and gradients of physical and chemical cues to organise engrafted and/or infiltrating cells (Yao *et al.*, 2010; Ceballos *et al.*, 1999; Maeda *et al.*, 1993; Eastwood *et al.*, 1998). Various materials are being explored, with surface modifications to support cell attachment and the incorporation of growth factors. Ideally the scaffolds would satisfy many properties, for example they would be:

- **Biocompatible**, to be able to support normal cellular behaviours, without eliciting any undesirable effects or immune responses.
- **Biodegradable**, to be able to degrade after the regeneration process and be remodelled or resorbed into the host tissue. This would avoid the requirement for a second operation to remove the device, which is currently required for non-biodegradable scaffolds (Lundborg *et al.*, 2004). Clinical and experimental data

suggest that the ideal scaffold should biodegrade in 1-2 years (Bell and Haycock, 2012).

- **Suitable, in terms of its mechanical properties**, to be able to withstand the loads that nerves are subjected to during normal daily activities, i.e. bending and stretching.
- **Easy to handle and suture**, to be robust enough for easy handling and capable of implantation.

These properties are mainly determined by the scaffold material, manufacturing process and structure. The types of scaffolds used can be divided into two categories: natural and synthetic materials, which will now be discussed in more detail.

#### **1.4.1 Neural scaffolds**

##### **1.4.1.1 Natural biomaterials**

Naturally-derived materials, such as the major components in ECM: collagen, laminin and fibronectin, have beneficial properties such as stimulating Schwann cell adhesion, migration and proliferation (Babington *et al.*, 2005; Grimpe and Silver, 2002; Gardiner *et al.*, 2007).

##### Collagen

Collagen is a large complex family of molecules, most commonly found as fibrous bundles, that interact with each other and other ECM molecules to provide a range of structures and functions throughout tissues of the body, for example, bone, cartilage, tendon, cornea, blood vessels, skin and nerve (Cen *et al.*, 2008). Collagen has a triple  $\alpha$ -helical structure, dependent on a highly characteristic sequence of amino acids, with glycine in every third position and also has a high content of proline and hydroxyproline



(Gordon and Hahn, 2010). Native type I collagen can aggregate into fibrils (fibrillogenesis). In fibrillogenesis, the collagens are cleaved by specific enzymes (procollagen metalloproteinases). Fibrillogenesis would not occur without these proteinases (Alovskaya *et al.*, 2007). Collagen is a highly conserved protein across species and there are various types of collagen currently being used in the clinic for peripheral nerve repair (see table 1.1 in section 1.3.2.1; Meek and Coert, 2008). Collagen has also been used in the clinic for cosmetic surgery (e.g. Zyplast, Zyderm), nerve (e.g. Integra) and skin (e.g. Apligraf).

Various methods have been used for producing aligned collagen materials. These include: high strength magnetic field (Guido and Tranquillo, 1993); micro-fluidic channels (Lee *et al.*, 2006); electro spinning (Barnes *et al.*, 2007); hydrodynamic flow (Edwina *et al.*, 2011) and cellular self-alignment in tethered gels (Phillips *et al.*, 2005). Additionally, collagen can interact directly with cells to influence cell adhesion, growth and differentiation, and play an important role in supporting axon growth and synaptic connection and maintenance (Fox, 2008).

### Fibrin

Fibrinogen molecules are comprised of two sets of disulfide-bridged  $\text{A}\alpha$ -,  $\text{B}\beta$ -, and  $\gamma$ -chains. Each elongated 46 nm structure contains two outer D domains connected to a central E domain by a coiled-coil segment (Laurens *et al.*, 2006). Fibrin is formed after thrombin cleavage of fibrinopeptides A and B from fibrinogen  $\text{A}\alpha$ - and  $\text{B}\beta$ -chains, thus initiating fibrin polymerization. Double-stranded fibrils form through end-to-middle domain (D:E) associations, and form a network of fibrin fibres which create a clot network (Laurens *et al.*, 2006). Fibrin plays an important role in the repair process after PNI. Within the first 24 hours after PNI, a fibrin cable forms between the two nerve

stumps, serving as a scaffold for cell migration, and also becomes populated with ECM proteins (Liu, 1992; Williams *et al.*, 1983).

Fibrin is currently being used in the clinic in the form of 'fibrin glue', as an alternative to micro-surgical sutures in peripheral nerve repair (Anani and El-Sadek, 2009) and as an outer tube and as a filler for conduits (Kalbermatten *et al.*, 2009). Improved regeneration was observed for the repair of a 15 mm gap in rabbit peroneal nerve using a vein graft filled with autologous fibrin glue (Choi *et al.*, 2005). The commercial kits for fibrin glue comprise of fibrinogen and thrombin, which react to form fibrin at the time it is being used (Currie *et al.*, 2001).

#### Other natural biomaterials

Other ECM proteins have also been used to engineer nerve repair devices; these include laminin (Kuappila *et al.*, 1993; Toba *et al.*, 2002), fibronectin (Whitworth *et al.*, 1995; Ahmed and Brown, 1999), hyaluronic acid (Ozgenel, 2003; Wang *et al.*, 1998; Seckel *et al.*, 1995), keratin (Lin *et al.*, 2012; Hill *et al.*, 2011; Apel *et al.*, 2008), chitosan (Wang *et al.*, 2012; Wang *et al.*, 2005) and silk fibroin (Huang *et al.*, 2012; Ghaznavi *et al.*, 2011; Yang *et al.*, 2007).

Laminin can be found in tissues such as endothelium, smooth muscle and bone marrow (Durbeej, 2010; Miner, 2008). It has been shown that the expression of laminin binding integrin subunits is upregulated in DRG neurons after sciatic nerve transection in rats (Wallquist *et al.*, 2002), and is considered to play an important role in peripheral nerve regeneration (Wallquist *et al.*, 2002; Fried *et al.*, 2005). Laminin, collagen, fibrin and hyaluronate matrices were compared within tubes for peripheral nerve repair. It was found that longer axons were extended and more axons innervated their targets in the

repairs using a laminin matrix (Labrador *et al.*, 1998; Navarro *et al.*, 1996). However there have been contrasting results, for example, Valentini and colleagues found that collagen and laminin-containing gels impeded regeneration in the rat (Valentini *et al.*, 1987).

In the repair process after PNI, hyaluronic acid plays a role in organising the ECM in the fibrin matrix phase of regeneration to facilitate migration of regenerating axons (Wang *et al.*, 1998). Topical application of hyaluronic acid to transected and immediately repaired rat sciatic nerve has been shown to prevent scar formation, resulting in faster functional recovery (Ozgenel, 2003). It also permits increased nerve conduction velocities after a 12 week recovery period following primary repair of sciatic nerve with a topical application of hyaluronic acid, compared to application of saline (Ozgenel, 2003). Nerve conduction velocities are also increased when hyaluronic acid is injected into conduits bridging the gap in rat sciatic nerve after a 4 week recovery period, compared to saline controls (Wang *et al.*, 1998).

Keratin gel has been used to fill empty conduits and improved functional recovery was observed in a mouse model after 6 months, compared to an empty conduit or an autograft (Apel *et al.*, 2008).

#### 1.4.1.2 Synthetic materials

The main advantage with using synthetic materials is that their chemical and physical properties, such as porosity, degradation rate, and mechanical strength, can be controlled. The biocompatibility of some synthetic materials is the main challenge, because they require surface modifications to support cell attachment and adhesion if they are to be used as core elements of PNI repair conduits (Bell and Haycock, 2012); and so laminin, collagen I and fibronectin have been used as coatings (Bell and Haycock, 2012).

Silicone is a non-biodegradable synthetic material that has been investigated for use as an outer tube in peripheral nerve repair since the 1960s (Gu *et al.*, 2011). The inert and flexible properties of silicone make it a useful experimental tool (Lundborg *et al.*, 1982). However the use of silicone in the clinic may cause a chronic foreign body reaction that could ultimately inhibit full functional recovery because silicone is non-biodegradable and remains *in situ* as a prosthesis (Merle *et al.*, 1989). Therefore a second operation would be required to remove the tube, which has clear disadvantages to the patient.

Biodegradable synthetic scaffolds have been fabricated for use in peripheral nerve repair, including poly(lactic acid) (PLA) (Evans *et al.*, 2002; Evans *et al.*, 2000), poly(caprolactone) (Bertleff *et al.*, 2005), polyesters such as polyglycolic acid (PGA) for Neurotube<sup>®</sup> (Shin *et al.*, 2009) and poly-3-hydroxybutyrate (PHB) (Young *et al.*, 2002). These can be fabricated with tailored properties, for example a suitable degradation rate and permeability. In PLA-based scaffolds, these properties can be controlled by electrospinning the PLA with miscible poly(lactide-co-glycolide) (PLGA) random copolymers (Kim *et al.*, 2003).

### 1.4.2 Growth factors

Neurotrophic factors play an important role in nerve regeneration; they promote neuronal growth and survival (Rich *et al.*, 1989; Whitworth *et al.*, 1996; Sterne *et al.*, 1997; Bloch *et al.*, 2001). They are produced and secreted by the cells of the nervous system (for example, Schwann cells) and are known to regulate neural cell division, survival, and neurite outgrowth of certain neuron populations (Lewin and Barde, 1996; Terenghi, 1999). Many neurotrophic factors have been identified, and some of the main ones are listed below.

- Nerve Growth Factor (NGF): This neurotrophin is vital for the development and the survival of PNS neurons. NGF is synthesised in peripheral targets. NGF binds to specific cell surface receptors on the nerve terminals and is retrogradely transported to the cell bodies of the neurons. The decrease in retrograde axonal transport of endogenous NGF after PNI informs the neuronal cell body that its axon has been disconnected from its target. NGF is secreted from denervated peripheral targets for a period of time post-injury, and this facilitates reinnervation, for example in laboratory tests involving rats with severed sensory nerves (Rich *et al.*, 1989; Rush *et al.*, 1995; Bloch *et al.*, 2001). NGF has been shown to act specifically on primary sensory neurons and on sympathetic neurons (Levi-Montalcini, 1987). It is needed for collateral sprouting of nociceptive and sympathetic axons into denervated skin (Gloster and Diamond, 1992). However it has been shown that the addition of NGF after PNI could also delay the regeneration process (Gold, 1997).
- Neurotrophin-3 (NT-3): NT-3 is produced at the motor end plates of adult skeletal muscles and has a trophic role on neurons (motor, sensory and autonomic) innervating muscles (Braun *et al.*, 1996).

- Fibroblast Growth Factor, basic (FGF-2): FGF-2 has been shown to be the most important factor for the initiation of nerve repair after trauma or injury (Grothe and Nikkah, 2001; Meisinger *et al.*, 1996). It has been shown to increase axonal branching, enhance regeneration and promote Schwann cell proliferation *in vitro* and *in vivo* (Klimaschewski *et al.*, 2004; Jungnickel *et al.*, 2006; Davis and Stroobant, 1990).
- Glial derived neurotrophic factor (GDNF): GDNF has been shown to have a trophic effect on sensory, motor and autonomic neurons *in vivo* (Hoke *et al.*, 2000; Trupp *et al.*, 1995). It has also been shown to have an effect on neuronal cell survival after axotomy (Zhao *et al.*, 2004; Henderson *et al.*, 1994).
- Others: brain-derived neurotrophic factor (BDNF), insulin-like growth factor (IGF), ciliary neurotrophic factor (CNTF), which can induce pro-regenerative responses in neurons (Kirsch *et al.*, 2003; Funakoshi *et al.*, 1993).

The use of exogenously applied neurotrophic growth factors can be an effective method of enhancing PNS nerve regeneration. The NTFs can be conjugated directly to the scaffolds for an enhanced biological effect (Bell and Haycock, 2012). Further research and development of devices to deliver these neurotrophic factors to the nerve injury site is required. Current challenges that are faced in the delivery process include local toxicity and poor stability associated with these factors.

### **1.4.3 Support cells**

It is widely reported that conduits filled with glial cells show much better regeneration for longer gaps (> 15 mm in rat, and > 30 mm in human) compared to acellular conduits (Bryan *et al.*, 2000; Bellamkonda, 2006; Gu *et al.*, 2011; Rodrigues *et al.*, 2012). Naturally occurring peripheral nerve regeneration in the body involves Schwann cells, which support axonal regeneration by clearing debris, secreting growth factors and ECM proteins and guiding axonal growth (Frostick *et al.*, 1998; Hall, 2005; Madduri and Gander, 2010). Cells could be delivered to the site of injury within a hollow tube, within a hydrogel, or on the surface of aligned fibres or channels. Schwann cells are a potential cellular source for supplying neurotrophic factors at the injury site (Rodrigues *et al.*, 2012). Other cells that may also have the potential to enhance nerve regeneration are stem cells i.e. mesenchymal stem cells (MSCs) and neural stem cells (NSCs), which are discussed in more detail in section 1.4.3.2

#### **1.4.3.1 Schwann cells**

The role of Schwann cells in the natural repair and regeneration processes of damaged nerves makes them obvious candidates for use in the development of an implantable repair device to provide support and guidance to regenerating axons following PNI. Promising results have been reported in the rat sciatic nerve model of PNI that show implanted Schwann cells assisting in the regeneration process (Anselin *et al.*, 1997; Bryan *et al.*, 2000; Hadlock *et al.*, 2000; Phillips *et al.*, 2005).

There are several challenges facing Schwann cell therapies, in particular the source and availability of the cells. Currently there is no clinically approved Schwann cell line. Obtaining autologous Schwann cells would require an invasive nerve biopsy, which carries some of the same disadvantages as the nerve autograft therapy. Autologous

Schwann cells could alternatively be obtained from a pre-degenerated nerve (at the injury site) to avoid sacrificing a healthy nerve. However, for any autologous Schwann cell source, the long periods currently required for the expansion of these cells *in vitro* would add a time delay to the surgery to repair the nerve (Gu *et al.*, 2011). An allogeneic source of Schwann cells has been explored; however, this would require the patient to be immunosuppressed to reduce the risk of the cells being rejected (Gu *et al.*, 2011). An alternative to these approaches would be to use Schwann cell-like cells that have been differentiated from stem cells.

#### **1.4.3.2 Stem cells**

Stem cells are cells that have the ability to self-renew and differentiate, giving rise to at least one other cell type. There are three potential sources of stem cells that can be used in tissue engineering: embryonic stem cells (ESCs), adult stem cells (ASCs) and induced pluripotent stem cells (iPS). ESCs are pluripotent cells derived from embryos that have been fertilised *in vitro*. They have the ability to self-renew through mitotic cell division, and have the capability for unlimited, undifferentiated proliferation. This, combined with their ability to give rise to any somatic cell except extra-embryonic tissue, gives them great potential for use in medical therapies. ASCs are stem cells harvested from adults, e.g. mesenchymal stem cells (MSCs) from bone-marrow or adipose tissue. Additionally, normal somatic cells can be taken from an adult and de-differentiated to form iPS, which are ESC-like cells. This is ethically less controversial than using ESCs in an allogeneic therapy, but has not been shown to be safe and effective in therapy yet.

Researchers have investigated the potential of stem cells to be used in nerve regeneration. Implanted neural stem cells have been shown to participate in tissue repair



and regeneration after injury to promote regeneration of peripheral nerve (Murakami *et al.*, 2002; Marchesi *et al.*, 2007; Rodrigues *et al.*, 2012). Table 1.2 shows some of the different types of adult stem cells that have been explored for peripheral nerve repair.

Cell type/ source	Study	Species/ Strain	Model	Major finding
BM-MSC	Hu <i>et al.</i> , 2007	Rhesus monkey	40 mm gap in ulnar nerve, 6 month recovery period.	Enhanced regeneration (more axons) and functional recovery, as assessed by muscle recovery and electrophysiological studies, compared to acellular controls.
	Chen <i>et al.</i> , 2007	Sprague- Dawley (SD) rat	15 mm gap in sciatic nerve, 10 week recovery period.	Improved walking behaviour as measured by footprint analysis, reduced loss of gastrocnemius muscle weight and greater number of regenerating axons within the tube, compared to control (acellular 2 % gelatin).
	Dezawa <i>et al.</i> , 2001	Wister rat	15mm gap in sciatic nerve, 3 week recovery period.	Differentiated BM-MSCs, enhanced regeneration as assessed by axon numbers and myelination, compared to undifferentiated BM- MSCs.
	Zhang <i>et al.</i> , 2004	SD rat	Injected into mechanically injured sciatic nerve, 3 week recovery period.	MSCs had differentiated into Schwann cell-like cells <i>in vivo</i> .
	Shimizu <i>et al.</i> , 2007	Wistar rat	10 mm gap in sciatic nerve, 3 week recovery period. With immunosuppress ion (human BM- MSCs).	Axons regenerated across the gap. Undifferentiated MSCs and those that differentiated into S100- positive cells were compared. More axons regenerated when using the differentiated cells.
ADSCs	Reid <i>et al.</i> , 2011	SD Rat	10 mm gap in sciatic nerve, 2 week recovery	Differentiated ADSCs were injected within PCL tubes before implantation. DRG protection

			period.	from apoptosis, compared to empty tube controls.
	Di Summa <i>et al.</i> , 2010	SD Rat	10 mm gap in sciatic nerve, 2 week recovery period.	Axons regenerated further into the conduit with differentiated ADSCs compared to the empty tubes, but not as far as in devices containing differentiated MSCs and Schwann cell repairs.
	Sun <i>et al.</i> , 2011	SD Rat	8 mm gap in facial nerve branch, 8 week recovery period.	More axonal regeneration and better reinnervation outcomes with ADSCs compared to the acellular control.
Hippocampal neuronal progenitor cells	Murakami <i>et al.</i> , 2003	Fischer rat	15 mm gap in sciatic nerve, 6 or 10 week recovery period.	After 10 weeks, more myelinated axons and enhanced electrophysiological recovery, compared to acellular controls.
Neonatal skin/neural crest-like precursors	Marchesi <i>et al.</i> , 2007	Wistar rat	16 mm gap in sciatic nerve.	More regenerated axons in the cellular repairs, compared to acellular controls.
	McKenzie <i>et al.</i> , 2006	Shiverer or wild type mouse	Sciatic nerve was crushed and cells were injected into the nerve distal to the injury, 6 week recovery period.	Differentiated skin-derived precursor cells can myelinate axons in Shiverer mice (genetically deficient in myelin basic protein).

**Table 1.2 Summary table for cells that have been used in peripheral nerve repair** (Rodrigues *et al.*, 2012, Walsh and Midha, 2009) BM-MSCs = bone marrow-mesenchymal stem cells; ADSCs = adipose-derived stem cells.

Stem cells could either be used in their “stem” state or pre-differentiated to the desired cell type prior to implantation. Delivery of undifferentiated stem cells to the injury site can encourage the stem cells to differentiate into the appropriate cell type *in vivo* (e.g. a Schwann cell-like cell in the case of PNI) as a result of cues from their microenvironment. *In vitro* studies have demonstrated that neural stem/progenitor cells in co-culture with cells from the nervous system will adopt a phenotype similar to that of their neighbouring cells. For example, dorsal root ganglion cultures (mixed cell population of neurons and glia) will induce differentiation of neural stem cells into a peripheral neuron, Schwann cell or smooth muscle phenotype (Brannvall *et al.*, 2008).

#### **1.4.3.3 Considerations for translation of cell therapies to the clinic**

The use of stem cells in regenerative medicine is a relatively new field that is quickly expanding. Previous accomplishments using stem cells in the clinic encourage further research on stem cells for future cell therapies (Hayani *et al.*, 2007; Rama *et al.*, 2010); although there are many issues associated with their use at the moment, such as their source and availability, the lack of control over cell differentiation and their long term safety.

Recent reviews have predicted that the optimal peripheral nerve repair device would include a combination of features including guidance and the presence of living cells (Bellamkonda, 2006; Bell and Haycock, 2012; Gu *et al.*, 2011). Under current regulations, the European Medicines Agency (EMA) categorises a cell-based therapy as “an advanced therapy medicinal product” (ATMP). The nerve repair device developed in this study would be further classed as a tissue engineered product, which is defined by the EMA as follows.

*“A product that contains or consists of engineered cells or tissues and is presented as having properties for, or is used in, or administered to human beings with a view to regenerating, repairing, or replacing human tissue. A tissue engineered product may contain cells or tissues of human or animal origin, or both. The cells or tissues may be viable or nonviable. It may also contain additional substances such as cellular products, biomolecules, biomaterials, chemical substances, scaffolds, or matrices.”*

The US Food and Drug Administration (FDA) classify such a device as a combination product: biological (derived from living sources) and medical device class III (intended to affect the structure or function).

There are many hurdles to be overcome before a cell therapy can reach the patient. These include: identifying cells/materials that will not cause adverse effects such as formation of tumours/ectopic tissue; fully defining the production process and final product; meeting regulations and designing appropriate assays to classify the product; confirming safety and efficacy. These hurdles and safety issues in some part explain why only one autologous cellular nerve repair device has progressed to clinical trials (Sabelman and Hentz, clinical trial, 1999).

#### **1.4.4 Guidance structures within tissue engineered scaffolds**

Anisotropic guidance structures are considered to be critical within a peripheral nerve repair device to efficiently bridge large nerve gaps (Kim *et al.*, 2008; Gupta *et al.*, 2009; Wang *et al.*, 2011; Daly *et al.*, 2012). When engineering intraluminal guidance structures, it is important to consider the scale of the different structural elements; nano- (tropocollagen, the molecular component of a collagen fibre ~300 nm), micro- (collagen

fibrils  $\sim 1 \mu\text{m}$ ) and macro-scale (collagen fibres  $\sim 10 \mu\text{m}$ ). The scale of the structural elements determines the dimensions of the environment on a cellular level. Cells binding to channels or fibre-based scaffolds with micro-scale architecture flatten and spread over them, similar to how they would in monolayer culture, representing a pseudo-third dimension. The scale of the material relative to the cells on/within it, plays an important role in cell phenotype, influencing cell shape and gene expression (Dutta and Dutta, 2009; Leong *et al.*, 2003; Behonick and Werb, 2003; Cukierman, 2001). Cells also respond differently when cultured in 3D, compared to 2D cultures, and can adopt more *in vivo*-like morphologies in 3D culture (East *et al.*, 2010). In 3D culture, the cells are able to attach to the substrate through most of their membrane surface (Stevens and George, 2005).

The orientation of the scaffold elements directly affects its mechanical properties and also provides topographical cues to cells (Murugan and Ramakrishna, 2007; East *et al.*, 2010; Nisbet *et al.*, 2009). Directional organisation is displayed in the cell shape and cytoskeleton. Contact-guided cellular alignment is primarily due to the orientation of actin filaments or microtubules (Oakley and Brunette, 1993; Wojciak-Stothard *et al.*, 1995). Weiss was first to correlate the orientation of substrate and the directional growth of cells as contact guidance (Weiss *et al.*, 1945). Table 1.3 provides a summary of some of the materials and techniques that have been reported to create anisotropic guidance substrates for peripheral nerve repair.

Technique	Material	Structure	Result	Reference
Magnetic alignment	Collagen I	Aligned fibres	guided neurite outgrowth	Guido and Tranquillo, 1993; Ceballos <i>et al.</i> , 1999; Dubey <i>et al.</i> , 1999
	Fibrin			Dubey <i>et al.</i> , 2001
Injection moulding	Poly(lactic-co-glycolic acid)	Porous conduits with longitudinal channels	Reduced dispersion of regenerating axons, guided outgrowth	Hadlock <i>et al.</i> , 2000; Sundback <i>et al.</i> , 2003
	Collagen	Micro-fluidic channels	Guided channels	Lee <i>et al.</i> , 2006
Electrospun fibers	Collagen fibre bundles	Aligned fibers	Improved regeneration in rat sciatic nerve model	Tong <i>et al.</i> , 1994
	Poly-[epsilon]-caprolactone (PCL)	Nanofibres	Guided cell migration and neurite outgrowth	Schnell <i>et al.</i> , 2007
	Polyamide	Aligned filaments	Supported regeneration across 15mm gap in rat sciatic nerve model	Lundborg <i>et al.</i> , 1997
Self-alignment in tethered gels	Collagen type I	Columns of aligned cells within an aligned collagen matrix	improved regeneration <i>in vivo</i> in rat sciatic nerve model	Phillips <i>et al.</i> , 2005

**Table 1.3 Some of the current techniques and materials used to fabricate anisotropic neural scaffolds**

Hydrogels consist of nano-scale fibres and represent true 3D substrates. They possess the desired properties for engineering: capacity for water retention, nano/micro-porosity to allow cells to grow and arrange in 3D, biodegradability and porosity to permit oxygen and nutrient diffusion (Dutta and Dutta, 2009). Phillips and colleagues used a tethered hydrogel with columns of aligned Schwann cells to repair a 5 mm gap in rat sciatic nerve (Phillips et al., 2005). In this study the cellular hydrogel was tethered within a silicone tube. The Schwann cells in the collagen formed stable integrin-mediated attachments with the collagen fibrils. Over time, the cells generated contractile forces, which led to gel compaction (Brown and Phillips, 2011). The tethering self-aligning system avoids the need to manufacture elaborate scaffolds with surface modification to support cell attachment, and for a cell-seeding and/or cell alignment step. It also uses native collagen rather than synthetic materials.

The high fluid content of hydrogels means that they have poor mechanical stability (Cheema *et al.*, 2007), limiting their use as a scaffold for tissue engineering applications. If the gels can be made mechanically stable then a simple and effective aligned cellular material could be made, which is the focus of this project.

Brown and colleagues previously reported that a compressive load can be applied to fully hydrated collagen gels to rapidly remove most of the interstitial fluid from the gel (Brown *et al.*, 2005). This increases the collagen and cell density by ~ 50 fold without affecting cell viability, producing more robust cellular collagen sheets; this process is called plastic compression (Brown *et al.*, 2005).

This project began with the hypothesis that combining the tethered self-alignment technology with the plastic compression process could produce robust, mechanically



stable collagen sheets with chains of aligned supporting cells. The key advantage of this approach is that it achieves a stable 3D structure without the use of chemical cross-linking agents, and provides guidance, neurotrophic factors and biological cues in a single approach. The purpose of this work was to develop a material that could promote guided neuronal growth for use in a peripheral nerve repair device.

## 1.5 Aims and objectives

The overall aim of this PhD was to develop an implantable tissue-engineered device for the surgical repair of the peripheral nervous system. This was divided into three main objectives:

1. To develop and optimise a robust biomaterial with highly aligned cells [Engineered Neural Tissue (EngNT)] that could potentially form the basis of a peripheral nerve repair device.
2. To engineer an 'endoneurium' using EngNT that supported the re-growth of axons across the gap in injured nerves.
3. To investigate the feasibility of constructing a repair device from EngNT using clinically relevant cells and materials.

Objective 1 was addressed by first investigating whether the alignment achieved in tethered hydrogels could be stabilized when the gel is removed from the tethering bars for implantation, and optimising EngNT. An *in vitro* co-culture experiment with primary adult neurons was used to investigate whether EngNT could support guided neurite outgrowth. The next step (objective 2) was to investigate whether EngNT could form the basis of a functional peripheral nerve repair device *in vivo*. This was addressed through the exploration of two different EngNT arrangements (rods and sheets) within an outer tube in the short gap rat sciatic nerve model, with the best arrangement taken forward for testing in a long gap model, which is representative of the clinical situation. The final part of this study was addressed by testing different types of stem cells (undifferentiated and differentiated) within EngNT and assessing their ability to promote guided neurite outgrowth *in vitro*. Promising cell types were taken forward for testing in a pilot *in vivo* study to assess whether they could support neuron regeneration across a long gap in the rat sciatic nerve.

## 2.0 Materials and methods

### 2.1 Materials

The following tables list the cell lines purchased (table 2.1), the consumables (table 2.2), and the antibodies (table 2.3) used for this project.

Cell line	Supplier	Catalogue number
F7 Schwann cell line, rat	Health Protection Agency Culture Collections, UK	93031204
ReNcell CX cells, human	Millipore, UK	SCC007

**Table 2.1 Cell lines used in this project**

This table includes the names of the cell lines, suppliers and catalogue numbers.

Reagent/solution/other	Supplier	Catalogue number
Dulbecco's modified Eagle's medium (DMEM)	Sigma-Aldrich, UK	D6426
Fetal bovine serum (FBS/FCS)	Sigma-Aldrich, UK	F74524
Penicillin-streptomycin (P/S)	Sigma-Aldrich, UK	P0781
<b>DMEM-complete</b> is DMEM supplemented with 10% FCS and 1% P/S		
ReNcell Neural Stem Cell Maintenance Medium	Millipore, US	SCM005
Trypsin-EDTA solution (1X)	Sigma-Aldrich, UK	T3924
Accutase™	Millipore, US	SCR005
Poly-D-lysine	Sigma-Aldrich, UK	P7886
Poly-L-lysine	Sigma-Aldrich, UK	P6282
Laminin	Sigma-Aldrich, UK	L-2020
Phosphate buffered saline (PBS)	Sigma-Aldrich, UK	P4417
Paraformaldehyde (PFA)	Fischer-Scientific, UK	P/0840/53
Sodium borate	BDH, UK	30231
Uranyl acetate	Agar Scientific, UK	R1206A
Osmium tetroxide	Agar Scientific, UK	R1015
Dimethyl sulfoxide (DMSO)	Sigma-Aldrich, UK	D5879
Cytosine Arabinoside (Ara-C)	Sigma-Aldrich, UK	C1768
Collagenase type IV	Sigma-Aldrich, UK	C9407
$\epsilon$ -amino Caproic acid (E-ACA)	Sigma-Aldrich, UK	A2504

2-mercaptoethanol	Sigma-Aldrich, UK	M3148
All-trans-retinoic acid	Sigma-Aldrich, UK	R2625
Platelet-derived growth factor - AA (PDGF-AA)	PeptoTech, UK	315-17
Basic fibroblast growth factor (FGF-2)	Sigma-Aldrich, UK	F0291
Forskolin	Sigma-Aldrich, UK	F6886
Glial growth factor-2 (GGF-2)	Millipore, US	GF030
Neuregulin-1 (NRG-1)	Millipore, US	01-201
Recombinant human fibroblast growth factor-basic (FGF-2)	Millipore, US	GF003
Epithelial growth factor (EGF) human recombinant protein	Millipore, US	GF144
Minimum essential medium (MEM) 10X	Sigma-Aldrich, UK	M0275
Rat tail collagen type I	First Link (UK) Ltd.	60-30-810
Bovine collagen type I	Invitrogen™ Life Technologies, US	A10644-01
Sodium hydroxide (NaOH)	Fischer-Scientific, UK	S/4930/17
Fibrinogen (Fb)	Sigma-Aldrich, UK	F8630
Thrombin (Th)	Sigma-Aldrich, UK	T9549
CellTracker™ Green CMFDA	Invitrogen™, US	C7025
Hoechst 33258 (Bisbenzimidazole)	Sigma-Aldrich, UK	861405

Propidium Iodide (PI)	Sigma-Aldrich, UK	81845
Trypan blue solution (0.4%)	Sigma-Aldrich, UK	T8154
Toluidine blue	VWR, UK	JTW143-3
Triton® X-100	Sigma-Aldrich, UK	T9284
Goat serum	Dako, Denmark	X0907
FluorSave™	CalbioChem®, UK	345789
Isoflurane anaesthetic	Minrad Inc, UK	From the pharmacist
Rimadyl analgesic	Pfizer, US	From the pharmacist
Lacri-lube	Allergan®, UK	From the pharmacist
Opsite skin spray	Smith & Nephew, UK	From the pharmacist
10-0 sutures	eSutures	2830G
4-0 sutures	Westons	W392H
NeuraWrap™	Integra LifeSciences, US	NW340
Silicone tubing (medical grade)	SF Medical, US	SFM3-3050
OCT Embedding matrix	Thermo Scientific	12678646
Gelatin from porcine skin, type A	Sigma-Aldrich, UK	G1890

**Table 2.2 Consumables used in this project**

This table includes the names of the reagents, solutions and other, the supplier and catalogue numbers, which were used in this project.

Primary antibody	Dilution	Supplier	Catalogue number	Secondary antibody	Dilution	Supplier	Catalogue number
Rabbit, polyclonal anti-S100	1:200	Dako, Denmark	Z0311	DyLight® 488 or 549. Goat anti-rabbit IgG (H+L)	1:200	Vector Laboratories, US	DI-1488 or DI-1549
Rabbit, polyclonal anti-glial fibrillary acidic protein (GFAP)	1:300	Dako, Denmark	Z0334				
Rabbit, anti-integrin $\beta$ 1	1:500	Millipore, US	AB1952-20				
Rabbit, anti-nerve growth factor receptor p75	1:200	Chemicon, UK	AB1554				
Rabbit, polyclonal anti-sox 10	1:200	Millipore, US	MAB5727				
Mouse, monoclonal anti- $\beta$ -tubulin III	1:400	Sigma-Aldrich, UK	T8660	DyLight® 488 or 549. Goat anti-mouse IgG (H+L)	1:200	Vector Laboratories, US	DI-2488 or DI-2549
Mouse, anti-neurofilament	1:1000	Covance, UK	AMI-35R				
Mouse, anti-nestin	1:200	Millipore, US	MAB5326				
Mouse, anti-CD54	1:100	Millipore, US	MAB2130				
Mouse, anti-CD45	1:100	Millipore, US	2003607				
Mouse, anti-CD14	1:000	Millipore, US	2003608				

**Table 2.3 Antibodies used in this project**

The table includes the names, suppliers and catalogue numbers of the antibodies used within this project, and the dilutions they were used at.

## **2.2 Cell culture**

### **2.2.1 Schwann cells (F7 cell line)**

The rat Schwann cell line SCL 4.1/F7 (obtained as frozen stocks from the Health Protection Agency) was originally derived from neonatal Wistar rat Schwann cells (Haynes *et al.*, 1994). These cells were chosen for the initial experiments to optimise the production of EngNT, to ensure a ready supply of cells in the quantities required.

Cells were cultured on standard tissue culture plastic and the nutrient medium, DMEM-complete, was replaced every 2-3 days until cells were approximately 80 % confluent, as observed under phase-contrast microscopy, at which point they were either sub-cultured or used for experiments. Cells were removed from the culture dishes by trypsinisation with 0.25 % trypsin-EDTA solution for 7-10 minutes at 37 °C, 5 % CO<sub>2</sub> in air; and were recovered by centrifugation at 400 x g for 5 minutes and the pellet was resuspended in DMEM-complete for use in the various systems in this study.

### **2.2.2 Primary adult rat neurons**

All animal tissue was obtained according to the UK Home Office regulations following approval by the Open University Animal Ethics Advisory Group. Adult rats were euthanized by carbon dioxide asphyxiation (schedule 1 method) according to the UK Animals (Scientific Procedures) Act 1986.

To obtain the dorsal root ganglia (DRGs), first the spinal column was excised from adult Sprague-Dawley rats (250-350 g) that were culled using carbon dioxide (CO<sub>2</sub>) asphyxiation. The column was divided in half in the sagittal plane to expose the spinal cord, and the cord tissue was removed to expose the DRG and roots in the intervertebral foramen. Using the Olympus SZ40 dissecting microscope with Volpi, Intralux® 6000



optical fibre light source, the DRGs were removed and placed in a petri dish containing DMEM-complete. Twenty DRGs were collected from the thoracic and lumbar regions, and cleaned by removal of the roots, capsule and capillaries. Cleaned DRGs were placed in a fresh petri dish containing DMEM-complete. The cleaned DRGs were dissociated after incubation in 2 ml 0.125 % collagenase type IV (prepared in serum-free DMEM medium supplemented with 100 µg/ml P/S solution) at 37 °C, 5 % CO<sub>2</sub> in air for 90 minutes. The collagenase-treated explants were mechanically dissociated (trituated) with a 1 ml Gilson pipette. Collagenase was removed by two 20 ml spin washes in DMEM-complete at 400 x g for 5 minutes. The pellet was resuspended in DMEM-complete supplemented with 0.01 mM cytosine arabinoside (to deplete the dividing satellite glial cells and any fibroblasts, leaving an enriched primary culture of adult rat neurons), and plated in a poly-d-lysine (PDL)-coated (50 mg/ml, RT, 30 minutes) T75 flask (1-2 rats per flask) and incubated at 37 °C, 5 % CO<sub>2</sub> for 24 hours before use.

DRG neurons were maintained in PDL-coated flasks and used within 48 hours. They were removed by trypsinisation with 0.25 % trypsin-EDTA solution for 7-10 minutes at 37 °C, 5 % CO<sub>2</sub>. Cells were recovered by centrifugation at 400 x g for 5 minutes and then resuspended in DMEM-complete medium for use in the various systems in this study.

### **2.2.3 Primary rat bone marrow-mesenchymal stem cells**

The femurs of 20 day old Sprague-Dawley rats were harvested from both hind legs following CO<sub>2</sub> asphyxiation. Femurs were trimmed to exclude the proximal and distal epiphyses and trimmed of excessive muscular tissue. The bone marrow was flushed out with DMEM-complete using a 23G needle. Bone marrow was flushed from both

directions, in turn, until all material was recovered. The bone marrow was mechanically dissociated using a 1ml pipette and plated on to PDL-coated T75 flasks (1-2 rats per flask; flasks coated as previously described). Daily media changes were required to remove the non-adherent haematopoietic cells. Cells were used when 80 % confluent without passaging, at which point they were dissociated by trypsinisation (as described previously).

#### **2.2.4 Primary rat Schwann cell-like cells derived from adipose stem cells**

Adipose-derived stem cells (ADSCs) were isolated and differentiated into Schwann cell-like cells by Dr Paul Kingham, Umea University, Sweden, using previously published protocols (Kingham *et al.*, 2007).

##### Isolation of ADSCs

ADSCs were obtained from adult Sprague-Dawley rats. Visceral fat encasing the stomach and intestines was carefully dissected and minced using a sterile razor blade. Tissue was then enzymatically dissociated for 60 minutes at 37 °C using 0.15 % (w/v) collagenase type I. The suspension was passed through a 70 µm filter to remove undissociated tissue, enzymes were neutralized by the addition of Modified Eagle Medium (α-MEM) containing 10 % (v/v) foetal bovine serum (FBS) and cells were recovered by centrifugation at 800 × g for 5 minutes. The stromal cell pellet was resuspended in MEM containing 10 % (v/v) FBS and 1 % (v/v) P/S solution. Cultures were maintained at sub-confluent levels in a 37 °C incubator with 5 % CO<sub>2</sub> and passaged with trypsin-EDTA as required.

### Differentiation of ADSCs to a Schwann cell phenotype

Growth medium was removed from sub-confluent ADSC cultures at passage 2 and replaced with medium supplemented with 1 mM  $\beta$ -mercaptoethanol for 24 h. Cells were then washed and fresh medium supplemented with 35 ng/ml all-trans-retinoic acid was added. A further 72 h later, cells were washed and medium replaced with differentiation medium: cell growth medium supplemented with 5 ng/ml platelet-derived growth factor-AA (PDGF-AA), 10 ng/ml basic fibroblast growth factor (bFGF), 14  $\mu$ M forskolin (FSK) and 252 ng/ml glial growth factor (GGF-2). Cells were incubated for 2 weeks under these conditions, with fresh medium added approximately every 72 h.

The resulting Schwann cell-like cells were cultured on standard tissue culture plastic and the nutrient medium [DMEM-complete supplemented with 10 mM FSK, 100  $\mu$ g/ml bFGF, 100  $\mu$ g/ml Neuregulin-1 (NRG1)] was replaced every 2-3 days until cells were approximately 80 % confluent, as observed under phase-contrast microscopy, at which point they were either sub-cultured or used for experiments before passage 8. Cells were passaged by trypsinisation, as described previously. Cells were recovered by centrifugation at 400 x g for 5 minutes and the pellet was resuspended in DMEM-complete for use in the various systems in this study.

#### **2.2.5 Human neural progenitor cells (ReNcell CX cell line)**

ReNcell CX (Millipore UK Ltd.) is an immortalized human neural progenitor cell line with the ability to readily differentiate into neurons and glial cells (ReNcell CX immortalized cell line, Millipore, 2012, SCC007, data sheet). ReNcell CX was originally derived from the cortical region of human fetal brain.

Undifferentiated CX cells (uCX) were cultured on laminin-coated flasks (20  $\mu\text{g}/\text{ml}$  laminin in DMEM/F12 for at least 4 h at 37 °C, 5 %  $\text{CO}_2$ ). Cells were cultured in ReNcell NSC Maintenance Medium supplemented with 20 ng/ml FGF-2 and 20 ng/ml EGF. Nutrient medium was replaced every 2-3 days until cells were approximately 80 % confluent, as observed under phase-contrast microscopy, whereupon they were either sub-cultured or used for experiments. Cells were dissociated with 3-5 ml Accutase™ for 3-5 minutes at 37 °C, 5 %  $\text{CO}_2$  and cells were recovered by centrifugation at 300 x g for 3-5 minutes.

#### Differentiation of uCX to a population of mixed glia

Differentiation was initiated when cells were approximately 50-60 % confluent (to prevent overgrowth of the cells by the end of the two-week differentiation protocol), by replacing medium with fresh ReNcell NSC Maintenance Medium that did not contain FGF-2 and EGF. Medium was replaced every 2-3 days for 2 weeks, with no FGF-2 and EGF in the basal medium. Cells were dissociated with 3-5 ml Accutase™ for 3-5 minutes at 37 °C, 5 %  $\text{CO}_2$  and were recovered by centrifugation at 300 x g for 3-5 minutes.

## **2.3 3D hydrogels**

After trypsinisation of cells to be used in culture systems, the number of cells recovered was determined using a haemocytometer. The haemocytometer was moistened and a coverslip was fixed over the top, creating a chamber between the coverslip and the haemocytometer. Cell suspension (7  $\mu$ l) was added to this chamber and then observed under the 10X objective on a light microscope. The number of cells in the grid of the four corners (16 squares per corner) were counted. The total number of cells was divided by four to give an average per corner, and then multiplied by  $10^4$  to give the number of cells per ml. 3D hydrogels (collagen type I or fibrin) were prepared as described below. Details of the cell densities used in the gels are provided for individual experiments or protocols.

### **2.3.1 Collagen type I**

Type 1 collagen (2 mg/ml in 0.6 % acetic acid) and 10x MEM were mixed and kept at 2-4 °C until neutralisation with drop-wise addition of concentrated (10 mM) and dilute (1 mM) sodium hydroxide (NaOH). Collagen/MEM solution was mixed by swirling after each addition of NaOH and neutralisation was indicated by a colour change of phenol red pH indicator in the medium (from yellow to peach/orange). The neutralised collagen/MEM solution was then added to the cell suspension containing the appropriate number of cells, and swirled to mix, in a final mixture ratio of: 80 % (v/v) collagen, 10 % (v/v) 10x MEM and 10 % (v/v) cell suspension. The gel mixture was dispensed into appropriate culture vessels or moulds (section 2.4) and left to set for 10-15 minutes at 37 °C before overlaying with appropriate culture medium.

### 2.3.2 Fibrin

Fibrinogen (5 mg/ml in PBS) was mixed with the appropriate cell suspension (in DMEM-complete), and then added to the thrombin (2 U/ml in PBS). These were mixed slowly by triturating in a final mixture ratio of: 67 % (v/v) fibrinogen, 16.5 % (v/v) cell suspension and 16.5 % (v/v) thrombin. Gels were cast into the tethered moulds (see section 2.4.1 for detail) and left to set for 20 minutes at 37 °C. Gels were then topped up with 7 ml of culture media containing 1 mg/ml of  $\epsilon$ -Amino Caproic Acid (E-ACA), to inhibit enzymatic degradation of the fibrin gel by fibrinolysis. E-ACA prevents the binding of plasmin to fibrin and thus blocks fibrinolysis. Fibrin tethered gels were left for 18 hours to permit contraction.

## 2.4 Engineered neural tissue protocol

EngNT is a tissue-like robust hydrogel with highly aligned cells (prepared as described in East *et al.*, 2010). Rat tail and bovine collagen I, and fibrin hydrogels were used for preparation of EngNTs for the experiments in this project. The process for making EngNT can be divided in two parts: making tethered gels, and then stabilising them using the plastic compression process (figure 2.1).

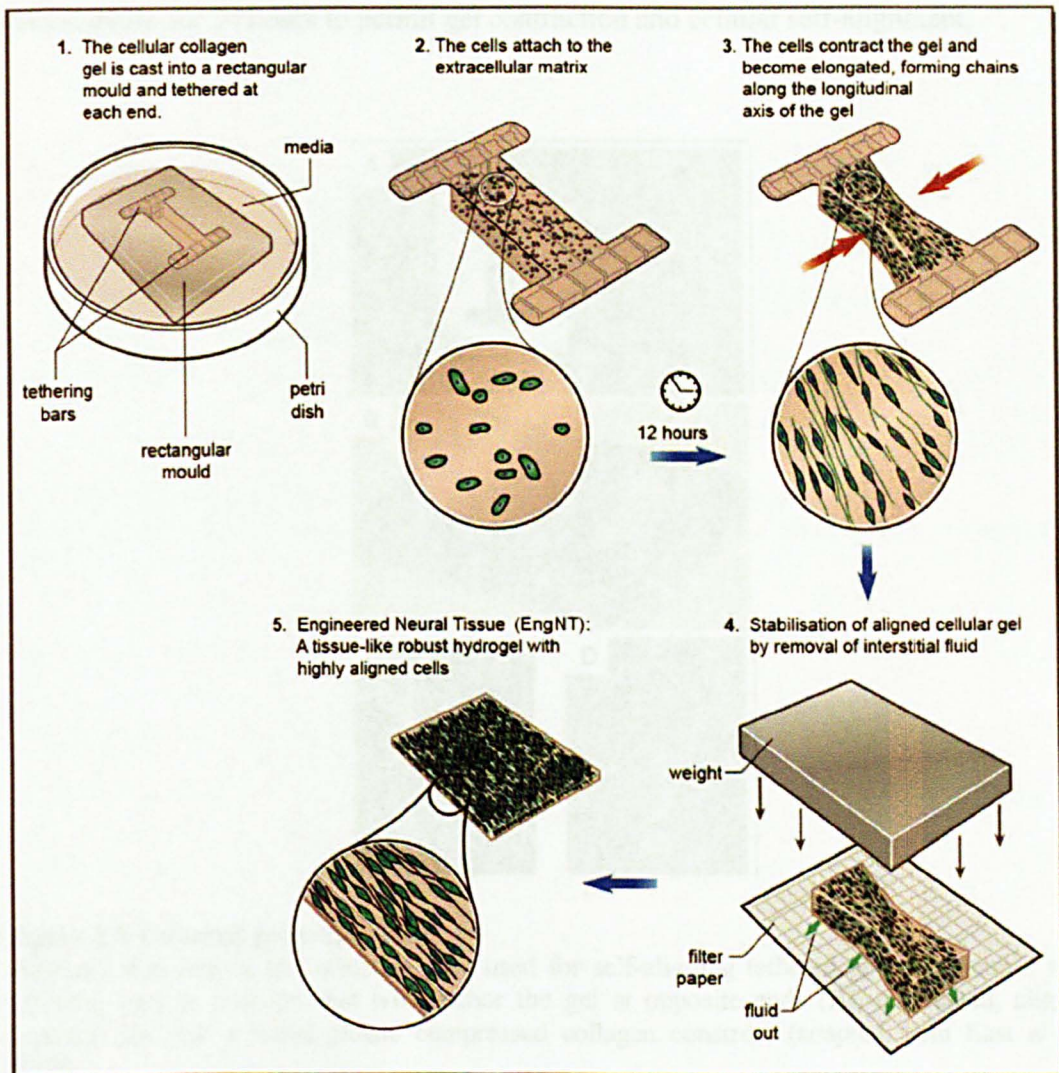


**Figure 2.1 Production of EngNT**

This shows the general scheme for the production of EngNT using collagen. However the materials and timings were varied in the experiments.

### 2.4.1 Tethered cellular gels

Cellular hydrogels were prepared as described in section 2.3 and cast in the tethering system (Figure 2.2), which was within a petri dish and on a cold block to reduce the rate of fibrillogenesis. The cellular collagen solution was integrated with the tethering bars using a 200  $\mu$ l Gilson pipette, incubated for 10-15 minutes to allow it to set at 37 °C, 5 % CO<sub>2</sub> and then overlaid with 7 ml of DMEM-complete medium before returning it to the incubator for 24 hours to permit gel contraction and cellular self-alignment.

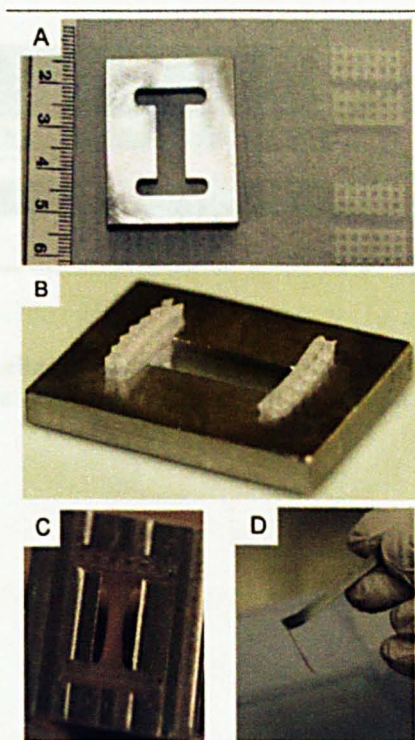


**Figure 2.2 Tethered gel preparation**

Stainless steel mould and tethering bars used for self-aligning tethered gels (A), mould with tethering bars in position that will anchor the gel at opposite ends (B), contracted, aligned hydrogel (c), and a rolled plastic compressed collagen construct (adapted from East *et al.*, 2010).

The cells within this tethering system self-align along the long axis of the gel as a result of the tension they generate between the two attachment sites (Eastwood, 1998; Brown and Phillips, 2004; Phillips *et al.*, 2005; Alovskaya *et al.*, 2007).



## 2.4.2 Plastic compression

Plastic compression (Brown *et al.*, 2005) is the process used to stabilise the cellular alignment in the hydrogel (figure 2.3), once it is removed from the tethering system. This process involves loading the gel with a 120 g weight to irreversibly expel most of the interstitial fluid held within the mesh of collagen fibrils (the fluid being absorbed by filter papers), thereby increasing the matrix and cell density and producing a robust, aligned cellular hydrogel (EngNT).

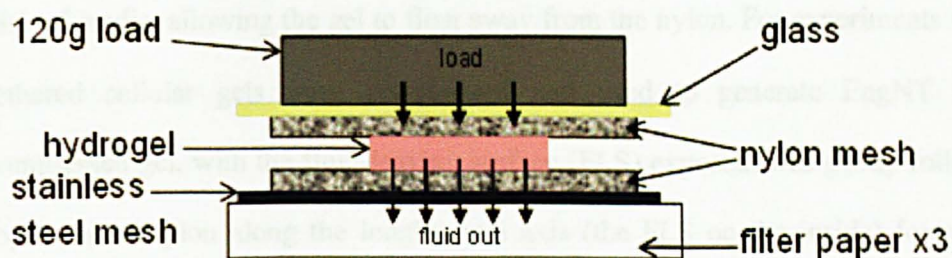


**Figure 2.3 Stabilisation of cellular alignment by plastic compression**

The gel is placed between the two nylon meshes, and the weight is applied for 1 minute (unless otherwise stated).

Fully-hydrated gels in 24 well-plates were gently removed using a spatula (for initial experiments in chapter 3). Tethered gels were cut away from tethering bars (in the stabilisation process), so the tethering mould could be gently lifted away from the gel. The gel was placed between the two nylon meshes and the 120 g load was applied for 1 minute (unless otherwise stated). For experiments to assess cell survival and alignment post-plastic compression, and for co-culture with DRGs, the top layer of nylon mesh was slowly peeled away leaving the bottom layer of nylon still in contact with the compressed gel. The compressed gel on the nylon mesh was then submerged in a petri dish of media, allowing the gel to float away from the nylon. For experiments where the tethered cellular gels were compressed and used to generate EngNT rods, the compressed gel, with the fluid-leaving surface (FLS) exposed, was gently rolled off the top layer of nylon along the longitudinal axis (the FLS on the inside) forming a rod shaped structure (Figure 2.2D). These rods were then placed in a petri dish of DMEM-complete and, when cut to size, were ready for device assembly.

### **2.5 *In vitro* co-culture of EngNT with neurons**

EngNT was made as described in the previous section. DRG neurons were prepared as described in section 2.2.2. These were seeded onto the surface (not the FLS) of EngNT sheets in a petri dish with no medium, allowed to settle for 30 minutes, then constructs were immersed in culture medium at 37 °C in a humidified incubator with 5 % CO<sub>2</sub>/95 % air. After 3 days the EngNT-neuron co-cultures were washed briefly in phosphate buffered saline (PBS) and fixed with 4 % paraformaldehyde (PFA) for 24 hours, then immunofluorescence staining was carried out as described in section 2.9.1, to detect  $\beta$ III-tubulin-positive neurons and to label the cells used in the EngNT with a suitable antibody against a specific marker.

## **2.6 Tensile testing**

This experiment was conducted by Dr Darren Burke from Bose Limited. Tensile testing was used to compare the mechanical behaviour of fresh rat sciatic nerve and acellular sheets of plastic compressed collagen. For this experiment, 40 mm lengths of sciatic nerve (starting from 5 mm distal to the hip joint) were collected from female 240-300 g Sprague-Dawley rats killed by CO<sub>2</sub> asphyxiation, and acellular plastic compressed sheets of collagen were made. Nerves were maintained at their *in situ* length on a frame made from a piece of card. For each experiment, nerves and sheets of collagen were connected to a Bose ElectroForce 3100 system (Bose, UK). Each nerve or construct was stretched at a rate of 1mm per minute and was tested until point of breakage. WinTest Control software was used to produce force/extension curves, from which the resistance to deformation of each nerve and sheet of collagen could be assessed.

## **2.7 *In vivo* testing in the rat sciatic nerve model**

### **2.7.1 Device assembly**

The outer sheath of the device (a silicone tube with a longitudinal slit or NeuraWrap™) was cut to 8 mm for a 5 mm gap and 18 mm for a 15 mm gap to allow a 1.5 mm overlap with each nerve stump. EngNT rods or sheets were positioned within the conduits. The silicone closed naturally due to its elastic structure, and NeuraWrap™ was closed using 10-0 sutures along the seam.

### **2.7.2 Surgery**

Surgery and animal care were performed in compliance with institutional guidelines, under a Home Office Licence. Adult (250-400 g) Sprague-Dawley rats (a transgenic  $\beta$ -actin-green fluorescent protein (GFP) reporter line or wild type) were deeply anaesthetised by inhalation of isoflurane and oxygen, and maintained under anaesthetic

with a gas mask throughout the surgery, which was carried out on a heated table (set to 40°C). The breathing of the animals was monitored throughout the surgery as an indication of depth of anaesthesia, and the anaesthetic dose was adjusted accordingly. Lacri-lube eye ointment was applied to both eyes of the rat to prevent drying during the surgery. The skin over the left femur was shaved and a 3 cm lateral skin incision was made parallel to and approximately 5 mm dorsal to a straight line between the knee and hip joint, to reveal the intermuscular plane, which was then separated using blunt dissection to expose the sciatic nerve. Viewed with a Zeiss Stemi DV4 spot stereomicroscope, the sciatic nerve was separated from surrounding tissue before a transection was made in the nerve mid-way between the hip and the knee, above the bifurcation. The repair device or graft was secured to the proximal and distal stumps of the transected nerve with 2-3 surgeon's knots per stump, using 10.0 non-absorbable nylon sutures. The injury site was closed with separate fascia and skin sutures. 0.1 ml Rimadyl analgesic was administered sub-cutaneously to the injury site and Opsite skin spray was sprayed over the sutured skin wound to reduce the risk of infection and the animal disrupting the wound. Animals that were immunosuppressed received an injection (sub-cutaneous) of Cyclosporine A (15 mg/kg) 24 hours prior to the surgery and then daily throughout the recovery period.

During recovery, animals were kept separately in a heated chamber and monitored closely until they had regained consciousness before being returned to their previous social group. Animals had free access to food and water after recovery from anaesthesia. All rats were kept in cages within ventilated Scantainers with room temperature maintained at  $21 \pm 0.5^\circ\text{C}$  and a lighting condition of 12 hour light/dark cycle. For each experiment, the weight of the animals was monitored. Animals were culled following the recovery period using CO<sub>2</sub> asphyxiation.

### **2.7.3 Device harvest**

Repaired nerves were excised under a dissecting microscope and harvested devices with proximal and distal stumps were maintained at *in situ* tension using a card frame, which keeps the nerve at the same length during fixation.

### **2.7.4 Gastrocnemius muscle dissection**

The gastrocnemius muscle is the major calf muscle on the posterior surface of the lower hind leg. Both the experimental and contralateral gastrocnemius muscles were exposed and then separated from the surrounding tissues before being cut out at the Achilles tendon and knee to be weighed.

## **2.8 Sectioning**

### **2.8.1 Vibratome sections**

The vibratome was used to section devices which had a silicone outer tube. Following fixation by immersion in 4 % PFA overnight at 4 °C, the fixative was aspirated and the tissue was washed (3 changes of PBS for five minutes for each wash). The tissue was then embedded in warmed (37 °C) 20 % gelatin in PBS and left to set for 20-30 minutes at 4 °C before adding 4 % PFA at 4 °C overnight. The fixed gelatin block was secured to the specimen holder with super glue and 100 µm thick sections were cut using the Leica vibratome VT1000. Sections were collected in water using a fine brush and stored in PBS prior to immunostaining.

### **2.8.2 Cryo-sections**

Frozen sections were cut from the devices which were implanted within the NeuraWrap™ outer tube. Following fixation by immersion in 4 % PFA overnight at 4 °C, the fixative was aspirated and the tissue was washed in PBS. Tissue was placed in a

rectangular plastic mould and overlaid with OCT at room temperature. It was oriented and frozen quickly in liquid nitrogen. The frozen block containing the tissue was removed from the mould and secured to the specimen holder with OCT in the required orientation in the -25 °C cutting chamber of a Leica CM1900 Cryostat. 10 µm sections were cut and collected on poly-L-lysine (PLL) coated slides and immunostained immediately.

## **2.9 Staining**

### **2.9.1 Immunofluorescence labelling protocol**

The following method was used to stain fully hydrated gels, EngNT (with and without neurons) and tissue sections from harvested devices and autograft repairs.

Following fixation of gels by incubation in 4 % PFA overnight at 4 °C, the fixative was aspirated and material was washed. Washes for the gels: 3 changes of 2-3 ml PBS for five minutes for each wash; washes for tissue sections on slides: immersed in 300 ml PBS). Samples were then incubated in 0.1 % Triton-X solution for 30 minutes. After another wash in PBS, the material was immersed in a blocking solution containing 5 % goat serum in PBS for 40 minutes. Following another wash, material was incubated with primary antibody(s) at the appropriate dilution(s) in PBS (see table 2.3) for 18 h at 4 °C. After 18 h, the material was washed and then incubated with secondary antibody(s) at the appropriate dilution(s) (see table 2.3) and Hoechst 33258 (1:1000) in PBS for 90 minutes. Finally the material was washed and stored in PBS ready for microscopy.

For staining cells on coverslips the following adaptations were made to the above immunofluorescence protocol: primary and secondary antibody incubation was for 90

and 45 minutes, respectively, at room temperature. Coverslips were mounted on slides using FluorSave™.

### **2.9.2 Flow cytometry**

Following fixation of cells in suspension with 4 % PFA for 10 minutes at 4 °C, cells were washed and then stained in suspension. Washes were carried out by the addition of 5 ml PBS and centrifugation at 400 x g for 5 minutes. After the first wash, the cell pellet was resuspended in 1 ml of 0.1 % Triton-X solution for 1 minute and then washed. Cells were then resuspended in 500 µl of blocking solution containing 5 % serum in PBS and incubated for 30 minutes at 4 °C. Cells were washed and counted, and then resuspended into tubes each containing  $2 \times 10^5$  cells. Following this, 10 µl of primary antibody (anti-CD54, 1:10 dilution) was added to each tube and incubated for 1 hour at 4 °C. Next 1 ml PBS was added and cells were washed by centrifugation, before incubation of 100 µl of the secondary antibody (dilution 1:40) for 40 minutes at 4 °C. Cells were washed with 500 µl PBS and then resuspended in 300 µl PBS before being read using the FACSCalibur. Data was analysed using CellQuestPro software.

### **2.9.3 CellTracker™ staining**

Living cellular EngNT was incubated with green CellTracker™ (50 µg in 10 µl DMSO) at 1:1000 in cell culture media for 45 minutes at 37 °C in a humidified incubator. Gels were then washed with media before fixing or using in *in vitro* experiments.

## **2.10 Electron microscopy**

### **2.10.1 Scanning electron microscopy**

EngNT sheets were fixed in 4 % paraformaldehyde in PBS for 24 hours at 4 °C. They were then prepared for SEM by Francis Colyer. They were post-fixed in 1 % osmium tetroxide in phosphate buffer (PB), dehydrated through a graded series of acetone and infiltrated in liquid carbon dioxide in a critical point drying apparatus (Polaron, UK) before drying at the critical point of 31 °C. The dried samples were mounted on aluminium SEM stubs with double-sided carbon sticky tabs (Agar Scientific, UK), sputter coated with gold (Polaron sputter coater SC7640, UK) and examined by Gordon Imlach in a Zeiss Supra 55 VP field emission guns scanning electron microscope (FEGSEM) at 3 kV.

### **2.10.2 Transmission electron microscopy**

After excision and dissection of the middle of the repair constructs, samples were fixed in 4 % PFA in PBS for 24 h at 4 °C. These were then prepared and imaged by Heather Davies. Samples were post-fixed in 1 % osmium tetroxide in PB, dehydrated through a graded series of acetone, flat-embedded in Epon epoxy resin and polymerised at 60 °C for 48 h. Semi-thin sections of 1 µm were cut using a glass knife on a UCT ultramicrotome (Leica, UK), dried onto poly-L-lysine coated microscope slides and stained with 1% toluidine blue with added 5% sodium borate. Ultrathin sections of 70 nm were cut with a diamond knife (Diatome, UK) and collected on copper slot grids with Pioloform/carbon support films. Sections were counter-stained with aqueous uranyl acetate and Reynolds' lead citrate before examination in a JEM 1400 transmission electron microscopy at 80kV (TEM) (JEOL, UK).



## **2.11 Analyses**

### **2.11.1 Cell death quantification**

Cell death analysis was by propidium iodide (PI) exclusion and Hoechst 33258 was used as a counterstain to establish total cell numbers. PI is commonly used as a marker of cell death because it only enters cells with damaged plasma membranes (i.e. those undergoing late apoptotic and necrotic cell death) where it binds to DNA. Cell death thus results in cells with condensed, bright red PI-stained nuclei. Cellular gels were incubated with PI (20 mg/ml, used at 1:100) and Hoechst 33258 (1 mg/ml, used at 1:1000) in cell culture medium for 30 minutes at 37 °C, 5 % CO<sub>2</sub> and then washed with three changes of cell culture medium for 10 minutes for each wash.

### **2.11.2 Assessment of cellular alignment**

Confocal microscopy (Leica SP5) was used in the assessment of cell alignment in EngNT. Equivalent fields were analysed per gel using a standardised sampling protocol (figure 2.4A). Images were captured using a x40 oil immersion lens; z-stacks were 20 µm with a step size of 1 µm. Image analysis was conducted using Volocity™ software (Perkin Elmer, Waltham, MA) running automated 3D image analysis protocols to measure the angle of cell alignment in each field relative to the long axis of the gel (figure 2.4B).

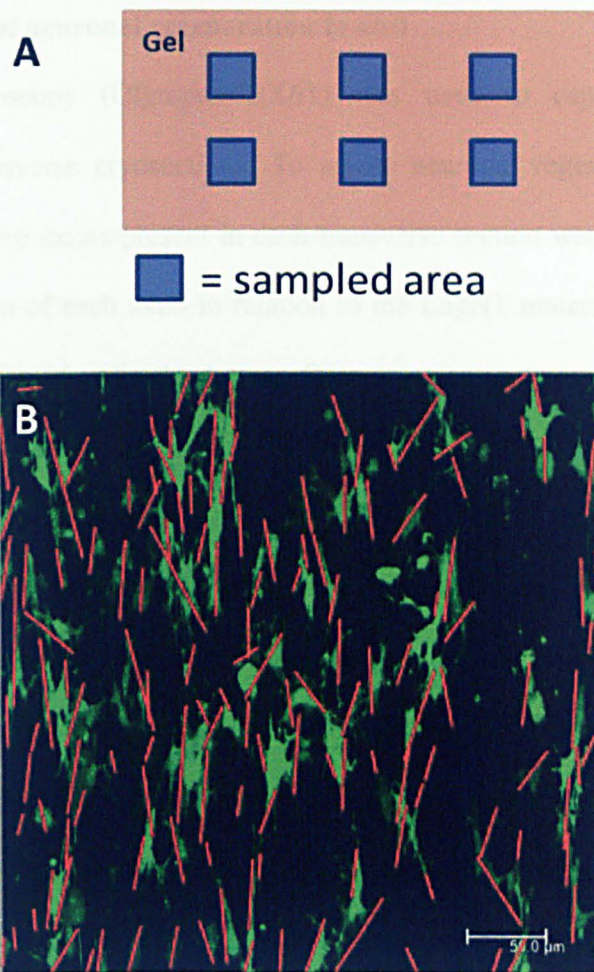


**Figure 2.4 Automated 3D analysis of cell alignment in EngNT using Volocity™**

Sample fields of hydrated and compressed gels looking down at the surface on which DRG neurons were seeded (A); and the automated analysis using Volocity™ recognises the cells, in EngNT-Schwann cell in this example, based on colour and intensity. Volocity™ assigns a line for the longest length and reports the angle of deviation from the long axis of the gel (B).

### 2.11.3 Assessment of neurite growth *in vitro*

Confocal microscopy (Leica SP5) was used in the assessment of neurite outgrowth on EngNT. The same image acquisition protocol was used as described in section 2.11.2. Image analysis was conducted using Volocity™ software (Perkin Elmer, Waltham, MA) running automated 3D image analysis protocols to measure the length and orientation of each neurite for each field. Volocity™ recognises the neurites based on colour channel and intensity and traces over them using the ‘skeletal length’ tool, which gives length (μm) and bearing (degrees) read outs relative to the long axis of the gel, to enable the amount and direction of neurite growth to be quantified.

#### 2.11.4 Assessment of neuronal regeneration *in vivo*

Fluorescence microscopy (Olympus BX61) was used to capture images from immunostained transverse cryosections. To assess neuronal regeneration, all of the neurofilament positive axons present in each transverse section were counted. In some cases the localisation of each axon in relation to the EngNT material was assessed, in which case EngNT was visualised using autofluorescence.

#### 2.11.5 Analysis of myelin *in vivo*

At least 50 myelin profiles were sampled from each of 5 electron micrographs at the mid-point of the constructs that were taken from the densest regions of regeneration, identified using corresponding semi-thin sections. For each myelinated axon, the axon diameter and fibre diameter (axon + myelin sheath) were measured at the widest part of the fibre. For the unmyelinated axons, only the axon diameter was measured. Measurements were made using Image J software, Figure 2.5 summarises this process.

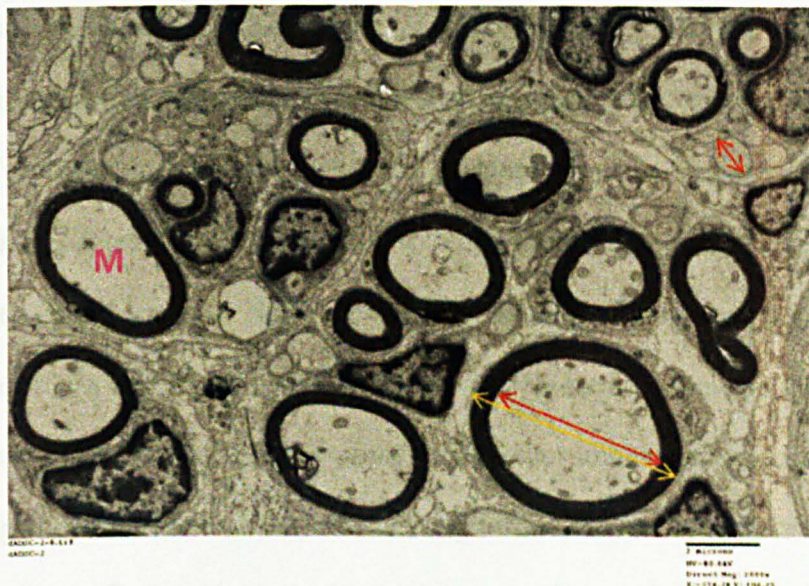


**Figure 2.5** Example measurements to assess myelination from an electron micrograph using Image J. M = myelinated axon. Axon diameter measurements are shown using the red arrows and fibre diameter measurement is shown using the orange arrow.

### **3.0 Development and optimisation of Engineered Neural Tissue (EngNT)**

#### **3.1 Introduction**

An important area of research in neural tissue engineering is concerned with how to promote and guide neurite extension across a gap in a damaged nerve (Bellamkonda, 2006, Daly *et al.*, 2012; Bell and Haycock, 2012). Directing regeneration is important for an efficient repair and to increase the likelihood of a functional outcome, as guided axons will reach their targets faster than those crossing a gap without guidance, reducing the time in which a target organ is denervated (Hall, 2005). It is widely agreed that the presence of living cells is essential for supplying the signals required for optimal neurite extension and for the repair of gaps larger than 3 cm in human nerve/s (Duemans *et al.*, 2010).

Schwann cells tend to be the starting cell type for tissue engineers developing a repair device because they are the appropriate resident PNS glial cell type and play an important role in the regeneration process (Rodrigues *et al.*, 2012). Previous studies have investigated how alignment of Schwann cells can affect neuron regeneration, providing topographical and biochemical guidance cues to regenerating neurites (Thompson and Buettner, 2005; Weinstein, 1999; Rodrigues *et al.*, 2012). Schwann cells secrete factors such as NGF and deposit laminin, which have been shown to enhance the effects of Schwann cell topography and orientation. Some approaches focus on the development of anisotropic materials that confer alignment to seeded Schwann cells (e.g. guidance cues on the material through the influence of surface architecture such as, channels, fibres and grooves), which in turn direct neurite outgrowth (Lietz *et al.*, 2006). The migratory movement of cells and their interactions with the physiochemical properties of their substrata was first described by Weiss as contact-

guidance, from his experiments on cell and axon orientation (Weiss, 1934; Weiss, 1945).

In previous investigations in this area, Schwann cells were cultured on the surfaces of three-dimensional scaffolds, owing in large part to the relative ease of fabrication of surfaces using many different materials. Ultimately it is the presence of the aligned Schwann cells that is important, and efforts to align the material are generally aimed at causing alignment of Schwann cells rather than a direct effect on neurites. Some studies have used endogenous tension from cell contraction to align cells (Eastwood *et al.*, 1998, Phillips *et al.*, 2005, East *et al.*, 2010). This approach of enabling the Schwann cells to self-align due to tension is employed in this project.

It is widely agreed that Schwann cell-neurite interactions are very important during regeneration, and Schwann cells and neurons are usually found to be in close contact *in vivo* and in experimental models (Terenghi *et al.*, 1999). Additionally, there is a lot of evidence to suggest that a cellular element is needed for regeneration across gaps larger than 3 or 4 cm in human (Bellamkonda, 2006; Gu *et al.*, 2011; Rodrigues *et al.*, 2012). Therefore, it is rational to include a cellular element and focus on aligning this directly, instead of developing an aligned material and waiting for the seeded cells to migrate and elongate on and along it.

A wide variety of materials have been evaluated for nerve repair. These can be divided into two categories: native materials and synthetic materials. Native tissues such as autologous vein (Risitano *et al.*, 2002) and autologous muscle (Battiston *et al.*, 2000) have been used as nerve guidance conduits. Although they are able to successfully support neuronal regeneration, the disadvantage remains that there is a limited source of

these tissues and the lack of Schwann cells is also a disadvantage for longer gaps. As a result, materials made from extracellular matrix (ECM) proteins have been explored, such as collagen (Yoshii *et al.*, 2001; Dubey *et al.*, 1999; Ceballos *et al.*, 1999), laminin (Kuappila *et al.*, 1993; Toba *et al.*, 2002), fibrin (Kalbermatten *et al.*, 2009) and fibronectin (Whitworth *et al.*, 1995; Ahmed *et al.*, 1999). The FDA-approved bovine collagen I tube, NeuraGen™, is currently used in the clinic for repairs up to 3 cm in length.

Another alternative for nerve repair is to use synthetic conduits, which are chemically pure, easier to make into elaborate structures, better suited to GMP production, cheaper, less likely to transmit disease, easier to source and less immunogenic than biological materials. The degradation time of bio-degradable synthetic materials such as poly(glycolic acid) (PGA) and poly(lactic acid) (PLA) can, for example, be manipulated (Evans *et al.*, 2000; Evans *et al.*, 2002). There are currently FDA-approved synthetic conduits available, such as Neurotube (PGA) and Neurolac [poly(DL-lactide-caprolactone)] (PLC), for short gap repairs up to 3 cm.

It is important to consider scaffold degradation when developing materials for implantation. The initial scaffold for any implanted 3D tissue that is not intended to be a permanent prosthesis must eventually be resorbed. Importantly, the timescale for the degradation of the implanted scaffold needs to relate to the formation of new, replacement tissue from the resident cells. The implanted scaffold must be resorbed to avoid compression of the regenerated nerve, which could become restricted as it gets thicker. However the implanted scaffold must not degrade before the new nerve tissue has formed or it could compromise mechanical integrity. Native protein-based materials, where fibrillogenesis and potential for telopeptide cross-linking sites are not

impaired (Marenzana *et al.*, 2006) represent a natural part of the cell-matrix environment, participating in biological turnover and remodelling. They tend to be removed by cell action as new matrix is produced, with no harmful breakdown products. Based on this and because of previous expertise, this project used natural protein materials, rather than synthetic polymers.

The matrices explored here for the development of an Engineered Neural Tissue (EngNT) are collagen I and fibrin:

- i) Collagen I is the most abundant ECM protein in mammalian tissue and it is the predominant structural protein present in peripheral nerve tissue (Ricard-Blum, 2010; Soderhall *et al.*, 2007). Collagen fibrils and their networks play a dominant role in maintaining the structural integrity of ECM, while being highly dynamic and undergoing constant remodelling (Cen *et al.*, 2008). Collagen is one of the most widely used materials for three-dimensional cell culture and tissue-engineering applications, partly because of the ability of purified collagen I monomers to self-assemble into three-dimensional gels at physiological temperature and pH.
- ii) Fibrin was also selected for consideration based on its role in the natural repair process that occurs in wound healing. After peripheral nerve injury where defects are repaired using an empty conduit, on day 1 the conduit will be filled with blood proteins (Belkas *et al.*, 2004). In days 2-6 an hourglass shaped fibrin cable forms between the two nerve stumps (for short defects) and in days 7-14 support cells migrate on to the protein cable and other ECM proteins are deposited. Axon elongation (regeneration) begins from day 15 (Belkas *et al.*, 2004). Using fibrin to make EngNT to form the core of a repair device may

therefore speed up the repair process by removing the delay due to formation of the fibrin tissue bridge.

Several methodologies exist for using collagen and fibrin to guide axonal regrowth (Ahmed *et al.*, 2000; Dubey *et al.*, 2001; Phillips *et al.*, 2005); the method used in this study is a tethering system. The tethering approach results in an aligned cellular hydrogel that provides multiple stimuli in an effort to mimic the milieu of signals normally found in a nerve autograft, i.e. biological, physical and chemical. It facilitates cell growth, organisation and differentiation, permitting the cells to self-align and remodel the matrix generating a three-dimensional environment for repair and regeneration.

The Open University owns the granted patent for self-alignment of cells in tethered 3D hydrogels in Europe, US, Canada and Australia (Brown and Phillips, 2004). It is a simple and effective way of aligning cells in a 3D environment and has been used to generate tissues with aligned architecture, such as cardiac muscle (Boudou *et al.*, 2012) and nervous system tissue (Phillips *et al.*, 2005; East *et al.*, 2010). Our lab has shown that aligned Schwann cells within a tethered collagen gel can promote and guide neuron regeneration *in vitro* and *in vivo* (Phillips *et al.*, 2005). In that study the cellular collagen gel was tethered within the conduit before implantation, generating aligned Schwann cells in a 3D collagen environment. This device guided neuronal regeneration across a 5 mm gap in the rat sciatic nerve model more effectively than an empty tube control. However there is limited scope for scale up and translation of that design, which relies on a hydrated hydrogel remaining tethered within a conduit, due to the skill required for integration and potential for tethering to fail during handling, implantation or post-implantation. The initial aim of this project therefore was to retain the aligned cellular



architecture achieved in these 3D tethered gels but to develop the material to a more stable and robust form.

Plastic compression, a method developed by Brown *et al.*, increases the mechanical strength and stability of hydrogels by irreversibly removing most the interstitial fluid from the gel, generating a more dense and robust material (Brown *et al.*, 2005). Plastic compression has been used to stabilise collagen hydrogels containing various cell types including rat astrocytes (East *et al.*, 2010), human limbal epithelial cells (Levis *et al.*, 2010), human bladder smooth muscle cells (Micol *et al.*, 2011) and human osteosarcoma cells (Bitar *et al.*, 2008) with no reported adverse effects on cell viability. Plastic compression technology is commercially available (RAFT™ by TAP Biosystems) for the fabrication of tissue-like constructs. The Open University and TAP Biosystems are currently working in collaboration to develop an advanced RAFT™ process for the production of aligned tissue-like constructs, combining the plastic compression and tethering technology.

In preliminary studies aiming to understand the effect of aligning astrocytes on neuronal growth, tethered collagen I gels with aligned astrocytes were successfully compressed to generate robust constructs in which astrocyte alignment was maintained (East *et al.*, 2010). We hypothesized that this method could be developed further in order to stabilise tethered hydrogels with PNS glia, retaining the cellular alignment following their removal from the tethering system. This could enhance the mechanical properties so the material can withstand surgical handling and movement *in vivo* after implantation.

This study first tested the hypothesis that combining cellular self-alignment and the plastic compression process will produce a robust cellular biomaterial with the potential

to support and guide neuronal growth. This was tested by a series of experiments with the following aims:

- (i) to investigate Schwann cell survival after plastic compression of collagen gels;
- (ii) to assess whether the cellular alignment achieved in tethered rectangular collagen gels was retained following plastic compression and whether plastic compression was sufficient to stabilise the alignment;
- (iii) to assess whether neurons cultured on the surface of this engineered neural tissue (EngNT) with aligned Schwann cells (EngNT-Schwann cell) can extend neurites in a directed manner.

Fibrin was also explored as an alternative hydrogel to collagen, repeating the key experiments for the development of the collagen EngNT.

Despite the evidence that cellular therapies enhance regeneration, the application of such therapies in the clinic currently faces a number of biological and regulatory hurdles, mainly regarding the source and availability of cells (Bell and Haycock, 2012). Approved decellularised nerve guides are currently available, such as Avance™ from AxoGen for nerve defects up to 7 cm. In these, native nerve has been stripped down to its extracellular matrix, removing immunogenic cell components and retaining the intricate ECM architecture. Such decellularised nerves have been shown to provide a 3D scaffold to support regeneration in experimental and clinical studies (reviewed by Szykaruk *et al.*, 2012). In consideration of these findings, the potential of aligned Schwann cells to precondition the collagen biomaterial, before they are freeze-killed, leaving a decellularised guidance matrix was assessed in the present study; in terms of the ability of the decellularised material to support and direct neuronal growth.

## 3.2 Results

### 3.2.1 Schwann cell characterisation

The rat Schwann cell line SCL 4.1/F7 (Haynes *et al.*, 1994) was used for the initial experiments to develop and optimize the protocols and designs of the material. The Schwann cells were plated on coverslips and stained to confirm they were S100 positive, a marker for Schwann cells (Spreca *et al.*, 1989) (figure 3.1).

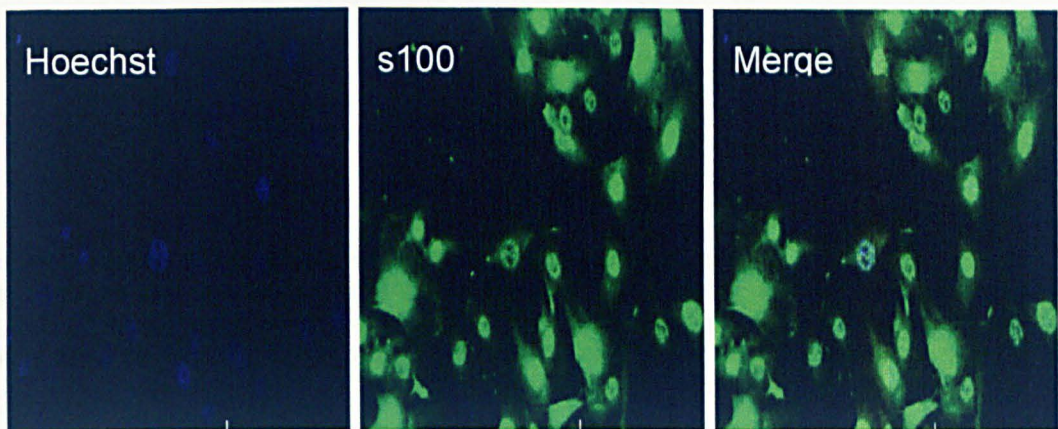


**Figure 3.1 Schwann cells on coverslips stained to detect S100**

Schwann cells were plated on coverslips and fixed after 24 hrs before staining to detect S100.

The first step was to establish the optimum Schwann cell seeding density to give consistent and reliable contraction of collagen gels within 12 hours. This is important because sufficient gel contraction is needed in the tethered gels to ensure cellular self-alignment. Contraction profiles were generated using a range of Schwann cell seeding densities within a 2 mg/ml collagen gel (figure 3.2). Subsequent experiments were conducted using a cell density of  $4 \times 10^6$  cells/ml, which gave over 70% contraction (figure 3.2).

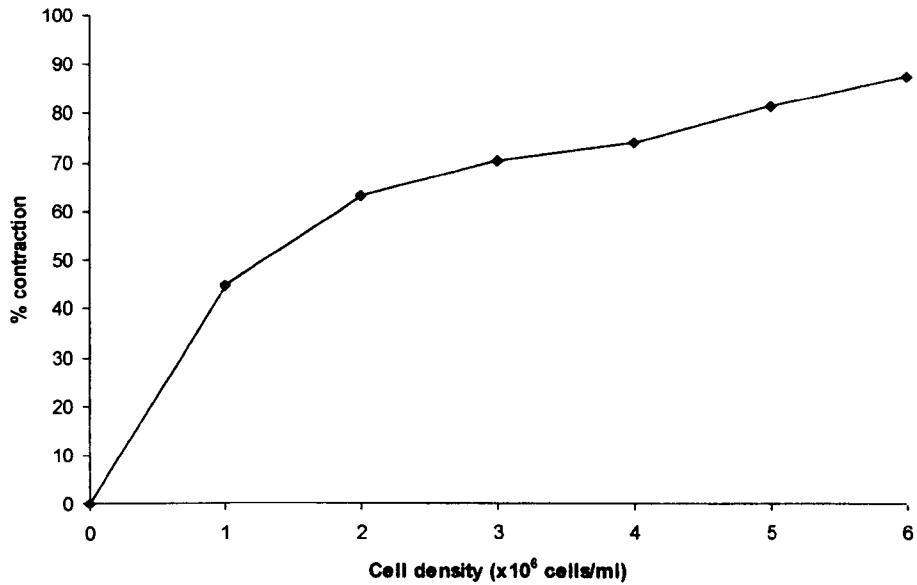


**Figure 3.2 Contraction profile for Schwann cells in collagen gels**

Cells were seeded at a range of seeding densities ( $1-6 \times 10^6$  cells/ml) within 300  $\mu$ l collagen gels (2 mg/ml) in a 96-well plate. Following a 12 h incubation, gels were photographed and % contraction determined [(% contraction = (cross-sectional (cs) area of gel at 0 h – cs area of gel at 12 h) / (cs area of gel at 0 h)]. Data are means  $\pm$  SEM from 4 separate gels.

**3.2.2 The effect of plastic compression on Schwann cell death**

To assess the effect of plastic compression on Schwann cell death, collagen gels containing Schwann cells in wells of a 96-well plate were subjected to plastic compression for 1 or 5 minutes. Cell death was assessed using propidium iodide and Hoechst 1 hour after compression or after a further 20 hours in culture and compared with uncompressed control gels. Three fields of view were sampled per gel. Two time points were used to determine the relative contribution of immediate or delayed mechanisms to any cell death. There was no significant difference in the amount of cell death observed following 1 or 5 minute plastic compression at both 1 hour ( $183 \pm 25$  cells were counted per gel) and 20 hours ( $132 \pm 14$  cells were counted per gel) compared to controls (Figure 3.3, one-way ANOVA,  $P > 0.05$ ). There was a significant

difference in the amount of cell death observed in the control gels that were stained either 1 or 20 hours after compression (T-test,  $P < 0.005$ ).

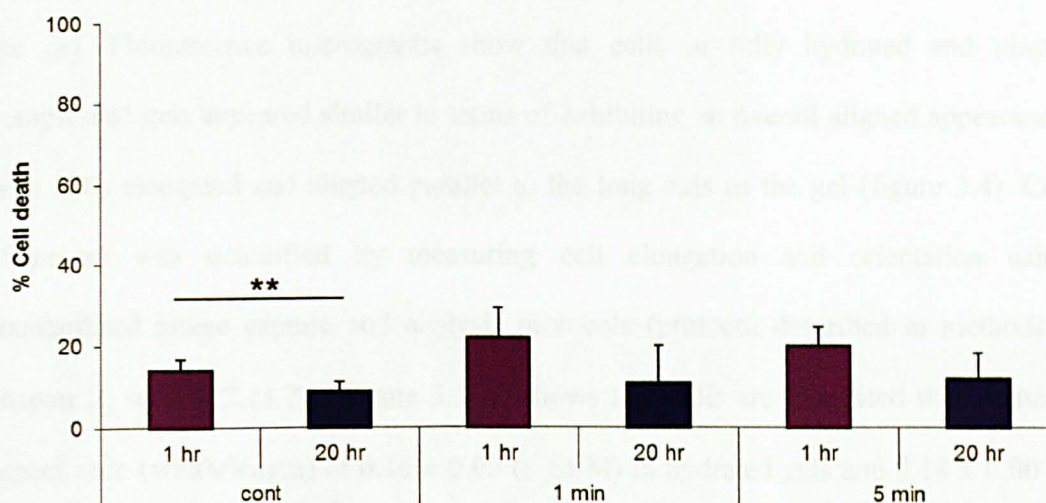


**Figure 3.3 The effect of plastic compression on Schwann cell viability**

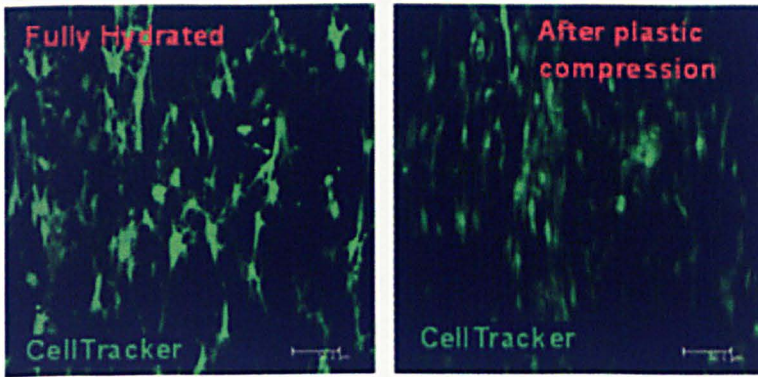
There was no significant difference in the amount of cell death observed between 1 minute compression or 5 minutes compression assayed at 1 and 20 hours post-compression, or in uncompressed control gels,  $P > 0.05$ . However, the amount of cell death differed significantly in the uncompressed control gels that were stained 1 and 20 hours after the gels had set,  $**P < 0.005$ .  $n = 6$  independent gels.

### 3.2.3 The effect of plastic compression on Schwann cell alignment

After confirming that plastic compression did not cause cell death, the next part of this investigation was to assess cellular alignment post-plastic compression. It is speculated that if the matrix stiffness is increased so that cytoskeletal contraction force is no longer sufficient to deform it in a way that results in cells losing their alignment or overall changes in gel size/shape, it could limit further remodeling of the collagen matrix by the cells. Therefore it was hypothesized that, by increasing the cell and collagen density, plastic compression could stabilize the cellular alignment observed in fully hydrated tethered collagen gels, producing a robust and mechanically stronger aligned biomaterial.

To assess cellular alignment, cells within tethered gels were labelled with CellTracker™ dye and analysed either before or after plastic compression. Schwann cell alignment was determined by comparing the angle of the long axis of each cell to the long axis of the gel. Fluorescence micrographs show that cells in fully hydrated and plastic compressed gels appeared similar in terms of exhibiting an overall aligned appearance, with cells elongated and aligned parallel to the long axis of the gel (figure 3.4). Cell alignment was quantified by measuring cell elongation and orientation using standardised image capture and analysis protocols (protocol described in methods – chapter 2, section 2.11.2). Figure 3.5 (i) shows that cells are elongated with a mean aspect ratio (width/length) of  $0.16 \pm 0.00$  ( $\pm$  SEM) in hydrated gels and  $0.18 \pm 0.00$  ( $\pm$  SEM) in plastic compressed gels (i.e. about 6 times longer than their width). This difference is not significant, demonstrating that the alignment is stabilised post-plastic compression. Figure 3.5 (ii) shows a frequency distribution of the angle of deviation of cell orientation from the long axis of the gel. There is a clear trend showing that most of the cells were orientated parallel to the long axis of the gel. The quantification revealed that  $63 \pm 15\%$  ( $\pm$  SEM) of the cells within the fully hydrated gel and  $51 \pm 12\%$  of cells within the plastic compressed gel, did not deviate by more than  $20^\circ$  from the long axis of the gel. Additionally, only  $11 \pm 7\%$  and  $16 \pm 5\%$  ( $\pm$  SEM) of the cells within, respectively, the fully hydrated and plastic compressed gels deviated by more than  $50^\circ$  from the long axis of the gel.

(i)



(ii)

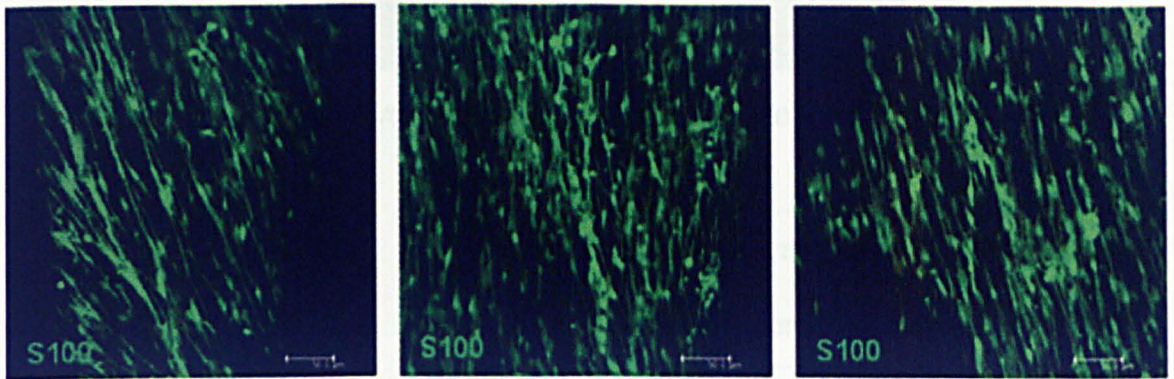


**Figure 3.4 Self-aligned Schwann cells in fully hydrated and plastic compressed gels**

(i) Representative confocal micrographs showing Schwann cells (green) labelled with CellTracker™ dye in a fully hydrated gel and in a compressed gel; (ii) and within EngNT using immunofluorescence, z-distance 20  $\mu\text{m}$ , step size 1  $\mu\text{m}$ . Scale bars are 50 $\mu\text{m}$ .

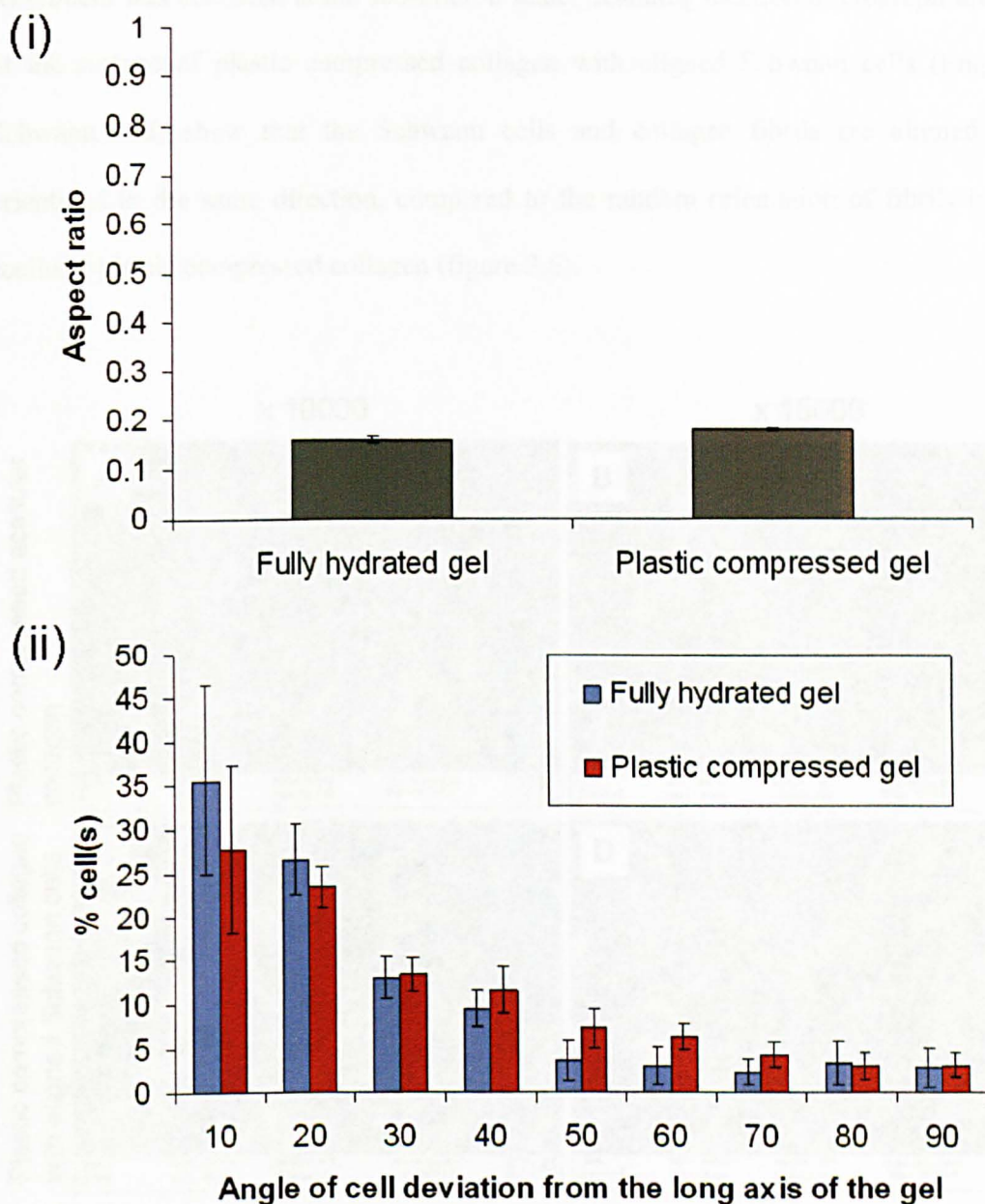


**Figure 3.5 Schwann cell elongation and orientation pre- or post-plastic compression**

(i) The aspect ratio (width/length) of cells was not significantly different in gels pre- or post-plastic compression. (ii) Frequency distribution of the angle of deviation of cell orientation from the long axis of the gel in 10 degree bins. Data are means  $\pm$  SEM from 3 gels, 6 regions per gel were analysed.



Alignment was also seen at the sub-micron scale. Scanning electron micrograph images of the surface of plastic compressed collagen with aligned Schwann cells (EngNT-Schwann cell) show that the Schwann cells and collagen fibrils are aligned and orientated in the same direction, compared to the random orientation of fibrils in the acellular plastic compressed collagen (figure 3.6).

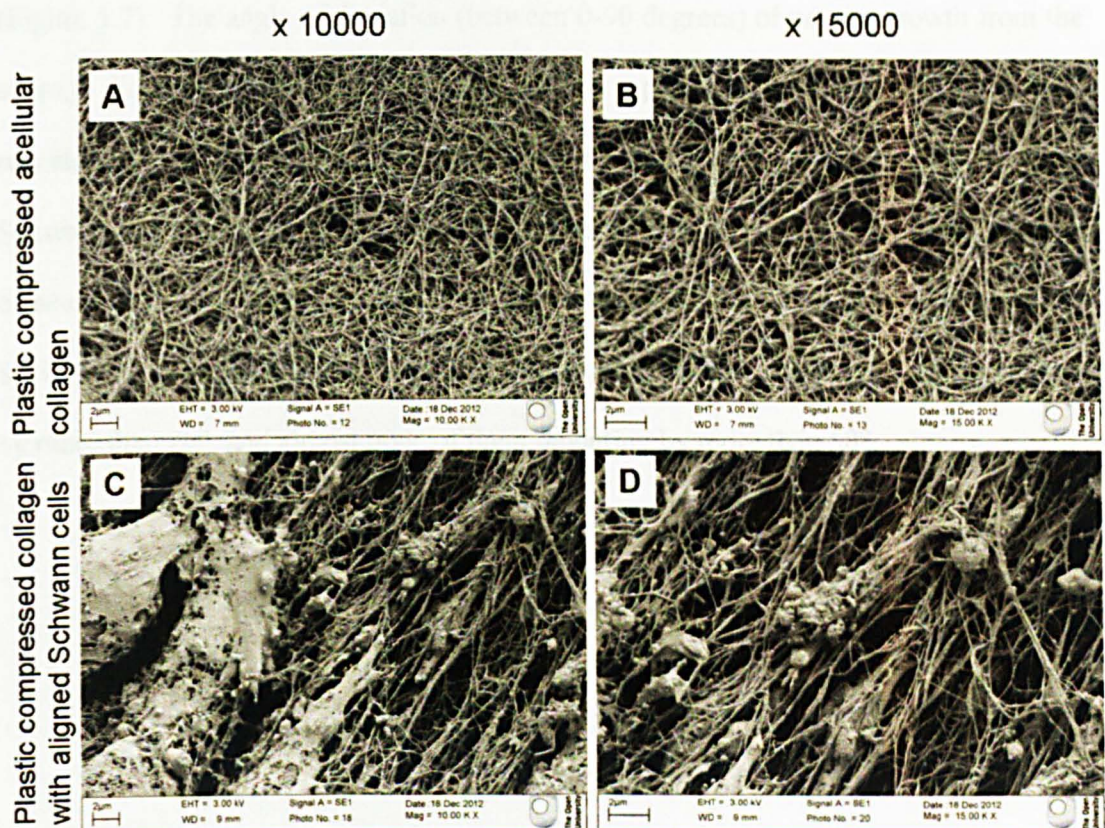


**Figure 3.6 Scanning electron micrographs of plastic compressed collagen with aligned cells and without cells**

Scanning electron micrographs of the surface of plastic compressed acellular collagen (A-B) and plastic compressed collagen with aligned Schwann cells (EngNT-Schwann cell) (C-D) at low (left) and high (right) magnifications. Scale bars are 2 µm.

These initial studies indicated that sheets of robust aligned cellular biomaterial could be formed using Schwann cells to self-align within a tethered collagen gel that was then stabilized using plastic compression.

### **3.2.4 Neuronal growth on the surface of collagen EngNT-Schwann cell**

The next stage was to investigate neuronal growth on the surface of EngNT-Schwann cell and to assess whether the cellular alignment could confer alignment to growing neurites. Primary adult rat neurons were cultured on the surface of EngNT-Schwann cell for 3 days before fixing overnight and then immunostaining to detect S100 (a marker for Schwann cells),  $\beta$ III-tubulin (a marker for neurons) and Hoechst to label cell nuclei (Figure 3.7). The angle of deviation (between 0-90 degrees) of neurite growth from the average direction of Schwann cell alignment on a per field basis was measured. This revealed that the angle of neurite growth observed after 3 days corresponded to the local Schwann cell alignment within EngNT-Schwann cell. Figure 3.8 shows the distribution of neurite deviation from the angle of local Schwann cell alignment, with approximately 80% of neurites not deviating from the orientation of the local Schwann cell population by more than 20°, and almost none of them deviating by more than 50°.

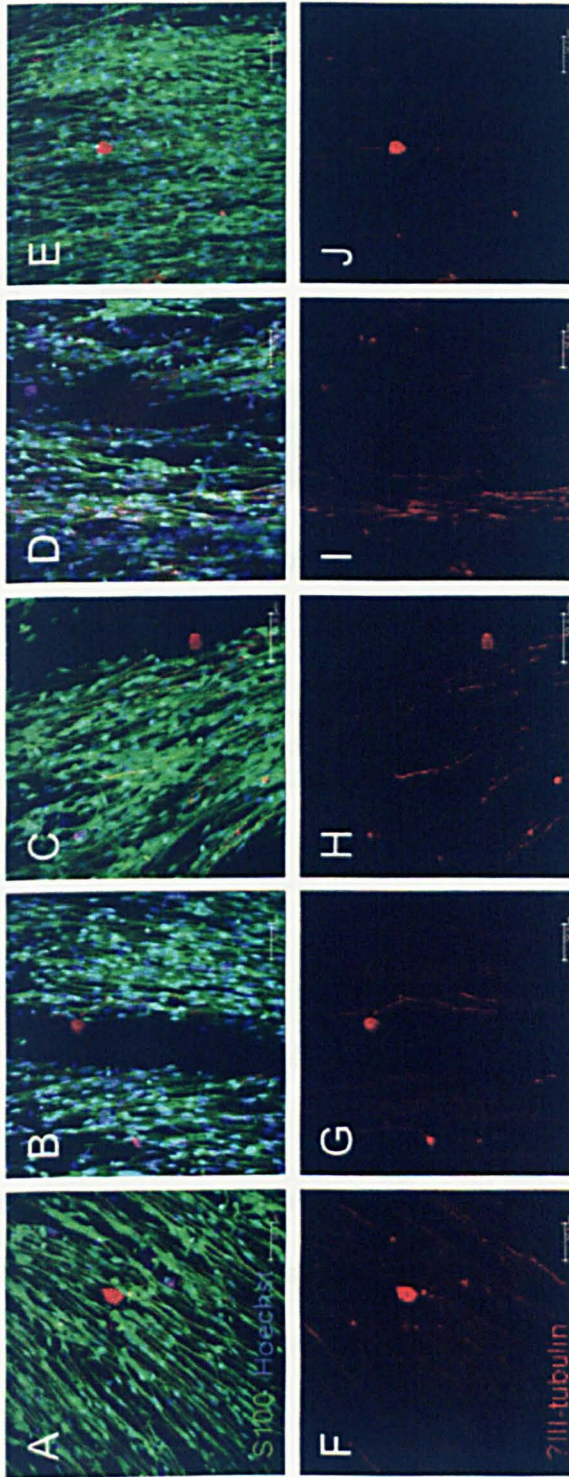


**Figure 3.7 Neuronal growth on EngNT-Schwann cell**

Five merged confocal micrographs showing the Schwann cells (green) within the collagen EngNT-Schwann cell and the neurites (red), stained for S100 and  $\beta$ III-tubulin respectively. Nuclei (blue) were labelled with Hoechst (A-E). An image containing the red channel only is also shown for each field (F-J). Scale bars are 50 $\mu$ m.

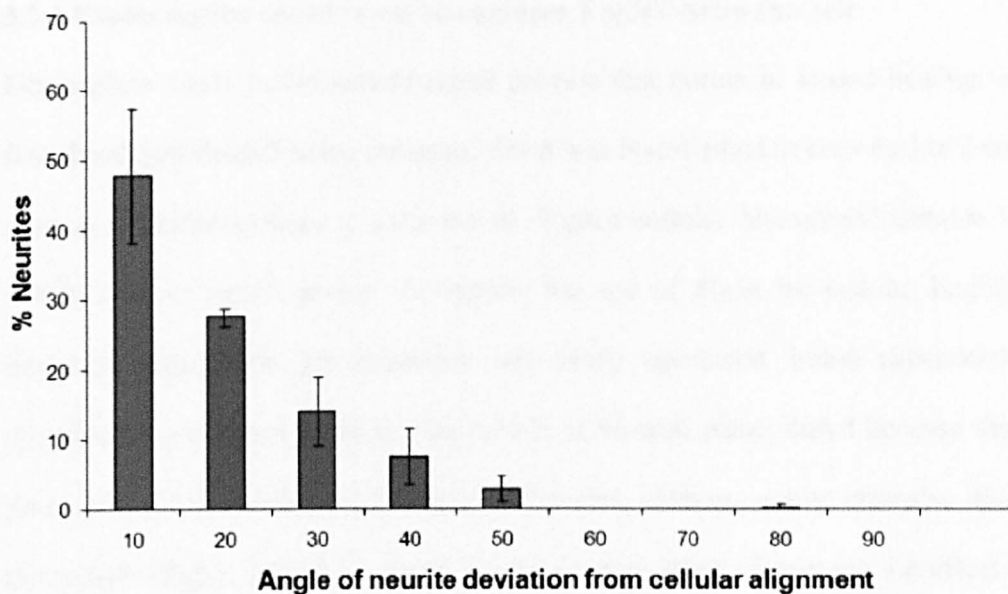


**Figure 3.8 Orientation of neuronal growth on EngNT-Schwann cell**

Frequency distribution showing the angle of neurite deviation from the Schwann cell alignment angle in that field (determined using automated analysis in Volocity, see section 2.11.3), 332 neurites were counted in total. Data are means  $\pm$  SEM from  $n=3$  independent gels, 6 regions per gel were analysed.

The images in figure 3.7 show that the Schwann cells within EngNT formed parallel chains, which were usually continuous within a field of view. The neurites appear to be growing along parallel chains of Schwann cells. The neurite length that was in contact with a Schwann cell was measured and expressed as a percentage of the total neurite length on a per field basis;  $91 \pm 4\%$  ( $n = 3$ ) of extended neurites, were found to be in close contact with a Schwann cell.

### 3.2.5 Exploring the use of fibrin to engineer EngNT-Schwann cell

Fibrin plays a role in the natural repair process that occurs in wound healing. Having first developed EngNT using collagen, fibrin was investigated to see whether it could be used in a similar manner to generate an aligned cellular biomaterial suitable for use within a nerve repair device. To explore the use of fibrin for making EngNT with Schwann cells, fibrin gel formation was firstly optimised. Initial experiments that attempted to construct a contraction profile in 96-well plates failed because the fibrin gels could not be freed from the edges of the wells without causing extensive disruption to the gels (figure 3.9). As a result, it was not possible to determine the effect of cell density on contraction of the fibrin gels (as had been done for the collagen hydrogel). Thus the same cell density was used to produce a fibrin based EngNT as was used for the production of collagen EngNT-Schwann cell, namely  $4 \times 10^6$  cells/ml.

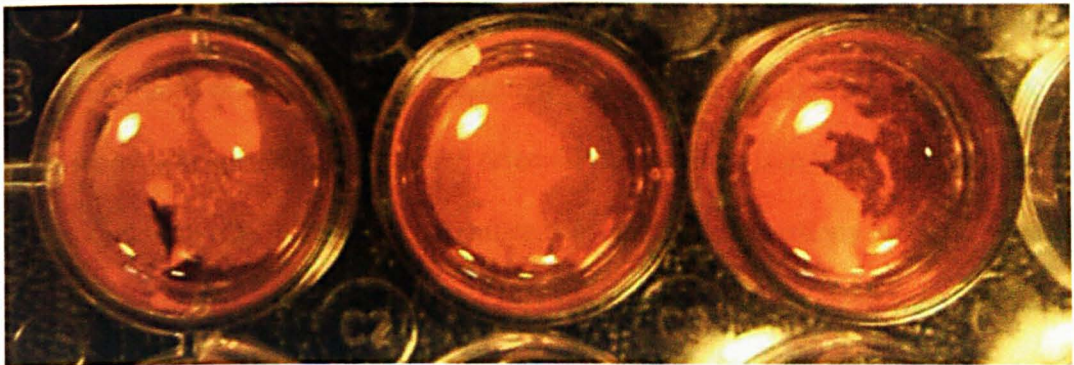


**Figure 3.9 Fibrin gel disruption in wells after attempting to free the edges**

Fibrin gels were photographed within the wells containing media after attempting to free the edges from the well using a needle, which caused much disruption.

Fibrin gel contraction in the stainless steel moulds was similar to what was observed with the tethered collagen hydrogels. The fibrin could be freed from the straight long edges of the mould using a scalpel without disrupting the gel. The first step was to assess cell death following plastic compression of fibrin gels containing Schwann cells by propidium iodide exclusion with Hoechst. This demonstrated that the plastic

compression process, when applied to cellular fibrin gels, did not increase cell death compared to uncompressed controls;  $2.0 \pm 1.5\%$  (mean  $\pm$  SEM, n=3) cell death was observed immediately after plastic compression, compared to  $2.0 \pm 0.4\%$  ( $\pm$  SEM, n=3) in the fully hydrated gels.

The next step was to investigate Schwann cell self-alignment in fully hydrated and plastic compressed fibrin gels. Schwann cells (S100, labelled green) appeared elongated and weakly aligned in uncompressed or plastic compressed fibrin gels (figure 3.10), compared to the Schwann cells in uncompressed or plastic compressed collagen (figure 3.4). Alignment relative to the long axis of the gel was quantified in the same way as in section 3.2.3, and Schwann cells in both fully hydrated and plastic compressed fibrin gels were elongated with cell aspect ratios (width/length) of, respectively,  $0.15 \pm 0.00$  and  $0.15 \pm 0.00$  (figure 3.11) (i.e. about 6 times longer than wide, comparable to the Schwann cell elongation seen in collagen gels). Gels were immunostained to detect S100 and cell orientation was quantified by image analysis following confocal microscopy. The quantification of cell orientation, in comparison to the long axis of the gel, shows that the cells were orientated in different directions with no overall alignment in hydrated or plastic compressed fibrin gels. However there were patches of alignment in areas. There was a similar distribution of cell orientation angles in hydrated and plastic compressed gels (figure 3.11).

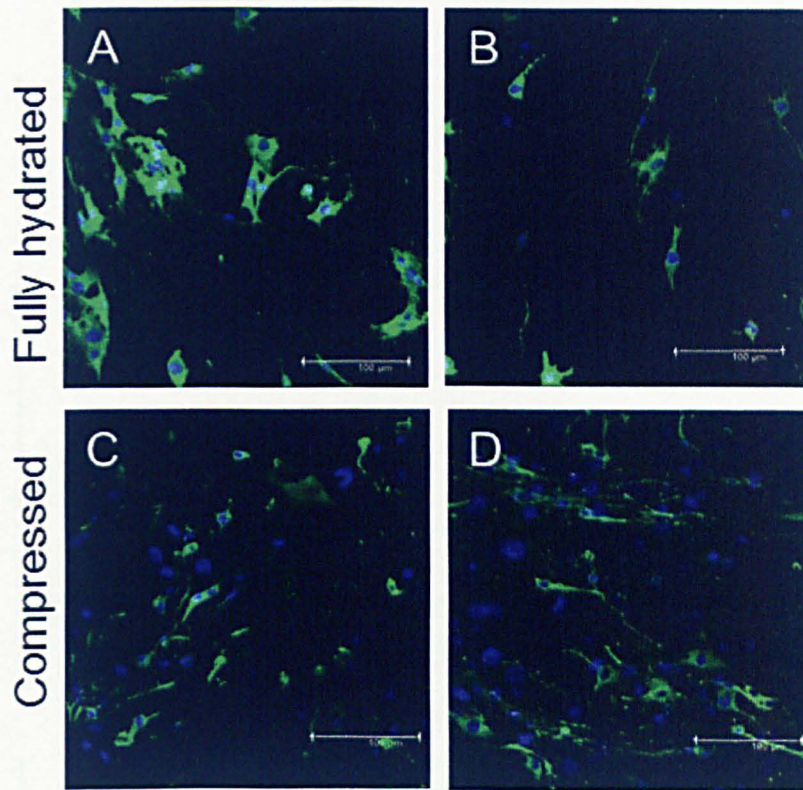


**Figure 3.10 Schwann cells in tethered hydrated or plastic compressed fibrin gels**  
 Representative confocal micrographs of the Schwann cells (green), labelled with S100, and nuclei (blue), labelled with Hoechst, in fully hydrated (A, B) or plastic compressed (C, D) fibrin gels. Scale bars are 100μm.

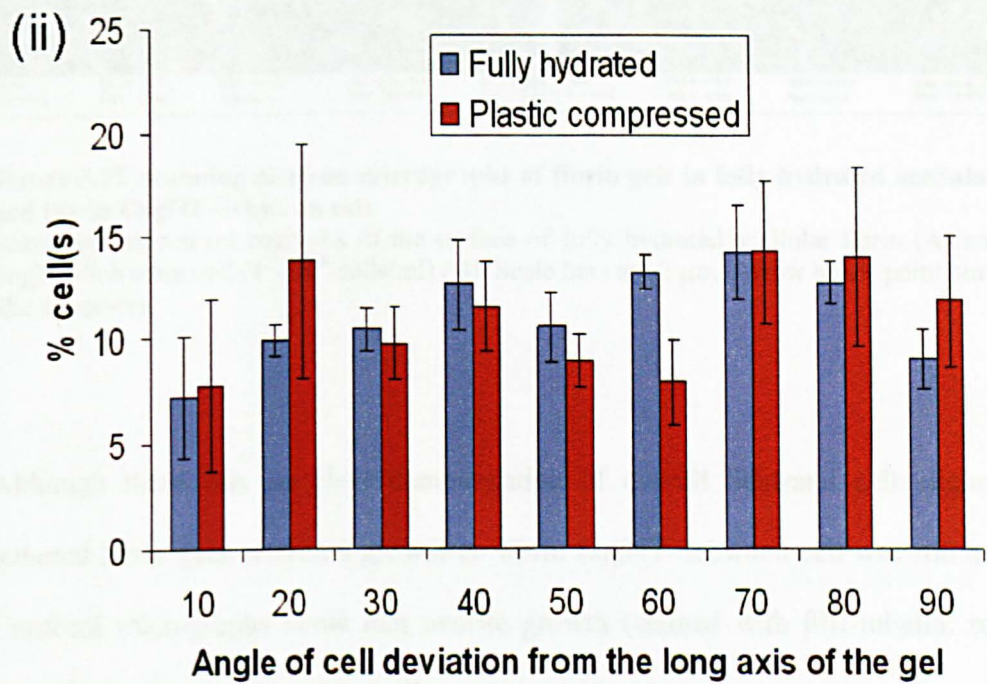
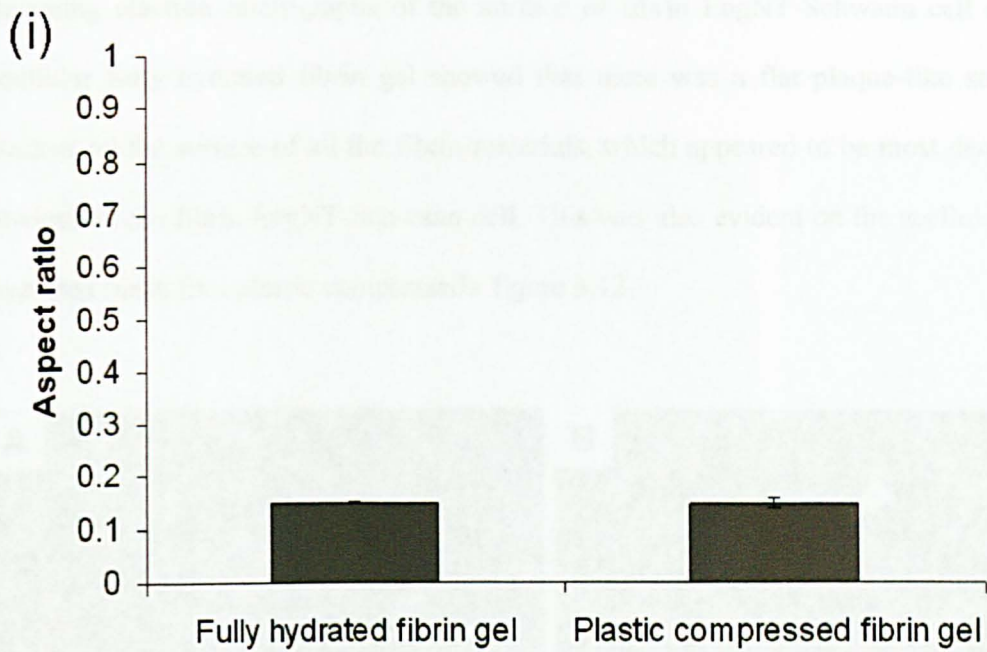


**Figure 3.11 Schwann cell elongation and orientation pre- or post-plastic compression of fibrin gels**

(i) The aspect ratio of the cells was not significantly different in gels pre- or post-compression.  
 (ii) Frequency distribution of the angle of deviation of each cell relative to the long axis of the gel. Data are means  $\pm$  SEM from  $n=4$  independent gels, 6 regions per gel were analysed.



Scanning electron micrographs of the surface of fibrin EngNT-Schwann cell and an acellular fully hydrated fibrin gel showed that there was a flat plaque-like structure evident on the surface of all the fibrin materials, which appeared to be most dense and obvious in the fibrin EngNT-Schwann cell. This was also evident on the acellular fully hydrated fibrin (not plastic compressed), figure 3.12.

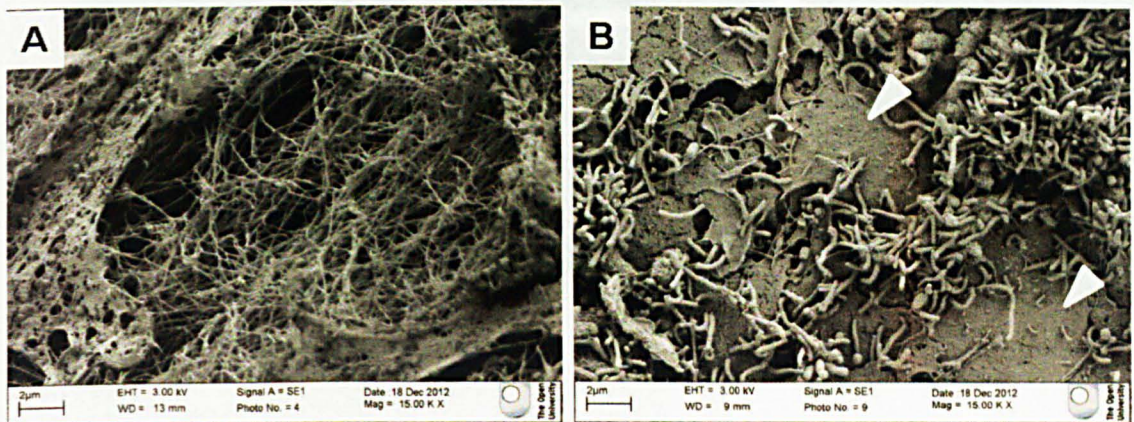


**Figure 3.12 Scanning electron micrographs of fibrin gels in fully hydrated acellular fibrin and fibrin EngNT-Schwann cell**

Scanning electron micrographs of the surface of fully hydrated acellular fibrin (A) and fibrin EngNT-Schwann cell ( $4 \times 10^6$  cells/ml) (B). Scale bars are 2  $\mu\text{m}$ . Arrow heads point out plaque-like structures.

Although there was no clear demonstration of overall Schwann cell alignment in tethered fibrin gels, neuronal growth on fibrin EngNT-Schwann cell was still assessed. Confocal micrographs show that neurite growth (stained with  $\beta$ III-tubulin, red) was associated with the Schwann cells (stained with S100, green) within fibrin EngNT-Schwann cell (figure 3.13). The degree of alignment was quantified in the same way as in section 3.2.4; i.e. the angle of neurite deviation from the mean direction that the Schwann cells are orientated in was determined on a per field basis. These measurements supported the observations from the images, which showed the majority

of neurite growth was along the Schwann cells;  $70 \pm 4\%$  ( $\pm$  SEM) of neurite growth did not deviate by more than  $20^\circ$  from the cell orientation on a per field basis (figure 3.13).

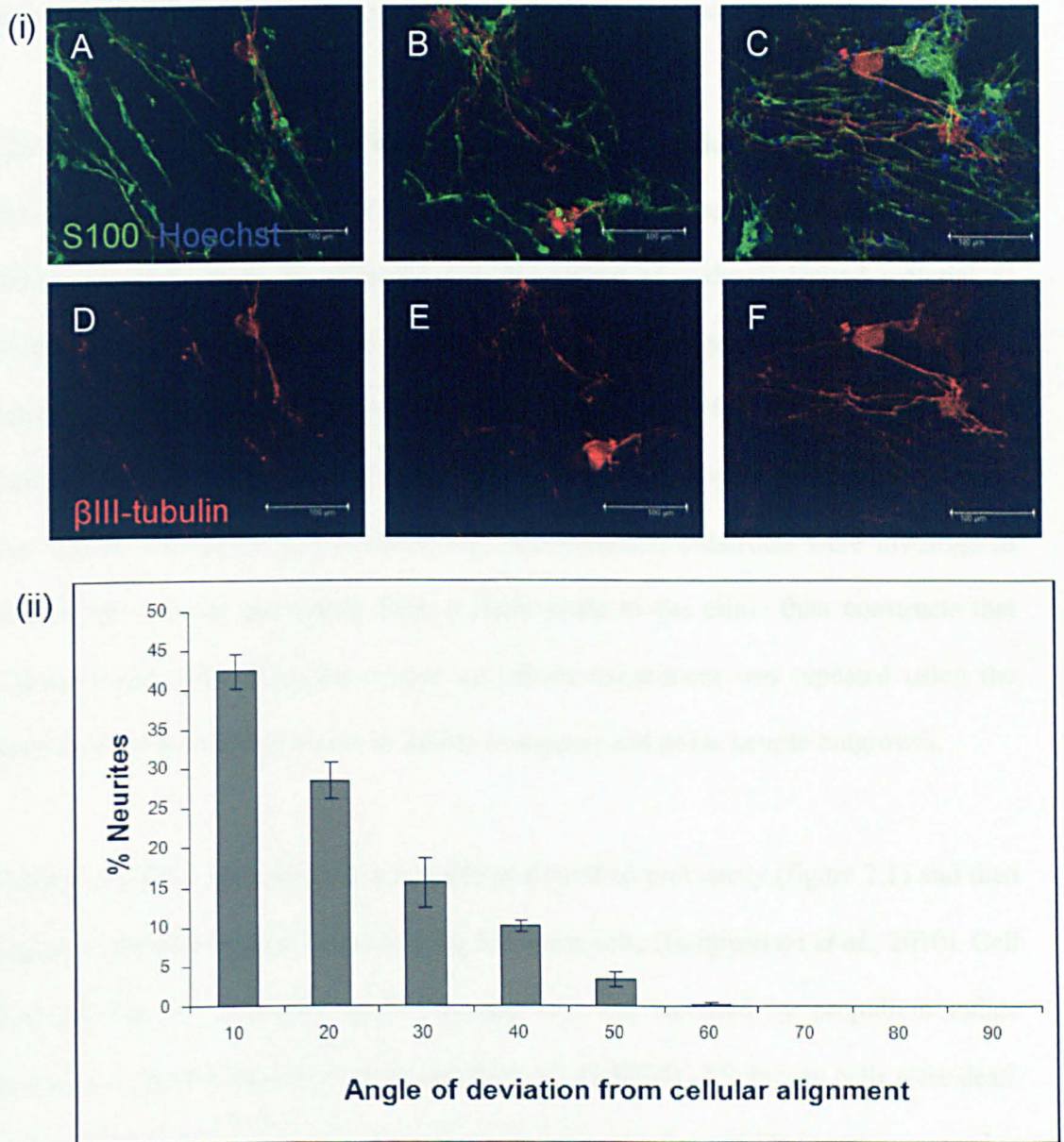


**Figure 3.13 Neuronal growth on fibrin EngNT-Schwann cell**

(i) Confocal micrographs showing Schwann cells (green) and neurons (red) stained for S100 and  $\beta$ III-tubulin, respectively, and Hoechst staining of nuclei (blue) (A-C). An image showing only the red channel is also shown for each field (D-F). Scale bars are  $100\mu\text{m}$ . (ii) Frequency distribution showing the angle of neurite deviation from the cellular alignment angle of that field; 570 neurites were counted in total. Data are means  $\pm$  SEM,  $n=3$  independent gels, 4 regions sampled by gel.

Thus, whilst the collagen EngNT-Schwann cell gave consistent and reliable alignment, the fibrin EngNT-Schwann cell showed a more complex pattern of localised orientation, and hence in further investigations only the collagen system was employed.

### **3.2.6 Exploring the use of decellularised collagen EngNT-Schwann cell**

In view of the overall aim of this project, to develop a nerve repair device for use in the clinic, this study went on to investigate the ability of a decellularised material to promote and guide neuronal growth. This is based on the hypothesis that the aligned Schwann cells could precondition the collagen biomaterial, before being freeze-killed to leave a decellularised guidance matrix. Having already shown that cellular constructs can support and guide neurite outgrowth, decellularised constructs were investigated because they would potentially have a faster route to the clinic than constructs that contain living cells. Thus the neuron co-culture experiment was repeated using the decellularised material to assess its ability to support and guide neurite outgrowth.

Collagen EngNT-Schwann cell was made as described previously (figure 2.1) and then dipped in liquid nitrogen once to kill the Schwann cells (Hadjipanayi *et al.*, 2010). Cell death in the freeze-killed EngNT-Schwann cell was assessed by propidium iodide exclusion with Hoechst and showed that  $96 \pm 3\%$  ( $\pm$  SEM) of Schwann cells were dead. Neurite outgrowth on the freeze-killed material (EngNT-freeze-killed) was compared to EngNT-Schwann cell and EngNT-acellular (no Schwann cells, plastic compressed collagen only). The images in figure 3.14 shows neurites that had been extended on the surface of these materials. Quantification of the neurite growth showed that there was 47-fold more neurite outgrowth (in terms of the total length extended in the sampled fields) on the live EngNT-Schwann cell material than on the EngNT-acellular biomaterial, and 26-fold more growth on the live EngNT-Schwann cell material than on

the EngNT-freeze-killed material (figure 3.14). These data highlight the importance of living Schwann cells for efficient nerve repair, and this will be discussed in some detail in section 3.3.

The direction of neurite outgrowth was assessed for all three materials by measuring the deviation of the angle of each neurite compared to the long axis of the gel. Consistent with previous findings from this study, there was a trend showing guidance of neurites parallel with EngNT-Schwann cell (figure 3.14). However there was no evidence of guidance by EngNT-acellular and little guidance provided by EngNT-freeze-killed (figure 3.14).

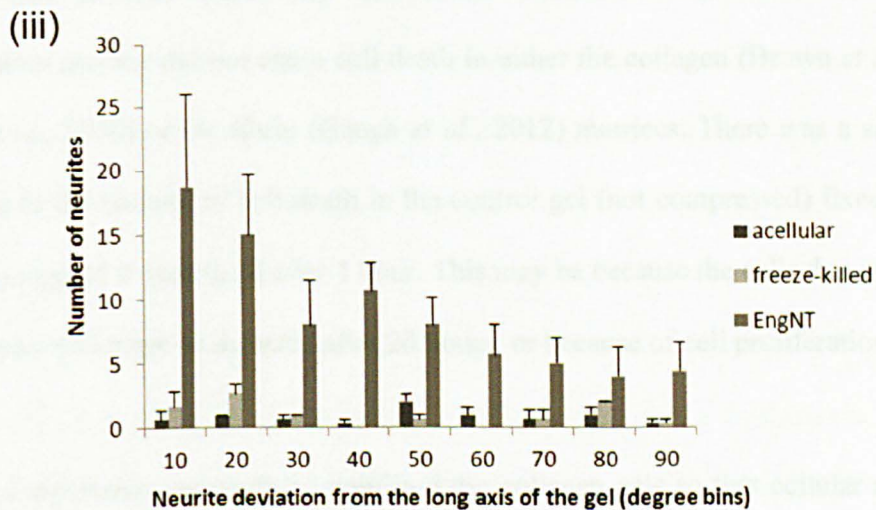
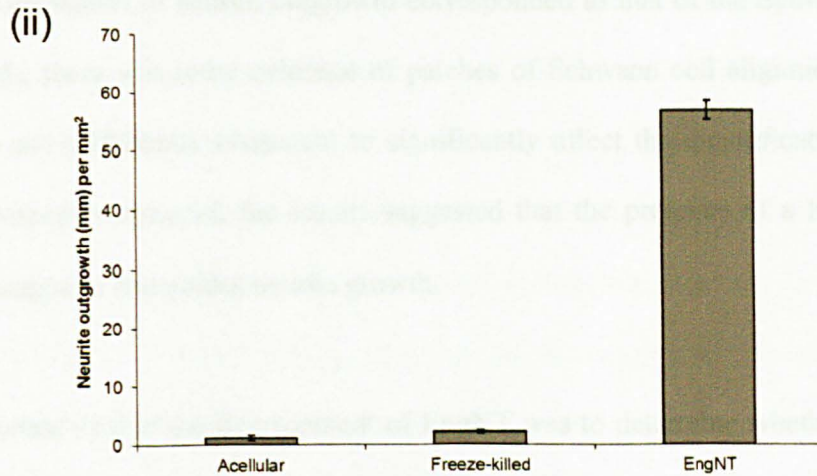
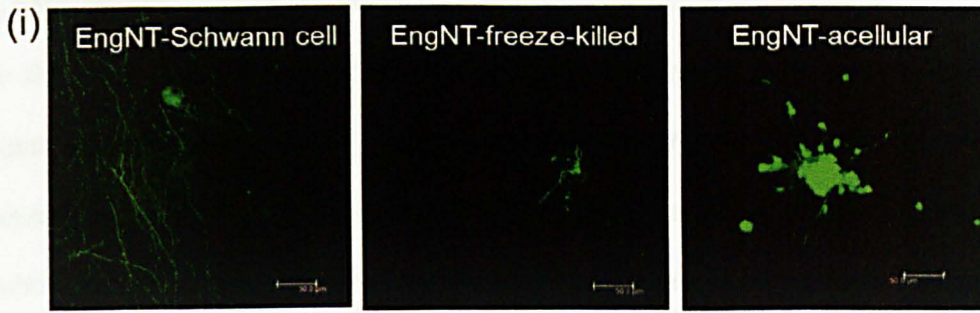


**Figure 3.14 Neuronal growth on EngNT-Schwann cell, EngNT-acellular and EngNT-freeze-killed**

(i) Confocal micrographs showing neurites (green) stained for  $\beta$ III-tubulin on EngNT-acellular, -freeze-killed and -Schwann cell. Scale bars are 50  $\mu$ m. (ii) The total length of neurite staining detected per mm<sup>2</sup> was compared in EngNT and freeze-killed and acellular controls; data are means  $\pm$  SEM from 3 independent co-cultures for each condition and 3 fields (total area 0.368 mm<sup>2</sup>) were sampled in each gel. (iii) The angle of neurite growth was compared to the longitudinal axis of the construct in each case; data are means  $\pm$  SEM of the number of neurites with angles of deviation from the long axis of the gel within each 10 degree bin.

### 3.3 Discussion

In this part of the study it has been shown that Schwann cells survive the plastic-compression process in both collagen and fibrin hydrogels. Schwann cell alignment achieved in tethered collagen gels was retained post-plastic compression. Co-culture of collagen EngNT-Schwann cells with neurons showed that neurite growth was supported and the orientation of neurite outgrowth corresponded to that of the Schwann cells. In fibrin gels, there was some evidence of patches of Schwann cell alignment. However this was not sufficiently consistent to significantly affect the quantification. In either type of substrate material, the results suggested that the presence of a living cellular element supports and guides neurite growth.

An important step in the development of EngNT was to determine whether the plastic compression process caused any cell death. Consistent with other findings, the stabilisation process did not cause cell death in either the collagen (Brown *et al.*, 2005; Levis *et al.*, 2010) or the fibrin (Haugh *et al.*, 2012) matrices. There was a significant decrease in the amount of cell death in the control gel (not compressed) fixed after 20 hours, compared to that fixed after 1 hour. This may be because the cells that are dead at 1 hour may no longer be detected after 20 hours; or because of cell proliferation.

Plastic compression successfully stabilised the collagen gels so that cellular alignment was preserved in collagen EngNT-Schwann cell immediately after and 3 days after plastic compression. This finding is consistent with a previous study using plastic compression to stabilise astrocyte alignment in collagen gels (East *et al.*, 2010), although in that study the persistence of alignment after compression was described but not measured. Although the mechanism for the stabilisation of alignment was not investigated here, it can be speculated that increased collagen concentration reduces the

ability of cells to undergo the alterations in shape and alignment associated with cytoskeletal contraction in a fully hydrated gel. This is in line with previous findings that show hydrogel rigidity and stiffness govern cell-matrix interactions during motility (Grinnell, 2003; Tomasek *et al.*, 2002).

Previous studies have investigated how plastic compression can be used to modulate the mechanical properties of cellular collagen I gels (Brown *et al.*, 2005) and fibrin gels (Haugh *et al.*, 2012), although East *et al.* were the only previous investigators to use plastic compression as a way to stabilise alignment specifically (East *et al.*, 2010). The plastic compression technology became commercially available in a multiwell plate format (RAFT™, TAP Biosystems, UK) during the course of this project, and is currently being developed in our lab to combine it with the self-alignment technology for the production of tissue-like constructs with aligned cells. If successful, that commercial development will provide a GMP-compliant production process that could be adapted to generate EngNT in a form that would be suitable for future translational studies.

The scanning electron micrographs showed that the Schwann cells and collagen fibrils were co-aligned, whereas the collagen fibrils in the plastic compressed acellular collagen were randomly oriented. This is in agreement with Eastwood and colleagues who imaged a fully hydrated tethered collagen gel with aligned fibroblasts using the scanning electron microscope, and showed both the cells and the collagen fibrils were aligned in the same direction (Eastwood *et al.*, 1998).

Both collagen I and fibrin matrices used to make EngNT created a permissive environment for neurites to elongate along Schwann cell columns, which guided and

promoted neurite outgrowth *in vitro*. These results are consistent with findings from previous co-culture experiments with DRG neurons and Schwann cells, that showed neurites were closely associated with columns of aligned Schwann cells (Thomson and Buettner, 2006). In this study, the majority of neurite outgrowth was in close contact with a Schwann cell, and grew parallel along the Schwann cell chains. This observation is in agreement with the current understanding of peripheral nerve repair, where neurite regeneration is associated with close contact with Schwann cells and/or their basal lamina (Guenard *et al.*, 1992; Dubey *et al.*, 1999; Thomson and Buettner, 2006). However, to understand the precise interactions between regenerating neurites and the Schwann cells within EngNT it would be interesting to study neurite growth cones using time lapse microscopy to see whether neurites seek and follow the aligned Schwann cells as one would predict, or whether some alterations to Schwann cell position and shape may occur in response to neuronal growth. The fluorescence images suggest that there is not a change in Schwann cell morphology because the surrounding Schwann cells, which are not in contact with a neurite, are similar in shape to the Schwann cells that are already in contact with a neurite.

In addition to the physical cues from the aligned cells and collagen fibrils, the biochemical influence of the live Schwann cells enhanced neurite outgrowth compared to acellular and freeze-killed controls. The cellular and freeze-killed EngNT-Schwann cell materials both provided guidance, but the presence of living cells resulted in considerably greater neuronal growth. This is consistent with reports demonstrating that denervated Schwann cells secrete the ECM components laminin 1 and 2 (merosin), which have been shown to promote neurite outgrowth *in vitro* (Anton *et al.*, 1994; Chen and Strickland, 2003; Cohen and Johnson, 1991). Denervated Schwann cells also secrete neurotrophins which aid regeneration (Rich *et al.*, 1989; Bloch *et al.*, 2001).



This is supported by studies that show the presence of living cells enhances neurite outgrowth by cell-neurite contact and through trophic factors (Thomson and Buettner, 2006; Richardson *et al.*, 2011; Seggio *et al.*, 2010) and is necessary for the repair of damaged nerves with a gap larger than 3 cm between the injured stumps in human (Nadim and Anderson *et al.*, 1990).

The overall aim for this part of the study was to develop and test EngNT *in vitro*. This has been done in terms of establishing the density of the cells required to generate sheets of EngNT and the time required for compression. In this part of the study it was established that the collagen was better than fibrin for the production of aligned EngNT-Schwann cell. Collagen I was used for subsequent experiments because it gave consistent and reliable contraction and alignment. Additionally, collagen I is a well-defined material, can be obtained in a GMP-compliant form and it is the material used in the RAFT™ system; which is also currently being used within the production of cornea transplants, for phase I clinical trials which are due to begin in 2013 (Genetic Engineering and Biotechnology News, 2012). The next step in this present study was to see whether EngNT-Schwann cell could be used as the basis for a repair conduit to support nerve regeneration *in vivo*, which is the subject of the next chapter.

## 4.0 Investigating ways to deliver EngNT within a nerve repair conduit

### 4.1 Introduction

The previous chapter showed that EngNT can support and guide neuronal growth *in vitro*. This material displayed structural characteristics and biological guidance cues that are beneficial for nerve repair; therefore it was appropriate to investigate ways in which it could be incorporated into a nerve repair conduit in order to bridge peripheral nerve lesions *in vivo*.

The addition of an 'engineered endoneurium' or core within a repair device would potentially be a way to improve current commercial options consisting of hollow nerve guidance conduits and decellularised allografts, which do not effectively support regeneration across gaps of more than 3 cm in humans (Deumans *et al.*, 2010). Insufficient levels of regeneration in 'empty' conduits may be attributed to the inadequate formation of a tissue bridge across the long gap in the initial stages of regeneration. This, in turn, will affect subsequent processes such as migration of host Schwann cells into the injury site, such that the guidance structure of the Bands of Büngner fails to form or is inadequate (Daly *et al.*, 2012). An appropriate core or intraluminal guidance structure in a conduit, could act as a replacement for, or speed up the formation of, the tissue bridge and/or the Bands of Bungner (Bellamkonda, 2006). Studies comparing conduits (empty tubes) to repair devices with a core, have found that the presence of intraluminal guidance structures enhances nerve regeneration in rat (10-20 mm gaps) (Yoshii and Oka, 2001; Ngo *et al.*, 2003; Kim *et al.*, 2008; Koh *et al.*, 2010) and in an 80 mm gap in a dog model (Matsumoto *et al.*, 2000). Others have added a cell component to the core of devices with intraluminal guidance structure and seen further enhancement to the regeneration process, when compared to acellular devices

(with guidance structures) or an empty tube in rat and dog models (Chang and Hsu, 2004; Kalbermatten *et al.*, 2007; Di Summa *et al.*, 2010; Ladak *et al.*, 2011). This indicates that cells and intraluminal guidance structures are beneficial within a nerve repair device.

The next step in this study was to use EngNT-Schwann cell to form the core of a peripheral nerve repair device. Bands of Büngner are known to be important for repair because columns of aligned cells provide a guidance structure and also secrete neurotrophic factors that promote regeneration (Dahlin and Brandt, 2004; Hall, 2005). The EngNT material could be used to create something analogous to this because it is an aligned collagen matrix containing aligned Schwann cells and it can potentially be arranged in various ways to form an 'engineered endoneurium' for a repair device. EngNT could promote the regeneration of axons by providing trophic factors, intraluminal guidance and Schwann cells. To explore this possibility, various core designs were developed using EngNT-Schwann cell and these were tested within an outer tube in the rat sciatic nerve model.

It is important that the outer tube or 'sheath' of the repair device can mimic the epineurium, containing the core and providing mechanical support at the repair site. The epineurium has been shown to be about 6.5 times stronger than the core in the rat sciatic nerve (Georgeu *et al.*, 2005); and ideally a repair device containing EngNT would have an outer tube with similar tensile strength and the ability to support sutures. Under normal physiological conditions peripheral nerves in the limbs bend and stretch, being exposed to combinations of tensile, shear and compressive stresses. The change in the length of a nerve caused by longitudinal tensile stress (for example as a result of joint movement) is called strain. Human nerves need to be able to bend and stretch to

accommodate up to 11% strain (Topp and Boyd, 2006). Changes to the structural components of peripheral nerves during surgery can lead to extraneural fibrosis and wound-bed adhesions and may cause increases in intraneural tension, which would compromise the clinical outcome (Hall, 2005). Localised increases in tension could also result from repair of nerves at joints in which a rigid outer tube is used, which could prevent the repaired nerve from bending with normal movement, so using materials that give a device appropriate mechanical properties is a critical feature of repair device design. For example, outer tube materials for repairing a nerve at a joint would ideally have more compliance than that for repairing a nerve at a location that would not need to bend (Phillips *et al.*, 2004; Mason and Phillips, 2011). It is potentially possible to engineer a more complex tailored outer sheath that could have a compliant section and a stiff section to match particular anatomical locations.

The first experiment in this chapter used a silicone tube as the outer part of the device, whereas later experiments used biodegradable conduits. Silicone tubes used to investigate peripheral nerve regeneration were described as a useful experimental tool for studying biological mechanisms in rat sciatic nerve (Lundborg *et al.*, 1982). It has subsequently been demonstrated that silicone tubes are well-tolerated in humans (Gu *et al.*, 2011), even five years after implantation (Lundborg *et al.*, 2004). The main objection to the use of non-biodegradable nerve guides, such as those made of silicone, is that they remain *in situ* as prostheses after the nerve has regenerated. Whilst this is not an issue in short term experimental models, the use of non-biodegradable tubes in the clinic can require a second surgery to remove the tube, which has clear disadvantages for the patient (Merle *et al.*, 1989).

Plastic compressed collagen was also explored for use as the outer sheath of a repair device. The potential advantages of this would be that the mechanical properties could be tailored, by varying the collagen concentration and amount of compression, to match those required at specific anatomical locations. Other conduits that have been used experimentally include: polylactic acid, poly caprolactone, silicone, fibrin and collagen (Schmidt and Leach, 2003, Angius *et al.*, 2012). Silicone tubes provided an economical way to test EngNT in initial experiments, but for later experiments that required a more clinically relevant conduit, NeuraWrap™, a clinically approved conduit was used.

Various biodegradable conduits which remain in the nerve injury site long enough to aid the repairs have been developed and are currently in clinical use. A literature search was conducted to identify the different commercially available tubes and materials for clinical use. Only 4 biodegradable synthetic conduits (by Integra LifeSciences, Polyganics, Synovis Micro Companies Alliance Inc. and Collagen Matrix Inc.), involving 3 materials (collagen, polycaprolactone and polyglycolic acid) have obtained the US FDA and the CE approval for clinical use (Kehoe *et al.*, 2012). These conduits are used to bridge gaps of less than 3 cm in damaged human peripheral nerves. They provide a conduit to concentrate factors, overall tissue guidance/containment, and reduce fibrosis/adhesion (Kehoe *et al.*, 2012; Schmidt and Leach, 2003).

After considering the various available conduits, the NeuraWrap™ tube was chosen for use in these experiments, partly because it is based on a similar material to EngNT, namely collagen type I (NeuraWrap™ is composed of cross-linked bovine collagen, whereas the EngNT was made from native rat tail collagen). Also, the NeuraWrap™ conduit has a longitudinal slit that allows it to be spread open, permitting insertion of the engineered core (figure 4.6 and 4.7), and the resilience of the material allows it to

recover and maintain closure when not being held open. The mechanical strength of the material is sufficient for it to be able to be sutured and NeuraWrap™ is flexible enough to be accommodated in the surgery site. While there was little data available about the mechanical properties of the tube, the publicly available summary from the FDA approval process states that “*NeuraWrap™ Nerve Protectors are able to hold a suture, resist repeated compression from surrounding tissues.*” (FDA approval number K041620, 2004 [http://www.accessdata.fda.gov/cdrh\\_docs/pdf4/k041620.pdf](http://www.accessdata.fda.gov/cdrh_docs/pdf4/k041620.pdf)).

Having used *in vitro* approaches for the development of EngNT (chapter 3), initial attempts to develop the assembly of an EngNT-based conduit were also made using *in vitro* techniques. Advantages of using *in vitro* models rather than *in vivo* testing for these initial experiments include: improved ability to control specific variables, greater accessibility for monitoring purposes, and more efficiency in terms of cost and time. In view of these advantages, and considering the principles of the 3Rs, it was decided to see whether a novel *in vitro* approach might allow testing of the ability of a construct made from EngNT to support and guide neuronal growth. However, a new *in vitro* model that attempted to use primary adult sensory neurons in culture to mimic the interaction between a nerve stump and a conduit containing EngNT was not successful. In these experiments dissociated DRG neuronal cell bodies were applied at one end of the EngNT devices so that neuronal growth through the device, from end to end, could be investigated, and two different approaches were tested. The first approach was to place the device vertically and seed the neurons at the top end. This was unsuccessful because the neuronal cell bodies were subsequently discovered to be distributed throughout the constructs rather than remaining at the top. The second attempt was to seed them within a gel at the top end; however this was also unsuccessful because the gel volume was too small to support a sufficient number of neuronal cells near the

device core. It was therefore decided that the priority was to move forward with the device development using conventional *in vivo* approaches.

A review of animal models used to study nerve regeneration from the 1950s to 2010, showed that 17 different peripheral nerves had been studied in 8 different species. The rat sciatic nerve model was the most commonly used model for the study of synthetic scaffolds; it was used for 86% of the studies reviewed (308 studies were reviewed in total) (Angius *et al.*, 2012). The gap size used in initial *in vivo* experiments, to compare the extent of directed neuronal growth in repair devices of different arrangements, was 5 mm at 2 or 4 weeks. While this is not a critical sized defect, so no difference would be expected in the amount of regeneration through an empty tube compared to a graft, it is a useful model for understanding how materials are likely to behave in a nerve repair situation (Angius *et al.*, 2012; Phillips *et al.*, 2005). The most optimal device design, in terms of the amount/density of neurite regeneration, was then used to repair a critical sized long gap (15 mm) in rat sciatic nerve, where an empty tube fails but a graft is able to bridge the gap and regeneration was assessed after 8 weeks.

The main objective of this part of the study was to engineer an ‘endoneurium’ that supported the re-growth of axons across the gap in injured nerves. In addition to this, the use of plastic compressed collagen as an outer sheath of a device was also assessed.

The following specific objectives/questions were addressed:

- (i) The first hypothesis that was tested, based on results from the previous chapter, was that EngNT-Schwann cell could support neuronal growth in a more directed manner *in vivo* than equivalent collagen constructs that were either acellular or contained unaligned Schwann cells.
- (ii) The next part was to investigate different arrangements of EngNT-Schwann cell to see which was the most optimal in terms of supporting neuronal growth.
- (iii) Following this, an experiment was carried out to investigate whether different numbers of cells and amounts of material, and different sizes of EngNT structures could affect the amount of neuronal regeneration through the device *in vivo*.
- (iv) Next a proof-of-principle experiment was conducted to assess the feasibility of using EngNT in the device core to repair a gap in the rat sciatic nerve that is representative of the clinical situation (15 mm).
- (v) Finally, a preliminary experiment compared the mechanical strength and stiffness of plastic compressed collagen to rat nerves and silicone tubes as a prelude to the possible future development of this material as the outer sheath component of repair devices requiring specific mechanical properties or non-standard dimensions.



## 4.2 Results

### 4.2.1 Investigating the contribution of cells and alignment to neuronal regeneration through EngNT rods *in vivo*

The first approach used to engineer ‘endoneurium’ was to roll the EngNT sheets into rods, bundle them together and then pack them within an outer tube to form the core of a repair device (figure 4.1). EngNT-Schwann cell, an equivalent cellular construct without alignment, and an acellular collagen construct control, were tested in a 5 mm gap in the rat sciatic nerve for 2 weeks. For each experimental group, 2 EngNT rods or controls (5 mm in length) were packed within a silicone tube (as shown in figure 4.2). A longitudinal slit was made in the silicone for the insertion of the engineered ‘endoneurium’, and three holes were made at each end for the suture material to pass through (figure 4.2). Each construct was then sutured at either end to the stumps of the rat sciatic nerve following a single transection. The animals used in this surgery showed no obvious external signs of inflammation/infection, weight loss or distress; and they all survived the entire period (2 weeks) of recovery post-implantation.

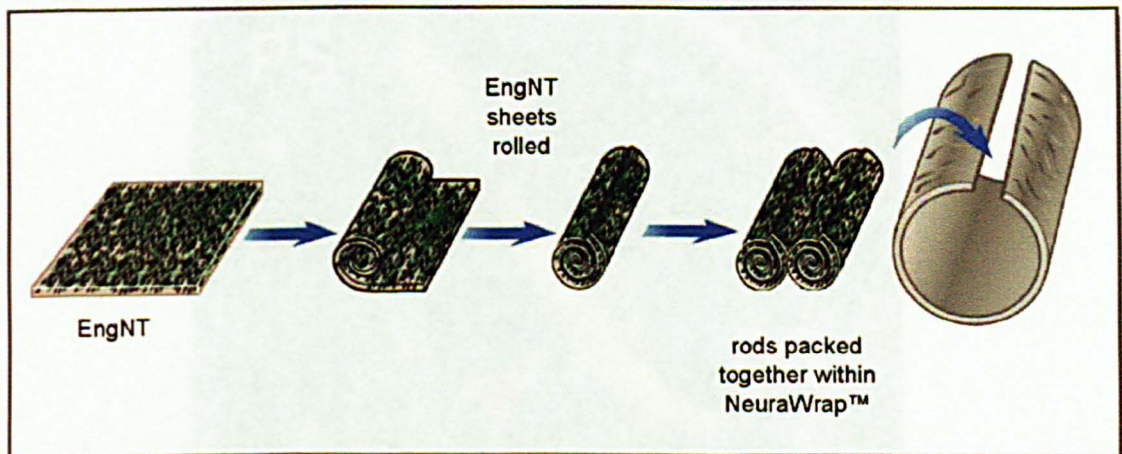


**Figure 4.1 The rod-based device design.**

Assembly of EngNT-Schwann cell rods to form the core of a peripheral nerve repair device.

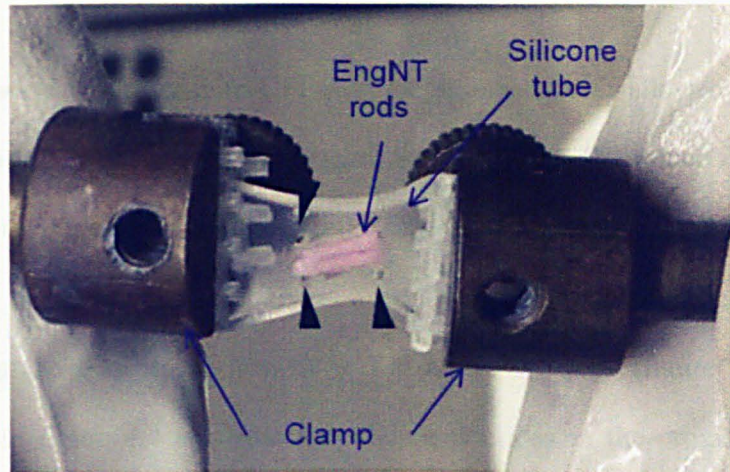


**Figure 4.2 Assembly of a nerve repair device with an EngNT core within a silicone tube**

A silicone outer tube was held open using a clamp and two EngNT-Schwann cell rods (5 mm in length) were positioned inside. Holes for the suture material are marked with arrow heads. The tube returned to its cylindrical shape when the clamp was removed, and the ends were trimmed so there was a length of 1.5 mm between the holes for sutures and the end of the tube.

The total amount of neuronal growth was not compared between treatment groups because inconsistent stump-core contact was observed in some samples after harvesting (figure 4.3).

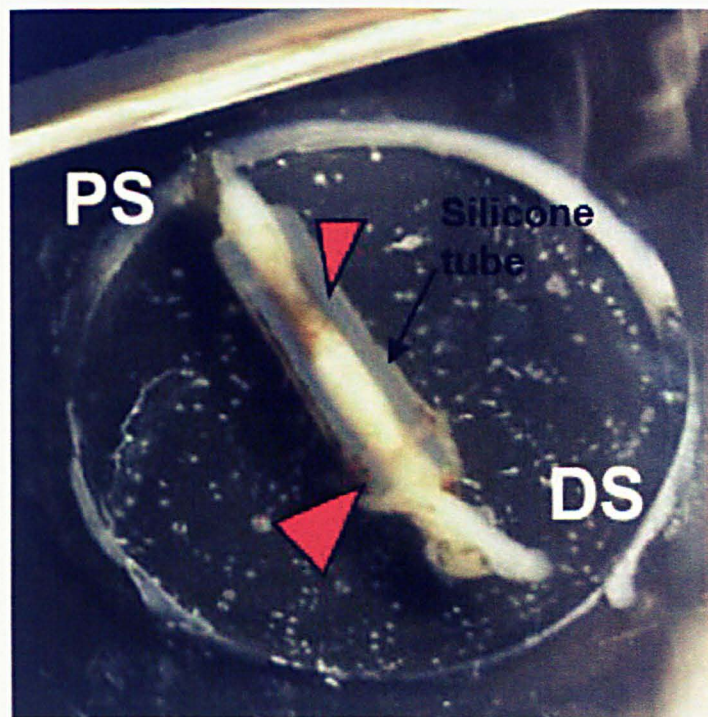
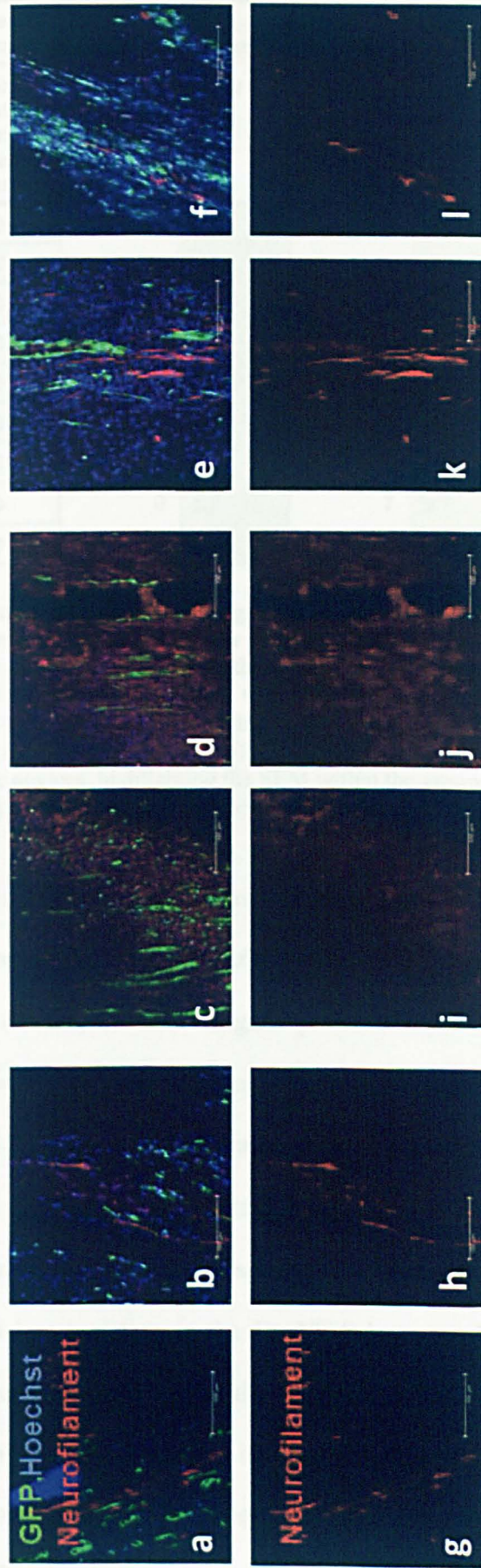


**Figure 4.3: EngNT-Schwann cell within a silicone outer tube after 2 weeks *in vivo*.** Embedded in 20% gelatin and fixed with 4% PFA. In this case, the ends of the EngNT, indicated by the arrow heads, did not make sufficient contact with the proximal stump, as was observed in some other samples. PS = proximal stump; DS = distal stump.

The devices were implanted into GFP-positive animals which allowed the infiltrating host cells to be distinguished from implanted Schwann cells. Combined fluorescence for Hoechst and GFP identified the host cells, whereas implanted cells were positive for Hoechst and negative for GFP. There were GFP-positive host cells present in all conditions but little neuronal growth in the acellular grafts (figure 4.4). Confocal micrographs in figure 4.4 are from longitudinal sections in the proximal part of the device, and show an overall longitudinally-aligned pattern of cell staining in all cases. The nature of neuronal growth within the device core was assessed by measuring how aligned each neurofilament-positive neurite was in relation to the long axis of the device, in longitudinal sections in the proximal part of the device. In all groups most of the neurites showed longitudinal alignment, although there was a trend towards more alignment in the EngNT condition (especially looking at the 20° deviation category) (figure 4.4B).

**A** EngNT-Schwann cell



**B**

device type:	EngNT-Schwann cell	Acellular	Unaligned
Angle of deviation from longitudinal axis	% frequency of neurites Means $\pm$ sem	% frequency of neurites Means $\pm$ sem	% frequency of neurites Means $\pm$ sem
10	46 $\pm$ 5	46 $\pm$ 27	47 $\pm$ 17
20	34 $\pm$ 6	22 $\pm$ 22	22 $\pm$ 7
30	13 $\pm$ 7	6 $\pm$ 6	18 $\pm$ 9
40	2 $\pm$ 2	7 $\pm$ 7	6 $\pm$ 2
50	0 $\pm$ 0	13 $\pm$ 13	3 $\pm$ 1
60	4 $\pm$ 2	0 $\pm$ 0	2 $\pm$ 2
70	0 $\pm$ 0	0 $\pm$ 0	1 $\pm$ 1
80	0 $\pm$ 0	7 $\pm$ 7	0 $\pm$ 0
90	0 $\pm$ 0	0 $\pm$ 0	1 $\pm$ 1

**Figure 4.4 Comparison of neurite alignment between EngNT with aligned Schwann cells, unaligned Schwann cells and acellular collagen *in vivo***

Neurite angle was measured relative to the long axis within the proximal part of the devices in a 5mm gap in the rat sciatic nerve after 2 weeks. (A) Confocal images from longitudinal sections in the proximal part of the device showing host cells (a-f) (GFP, green), nuclei (Hoechst, blue) and axons (g-l) (neurofilament, red); (B) Table showing the angle of neurite deviation from the long axis of the devices, highlighting the SEM within the groups. There was a directional trend for regenerating axons in all device groups. N=3, data are means  $\pm$  SEM.

The location of the regenerated axons was investigated to see whether they were within the rods or between the rods and results are shown in figure 4.5 part (A). In the EngNT-Schwann cell devices, the neurites grew preferentially within the rods. In the EngNT condition 95  $\pm$  5% of total neuronal growth within the device was within the rods, compared to 54  $\pm$  28% in the equivalent cellular constructs without alignment; and in the implanted material which contained no Schwann cells there were no neurites detected within the rods. No neurites were observed in the areas surrounding the rods, and there was less variation in the EngNT-Schwann cell group for the location of regenerating neurites, compared to the constructs without alignment and the acellular materials. Figure 4.5 part (B) shows the number of host cells (GFP-positive) within and between the rods. In all the device groups, over 90% of total host cells were present within rods rather than between the rods and the outer tube.

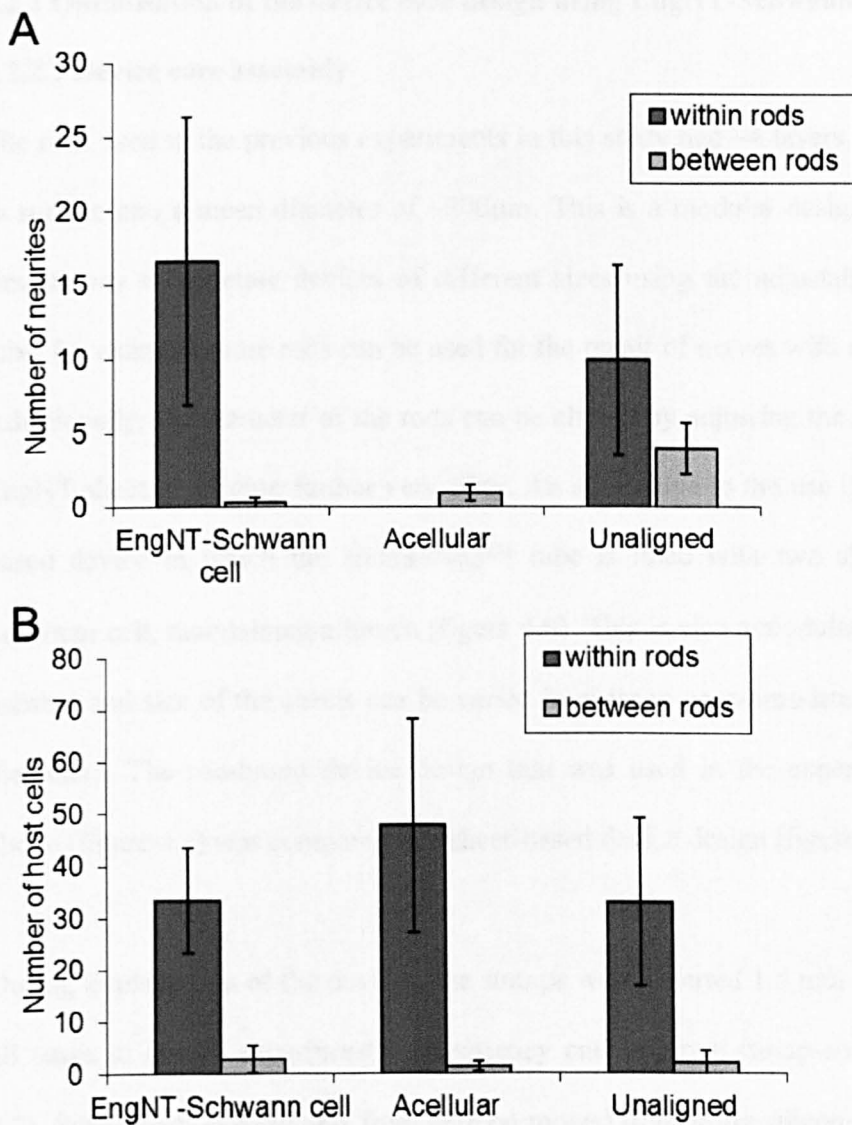


**Figure 4.5 The location of regenerating axons in the proximal part of the device**

(A) Neurites within the devices grew preferentially within the rods in the cellular devices and between the rods in the acellular devices; and (B) host cells in all device groups were present within the rods. N=3, data are means  $\pm$  SEM.

An optimal device core element would be expected to support more neuronal regeneration than the surrounding areas. In this case, despite the limitations of the experiment due to the inconsistent proximal stump interface, the EngNT-Schwann cell material demonstrated advantages over the unaligned or acellular controls in terms of distribution of regenerating neurons.

## **4.2.2 Optimisation of the device core design using EngNT-Schwann cell**

### **4.2.2.1 Device core assembly**

The rods used in the previous experiments in this study had ~4 layers from central axis to surface and a mean diameter of ~200 $\mu$ m. This is a modular design that provides a simple way to generate devices of different sizes using the adjustable NeuraWrap™ tube, for example more rods can be used for the repair of nerves with a larger diameter. Additionally, the diameter of the rods can be altered by adjusting the size of the initial EngNT sheet, providing further versatility. An alternative to the use of rods is a sheet-based device in which the NeuraWrap™ tube is lined with two sheets of EngNT-Schwann cell, maintaining a lumen (figure 4.6). This is also a modular design since the number and size of the sheets can be varied in order to accommodate a range of nerve diameters. The rod-based device design that was used in the experiments described above (figure 4.1) was compared to a sheet-based device design (figure 4.6).

During implantation of the devices, the stumps were inserted 1.5 mm into the device in all cases to ensure experimental consistency and improve stump-core contact (figure 4.7). Subsequent experiments from here on moved from using silicone to NeuraWrap™ as the outer tube material, which is a step towards making a translational device and also made the device assembly easier.

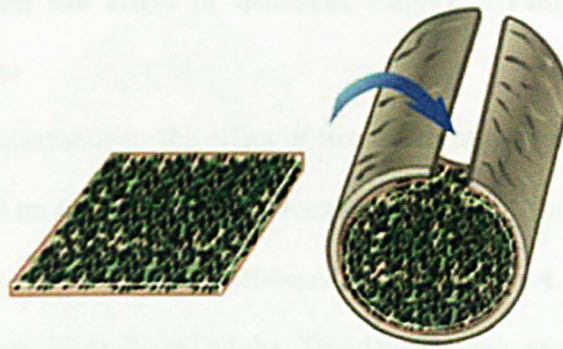


**Figure 4.6 The sheet-based device design**

The EngNT-Schwann cell sheet is placed on the inside surface of NeuraWrap™, maintaining a lumen. Two sheets were used in this experiment, one on top of the other.

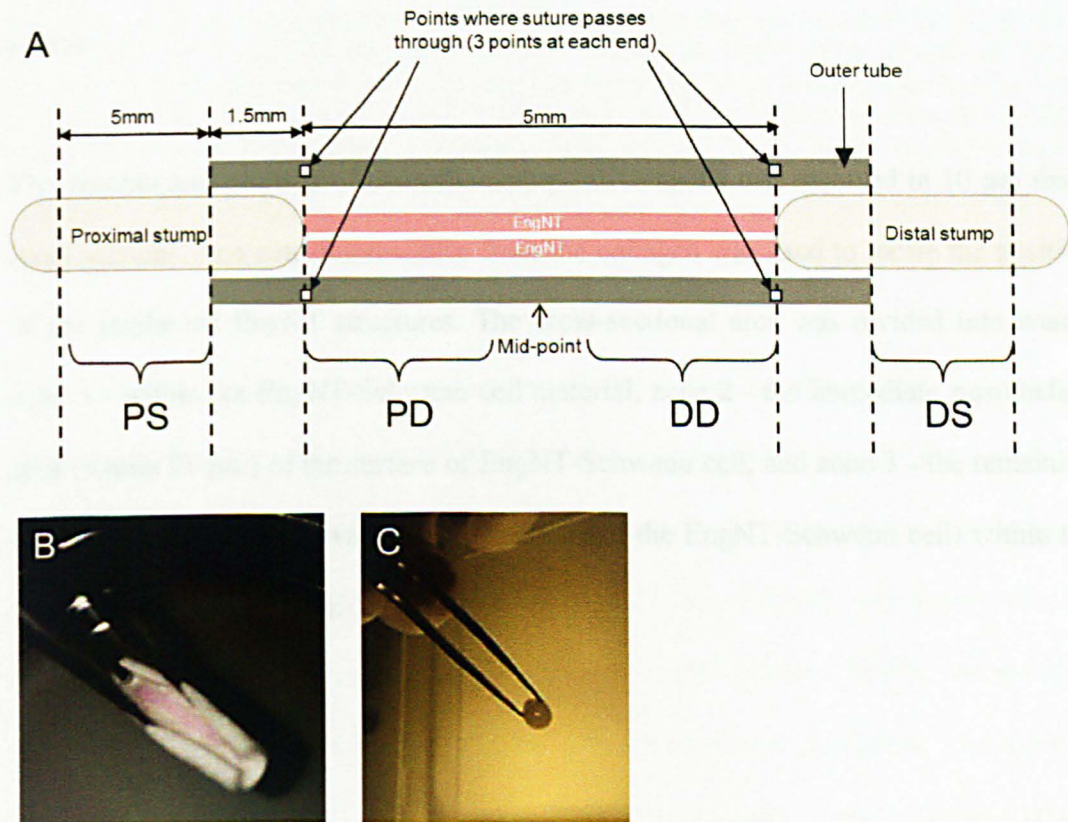


**Figure 4.7 Implantation of rod- and sheet-based devices within a NeuraWrap™ outer tube**  
 (A) A schematic of the implanted device, showing EngNT within the outer tube; PS = proximal stump, PD = proximal part of the device, DD = distal part of the device and DS = distal stump;  
 (B) A NeuraWrap™ outer tube (held open by forceps to prevent it from returning to its normal cylindrical shape), containing an EngNT-Schwann cell rod of 15 mm in length;  
 (C) End-on view of a closed NeuraWrap™ tube with two EngNT-Schwann cell sheets lining the lumen.



#### **4.2.2.2 Investigating the effect of different EngNT arrangements on neuronal regeneration *in vivo***

The next step was to investigate the effect of two different device designs (both within a NeuraWrap™ tube) on the amount of neuronal regeneration. The EngNT arrangements tested here were the rod-based and sheet-based designs (figure 4.1 and 4.6), which were compared to an empty NeuraWrap™ tube. The devices were assembled using the same amount of collagen and the same starting cell density for each design, then implanted into a 5 mm gap in the rat sciatic nerve. Devices were harvested after 4 weeks *in vivo*, and frozen transverse sections were taken from the centre of the proximal part of the device region (see figure 4.7 part A) and stained to detect neurofilament, a marker for axons.

The number and position of neurofilament-positive axons was assessed in 10 µm thick cross sections. The auto-fluorescence from the collagen was used to locate the position of the implanted EngNT structures. The cross-sectional area was divided into zones: zone 1 - within the EngNT-Schwann cell material, zone 2 - the immediate surrounding area (within 25 µm) of the surface of EngNT-Schwann cell, and zone 3 - the remaining area (more than 25 µm away from the surface of the EngNT-Schwann cell) within the conduit lumen (figure 4.8).

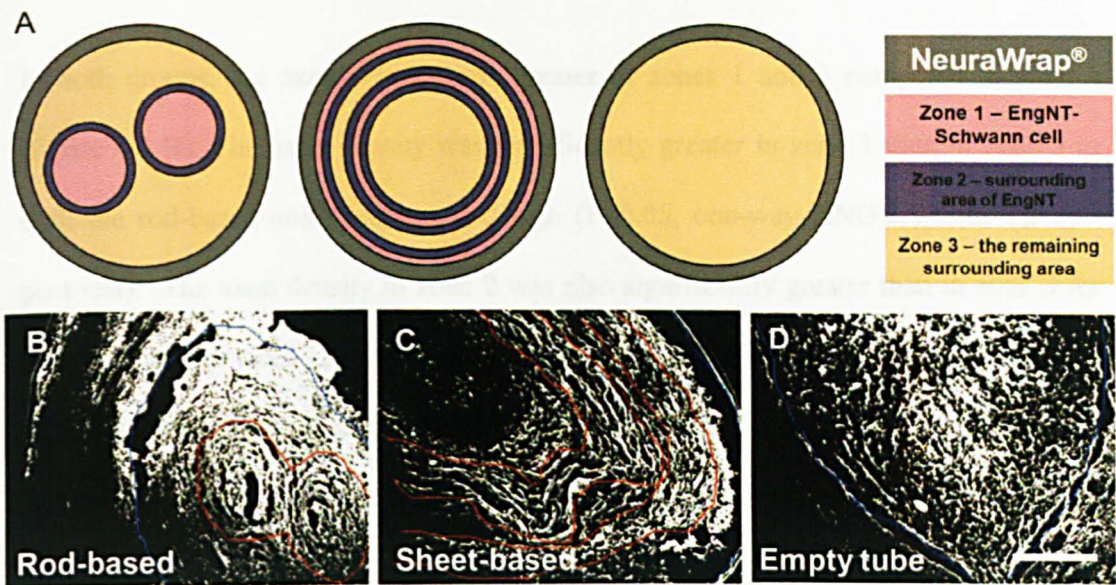


**Figure 4.8** The different zones within cross-sections from the rod- and sheet-based devices (A) A key to show the different zones within the implanted EngNT-Schwann cell and empty NeuraWrap™ devices after 4 weeks *in vivo* in a 5 mm gap in rat sciatic nerve (not drawn to scale); (B-D) are 10 μm cross sections, as observed using autofluorescence on a fluorescence microscope for the different device designs: EngNT-Schwann cell rods (B), EngNT-Schwann cell sheets (C), and the empty NeuraWrap tube (D). The red outlines the EngNT-Schwann cell material and the blue outlines the device core. Scale bar is 200 μm.

There was no significant difference between the three devices when comparing the total number of axons in the cross sections using a one-way ANOVA, figure 4.9 A. Although the same amount of material was implanted for each design, the cross sectional area of zone 1 in the sheet-based design,  $0.15 \pm 0.02 \text{ mm}^2$  (mean  $\pm$  SEM), was about twice the size of zone 1 in the rod-based designs,  $0.06 \pm 0.01 \text{ mm}^2$  (mean  $\pm$  SEM). The numbers of axons in the different zones were counted to give an axon density for each zone in each device (figure 4.9 B). There was a trend towards more axons in zone 1 of the sheet-based design ( $400 \pm 100$ , mean  $\pm$  SEM) than zone 1 of the rod-based design ( $200 \pm 40$ , mean  $\pm$  SEM) although there was considerable variability and the trend was not significant (using either t-test to compare the two zone 1 regions, or ANOVA to compare all zones).

In both groups, the axon density was greater in zones 1 and 2 compared to zone 3 (figure 4.9 B). The axon density was significantly greater in zone 1 than in zone 3 in both the rod-based and sheet-based design ( $P < 0.05$ , one-way ANOVA with Tukey's post-test). The axon density in zone 2 was also significantly greater than in zone 3 for the rod-based devices ( $P < 0.05$ , one-way ANOVA with Tukey's post-test). The axon density in zones 1 and 2 in the rod-based design appeared to be slightly greater than that in zones 1 and 2 in the sheet-based design, although this was not significant. The axon density in the empty tube group was similar to that of the zone 3 in both device designs and zone 2 of the sheet-based design. The axon density in the empty tube was lower than zone 1 in both devices, although this was not significant.

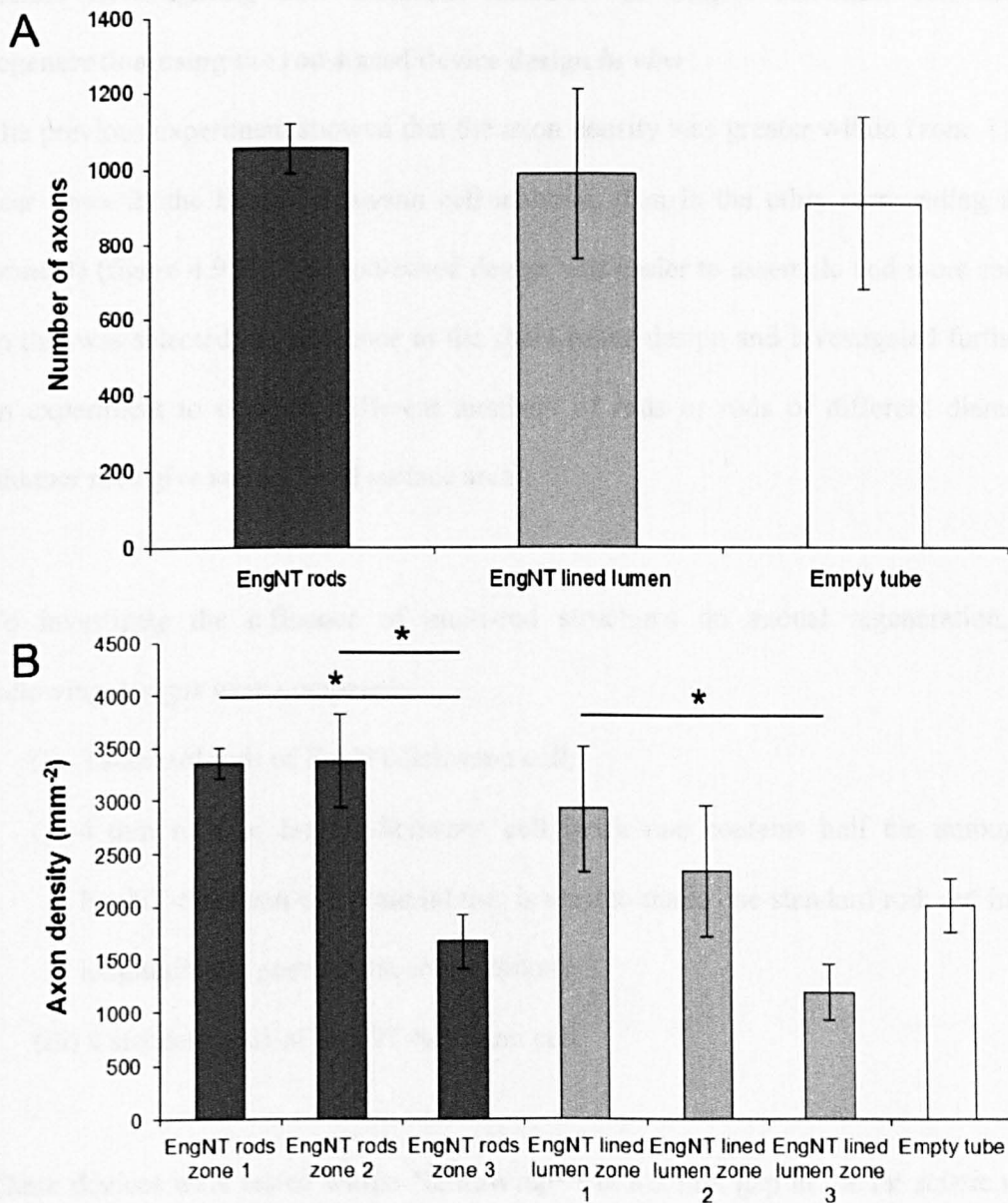


**Figure 4.9 The number and location of axons within cross sections from the proximal parts of rod- and sheet-based EngNT devices.** (A) There was no significant difference in the three devices when comparing the total number of axons per cross section (one-way ANOVA). (B) Axon density was greater in zones 1 and 2 (within or near EngNT-Schwann cell), compared to zone 3 in both device groups. This was significant between zones 1 and 3 for the rod-based and the sheet-based device designs; and between zones 2 and 3 for the rod-based devices (one-way ANOVA, \* $P < 0.05$ ,  $n = 4$ , data are means  $\pm$  SEM).

#### **4.2.2.3 Investigating how different amounts of EngNT-Schwann cell affects regeneration using the rod-based device design *in vivo***

The previous experiment showed that the axon density was greater within (zone 1) and near (zone 2) the EngNT-Schwann cell material, than in the other surrounding areas (zone 3) (figure 4.9 B). The rod-based design was easier to assemble and more robust, so this was selected in preference to the sheet-based design and investigated further in an experiment to compare different numbers of rods or rods of different diameters (thinner rods give an increased surface area).

To investigate the influence of multi-rod structures on axonal regeneration, the following designs were compared:

- (i) 2 standard rods of EngNT-Schwann cell;
- (ii) 4 thin rods of EngNT-Schwann cell (each one contains half the amount of EngNT-Schwann cell material that is used to make one standard rod; cut in half longitudinally post-plastic compression);
- (iii) 4 standard rods of EngNT-Schwann cell.

These devices were tested within NeuraWrap™ in a 5 mm gap in the rat sciatic nerve (n=3 animals per group). Devices were harvested after 2 weeks, which was a shorter time point than in the previous experiment, to permit examination of any differences in the initial amount of regeneration between the groups. The animals used in this experiment showed no obvious external signs of inflammation/infection, weight loss or distress, and they all survived the period of recovery after surgery. Frozen 10 µm thick longitudinal sections from the proximal part of the device and cross sections from the distal part of the device (figure 4.7 A) were stained to detect neurofilament protein.

In the proximal part of the devices the infiltrating axons were orientated longitudinally, with 50-75% of them deviating by less than 20° from the longitudinal axis (figure 4.10). There did not appear to be any clear advantage or disadvantage associated with any of the device designs in terms of orientation of neuronal growth in the proximal part of the device.

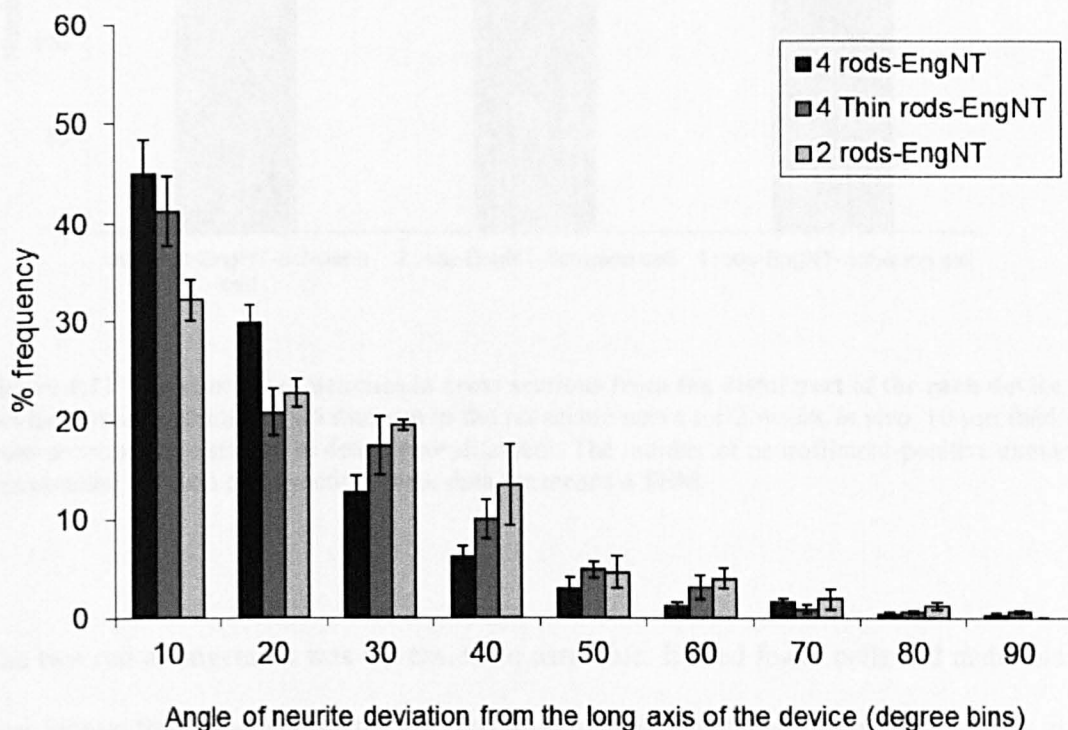


**Figure 4.10** Frequency distribution showing the angle of deviation of axon growth from the long axis of the device, in longitudinal sections from the proximal part of each device. There is a directional trend in all device groups, with a slightly higher proportion of neurites (~75%) in the 4 rods-EngNT devices deviating by less than  $\pm 20^\circ$  from the long axis, N=3, data are means  $\pm$  SEM.

Regeneration was assessed in the distal part of all the device groups. Figure 4.11 shows the number of neurites counted in cross sections from the distal part of each device (n=3 per group). There were not any clear differences in the amount of regeneration when there was more guidance material and cells (4 rods-EngNT) or increased surface area (thin rods-EngNT) compared to 2 rods-EngNT.

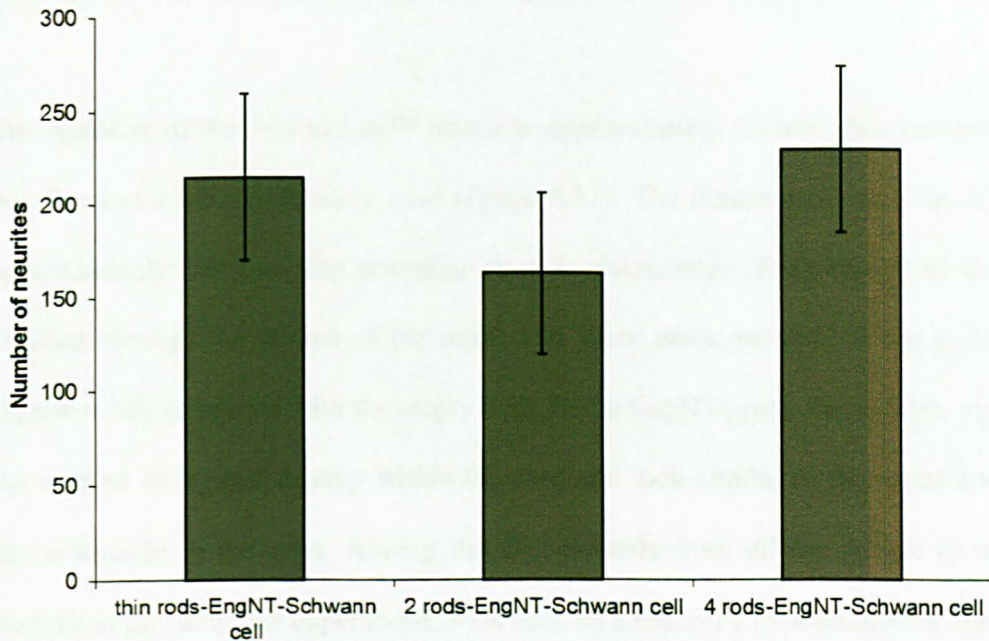


**Figure 4.11** The number of neurites in cross sections from the distal part of the each device. Devices were implanted in a 5 mm gap in the rat sciatic nerve for 2 weeks *in vivo*. 10  $\mu$ m thick cross sections were stained to detect neurofilament. The number of neurofilament-positive axons was counted for each cross section. N=3, data are means  $\pm$  SEM.

The two rod arrangement was the easiest to assemble. It used fewer cells and materials than having four rods, and so the two rod arrangement was taken forward for testing in the long gap (15 mm) model.

#### 4.2.3 *In vivo* proof-of-principle testing in the rat sciatic nerve

To test the ability of EngNT to support neuronal regeneration in a clinically more challenging model, compared to the short gap model, two EngNT rods were packed within NeuraWrap™ to form an implantable device (figure 4.1) and used to repair a critical-sized defect of a 15 mm gap in the rat sciatic nerve. The EngNT devices were compared to empty NeuraWrap™ tubes and to grafts taken from the sciatic nerves of littermates to simulate the clinical gold standard autograft. The extent of neuronal

regeneration across a 15 mm gap in the rat sciatic nerve was compared in these three surgical treatment groups, with assessment after 8 weeks of recovery.

The diameter of the NeuraWrap™ lumen is approximately 1.2 mm; this was similar to the diameter of the graft nerve used (figure 4.12). The diameter of one EngNT rod is approximately 200 µm. The scanning electron microscope (EM) images of the cross sections through the middle of the repair site show dense material in the graft group (figure 4.12), compared with the empty tube. In the EngNT group the rods are visible as the regions of highest density within the core and look similar to the appearance of a nerve fascicle in the graft. Among the first animals from all the groups to undergo surgery in this long gap experiment, 50% showed a tendency to autotomy, necessitating culling before the 8 weeks. Following veterinary advice, this was controlled in subsequent procedures by daily administration of 0.05 ml Carprofen analgesic. At the defined end-point, all the devices showed no signs of collapse, but there were some showing minor signs of degradation. In one instance, one of the empty tubes had degraded at the mid-point leaving only a thin visible tissue bridge; this was excluded from further analysis. There were no signs of adhesions and fibrosis in any of the repairs.

There were a number of outputs from this experiment, including EM analysis at the mid-point, muscle weight measurements, and histological analysis of various positions within the graft and stumps (figure 4.13). The next section (4.2.5.1) describes the results from the mid-point of the repair site in each group.



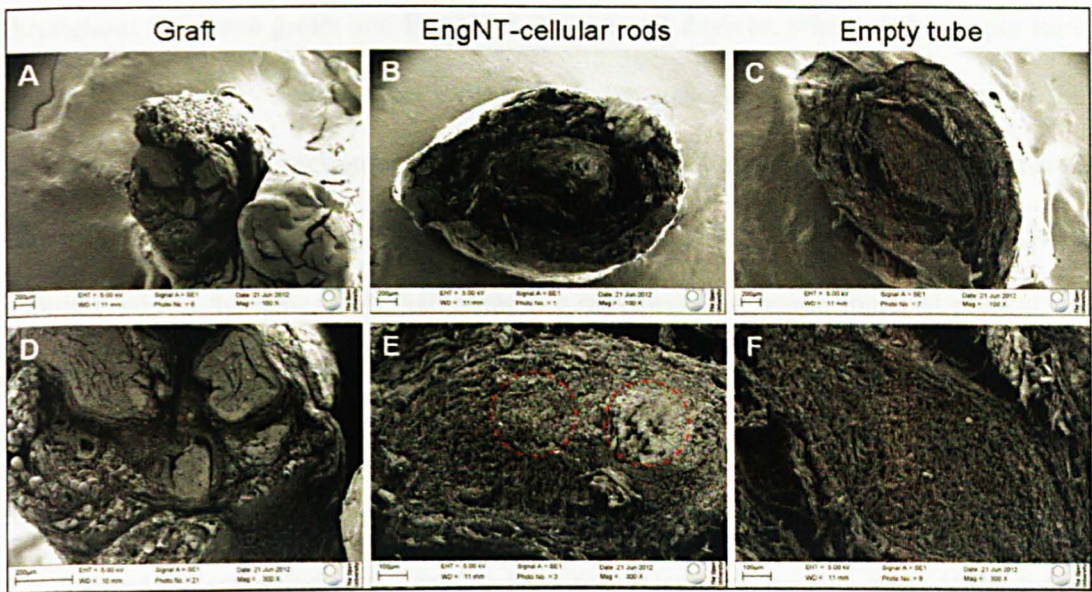


**Figure 4.12** Scanning electron microscopy images of the mid-point of the different device groups after 8 weeks *in vivo*

(A-C) Low power images of the mid-point of the devices after 8 weeks *in vivo*. Scale bars are 200  $\mu\text{m}$ . (A) graft, (B) EngNT-Schwann cell rods and (C) the empty NeuraWrap tube. (D-F) High power images of the core of the devices for graft, EngNT-cellular and empty tube, respectively. Scale bars are 100  $\mu\text{m}$ . Red outline in image E is around the EngNT rods.

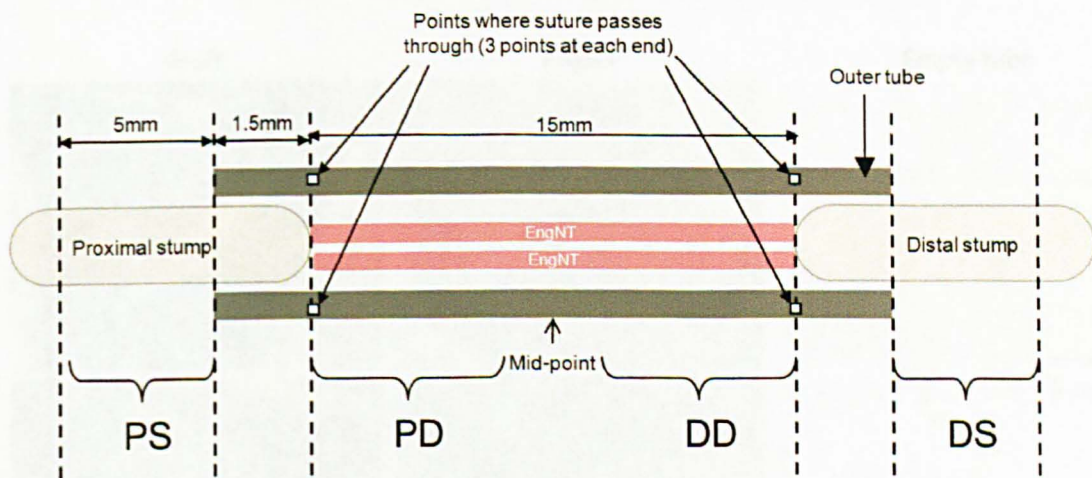


**Figure 4.13** Schematic of harvested device/graft with stumps, showing the 5 sampling positions for analysis

These are PS (proximal stump), PD (proximal part of the device), mid-point, DD (distal part of the device) and DS (the distal stump).

#### 4.2.3.1 Mid-point analysis

Transverse sections were taken from the middle of the repair site and prepared for transmission EM. Regenerated nerve tissue in each group was revealed in semi-thin sections using toluidine blue staining (figure 4.14). Dense neural tissue can be observed

throughout the nerve grafts and EngNT-Schwann cell devices, whereas the empty tube group had only very few patches of neural tissue present. Closer examination of the toluidine blue stained sections revealed the presence of longitudinally orientated nerve fibres at the mid-point of all the repairs, identified by the presence of dense myelin staining, within the densely stained areas. To maximise the neural material present for analysis in all groups, particularly in the empty tubes where the material was sparse, EM analysis was carried out in the densest areas of regeneration, as identified using the toluidine blue stain. Figure 4.15 shows transmission electron micrographs that reveal the detailed ultrastructure of the regenerated nerve tissue at the mid-point of the repair site. The axons were measured by image analysis from the electron micrographs, sampling  $1232 \mu\text{m}^2$  from each device in each group to capture at least 50 myelin profiles per repair.

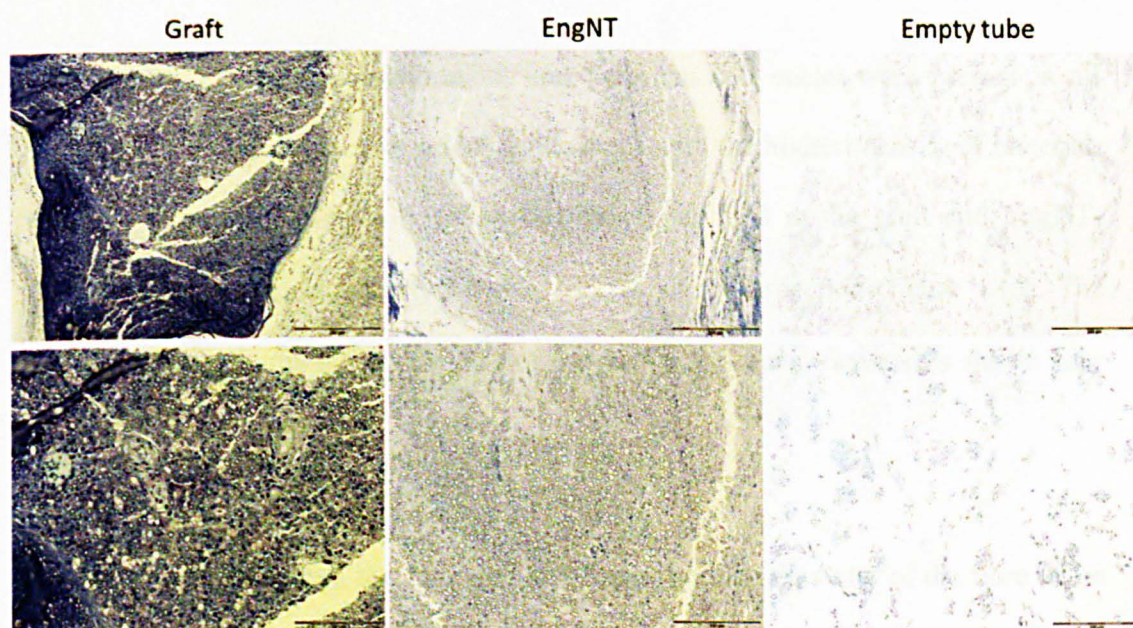


**Figure 4.14 Light micrographs of semi-thin transverse sections from the mid-point of each repair after 8 weeks *in vivo*, stained with toluidine blue**

Representative semi-thin sections stained with toluidine blue show the differences in density of neural tissue between the three groups at low (top row) and higher (bottom row) magnification (scale bars  $200 \mu\text{m}$  and  $100 \mu\text{m}$  respectively).

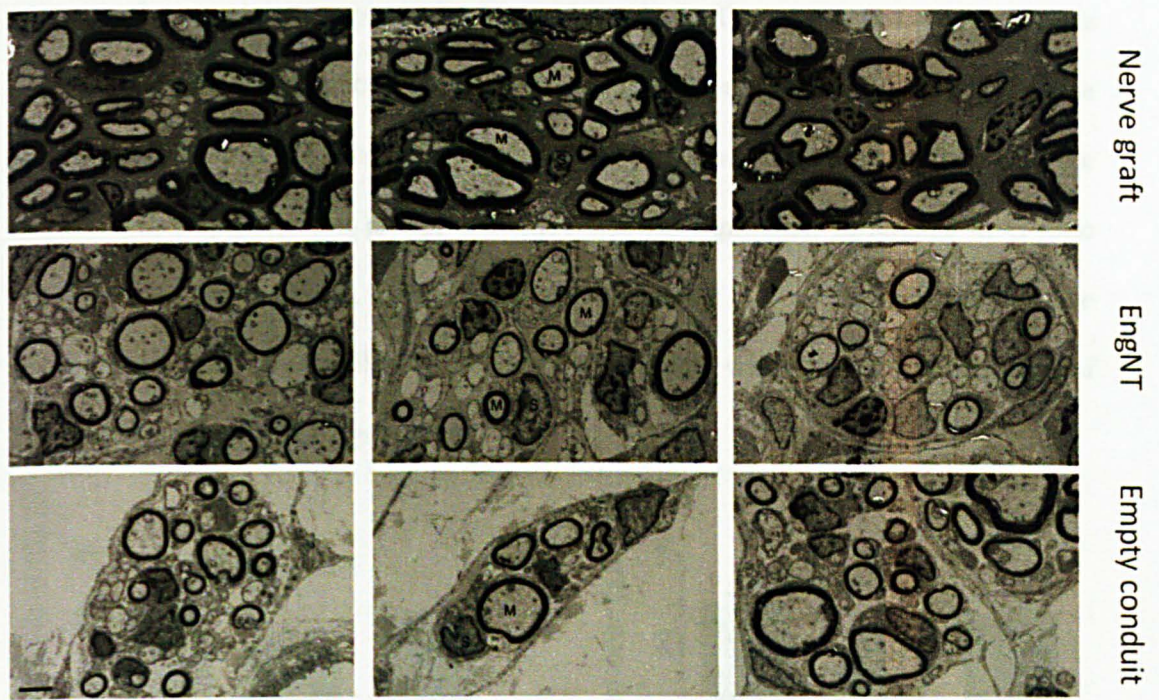


**Figure 4.15** Transmission electron micrographs of transverse sections through regenerated nerve at the mid-point of the repair site after 8 weeks *in vivo*

Areas with the highest density in each case were sampled for transmission EM (M = Myelinated axon, S = Schwann cell nucleus, scale bar 2  $\mu\text{m}$ ), with 10 fields selected from the densest regions of each corresponding semi-thin section (which was stained using toluidine blue).

Myelinated axons, unmyelinated axons and Schwann cell nuclei were present in all groups (figure 4.15). Even after selecting the areas with the highest density of material, there was a greater density of regenerated fibres per field in the graft and EngNT-Schwann cell, than in the empty tube device, by visual inspection (figure 4.15). The number of axons at the different points of the device was quantified and is shown later (figure 4.18).

For each myelinated fibre, the diameter of the axon and the diameter of the fibre (axon + myelin sheath) was measured, allowing the myelin thickness and the G-ratio (axon diameter/fibre diameter) to be determined and compared (figure 4.16) to explore the quality and extent of myelination present in each group. Both the axon diameter and the fibre diameter were significantly lower in the empty conduit group compared to the

nerve graft group when compared using a one-way ANOVA ( $P < 0.05$ ), whereas there was no significant difference between the EngNT-Schwann cell group and the nerve graft group (figure 4.16). The myelin was thicker in the nerve graft group than both the EngNT and empty conduit group, and there was no significant difference in G-ratio between the three groups, which was approximately 0.7 across all groups. The myelinated axons were smallest in the empty tube group, with a mean axon diameter of  $1.93 \pm 0.10 \mu\text{m}$  ( $\pm$  SEM), figure 4.16.

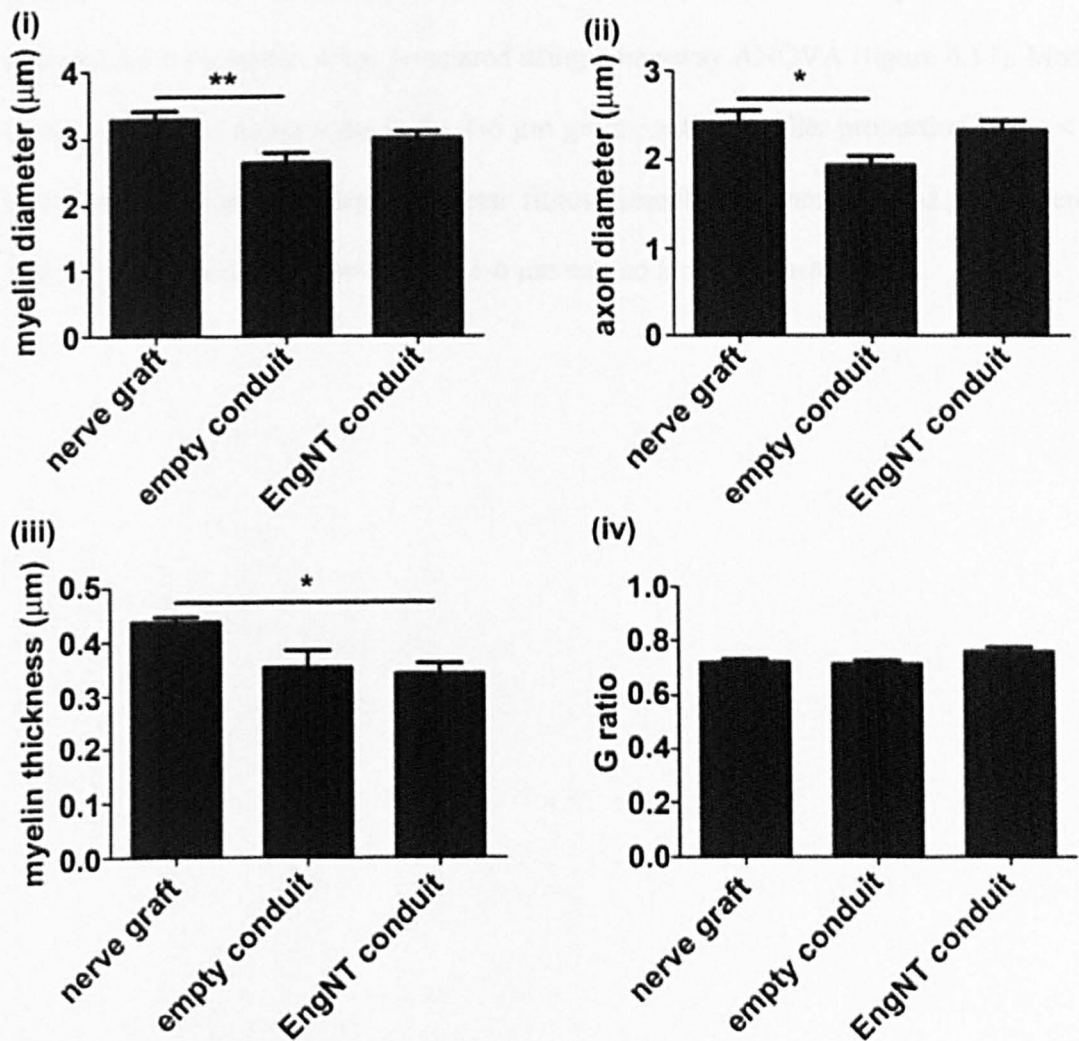


**Figure 4.16 Morphological analyses of regenerated nerve fibres at the mid-point of the repair site after 8 weeks *in vivo***

The following were assessed from transmission EM ultrathin sections: fibre diameter, axon diameter, myelin thickness and G ratio.  $1232 \mu\text{m}^2$  was sampled from each device in each group, to capture at least 50 myelin profiles per repair. Data are means  $\pm$  SEM,  $n = 5$  individual devices/grfts, \* $P < 0.05$ , \*\* $P < 0.01$ , one-way ANOVA with Tukey's post-test.

The regeneration of different fibre types can be evaluated in each device group. Fibre types were categorised according to axon diameter (classified into 4 groups:  $<1\ \mu\text{m}$ ,  $1\text{-}6\ \mu\text{m}$ ,  $6\text{-}12\ \mu\text{m}$  and  $12\text{-}20\ \mu\text{m}$ ) and whether it is myelinated or not (Michael-Titus *et al.*, 2010). The distribution of diameters for the unmyelinated and myelinated nerve fibres shows that the population of neuronal fibre types that EngNT supported was equivalent to that present in the nerve graft (figure 4.17). There was no significant difference in the proportions of the different types of fibres that were present in the regenerated nerve sampled for each repair, when compared using a one-way ANOVA (figure 4.17). Most of the myelinated axons were in the  $1\text{-}6\ \mu\text{m}$  group, with a smaller proportion in the  $<1\ \mu\text{m}$  group and very few larger diameter fibres present. The unmyelinated fibres were mainly  $<1\ \mu\text{m}$  in diameter with some  $1\text{-}6\ \mu\text{m}$  and no larger diameter fibres.

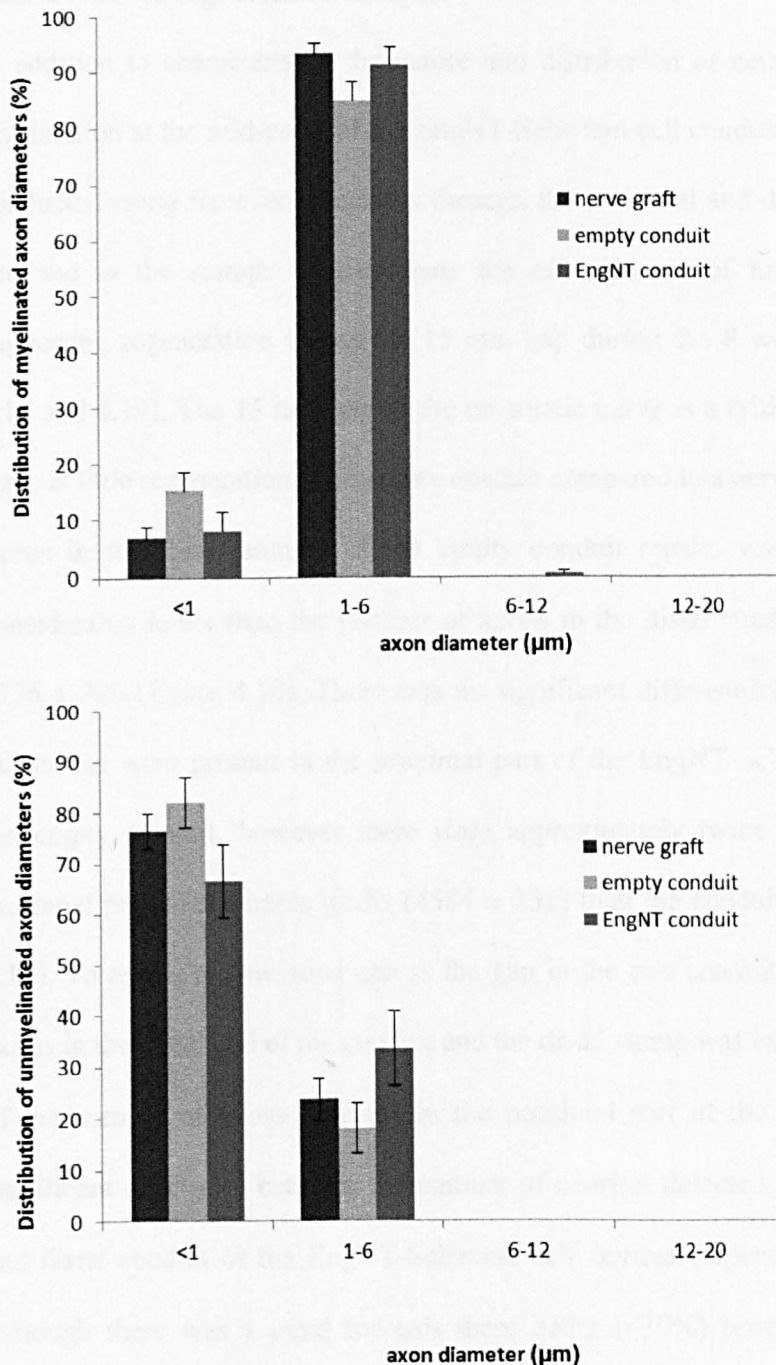
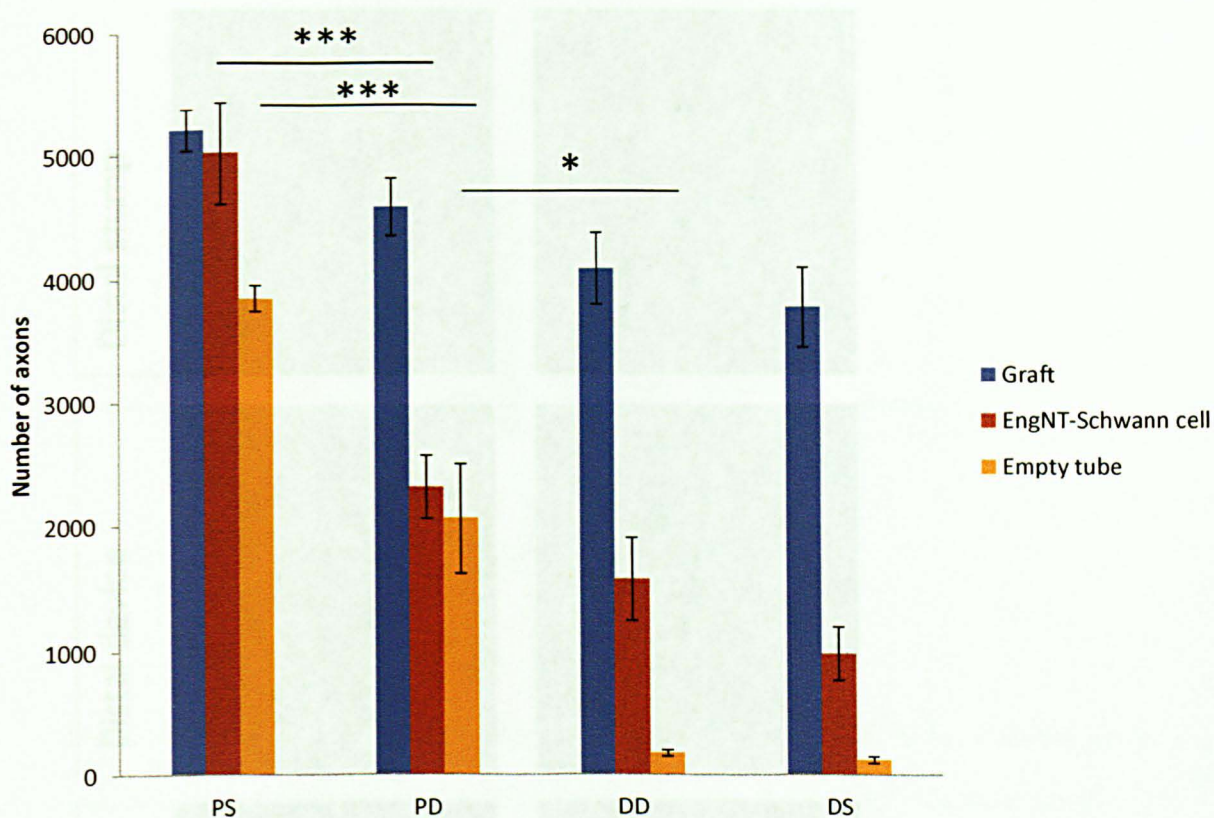


**Figure 4.17 Distribution of myelinated and unmyelinated fibres by diameter at the mid-point of the repair site after 8 weeks *in vivo***

The different fibre types are classified according to (i) whether they are myelinated or not and (ii) axon diameter: B and C fibres are <1 μm, Aδ and Aγ and B fibres are 1-6 μm, Aβ fibres are 6-12 μm and α fibres are 12-20 μm. Analysis was done from electron micrographs in a 1232 μm<sup>2</sup> sample area in the region where there was the most amount of regeneration in the mid-point of the device for each group. The proportion of the types of axons in the regenerated nerve was similar for each device group. No significant difference when compared using a one-way ANOVA, n=5 individual grafts/devices and data are means ± SEM.

#### 4.2.3.2 Neurite regeneration analysis

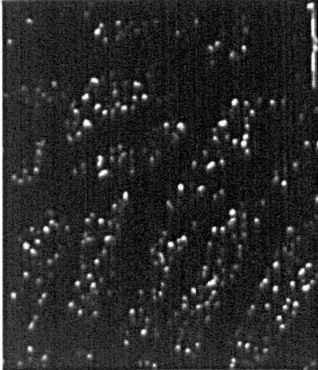
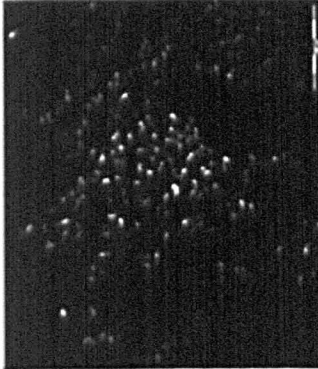
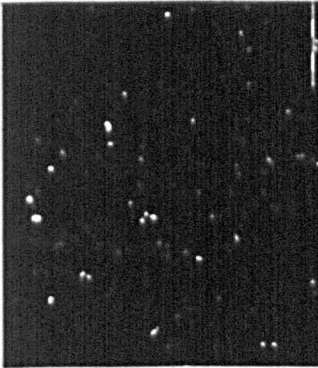
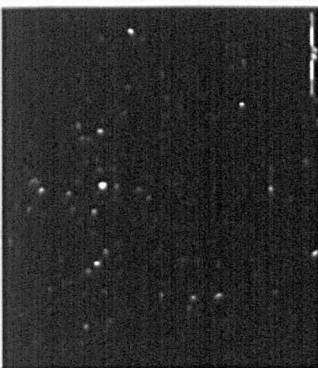
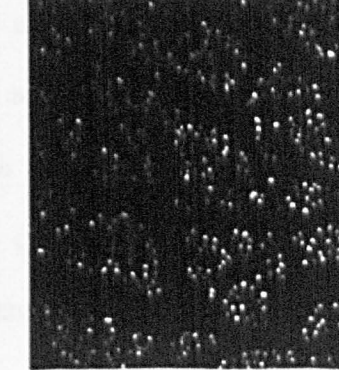
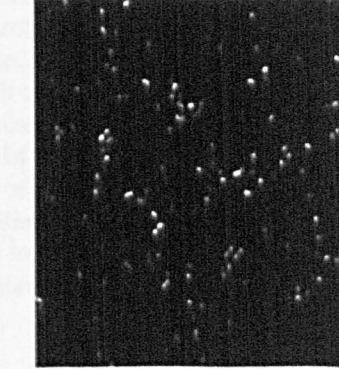
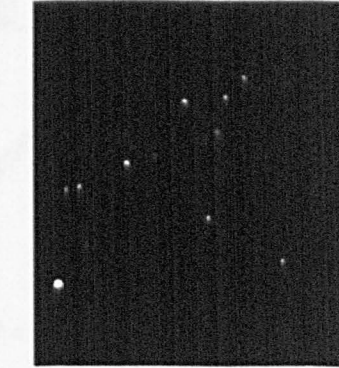
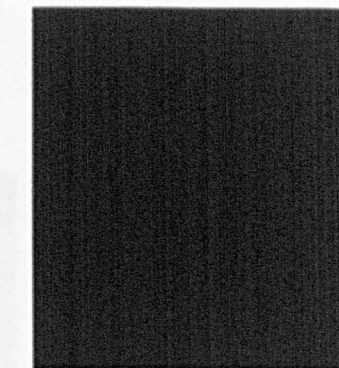
In addition to characterising the nature and distribution of neuronal regeneration and myelination at the mid-point of the EngNT-Schwann cell conduit, further analyses were conducted using transverse sections through the proximal and distal ends of the repair site and in the stumps to investigate the effectiveness of EngNT-Schwann cell in supporting regeneration across the 15 mm gap during the 8 week experiment (figure 4.18 and 4.19). The 15 mm gap in the rat sciatic nerve is a critical sized defect, where there is little regeneration in an empty conduit compared to a nerve graft. The number of axons in the distal stumps of the empty conduit repairs was  $105 \pm 29$ , which is considerably lower than the number of axons in the distal stumps of the graft repairs,  $3776 \pm 326$  (figure 4.18). There was no significant difference between the number of axons that were present in the proximal part of the EngNT-Schwann cell conduit and the empty conduit, however there were approximately twice as many axons in the proximal part of the nerve grafts ( $4584 \pm 231$ ) than the conduits ( $2014 \pm 501$ ) (figure 4.18). To assess regeneration across the gap in the two conduit groups, the number of axons in the distal end of the conduit and the distal stump was expressed as a percentage of the number of axons detected in the proximal part of the conduit. There was no significant difference between the number of neurites detected in the proximal conduit and distal conduit of the EngNT-Schwann cell devices (repeated measures ANOVA), although there was a trend towards there being (~30%) fewer neurites in the distal device than had entered the proximal part of the device (figure 4.19). In contrast, there were significantly (~90%) fewer neurites in the distal part of the empty conduit than entered the proximal part of the empty conduit.



**Figure 4.18 The number of regenerated axons in 10  $\mu\text{m}$  thick cross-sections from different parts of each device from each experimental group**

The ability of each conduit to support neuronal growth was assessed by comparing the number of axons detected at the different positions within the repairs. Total numbers of neurofilament-positive axons were counted per cross-section. PS = proximal stump, PD = proximal part of the device, DD = distal part of the device, DS = distal stump. Data are means  $\pm$  SEM,  $n = 5$  for all groups except EngNT-dADSC, which is  $n = 3$ . \* $P < 0.05$ , \*\*\* $P < 0.001$ , one way ANOVA with Tukey's post-test for  $n = 5$  repair groups.



A	Proximal stump	Proximal device	Distal device	Distal stump
EngNT				
Empty conduit				

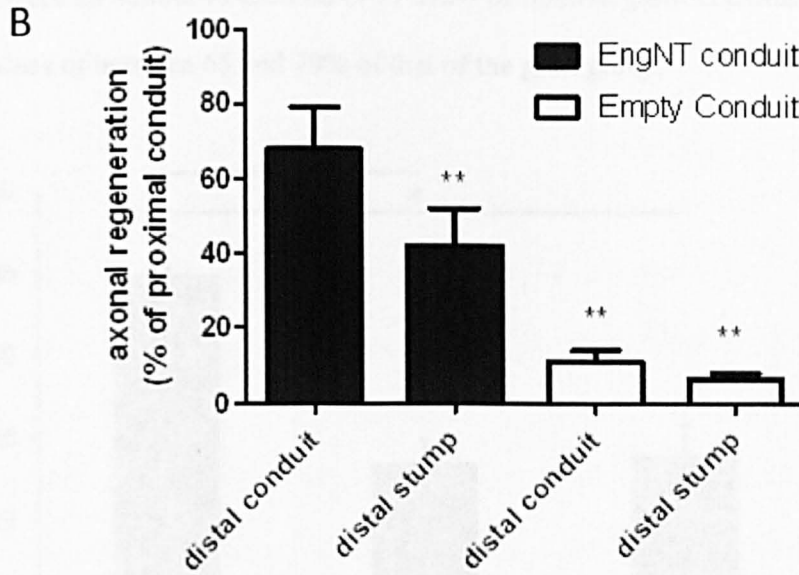


**Figure 4.19 Histological overview of axons (neurofilament-positive) in the different parts of the device**

Transverse sections were taken at different positions within NeuraWrap™ conduits containing EngNT and empty NeuraWrap™ controls, and in the distal nerve stumps, and neurofilament-positive regenerated axons were detected using neurofilament immunoreactivity. Scale bars are 100 μm (A). The ability of each conduit to support neuronal growth was assessed by comparing the number of axons detected at the proximal end to those detected at the distal end and in the distal stump (B). Data are means ± SEM showing the number of axons at each position as a % of those present in the proximal device (proximal device axon counts were 2313 ± 260 for EngNT and 2059 ± 446 for empty conduit). There was no significant difference in the number of axons present in the distal compared to the proximal EngNT conduit (\*\* $P < 0.01$ , \*\*\* $P < 0.001$ , repeated measures ANOVA with Dunnett's post-test comparing proximal regions to distal device in each case).

The atrophy of the gastrocnemius muscle, innervated by the sciatic nerve, gives an indication of the extent of motor neuron degeneration/regeneration. Relative muscle weight ratio, defined as the ratio of the gastrocnemius muscle weight from the experimental side to that of the contralateral control side (E/C), is therefore an additional way to estimate the regeneration of the motor neuron component in sciatic nerve (figure 4.20). The relative gastrocnemius muscle weight in the graft group was significantly greater than that in the EngNT-Schwann cell and empty tube groups ( $P = 0.025$ , one-way ANOVA and Tukey's test). The EngNT devices and empty NeuraWrap

repairs were all similar to each other in terms of relative gastrocnemius muscle weight, with values of between 65 and 70% of that of the graft group.

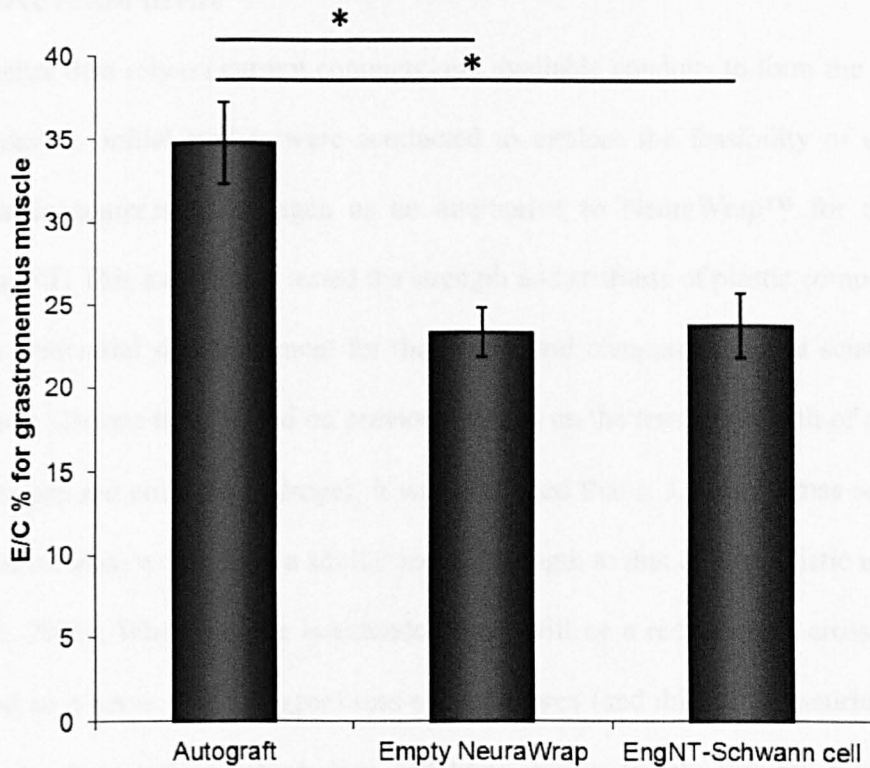


**Figure 4.20 Relative gastrocnemius muscle weight ratios after the 8 week recovery period for each experimental group**

The gastrocnemius muscles (innervated by the sciatic nerve) from both experimental and contralateral hind legs of the animal were dissected and weighed. This figure shows the percentage weight of the experimental/healthy gastrocnemius muscle. The graft group ratio was significantly greater than the EngNT-Schwann cell and empty tube groups,  $P = 0.025$  (one-way ANOVA with Tukey's post-test). Data are means  $\pm$  SEM,  $n = 5$ .

#### **4.2.4 Preliminary investigation into whether sheets of plastic compressed collagen would have the appropriate mechanical properties for use as an outer sheath for a nerve repair device**

Rather than rely on current commercially available conduits to form the outer sheath of a device, initial studies were conducted to explore the feasibility of using sheets of plastic compressed collagen as an alternative to NeuraWrap™ for the delivery of EngNT. This experiment tested the strength and stiffness of plastic compressed collagen as a potential sheath element for the device and compared it to rat sciatic nerve tissue and a silicone tube. Based on previous reports on the tensile strength of acellular plastic compressed collagen hydrogel, it was predicted that a 5.3 mm<sup>2</sup> cross-sectional area of this material would have a similar tensile strength to that of a rat sciatic nerve (Brown *et al.*, 2005). When a nerve is extended there will be a reduction in cross sectional area, and so a nerve with a bigger cross-sectional area (and thicker perineurium) could resist more stress before deformation and have greater tensile strength than a nerve of a smaller cross-sectional area.

The biomechanical behaviour of nerve, compressed collagen and silicone were tested by putting the materials under strain, increasing their length by 1 mm per minute, generating a load extension curve (figure 4.21). The x axis of the curve displays the extension as a percentage of the starting length and the y axis is the force required to stretch the material. The peak of the curve, the force at which the material fails, is defined as the tensile strength. If the slope of the curve is steep, as it is for silicone, the material is stiffer and less compliant to elongation than tissue giving a shallow curve, such as the nerve and compressed collagen samples (figure 4.21). The three rat sciatic nerves that were tested showed different tensile strength readings to each other but had a consistent characteristic profile in terms of the 'toe-region' (initial elongation with

relatively little resistance) followed by a linear extension profile (figure 4.21). They failed between 2-3 N load. The tensile strength of the plastic compressed collagen was similar to one of the nerves, which was 2 N. In contrast, the silicone curve had no ‘toe region’, and the stiffness, under the lower strains, was considerably greater than the plastic compressed collagen and nerves.

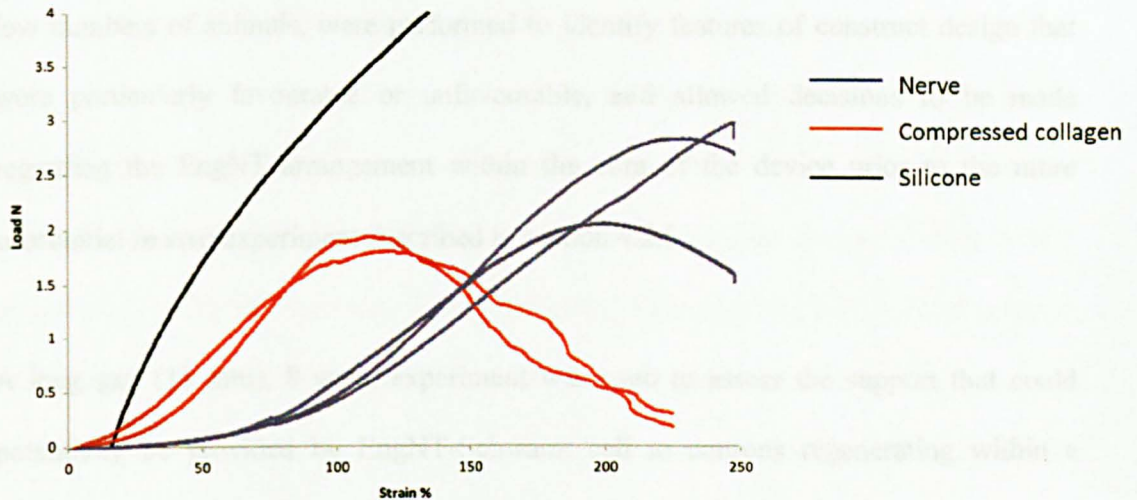


**Figure 4.21 Tensile strength testing of nerves and selected sheath elements**

Three different materials were tested, silicone (black), plastic compressed collagen (red) and rat sciatic nerve (blue). The maximal load for a material is a measure of its tensile strength (the load at which the material fails) and the slope of the linear part of the extension curve provides an indication of the stiffness of the material.

### 4.3 Discussion

In this work EngNT-Schwann cell was used to form the basis of a peripheral nerve repair device, and the results demonstrated that EngNT-Schwann cell devices can be used for the repair of critical sized defects in rat. Different arrangements and amounts of guidance material were initially tested within a silicone or NeuraWrap™ tube in a short gap (5 mm) model of rat sciatic nerve injury. These experiments, which used relatively low numbers of animals, were performed to identify features of construct design that were particularly favourable or unfavourable, and allowed decisions to be made regarding the EngNT arrangement within the core of the device prior to the more substantial *in vivo* experiment described in section 4.2.5.

A long gap (15 mm), 8 week experiment was used to assess the support that could potentially be provided by EngNT-Schwann cell to neurons regenerating within a conduit. At the mid-point of the repair there was considerably more tissue present in the EngNT group compared to the empty conduits, and electron microscopy revealed that the tissue associated with the EngNT contained densely packed nerve fibres associated with Schwann cells. Detailed analysis of the fibre types (based on diameter and presence of myelin) showed similar populations in all repair groups, with mainly smaller diameter fibres being present, in common with previous studies showing a shift towards smaller fibres in regenerating nerves compared to undamaged tissue (Ikeda and Oka, 2012).

Neuronal regeneration resembled the pattern observed *in vitro* (chapter 3), where neurites grew preferentially within the material that contained aligned Schwann cells, compared to the acellular and unaligned cellular material. Despite this, there was little difference in the orientation of neuronal growth between conduits containing aligned

and unaligned cells. Longitudinal orientation of neuronal regeneration was detected in acellular constructs too. Thus, in this short-gap model after 2 weeks, the presence of cells, aligned in EngNT or unaligned, did not significantly improve axonal guidance when compared to an acellular material.

A similar rolled conduit design, but with unaligned cells on the surface of unaligned collagen sheets, was reported by Goto *et al.* in 2009. They seeded primary rat Schwann cells on the surface of a collagen gel, above a calcium alginate gel on a porous membrane. The calcium alginate layer dissolved and the collagen gel layer with the Schwann cells detached and was then rolled to form a cellular device. In their culture study, they compared the rolled-rod design (which, like ours, had 3-4 layers of gel from central axis to the surface) with cells to a rolled-rod design without cells. They observed more neuronal growth between the layers in the rolled-rod design with cells, than in the equivalent device design without cells. This is in agreement with our findings, which showed more regenerating neurites within EngNT-Schwann cell rods than in acellular EngNT rods, and is also in agreement with most of the literature which shows neurites grow preferentially in close contact with Schwann cells (Guenard *et al.*, 1992; Fawcett and Keynes, 1990; Dubey *et al.*, 1999; Thompson and Buettner, 2006; Wang *et al.*, 2011).

EngNT could potentially be arranged in many different ways within a conduit. Two possibilities (rods and sheets) were compared and a clearer understanding of the distribution of neuronal regeneration associated with the constructs was obtained. The experiments demonstrated that the rod-based design supported a greater axon density within and adjacent to EngNT-Schwann cell than did the sheet-based design. Despite the increased EngNT volume and surface area present in the sheet constructs, there was

no associated increase in the axon density after 8 weeks, compared to the rod constructs. There was no significant difference in the numbers of neurites detected within the EngNT sheets compared to the EngNT rods (zone 1), although there was a trend towards the sheets containing a greater number (which may reflect the greater cross sectional area present in the sheets).

The increased cross-sectional area of the sheets compared to the rods (zone 1) may be due to the sheets being less compact and therefore more able to expand under physiological conditions. Rolling the EngNT into rods means they are likely to remain orientated longitudinally *in vivo*, in contrast to the sheet arrangement, which may twist or kink post-implantation. EngNT rolled to form rods will combine cell-level guidance provided by the EngNT-Schwann cell material with 'z' direction guidance across the cross section of the construct (Bellamkonda, 2006).

Neurite growth was observed within the layers of the rods, although it was hard to establish precisely whether the growth was on the surfaces or within the collagen. However when the amount of surface area (zone 2) was increased using sheets there was not an increase in the growth. This is in contrast with the study by Goto *et al.* where more growth was observed in the cellular rolled-rod design than in a cellular rod design (where there are no layers) (Goto *et al.*, 2009).

The rod-based devices were easier to handle and therefore could be assembled within conduits reproducibly, compared to the sheet-based devices in which it was difficult to position the layers of the material. The greater neurite density associated with the rods ( $3350 \pm 143$  axons/mm<sup>2</sup>) compared to the sheets ( $2920 \pm 587$  axons/mm<sup>2</sup>), although not significant, implies that multiple rods may be more optimal for regeneration within a



conduit than the equivalent amount of sheet material; so the rod-based design was taken forward for use in the subsequent experiments.

In the experiment to investigate the various EngNT rod formats, to see whether increasing the surface area by having thinner rods or increasing the amount of guidance material and cells by implanting more EngNT rods, would affect the amount of neuronal regeneration; there was a similar amount of regeneration in the distal parts of the devices for all device groups. The 5 mm gap model at 2 weeks may not fully demonstrate the advantages or disadvantages of the different device designs in terms of their ability to support neuronal regeneration. The differences between the devices in this respect may be better highlighted by using a 5 mm gap model at a shorter time point or a longer gap model at 2 weeks. A previous study by Yao and colleagues compared the number of axons that had grown through multi-channelled collagen conduits: 1-channel versus 2-, 4- and 7-channel conduits. No significant difference was observed between groups in a 7 mm gap for 6 weeks in the rat sciatic nerve model, showing that the difference in surface area did not affect the amount of axon regeneration in this model (Yao *et al.*, 2010). In this experiment, there was no difference in the amount of regeneration in the distal parts of the devices, if the rods are thinner, or double the number of them. This may be because in short gaps the presence or absence of Schwann cells makes little difference; it is only in longer gaps where they become more important (Angius *et al.*, 2012).

It would be interesting to examine other ways to organise EngNT within conduits in future experiments using critical-sized gaps, in order to optimise regeneration support and ease of assembly. Other tissue engineering approaches for the development of repair devices with intraluminal guidance structures are more conventional in their

approach (Bell and Haycock, 2012; Daly *et al.*, 2012; Nectow *et al.*, 2012), in which porous or fibrillar scaffolds are manufactured with surface modification to support cell attachment, followed with a cell seeding step prior to implantation. Similarly to the EngNT approach, these approaches can deliver cell-level and longitudinal guidance through the repair site and the designs can be adapted for the repair of different sized nerves. However they are in contrast to the EngNT approach in terms of their cell-scaffold relationship, where in EngNT the cells are more intimately associated with the matrix, which resembles natural endoneurium (aligned fibrils of type I collagen) (Mason and Phillips, 2011). The cell matrix interactions that shape the anisotropic structure in EngNT are similar to those that occur naturally in tissue development and remodelling, and the complex spatial and mechanical cues that arise when cells are forced to grow on stiff surfaces (such as within pores and channels or on the surfaces of fibres) are thus avoided (Grinnell, 2003; Phillips and Brown, 2011). Furthermore, the use of plastic compression to stabilise the material avoids the need for chemical cross-linking agents and retains the protein in a native state suitable for integration with host tissue.

Based on observations from the short gap experiments, EngNT-Schwann cell rolled to form rods was selected for a more detailed investigation of regeneration support *in vivo* using a longer gap. A 15 mm gap length and 8 week time point were appropriate for this investigation because under these conditions a clear difference in regeneration between the empty tube and the autograft group was evident, which was not apparent in shorter gap experiments (Angius *et al.*, 2012).

Investigation of nerve regeneration at the mid-point of the repairs, showed there was considerably more regenerated neural tissue present in the EngNT-Schwann cell groups

compared to the empty conduits, and electron microscopy revealed that the EngNT-Schwann cell contained densely packed nerve fibres associated with Schwann cells.

The quality of regeneration in the EngNT-Schwann cell devices, as quantified by transmission EM, is similar to that observed in the graft group. There was not much difference in the profile of myelin, axon and fibre diameter in the graft and EngNT groups. However, the fibre diameters were significantly greater in the graft group than the empty tube group (\*\* $P < 0.01$ ) and axon diameter was significantly lower in the empty tube group than the grafts (\* $P < 0.05$ ).

Detailed analysis of the fibre types (based on diameter and presence of myelination) showed similar populations in all repair groups, with mainly smaller diameter fibres being present, in common with previous studies showing a shift towards smaller fibres in regenerating nerves compared to undamaged tissue (Ikeda and Oka, 2012). At the 8 week time point in a 15 mm sized defect, there was no difference in the types of fibres that had regenerated. Axons that do not make peripheral connections undergo atrophy and eventually disappear, whereas axons that do make peripheral connections mature and enlarge in size (Allodi *et al.*, 2011). Perhaps therefore, in repairs where axons reinnervate target organs, a later time point than used in this study, fewer and/or larger axons would be observed. Also, one regenerating axon may support over 10 axon sprouts (Witzel *et al.*, 2005), which would decrease in time as they do not all make peripheral connections, so fewer axons may be observed at a later time point.

In addition to the transmission EM data obtained from the mid-point of the repair, histological analysis of the number of neurites present at 4 positions within the repaired

nerve revealed details about the ability of this initial EngNT-based device to support neuronal regeneration from proximal to distal stump.

Approximately half as many neurites entered the EngNT devices compared to the nerve graft, possibly because the two EngNT rods only occupied a fraction of the lumen so did not form a complete interface with the cross-section of the proximal stump. Future work should therefore include optimising the quantity and arrangement of EngNT components within a device in order to maximise proximal ingrowth. Of the neurites present in the proximal part of the EngNT-Schwann cell repair devices, approximately 70% successfully reached the distal part of the devices and approximately two thirds of these entered the distal stump. This was in contrast to the empty tube, where only 10% of the neurites present at the proximal end regenerated through the empty conduit.

The *in vivo* experiments demonstrated that there is potential for EngNT to be used within a nerve repair conduit in order to promote neuronal regeneration across a critical sized defect. The EngNT device was more effective than the empty conduit. Further work will be required to optimise the device design and investigate different amounts and arrangements of the EngNT within NeuraWrap™ to increase the amount of neuronal growth entering the device.

EngNT mimics neural graft tissue, in which key cellular features are known to contribute to the repair process (aligned Schwann cells in an aligned matrix). The aligned Schwann cells within EngNT resemble the Bands of Büngner to provide physical guidance cues to the regenerating axons. The *in vitro* experiments (chapter 3) suggest that the cells within EngNT secrete factors to promote regeneration, which is in line with previous reports (Hall, 2005; Rodrigues *et al.*, 2012). However, although

EngNT does not initially mimic the basement membrane, laminin structures, perineurial cells or vasculature, over time, the cells could modify the environment. By providing the essential elements (the Schwann cells, alignment and collagen), theoretically it is possible to facilitate modifications post-implantation, such as the laying down of other extracellular matrix proteins (e.g. laminin) or vascularisation as a result of blood vessels growing through the device.

There was no significant difference in the gastrocnemius muscle weight ratio for the experimental to the contralateral muscle. In a peripheral nerve regeneration study using a graft, empty fibrin conduit and a fibrin conduit with Schwann cells after a 16 week recovery period, higher muscle weight ratios were observed of  $0.51 \pm 0.03$  for the graft group and  $0.45 \pm 0.02$  for the repairs with implanted Schwann cells (di Summa *et al.*, 2011), compared to the ratio observed in this study with Schwann cells after 8 weeks ( $23.8 \pm 1.9$ ). Thus, suggesting that a longer-term group is needed to assess the effects of functional recovery.

The acellular plastic compressed native rat tail collagen ( $5.3 \text{ mm}^2$  cross sectional area) for use as a device sheath is close to rat sciatic nerve in terms of strength and stiffness. Therefore for a sheath to encompass a lumen that is 2 mm in diameter, the thickness of the sheath would need to be 1.3 mm, which is reasonable. It would be important to calculate the stiffness modulus to compare to other materials, including human nerve and NeuraWrap™. For example, if the cross sectional area is measured accurately then the stiffness modulus could be calculated. An initial attempt to estimate the stiffness modulus, indicated by the gradient of the linear part of the curve, is about  $2.43 \pm 0.33$  N/mm for plastic compressed collagen and  $2.25 \pm 0.18$  N/mm for rat sciatic nerve. These values are higher than those reported in the literature for rat sciatic nerve, which

are about  $0.37 \pm 0.13$  N/mm, as calculated from force/extension curves (Hayes *et al.*, 2007). This difference may be because the sciatic nerve has a number of branch points which may influence the local mechanical environment. Therefore, plastic compressed collagen for use as a sheath material shows promise in terms of its mechanical properties. There are studies that have shown that collagen guidance tubes enhance peripheral nerve regeneration, compared to silicone tubes (Chamberlain *et al.*, 1998; Spilker, 2000). Further to this, a study in 2012 also showed there was significantly less extraneural adhesion with collagen membranes than vein grafts, which are also currently used in the clinic, when tested in the rat sciatic nerve model after 3 months *in vivo* (Mathieu *et al.*, 2012). Further work is required to investigate other properties of plastic compressed collagen, including suture pull-out thresholds, degradation rate and resistance to extraneural adhesions. Since outer sheath development was not the main focus of the current project, this was not pursued further, and instead the remaining experiments focussed on testing core element constructs within the clinically approved NeuraWrap™ outer tube.

The main goal of this part of the study was to optimise the arrangement of EngNT within the core of a device in a short gap model (in terms of axon regeneration density), and then use the optimal device design to assess the feasibility of using EngNT in the device core to repair a gap in the rat sciatic nerve that is representative of the clinical situation (15 mm).

The standard EngNT rod constructs supported high density axon growth and there were not any clear advantages to increasing the surface area or quantities of EngNT-Schwann cell in terms of regeneration using the short gap and time point models. It has also been demonstrated that EngNT-Schwann cell can be used for the repair of critical sized

defects in which an empty conduit performs poorly compared to a nerve graft. The production of this device is simple, rapid and reproducible. The adjustable diameter of the NeuraWrap™ outer tube and the modular rod design would be advantageous for the production of a range of devices with different diameters. Finally, the three-stage process of self-alignment, plastic compression and rolling is potentially appropriate for scale-up and automation for use in clinical and commercial settings.

## **5.0 Investigating the feasibility of making an EngNT nerve repair device using clinically relevant cells and materials**

### **5.1 Introduction**

Having demonstrated that an implantable device containing EngNT-Schwann cell could support neuronal growth *in vivo*, this study went on to investigate the feasibility of constructing a repair device from EngNT using clinically relevant cells and materials. The design of the peripheral nerve repair device can be divided into two parts: the outer sheath and the core. A range of clinically relevant outer sheath materials are available (discussed in chapter 4) such as the NeuraWrap™ tube manufactured by Integra, which was used in these experiments. This part of the study begins to investigate some therapeutic cell types and collagen sources that can potentially be used to make EngNT to form the device core.

Schwann cells have been used in previous studies to promote regeneration in nerve repair models (Duncan *et al.*, 1981; Bunge, 1994; Ide, 1996; Terenghi, 1999; Wiberg and Terenghi, 2003; Angius *et al.*, 2012); however, for clinical use there are limitations to the availability of these cells. Autologous human Schwann cells would need to be derived from invasive nerve biopsies and sufficient numbers for regeneration would only become available after a lengthy expansion time *in vitro* (Guest *et al.*, 1997). Schwann cell-like cells derived from stem cells are therefore a more attractive source (Walsh and Midha, 2009). There are a range of cell types that can potentially be used within a nerve repair device, including autologous and allogeneic cells.



### **Autologous cells**

An autologous therapy is where the patient's own cells are used, whereas allogeneic cells are derived from another person. Autologous cells are generally considered to be more readily accepted by the patient because they do not provoke an immune reaction (Mosahebi *et al.*, 2002; Rodrigues *et al.*, 2012).

There are drawbacks associated with autologous cell therapies, including variability between patients in yield and quality of cells, a more complex clinical route to patients than with an off-the-shelf allogeneic therapy, and in particular the time delay that results from expanding the cell populations. Such delays can, in turn, delay the repair operation, which can negatively impact regeneration. A study by Wu *et al.*, compared nerve regeneration in the rat sciatic nerve model when it was repaired (using the primary repair method) at 1, 4, 6, 8 and 12 weeks after damage. Their results showed that whilst there was no significant difference in regeneration in the repairs carried out after 1 and 4 weeks in terms of compound muscle action potential (CMAP) amplitudes, repairs after 4 weeks showed reduced amplitudes (Wu *et al.*, 2013).

Adult stem cells can be obtained from the patient for use in an autologous therapy; however, before these cells can be approved for use in clinical applications, there are challenges to overcome such as availability of the cells, efficacy, safety and ethical issues. Table 1.3 (chapter 1) summarised some of the cell types that have been or are being used in research in the field of peripheral nerve repair. Schwann cells are embryologically derived from the neural crest (Le Douarin and Dupin, 2003; Woodhoo and Sommer, 2008). Some neural crest stem cells (NCSCs) persist in adults in sites of gliogenesis such as the sciatic nerve and dorsal root ganglia (DRG), and in the bulge area of hair and whisker follicles, where they give rise to melanocytes (Sieber-Blum *et*

*et al.*, 2004; Rodrigues *et al.*, 2012). A study by Aquino *et al.* has shown that mouse NCSCs can be differentiated into Schwann cell-like cells in the presence of neuregulins and implanted in suspension within a silicone tube to promote neuron regeneration in a 10 mm gap in rat sciatic nerve (Aquino *et al.*, 2006). Dental pulp is also a source of NCSCs that is easily accessible (Gronthos *et al.*, 2000). Some NCSCs express neural-progenitor protein markers, even in basal culture conditions (Janebodin *et al.*, 2011; Gronthos *et al.*, 2002). The main disadvantage is that the yield of NCSCs is low in comparison to adipose or bone-marrow tissue sources.

Bone marrow mesenchymal stem cells (BM-MSCs) are another source of adult stem cells, which have been extensively studied and characterised for use in cell therapies (Walsh and Midha, 2009). BM-MSCs can be differentiated into Schwann cell-like phenotypes expressing GFAP, S100 and p75 and have been used to enhance neuron regeneration (Dezawa *et al.*, 2001; Shimizu *et al.*, 2007). Wakao *et al.* have shown that autologous BM-MSCs differentiated *in vitro* to Schwann cell-like cells within a conduit containing a collagen sponge structure that filled the lumen, and promoted regeneration of median nerve injuries in monkeys (Wakao *et al.*, 2010). Interestingly, there have also been studies that have used undifferentiated BM-MSCs directly for peripheral nerve repair. A study by Hu *et al.* (2007) demonstrated that allogeneic decellularised nerves filled with autologous undifferentiated BM-MSCs also promoted functional recovery when placed in ulnar nerve gaps of non-human primates.

Autologous adipose tissue is another source of multipotent MSCs. Stem and progenitor cells usually make up less than 5% of the total cell population in adipose tissue (Fraser *et al.*, 2006), but this is 2500-fold more than the frequency of such cells in bone marrow (D'Ippolito *et al.*, 1999). The abundance of adipose-derived stem cells (ADSCs) and the

ability to collect large amounts of adipose tissue via liposuction potentially eliminates the need for cell expansion. A study that compared different sources of MSCs from the same rats, reported that ADSCs proliferate significantly faster than BM-MSCs *in vitro* (Yoshimura *et al.*, 2007). Culture studies have shown that ADSCs have protective effects on DRGs; and implantation of these cells causes significantly increased expression of mRNA of anti-apoptotic Bcl-2 and decreased mRNA of pro-apoptotic Bax and caspase-3 in DRGs, therefore promoting a neuro-protective effect (Reid *et al.*, 2011). Rat ADSCs differentiated into Schwann cell-like cells (dADSCs) express a range of Schwann cell proteins such as GFAP, p75 and s100 and can promote neurite outgrowth *in vitro* (Kingham *et al.*, 2007; Tomita *et al.*, 2012). It has also been reported that dADSCs can promote nerve regeneration in the rat sciatic nerve injury model (Gu *et al.*, 2012; di Summa *et al.*, 2010; Tomita *et al.*, 2012).

Certain important features of ADSCs mean that, compared with BM-MSCs, these cells offer advantages in terms of therapeutic potential. These features include a less invasive harvest procedure, high cell viability, and favourable culture and expansion properties. ADSCs have also shown promise in other therapeutic areas and are in clinical trials for autologous treatment of acute myocardial infarction (Europe, ClinicalTrials.gov Identifier: NCT01216995 and NCT00442806), chronic myocardial ischaemia (Europe, ClinicalTrials.gov Identifier: NCT00426868) and in the area of reconstructive surgery after lumpectomy in breast cancer (ClinicalTrials.gov Identifier: NCT00616135). Cytori Therapeutics, Inc. have developed a Tissue Processing System (the Celution® 800/CRS Device), which is approved for certain uses in Europe and which is used in the above clinical trials. This device automates and standardises the extraction, washing, and concentration of a patient's own ADSCs.

### **Allogeneic cells**

Alternative cell types are being used to create cell lines for potential allogeneic cell therapies. An allogeneic cell therapy is where the donor cells are not from the patient. Allogeneic cells are human in origin and potentially immunogenic and so are likely to evoke a reaction unless the patient is immunosuppressed prior to and post-implantation (Mosahebi *et al.*, 2002).

Potential allogeneic cell lines that could be used in EngNT within a repair device were identified through a comprehensive literature study (carried out in November 2012) to identify the cells currently used in clinical trials for nervous system cell therapies (reported in Table 5.1 in the next section). For example, the ReNcell CTX cells (human neural progenitors), which are currently in a clinical trial to treat Stroke, by ReNeuron (Guildford, UK); and MultiStem cells (human adult mesenchymal stem cells), which are currently in clinical trials for the treatment of multiple diseases and conditions, including neurological conditions by Athersys (Cleveland, Ohio, US).

Based on the literature study, the following cells were selected for investigation within this project:

- Adipose-derived stem cells differentiated into Schwann cells (dADSCs) – potential for high yield; derived from ADSCs which are in Table 5.1; existing technology for harvest and purification; literature on nerve repair.
- ReNcell CX neural progenitors: undifferentiated (uCX) and differentiated (dCX) – neural; availability of research grade equivalent cells ('CX' refers to the cell line available to buy for research, whereas 'CTX' refers to the cells used in their clinical trials); factor-free differentiation.

- Neural crest stem cells (NCSC) – potential for minimally invasive autologous harvest; demonstrated efficacy in SCI; correct Schwann cell lineage.
- Mesenchymal stem cells (MSC) – long-established transplantable cells; potential for allogeneic or ‘off-the-shelf’ use, for example MultiStem cells. The cells used in this study were primary rat bone-marrow mesenchymal stem cells.

Company	Cell type	Development	Indication
Geron (US)	GRNOPC1 (oligodendrocyte progenitor cells, derived and differentiated from hESCs)	Phase I 5 Patients treated.	Acute spinal cord injury. Therapy indicated at 7-14 days after injury.
ReNeuron (UK)	ReNcell CTX cells are neural progenitors (adult neural stem cells derived from 12-week-old foetal tissue). Committed, not pluripotent. Genetically engineered to be conditionally immortal. Some technology licensed from StemCells Inc.	Phase I/II First patient has been treated	Ischaemic stroke. Therapy indicated at 6 months to 2 years after injury. No immunosuppression
StemCells, Inc. (Europe)	HuCNS-SC (adult stem cells derived from fetal tissue).	Phase I/II First patient has been treated	Chronic spinal cord injury. Patients are immunosuppressed
Cytori Therapeutics, Inc. (Europe)	Autologous adipose-derived regenerative cells (ADRCs, also called ADSCs)	Phase I/II First patient has been treated.	Heart disease and reconstructive surgery. No immunosuppression
Advanced Cell Technology (ACT) (US)	Retinal pigment epithelial (RPE) cells derived from human embryonic stem cells	Phase I/II. 3 patients have been treated	Stagardt's Macular Dystrophy and dry AMD
Athersys, Inc.	Multistem® derived from human bone marrow	Phase I/II for all 3 areas investigated. Pre-clinical for spinal cord injury.	Cardiovascular disease, immune system disorders and neurological disorders like ischaemic stroke. Inflammatory bowel disease. No immunosuppression

**Table 5.1 Therapeutic cells currently in clinical trials for nervous system repair/regeneration**

Literature search was conducted in November 2012.

In this chapter, the results of using these three types of autologous cells (NCSCs, BM-MSCs, and ADSCs) and ReNcell CX (research grade) cells, for a potential allogeneic therapy, within EngNT are described. To investigate whether these cell types could be used to form EngNT and whether the resulting material would support and guide neurite outgrowth, they were first tested in the *in vitro* assay described in section 3.2.4. In cases where initial data looked promising, analysis of gel contraction and cellular alignment were carried out. The differentiated ADSCs (dADSCs) and the differentiated CXs (dCXs) were taken forward for testing *in vivo* in a pre-clinical model. The EngNTs with aligned cells were rolled into rods and tested within a NeuraWrap™ tube (see figure 4.1). Using the rat sciatic nerve model, repair of a long gap (15 mm) was assessed after 8 weeks. This was so the study could test the potential of therapeutic cells in a pre-clinical model, and use the previous long gap experiment (section 4.2.3) as control data.

In addition to exploring some of the possible options for selecting a clinically relevant source of cells for EngNT, this part of the study also explored suitable sources of collagen. Bovine collagen is currently being processed according to GMP regulations and implanted in various forms such as, for example, the NeuraWrap™ conduit for nerve repair. However the collagen that is generally used for current surgical purposes would not be suitable for EngNT since it tends to contain enzymatically prepared ateloptides rather than native acid-solubilised type I collagen. As a step towards finding a more suitable alternative to the acid-solubilised rat collagen used in the previous chapters, a commercially available source of bovine collagen was tested to see if it could be used to form EngNT.

The overall aim of this part of the study was to investigate the feasibility of constructing a repair device from EngNT using clinically relevant cells and materials. This was divided into two objectives:

- (i) To test bovine collagen type I for use in EngNT;
- (ii) To identify and test appropriate cell types, exploring both autologous and allogeneic cells *in vitro*. The cells that were able to promote guided neuronal growth *in vitro* were tested in the rat sciatic nerve model.

The rat sciatic nerve model was used to compare the nerve graft (current gold standard treatment), device containing EngNT-Schwann cell and an empty NeuraWrap™ tube to a device containing EngNT-dADSC rods and a device containing EngNT-dCX rods within a NeuraWrap™ tube. The aim of this *in vivo* experiment was to provide an indication of the efficacy of dADSCs and dCXs in a peripheral nerve therapy based on EngNT, to support and guide neuronal regeneration across a critical sized defect.



## 5.2 Results

### 5.2.1 Investigating the use of bovine collagen for the production of EngNT

A contraction profile using free-floating gels containing Schwann cells was established to give an indication of the ability of the cells to generate tension within bovine collagen gels. Figure 5.1 shows the contraction profile for Schwann cells in bovine and rat type I collagen (2 mg/ml) at a range of cell densities:  $1-6 \times 10^6$  cells/ml of gel. The percentage of gel contraction increased with cell density and began to plateau at a density of  $4 \times 10^6$  cells/ml in the bovine collagen gels. There was more contraction (80%) in the bovine collagen gels at this density than in the rat collagen gels, which was around 70%. Having established that similar contraction behaviour occurred with Schwann cells in bovine collagen as in rat collagen, the same Schwann cell density that was used in previous experiments,  $4 \times 10^6$  cells/ml, was used for subsequent experiments.

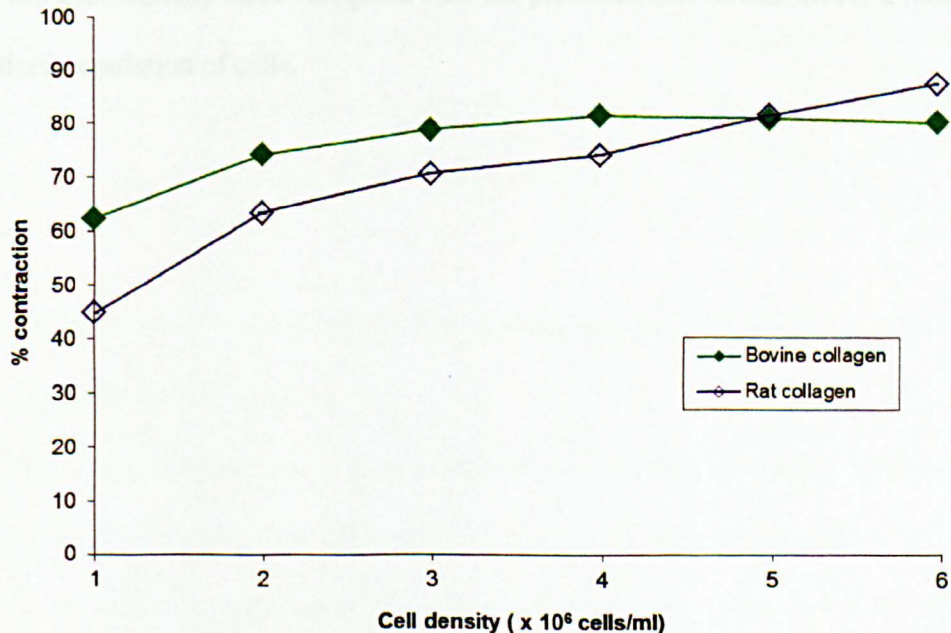


**Figure 5.1 Contraction profile for Schwann cells in bovine and rat collagen gels**

Schwann cells were seeded at a range of cell densities ( $1-6 \times 10^6$  cells/ml) within  $75\mu\text{l}$  collagen gels (2 mg/ml bovine or rat collagen) in a 96-well plate. Gels were photographed following overnight incubation and % contraction was determined  $\{[(\text{original gel area} - \text{contracted gel area}) / \text{original gel area}] * 100\}$ . Data are means  $\pm$  SEM from 4 replicate gels within one culture.

The next step was to assess the effect of plastic compression on Schwann cell survival in bovine collagen gels. Cellular gels were subjected to compression for 1 minute and cell death was assessed using propidium iodide and Hoechst immediately after compression. Less than 1% cell death was observed post-compression,  $0.9 \pm 0.7\%$  (mean  $\pm$  SEM; n=4).

Following this, cellular alignment was assessed in EngNT made using bovine collagen. Bovine collagen EngNT sheets with Schwann cells were fixed and stained to detect S100 and alignment was quantified as previously (chapter 3). Figure 5.2 A and B show the aligned Schwann cells in EngNT made using bovine collagen (cells were elongated and orientated in the same direction). Cell elongation was similar to that of Schwann cells in rat collagen, figure 5.2 C. The line of best fit shows that the degree of cell elongation is slightly less pronounced in bovine collagen than in rat collagen, but cells were still considerably more elongated than the predicted line of best-fit for a randomly organised population of cells.

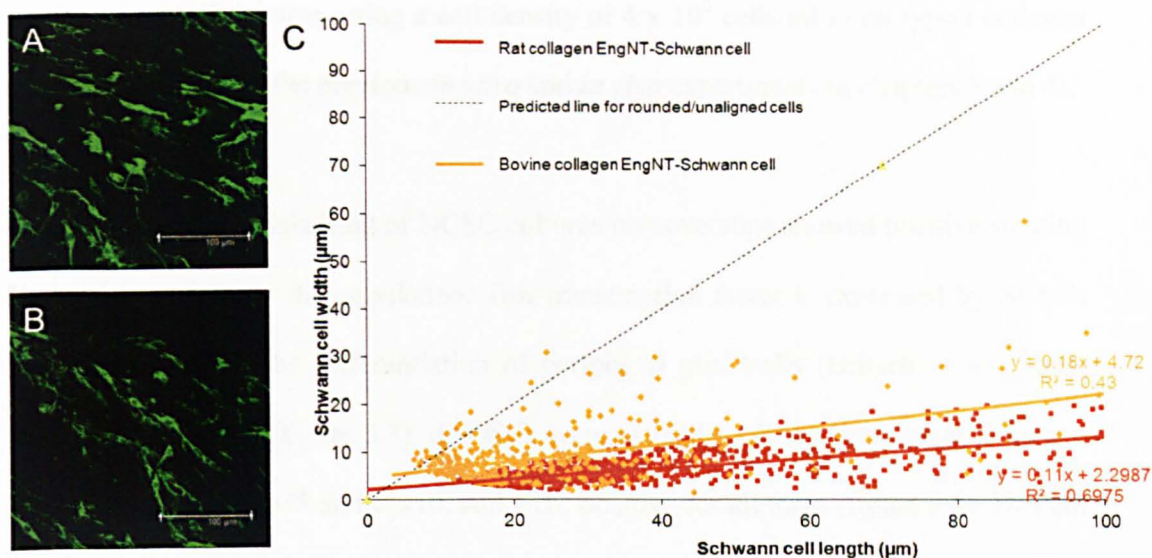


**Figure 5.2 Schwann cell orientation in EngNT made with bovine collagen**

**A-B**, Representative confocal micrographs showing Schwann cells (S100, green) in EngNT made with bovine collagen (z stack is 15-20µm thick, 1 µm step size). **C** Scatter plot showing the aspect ratio for each Schwann cell in the areas sampled, after compression in bovine (orange) and rat (red) type I collagen gels.  $4 \times 10^6$  cells/ml cell density was used. Sampled  $640,000 \mu\text{m}^2$  per gel,  $n=3$  independent gels.

These results indicated that Schwann cells can contract the bovine type 1 collagen matrix and self-align within the fully hydrated tethered gel. Schwann cell alignment is retained in bovine EngNT (post-plastic compression).

### 5.2.2 Cell characterisation of the different clinically relevant cell types investigated for peripheral nerve repair

The following cell types were tested experimentally within this study: primary rat hair follicle NCSCs, primary rat BM-MSCs, primary rat Schwann cell-like cells from ADSCs and undifferentiated and differentiated human neural progenitor cells (uCX and dCX, respectively). Initial characterisation of each cell population was followed by testing the ability of each cell type to form EngNT, this includes assessing cell survival post-plastic compression, cell alignment and ability of the material to promote guided

neurite outgrowth *in vitro*, using a cell density of  $4 \times 10^6$  cells/ml in rat type I collagen (the same collagen as the previous *in vitro* and *in vivo* experiments in chapters 3 and 4).

Immunofluorescence labelling of NCSC cultures on coverslips showed positive staining for Sox10 in 100% of the population. This transcription factor is expressed by NCSCs and plays a role in the differentiation of peripheral glial cells (Britsch *et al.*, 2001; Bremer *et al.*, 2011) (figure 5.3). dADSCs were stained to detect the typical Schwann cell markers, GFAP, p75 and sox10, and were positive for all three (figure 5.4). Dr Paul Kingham of Umea university (the supplier of these cells), previously characterised the cells by immunofluorescence and western blotting and showed they were positive for the same markers (Kingham *et al.*, 2007).

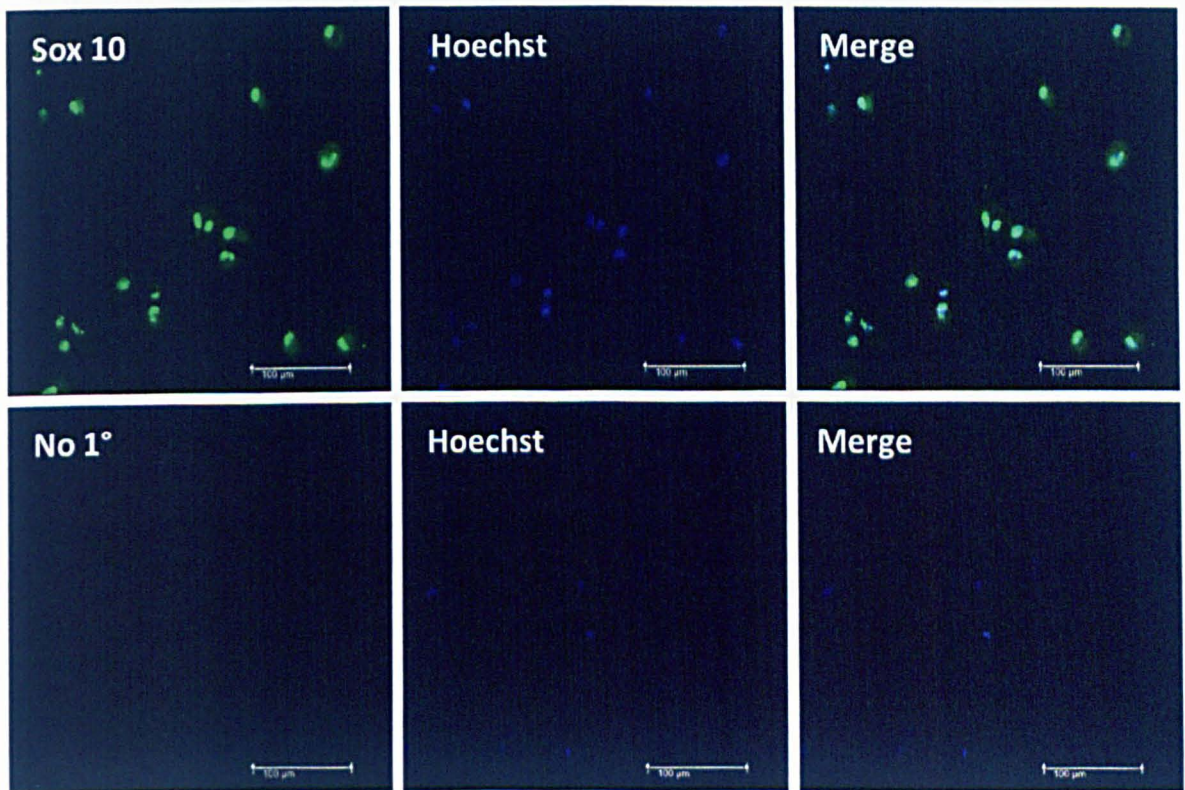


**Figure 5.3 Identification of Sox 10 in neural crest stem cells**

Immunofluorescence staining of cultured primary rat neural crest stem cells that were seeded onto coverslips and maintained in culture for 24 hours before fixation and immunolabelling to detect Sox10 (green). In the merged images, blue is Hoechst and green is Sox 10 staining. The top row shows an area positive for Sox 10 and the bottom row shows the negative control, no primary antibody. All NCSC nuclei were positive for Sox 10. Scale bars are 100 µm.

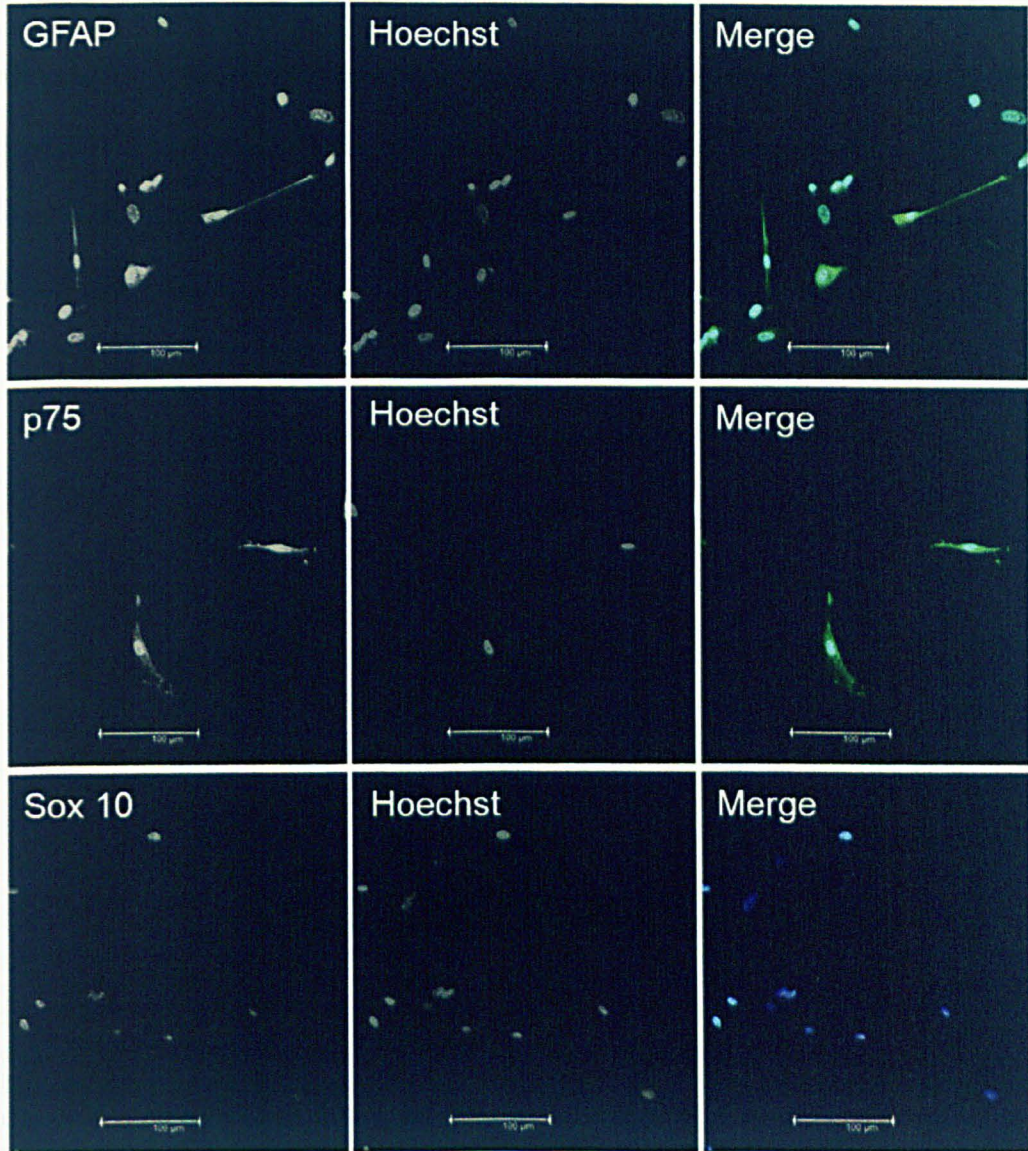


**Figure 5.4 Characterisation of dADSCs on coverslips**

Immunofluorescence staining of dADSCs on coverslips after 24 h in culture, for the typical Schwann cell markers: GFAP, p75 and Sox 10. (Scale bars are 100µm). In the merged images, blue is Hoechst and the green is for the antibody. dADSCs were positive for all of these markers.

Flow cytometry analysis was performed on BM-MSCs to detect anti-CD54, a marker for mesenchymal stem cells (Mafi *et al.*, 2011). BM-MSCs were positive for CD54 (figure 5.5) (isotype IgG1 antibody was included as a control). Immunofluorescence labelling of BM-MSCs on coverslips revealed that 51 % of the population of BM-MSCs was positive for anti-integrin  $\beta$ 1 (CD29), a marker present in mesenchymal stem cells (Mafi *et al.*, 2011).

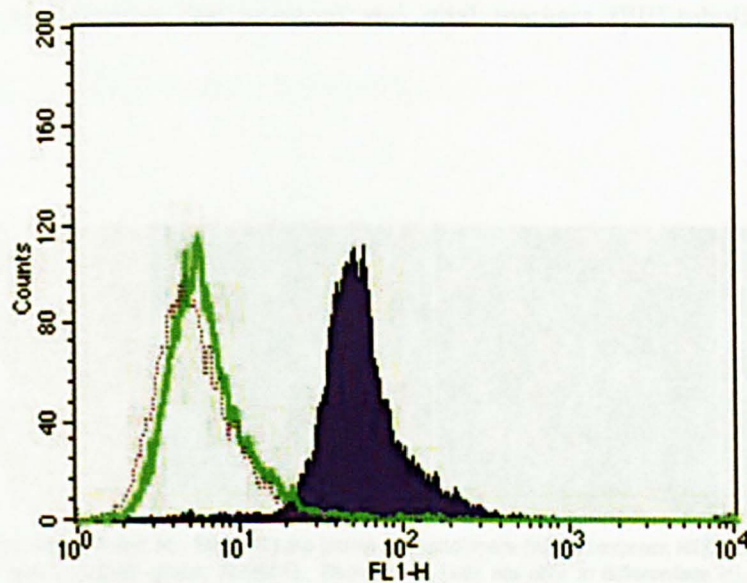
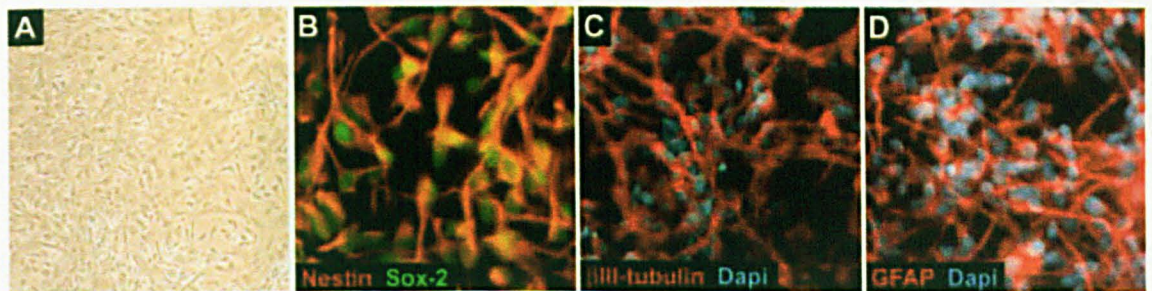


**Figure 5.5 Characterisation of BM-MSCs by flow cytometry**

Histogram showing CD54 expression on BM-MSCs (blue). Two experimental runs were carried out, with average median fluorescence for anti-CD54 of  $46.8 \pm 1.1$  (mean  $\pm$  SEM) and the average median fluorescence for the isotype IgG1 control was  $5.6 \pm 0.3$  (green peak). A no primary antibody control was also used, represented by the dashed pink peak.

The research grade ReNcell CX cells, were characterised previously by immunofluorescence staining by Millipore (figure 5.6), so no further characterisation was performed on this commercially-sourced cell line. The uCX cells were cultured with FGF-2 and EGF to maintain their undifferentiated state. The removal of these factors from the media initiates differentiation, which is a two week process. The uCX cells were positive for nestin, which is required for the self-renewal of neural stem cells (Park *et al.*, 2010), and sox-2, a marker for neural stem cells (Ellis *et al.*, 2004). The dCX cells were positive for neuronal and glial markers ( $\beta$ III-tubulin and GFAP, respectively).



ReNcell CX cells (Millipore Cat. No. SCC007) are grown as monolayers (A) and express NSC markers, Nestin (B, red; Cat. No. MAB5326) and Sox-2 (B, green; AB5603). ReNcell CX cells are able to differentiate into neurons expressing  $\beta$ III-tubulin (C; Cat. No. MAB1637) and glial cells expressing GFAP (D; Cat. No. AB5804).

**Figure 5.6** Characterisation of undifferentiated (A, B) and differentiated (C, D) CX ReNcells by supplier, Millipore (Reproduced from data sheet, Millipore, Cat. No. SCC007).

	S100	GFAP	p75	sox10	sox2	Nestin	CD54	integrin beta1
NCSC	-	-	-	✓	-	-	-	-
Rat BM-MSCs	-	-	-	-	-	-	✓	✓
uCX	-	-	-	-	✓	✓	-	-
dCX	-	✓	-	-	-	-	-	-
dADSCs	✓	✓	✓	✓	-	-	-	-

**Table 5.2** Summary table for cell characterisation

The ✓ indicates the cells are positive for the corresponding antibody; the - indicates where the test was not performed.

The primary rat neural crest stem cells were not explored further for use within the EngNT due to their low cell yield (less than one million cells were obtained after 2 weeks in culture). Following characterisation of the cell populations, BM-MSCs, dADSCs, uCX and dCX cells were selected for further testing. Cell death post-compression was assessed first using propidium iodide. Tethered gels were compressed following overnight incubation to permit gel contraction. Samples from compressed gels were stained with propidium iodide immediately after compression, and then fixed with 4% PFA and stained with Hoechst. As shown in table 5.3, there was little cell death post-compression for all the cell types tested.

Cell type	% cell death (means $\pm$ SEM) (n=4)
Rat BM-MSC	1.90 $\pm$ 0.28
Rat dADSC	0.50 $\pm$ 0.14
Human uCX	0.10 $\pm$ 0.03
Human dCX	0.20 $\pm$ 0.06

**Table 5.3 Cell death in compressed gels in rat collagen I gels**

Fully hydrated tethered gels ( $4 \times 10^6$  cells/ml) were incubated overnight to permit contraction before plastic compression. A sample from one end of the cellular EngNT was taken for live/dead analysis immediately after compression (before the remaining EngNT was used in the *in vitro* assay with neurons).



### 5.2.3 Assessing the capacity of (rat collagen) EngNT containing different cell types to support and guide neurite outgrowth *in vitro*

#### 5.2.3.1 Primary rat BM-MSCs

Rat BM-MSCs were tested as an initial way to investigate the feasibility of using the equivalent human cells to make EngNT (EngNT-BM-MSC). As previously in chapter 3, primary rat DRG neurons were cultured on the surface of this material, EngNT-BM-MSC, for 3 days before fixing overnight and then stained to detect  $\beta$ III-tubulin. Rather than conduct a detailed analysis of BM-MSC orientation within the EngNT, a more rapid assay was conducted to screen for the ability of the final material to support neurite growth and provide overall guidance parallel to the long axis of the construct. Figure 5.7 A-C show confocal micrographs of neurites that were extended on the surface. The direction of neurite outgrowth was measured in the sampled area ( $640,000\mu\text{m}^2$  per EngNT-BM-MSC), and there was no obvious directional trend (figure 5.7 part D). The total neurite length measured in the sampled area per EngNT-BM-MSCs was  $4233 \pm 1590\mu\text{m}$  (mean  $\pm$  SEM), which is low in comparison to the EngNT material with the other cell types tested (figure 5.13). No further analyses were carried out using the BM-MSCs, such as the quantification of BM-MSC alignment, because the amount of neurite growth extended on EngNT-BM-MSCs was lower than with the other cell types within EngNT (section 5.2.2.5).

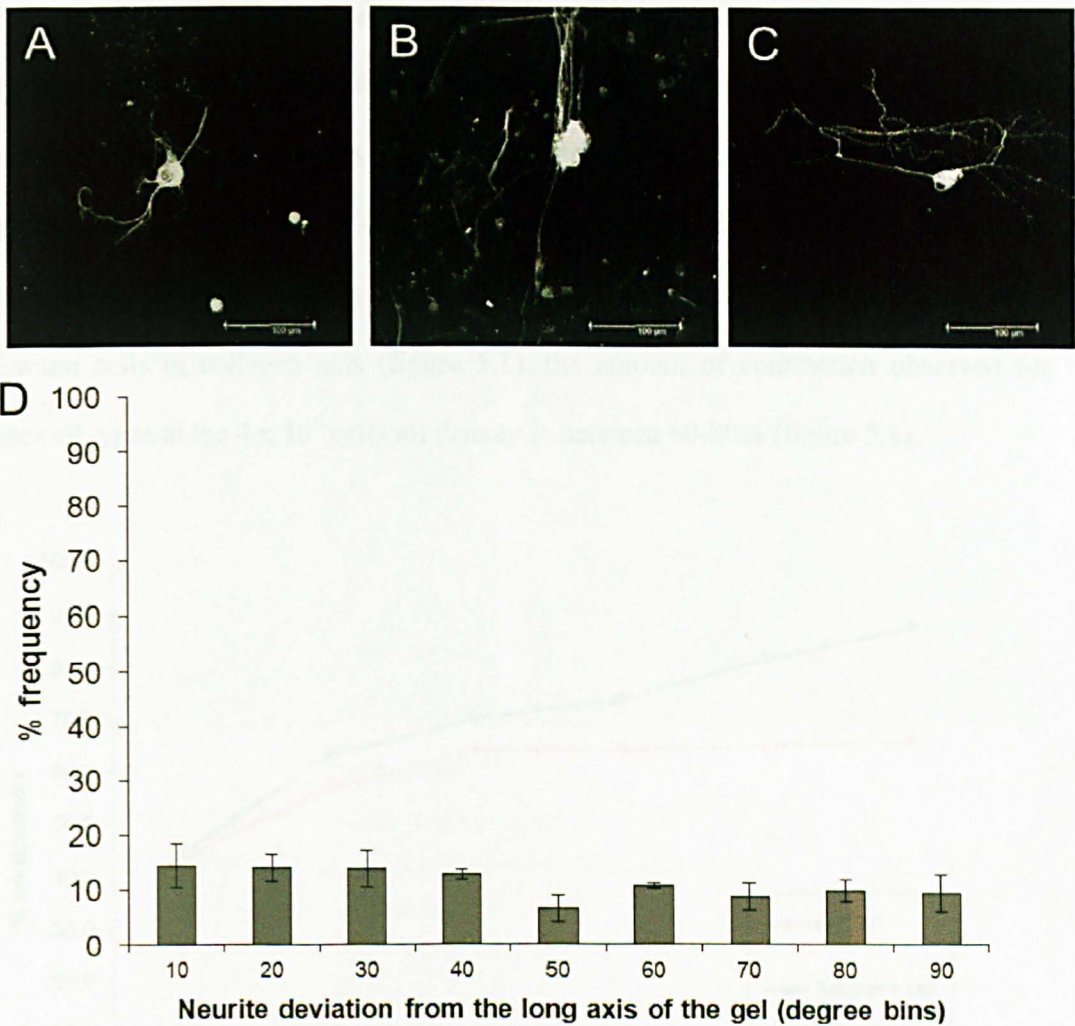


**Figure 5.7 Neurite outgrowth on the surface of EngNT-BM-MSCs after 3 days in culture**  
**A-C** Confocal micrographs of DRG neurons extending neurites ( $\beta$ III-tubulin, grey) on the surface, scale bars are 100  $\mu$ m; **D** Distribution of angle of neurite deviation from the long axis of the gel. Neurite length measured in the sampled area per EngNT-BM-MSCs was  $4233 \pm 1590 \mu$ m (mean  $\pm$  SEM). Data are means  $\pm$  SEM, n=4.

### 5.2.3.2 Schwann cell-like cells differentiated from rat ADSCs

Schwann cell-like cells differentiated from ADSCs (dADSCs) were tested as a potential source of cells for an autologous therapy. Before repeating the *in vitro* neuron co-culture experiment using EngNT-dADSC, the contractility of the cells was assessed in collagen gels at a range of cell densities  $1-6 \times 10^6$  cells/ml. Similar to prior observations with Schwann cells in collagen gels (figure 5.1), the amount of contraction observed for these cell types at the  $4 \times 10^6$  cells/ml density is between 60-80% (figure 5.8).

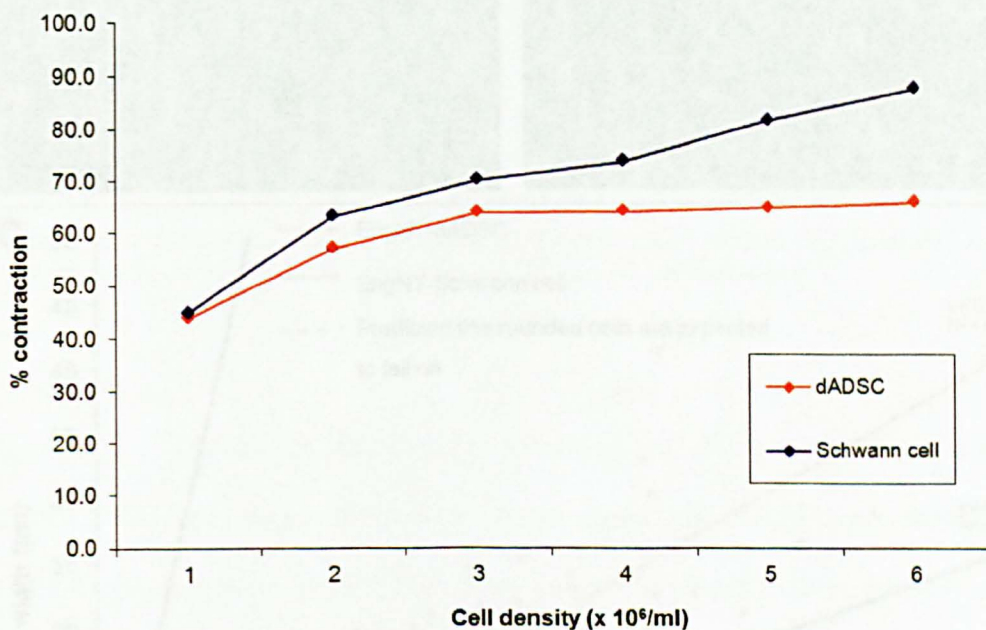
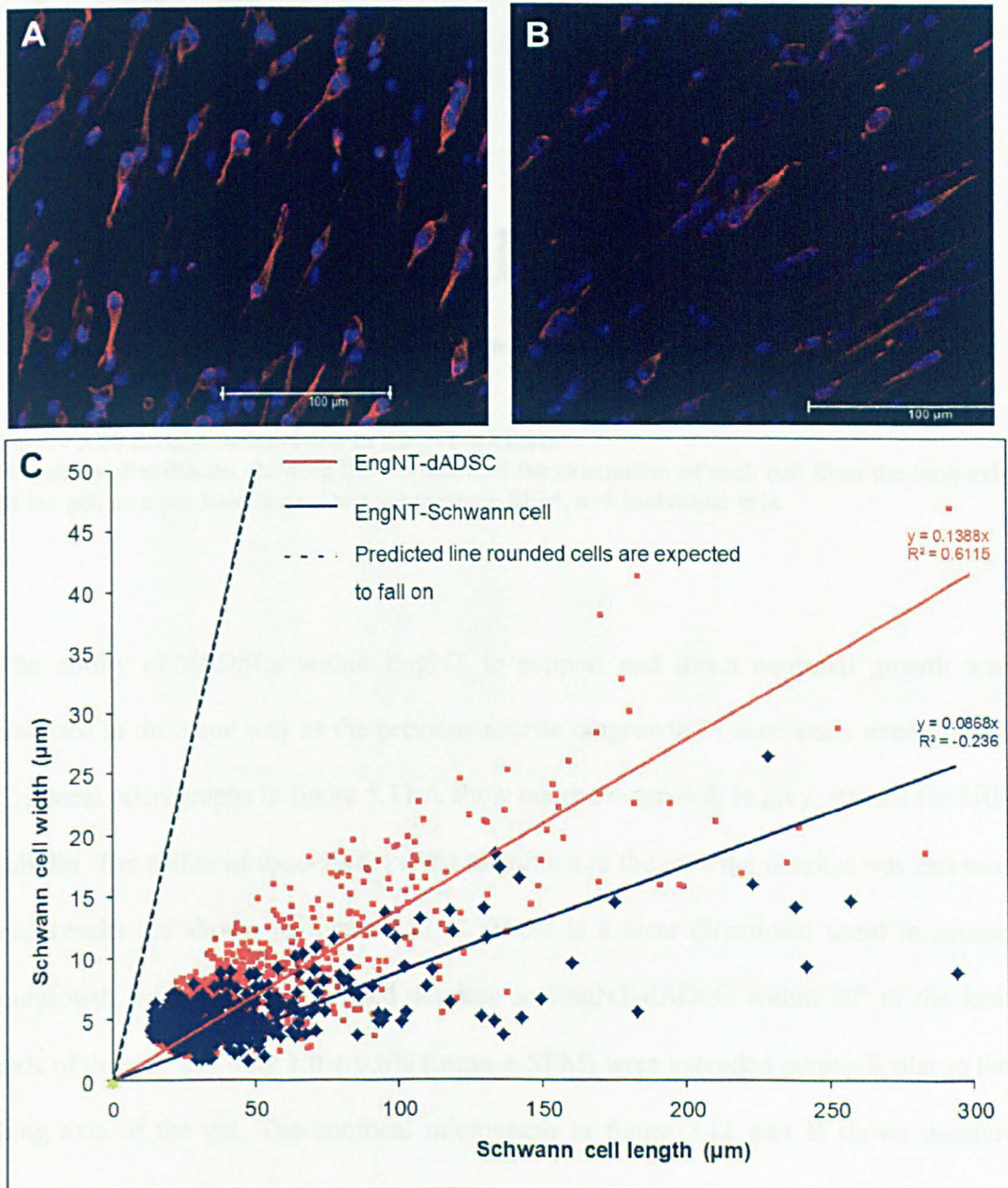


**Figure 5.8** Contraction profile for rat tail type I collagen gels with Schwann cells or dADSCs

Cells were seeded within  $75\mu\text{l}$  collagen gels (rat tail type I,  $2\text{mg/ml}$ ) in 96-well plates and photographed following overnight incubation to determine % contraction  $\{[(\text{original gel area} - \text{contracted gel area}) / \text{original gel area}] * 100\}$ . Data are means  $\pm$  SEM, from 4 replicate gels within one culture.

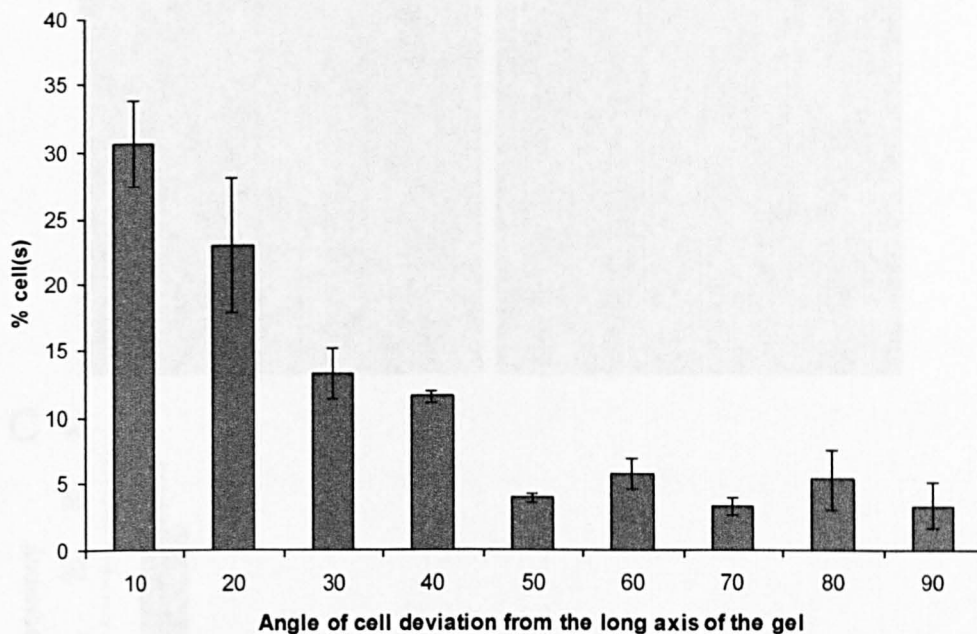
dADSC alignment and elongation within EngNT was quantified; EngNT-dADSC sheets were fixed after 24 hours and then stained to detect S100 immunoreactivity. Results are shown in figure 5.9 parts A and B. The confocal images show the aligned and elongated cells (red) within EngNT. Aspect ratio of cells was quantified and results are shown in

figure 5.9 part C; the degree of cell elongation is greater in EngNT-Schwann cell than in EngNT-dADSC. Cells were mostly orientated parallel to the long axis of the gel,  $54 \pm 8\%$  (mean  $\pm$  SEM) of the cells did not deviate from this by more than  $20^\circ$ , figure 5.10.



**Figure 5.9 Cell elongation within EngNT-dADSC**

**A and B** Confocal micrographs showing the cells (S100, red) within EngNT, scale bars are 100 µm; **C** Scatter plot showing each cell aspect ratio/elongation within EngNT-dADSC (red) and EngNT-Schwann cell (blue).  $n=3$  individual gels.



**Figure 5.10 dADSC orientation in EngNT-dADSC**

Frequency distribution showing the deviation of the orientation of each cell from the long axis of the gel, on a per field basis. Data are means  $\pm$  SEM, n=3 individual gels.

The ability of dADSCs within EngNT to support and direct neuronal growth was assessed in the same way as the previous neurite outgrowth *in vitro* assay experiments. Confocal micrographs in figure 5.11 A show neurite outgrowth in grey, stained for  $\beta$ III-tubulin. The ability of the cells to confer alignment to the growing neurites was assessed and results are shown in figure 5.11 C. There is a clear directional trend in neurite outgrowth, with 52% of extended neurites on EngNT-dADSC within 20° of the long axis of the gel, and only  $1.0 \pm 0.6\%$  (mean  $\pm$  SEM) were extended perpendicular to the long axis of the gel. The confocal micrograph in figure 5.11 part B shows neurites (green) growing along, and in very close contact with, dADSCs (red).

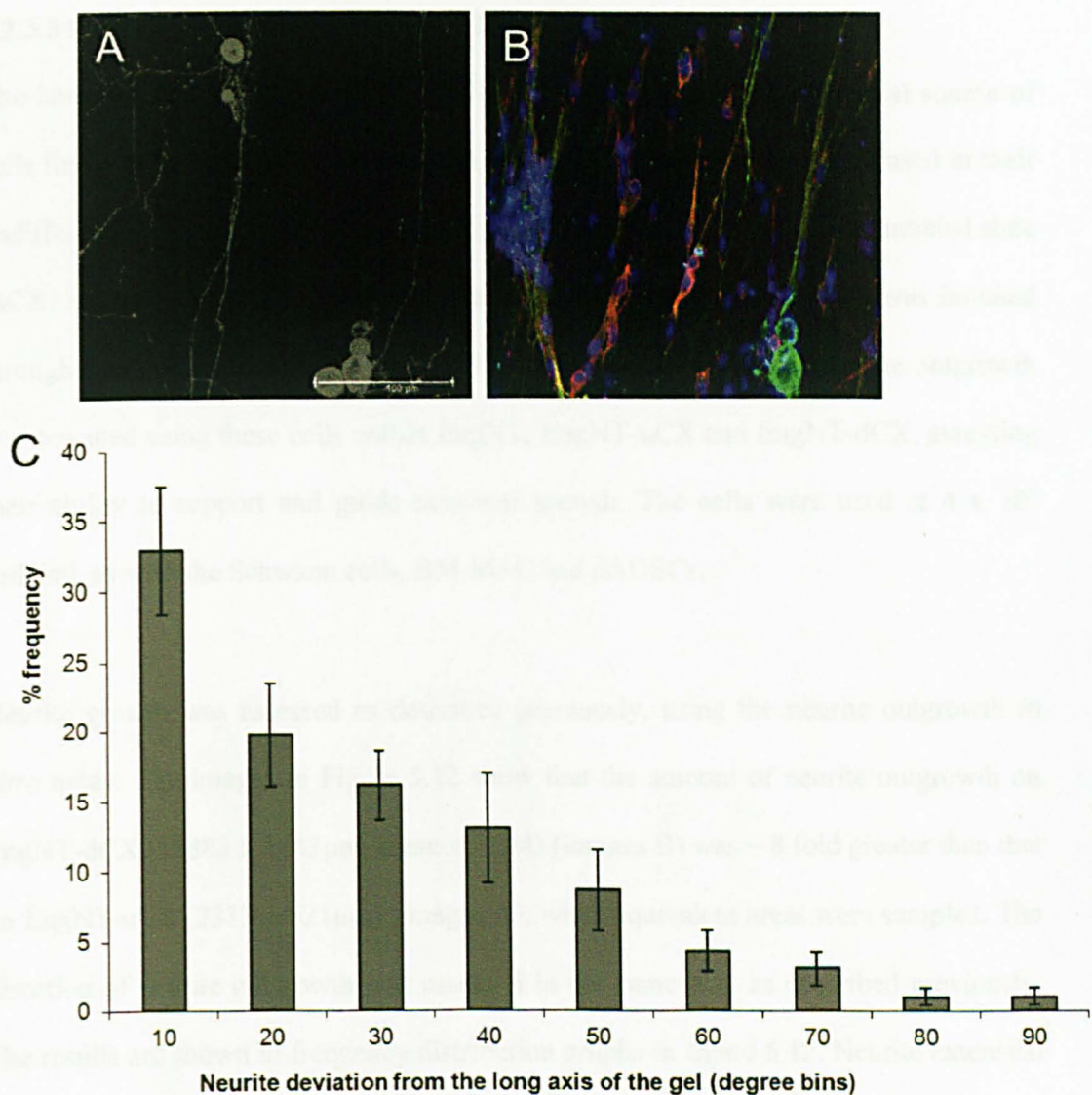


**Figure 5.11 Neurite outgrowth on EngNT-dADSC**

**A** Confocal micrographs of neurites stained for  $\beta$ III-tubulin (grey), scale bar is 100  $\mu$ m; **B** confocal micrograph showing dADSC (S100, red) and neurons ( $\beta$ III-tubulin, green) and **C** frequency distribution showing the angle of neurite deviation from the long axis of the gel. Total length of extended neurites in sampled area was  $9447 \pm 1710 \mu$ m, mean  $\pm$  SEM. Data are means  $\pm$  SEM, n=3 individual gels.

### 5.2.3.3 Human neural progenitor cells (ReNcell)

The human neural progenitor cells (ReNcell CX) were tested as a potential source of cells for an allogeneic approach to making therapeutic EngNT. They were used in their undifferentiated state (uCX) as supplied from Millipore, and in their differentiated state (dCX) as a population of mixed glia. The differentiation of the CX cells was initiated through the removal of growth factors. The *in vitro* assay to assess neurite outgrowth was repeated using these cells within EngNT, EngNT-uCX and EngNT-dCX, assessing their ability to support and guide neuronal growth. The cells were used at  $4 \times 10^6$  cells/ml, as with the Schwann cells, BM-MSCs and dADSCs.

Neurite growth was assessed as described previously, using the neurite outgrowth *in vitro* assay. The images in Figure 5.12 show that the amount of neurite outgrowth on EngNT-dCX ( $18888 \pm 1043 \mu\text{m}$ , mean  $\pm$  SEM) (images B) was  $\sim 8$  fold greater than that on EngNT-uCX ( $2313 \pm 521 \mu\text{m}$ ) (images A), when equivalent areas were sampled. The direction of neurite outgrowth was assessed in the same way as described previously. The results are shown in frequency distribution graphs in figure 5.12. Neurite extension on EngNT-uCX is quantified in figure 5.12 part C; the quantification supports the images showing the neurites were extended in all directions, because there was a similar portion of neurite outgrowth in all the angle ranges. There was a clear directional trend in neurite outgrowth on the surface of EngNT-dCX shown in figure 5.12 part D,  $46 \pm 6\%$  (mean  $\pm$  SEM) of neurites extended on EngNT-dCX do not deviate from the long axis of the gel by more than  $20^\circ$ . The amount of neuronal growth on the EngNTs with the different cell types tested is compared in figure 5.13.

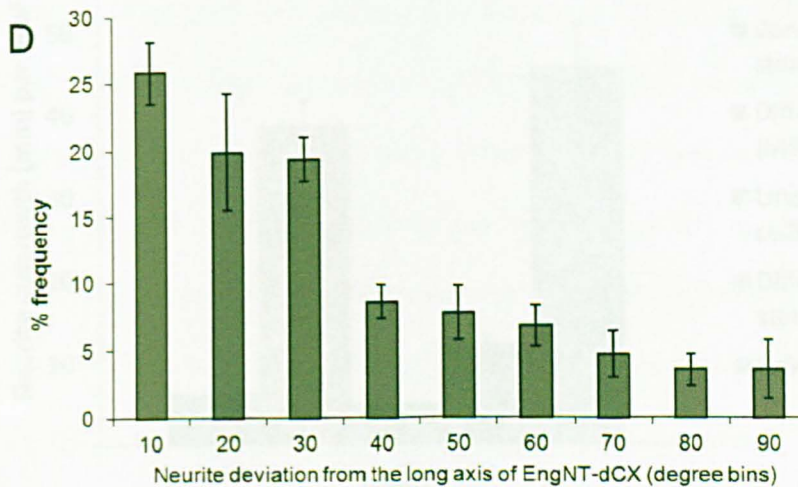
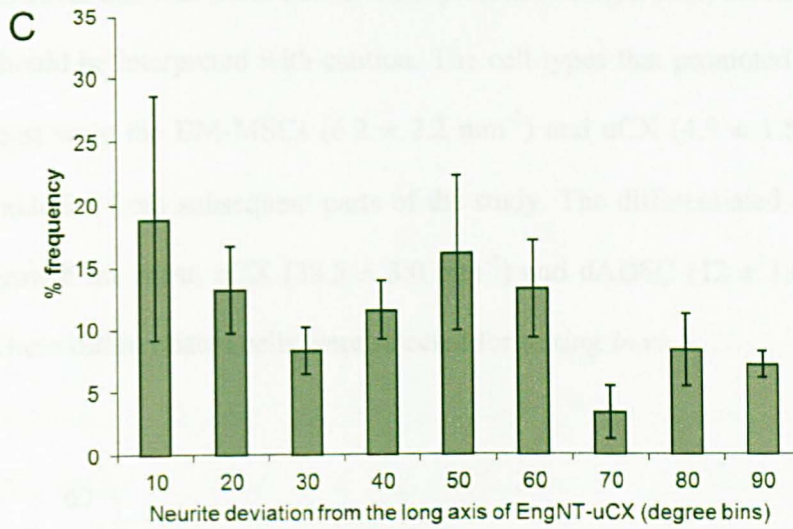
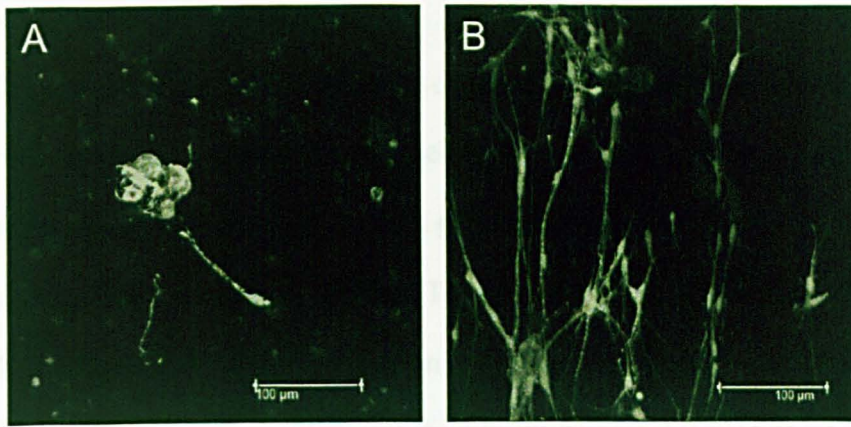


**Figure 5.12 Neuronal growth on the surface of EngNT-uCX and EngNT-dCX**

**A** Confocal micrograph showing neuronal growth ( $\beta$ III-tubulin, grey) on the surface of EngNT-uCX ( $2313 \pm 521\mu\text{m}$ , mean  $\pm$  SEM); **B** confocal micrograph of neuronal growth on EngNT-dCX ( $18888 \pm 1043\mu\text{m}$ ); and **C** Frequency distribution of neurite angle that have been extended on the surface of EngNT-uCX; and **D** Frequency distribution of neurites that have been extended on the surface of EngNT-dCX.  $n=4$  individual gels, data are means  $\pm$  SEM, scale bars are 100  $\mu\text{m}$ .



### 5.2.3.4 Cell type comparison

The relative ability of the different candidate cell types to support neurite extension *in vitro* on EngNT with the different cell types was compared by measuring the amount of neurite outgrowth per  $\text{mm}^2$  for each gel. Primary rat neurons from a single culture were seeded on the surface of the EngNTs with aligned Schwann cells, dADSCs, uCX and dCX. The results from the neuron co-culture on EngNT-BM-MSC were included, however this was from a different experiment using a different neuron culture so results should be interpreted with caution. The cell types that promoted neurite outgrowth the least were the BM-MSCs ( $6.2 \pm 2.2 \text{ mm}^2$ ) and uCX ( $4.9 \pm 1.5 \text{ mm}^2$ ) so these were excluded from subsequent parts of the study. The differentiated cells promoted neurite growth the most; dCX ( $38.5 \pm 3.0 \text{ mm}^2$ ) and dADSC ( $12 \pm 1.0 \text{ mm}^2$ ) (figure 5.13). These differentiated cells were selected for testing *in vivo*.

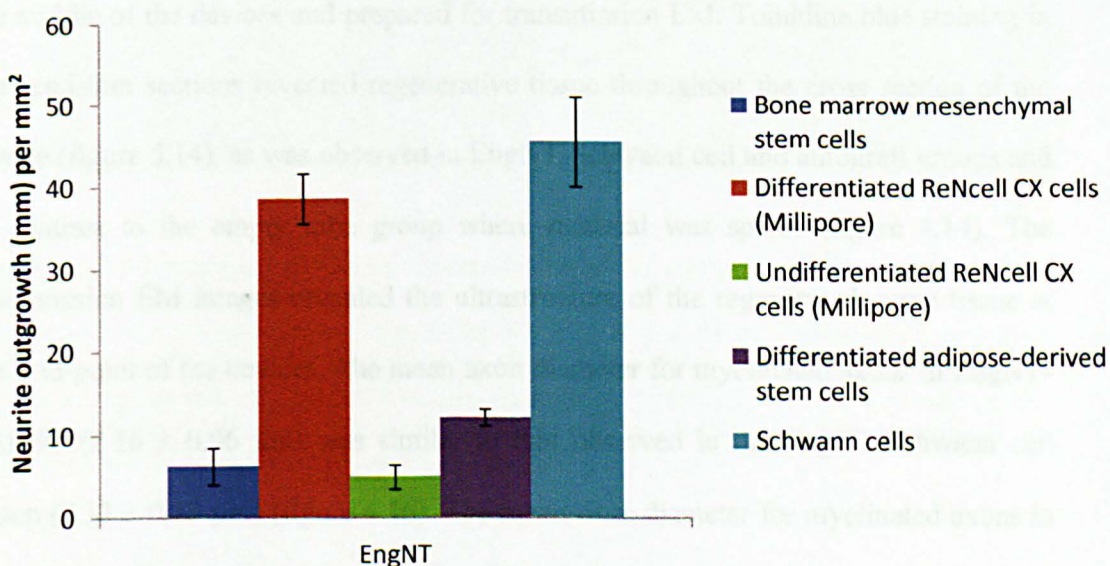


**Figure 5.13 Neurite outgrowth per  $\text{mm}^2$  quantification on aligned cellular EngNT**

The total length of neurite outgrowth measured in the sample region ( $640,000 \mu\text{m}^2$ ) of each EngNT, data are means  $\pm$  SEM,  $n=3$  individual gels.

#### 5.2.4 Initial *in vivo* testing in rat sciatic nerve

Having established that the dADSCs and the dCX cells could be used to generate EngNT which supported directed neuronal growth *in vitro*, they were taken forward for testing in the long gap (15 mm) *in vivo* model and compared to the groups tested in the previous long gap experiment (section 4.2.3): a nerve graft (obtained from litter mates to simulate the clinical gold standard autograft) and an empty tube. This was a preliminary experiment using small numbers of animals. These groups were compared using a 15 mm gap in the rat sciatic nerve with assessment after 8 weeks of recovery.

##### 5.2.4.1 EngNT-dADSC devices

To test the ability of EngNT-dADSC to support regeneration in the long gap model, two 15 mm rods were packed within a NeuraWrap™ outer tube to form the implantable device (n=3) (figure 4.1). As before (section 4.2.3), transverse sections were taken from the middle of the devices and prepared for transmission EM. Toluidine blue staining in the semi-thin sections revealed regenerative tissue throughout the cross section of the device (figure 5.14), as was observed in EngNT-Schwann cell and autograft groups and in contrast to the empty tube group where material was sparse (figure 4.14). The transmission EM images revealed the ultrastructure of the regenerated nerve tissue at the mid-point of the devices. The mean axon diameter for myelinated axons in EngNT-dADSC ( $2.16 \pm 0.06 \mu\text{m}$ ) was similar to that observed in the EngNT-Schwann cell group ( $2.33 \pm 0.10 \mu\text{m}$ ) (figure 4.16). The mean fibre diameter for myelinated axons in EngNT-dADSC was  $3.12 \pm 0.18 \mu\text{m}$ , which is approaching the mean fibre diameter measured for the graft group ( $3.29 \pm 0.13 \mu\text{m}$ ) and greater than that for the empty tube ( $2.64 \pm 0.14 \mu\text{m}$ ). Myelin thickness in EngNT-dADSC ( $0.48 \pm 0.08 \mu\text{m}$ ) was similar to that observed in the graft group ( $0.44 \pm 0.01 \mu\text{m}$ ), and greater than the myelin thickness in the empty tube and EngNT-Schwann cell groups ( $0.35 \pm 0.03$  and  $0.34 \pm 0.02 \mu\text{m}$ ,

respectively). Similar to the control groups, the g ratio in EngNT-dADSC was approximately 0.7 (figure 4.16). The different fibre diameters were evaluated as done previously (figure 4.17). The distribution of the different fibre types was similar in EngNT-dADSC to the graft, EngNT-Schwann cell and empty tube groups.

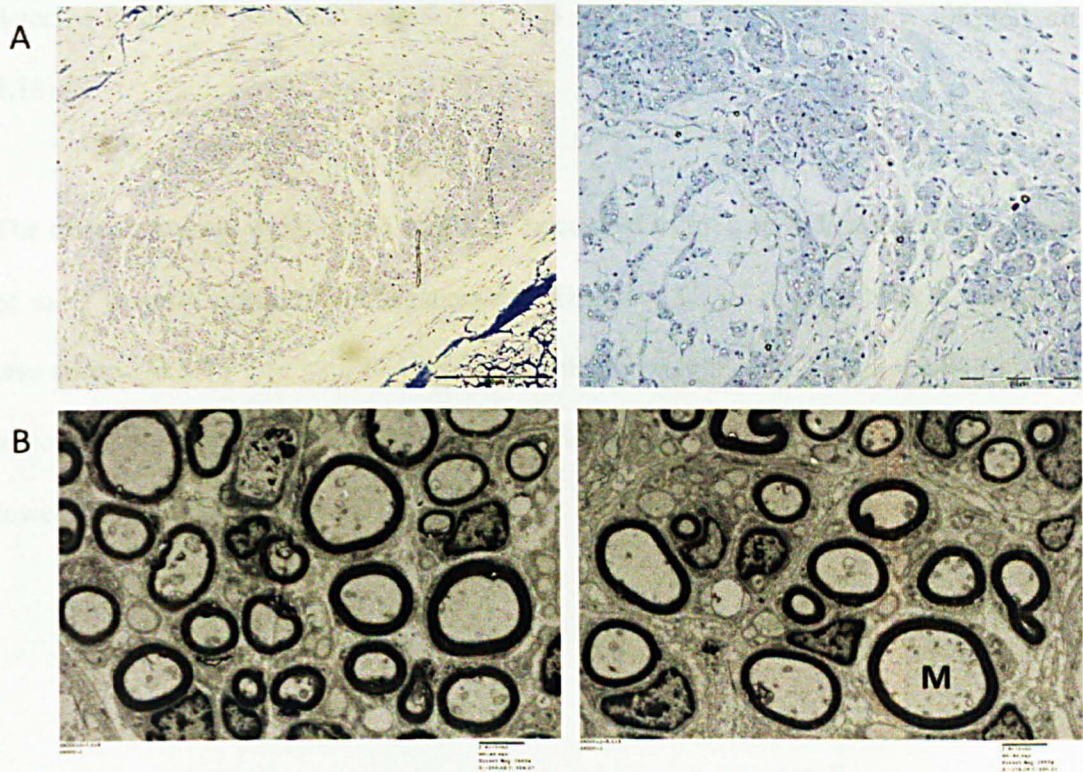


**Figure 5.14 Micrographs of transverse sections from the mid-point of the EngNT-dADSC devices after 8 weeks *in vivo***

Representative semi-thin sections stained with toluidine blue show the regenerated neural tissue within the device, as observed by light microscopy (A) scale bars are 200 and 100 µm for the images on the left and right, respectively. (B) Representative transmission electron micrographs taken from the areas of highest density (as determined from toluidine blue stained sections); S = Schwann cell nucleus, M = myelinated axon, scale bars are 2 µm.

Neurite regeneration was analysed using transverse sections through the proximal and distal parts of the device and in the stumps, to investigate if EngNT-dADSC could support regeneration across the 15 mm gap during the 8 week recovery period, as done previously. Figure 5.15 shows representative images of the neurofilament positive axons in the different parts of the repair site. The axon counts in the three EngNT-

dADSC devices tested gave a similar mean number of axons in the different parts of the device as were observed with EngNT-Schwann cell devices. There was a greater number of axons supported in the DD (distal part of the device) in the EngNT devices (EngNT-Schwann cell and EngNT-dADSC), compared to the empty tube group, which had  $290 \pm 112$  (mean  $\pm$  SEM) axons, which is approximately a third of the number detected in EngNT-Schwann cell ( $955 \pm 348$ ) and EngNT-dADSC ( $719 \pm 306$ ) (figure 4.18).

The relative muscle weight ratio was also calculated to give an indication of the extent of motor neuron regeneration/degeneration. EngNT-dADSC devices after 8 weeks *in vivo* to bridge a 15 mm gap, had a relative muscle weight ratio  $21.0 \pm 0.4$  % (n = 3), which is similar to that observed in EngNT-Schwann cell,  $23.8 \pm 1.9$  % (n = 5), and lower than that observed in the graft group,  $34.7 \pm 2.5$  % (n = 5).

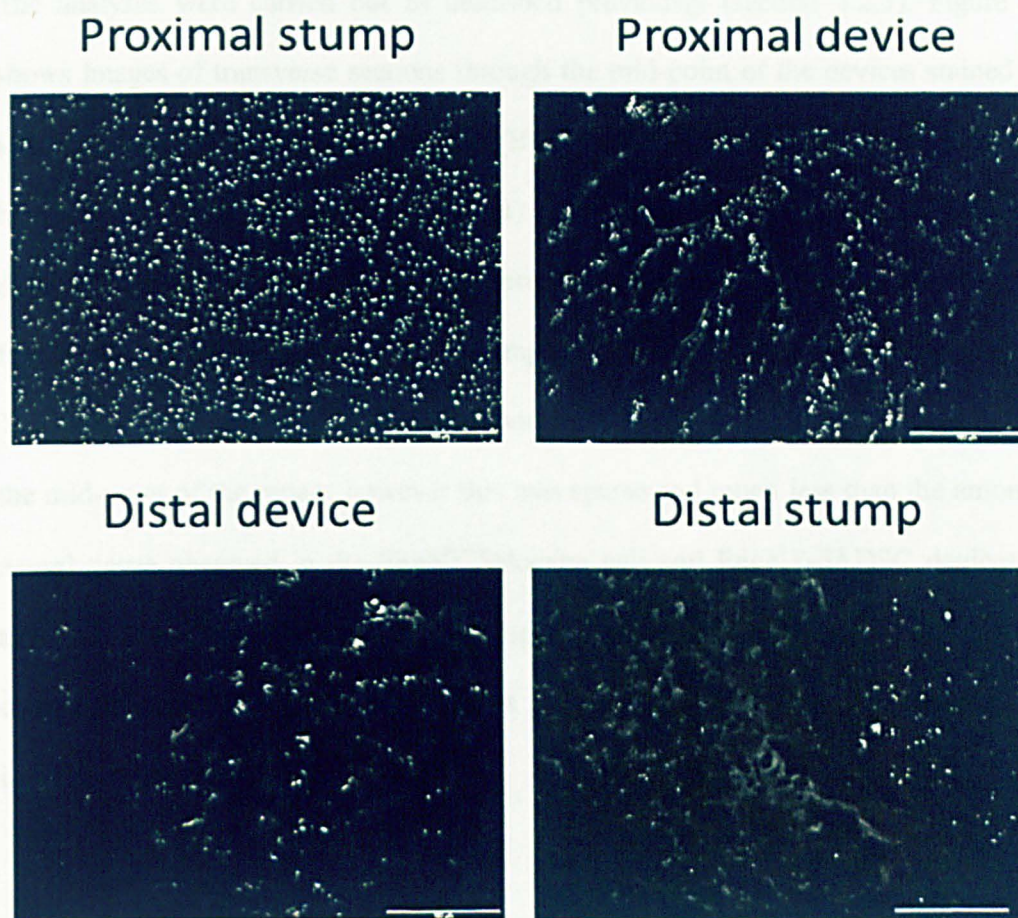


**Figure 5.15** Fluorescent micrographs of transverse sections through the different parts of the repair site after repair with EngNT-dADSC devices after 8 weeks *in vivo*. 10  $\mu\text{m}$  thick sections were stained to detect neurofilament, scale bars are 100  $\mu\text{m}$ .

#### 5.2.4.2 EngNT-dCX devices

EngNT-dCX devices were tested in the same way, within a NeuraWrap™ tube to bridge a 15 mm gap in the rat sciatic nerve (n=5) (figure 4.1). The dCX cells are human cells and so the animals were immunosuppressed using cyclosporine A (15 mg/kg) 24 hours prior to implantation and then daily throughout the recovery period. Two out of the five devices were pre-labelled with Hoechst to allow the implanted cells to be distinguished from the host cells in the harvested devices, in addition to using the GFP label expressed in host cells to distinguish them also.

The analyses were carried out as described previously (section 4.2.3). Figure 5.16 shows images of transverse sections through the mid-point of the devices stained with toluidine blue (A) and transmission EM (B). Two out of the five devices (one was pre-labelled with Hoechst and one was not) had regenerated tissue present within the devices, however no regeneration was observed in three of the devices (the images in figure 5.16 are representative of the two implanted devices that supported regeneration). The regeneration observed in the two devices (figure 5.16) shows myelinated axons at the mid-point of the repair, however this was sparse and much less than the amount of neural tissue observed in the EngNT-Schwann cell and EngNT-dADSC devices, and also less than that observed in the empty tube group. Although these cannot be compared directly as only the animals in the EngNT-dCX group received were immunosuppressed.

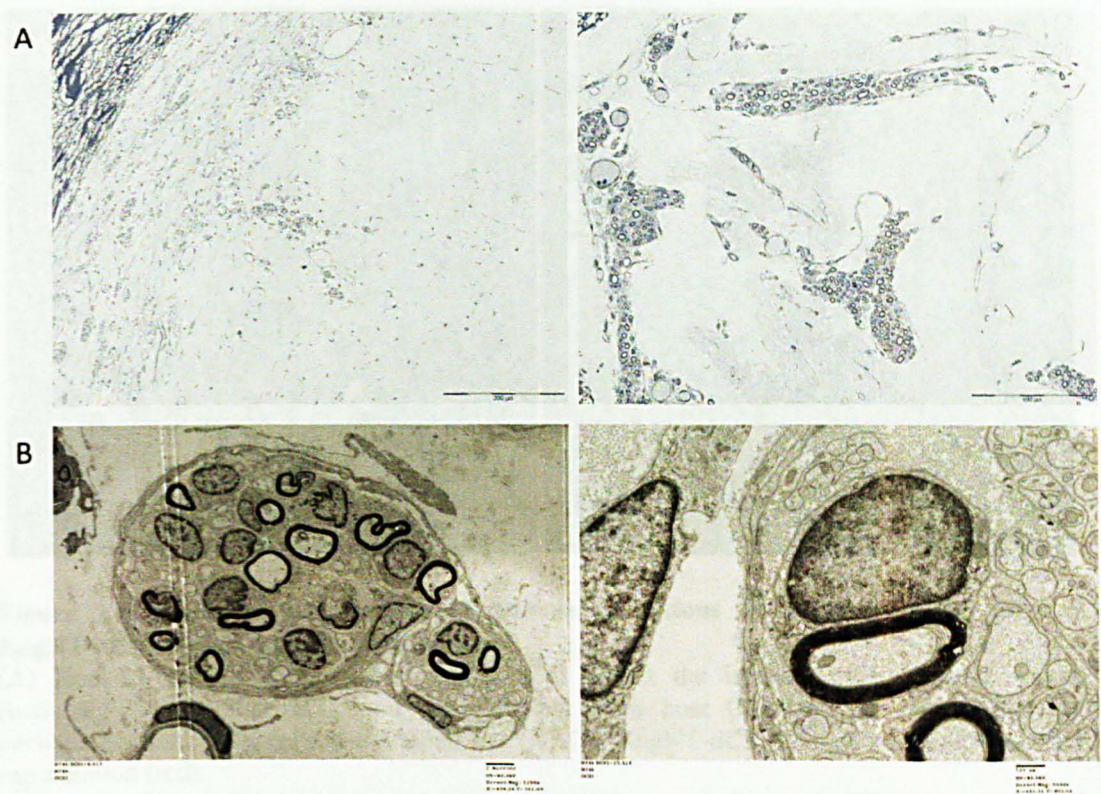


**Figure 5.16 Micrographs of transverse sections from the mid-point of the EngNT-dCX devices after 8 weeks *in vivo***

Representative semi-thin sections of two of the devices stained with toluidine blue show the neural tissue within the device, as observed by light microscopy (A) scale bars 100 µm; Representative transmission electron micrographs of the two devices taken from the areas of highest density (as determined by toluidine blue stained sections), S = Schwann cell nucleus, M = myelinated axon, scale bars are 2 µm and 500 nm for the images on the left and right, respectively.

Transverse sections were taken from the proximal part of the devices and stained to identify neurofilament positive axons. All devices were implanted into GFP+ rats, and there was evidence of Hoechst staining that was not associated with GFP+ cells, indicating persistence of the dCX cells at the repair site (figure 5.17 image A). The neurofilament-positive axons shown in red in image B indicated EngNT-dCX can support neuronal growth.

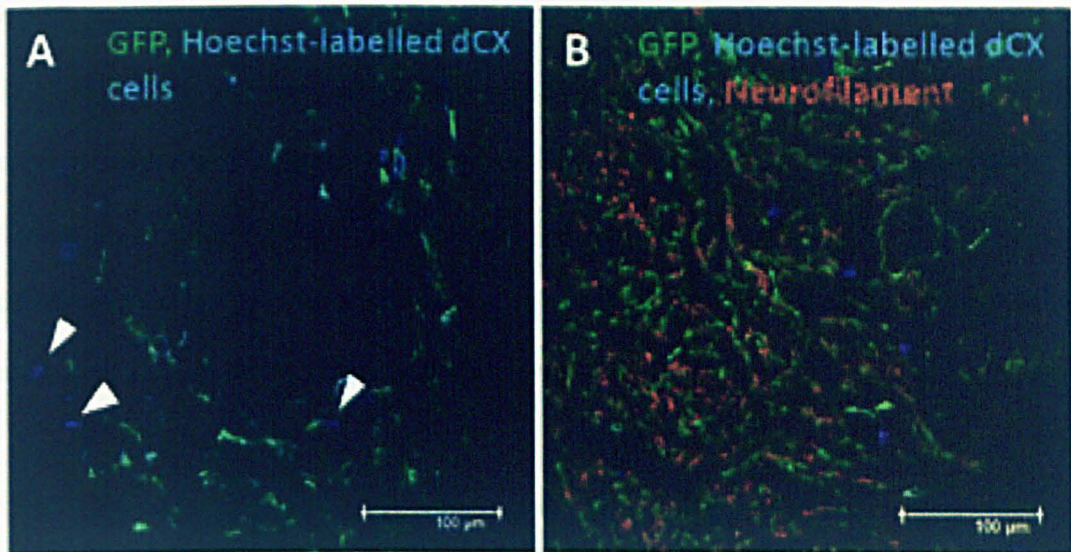


**Figure 5.17 Confocal micrographs of transverse sections from the proximal part of EngNT-dCX devices after 8 weeks *in vivo***

(A) Hoechst-labelled dCX nuclei were present within the implanted device at 8 weeks (indicated by white arrows), and were distinct from host GFP-labelled cells, indicating persistence of the dCX cells at the repair site (B) The EngNT-dCX devices supported neuronal regeneration (red).

At the time of device harvest, the relative muscle weight ratio was also calculated to give an indication of the extent of motor neuron regeneration/degeneration. This was greater than the other EngNT devices, at  $24.8 \pm 1.3 \%$  ( $n=5$ ), compared to  $21.0 \pm 0.4 \%$  for EngNT-dADSC ( $n=3$ ) devices and  $23.8 \pm 1.9 \%$  for EngNT-Schwann cell ( $n=5$ ) devices; but was lower than that observed in the graft group,  $34.7 \pm 2.5 \%$  ( $n = 5$ ).



### 5.3 Discussion

This part of the study tested whether clinically relevant cells and materials could be used to make a peripheral nerve repair device based on EngNT. Importantly, it demonstrated that sources of collagen and cells similar to those that have already been developed for use in clinical trials can be used to engineer neural tissue, providing useful evidence to underpin future translational studies.

This study showed that bovine collagen, which is more clinically relevant than rat collagen, supported Schwann cell self-alignment and could be subjected to plastic compression to produce EngNT. Studies have reported other cell types contracting bovine type I collagen, such as human gingival fibroblasts and human oral keratinocytes (Techatanawat *et al.*, 2011). The contraction profile experiment (section 5.2.1, figure 5.1) showed that the amount of contraction after 24 hours with Schwann cells was similar in both rat and bovine collagen. A study comparing contraction rates in type I rat and bovine collagen, using fibroblasts, showed that rat collagen had a slower contraction rate compared to bovine collagen over a 9 day period (Techatanawat *et al.*, 2011); though the contraction rates reported in that study were similar after a 24 hour period, which is in line with the results shown here.

The form of bovine collagen currently used in the clinic (e.g. for lip fillers in cosmetic surgery) is not suitable for use within this method, to form a hydrogel, because it contains telopeptide-free collagen, which cannot form a hydrogel. Collagen has been used for a considerable period of time in the clinic, providing evidence of safety and biocompatibility, making it desirable for use in more advanced tissue engineering. A study by Charriere *et al.* in 1989, showed that only a small percentage, 2.3%, of the

patients treated with bovine collagen implants had an adverse reaction, from the 656 patients tested (Charriere *et al.*, 1989).

The cells investigated in this study were: primary rat bone-marrow mesenchymal stem cells, Schwann cell-like cells from differentiated adipose-derived stem cells, undifferentiated and differentiated CX cells. Primary neural crest stem cells were considered initially but were not used for experiments. The neurite outgrowth *in vitro* assay was used to screen the cell types and showed the undifferentiated cells (BM-MSCs and uCX) did not enhance neurite outgrowth as much as the cells that had differentiated into glial cell types (dADSC and dCX).

Interestingly, other studies using rat BM-MSCs to repair rat sciatic nerve have shown that transplanting stem cells that are not fully differentiated can be effective due to subsequent *in vivo* differentiation (Zhang *et al.*, 2004; Chen *et al.*, 2007). Chen *et al.* showed the BM-MSCs differentiated post-transplantation into S100-positive Schwann cell-like cells that myelinated the regenerated axons (Chen *et al.*, 2007). Transplanting undifferentiated cells could be useful in the clinical setting because transplanting stem cells at the time of injury and permitting their differentiation to a Schwann cell-like phenotype *in vivo* would potentially reduce the delay associated with expanding and differentiating autologous cell populations. However, when comparing undifferentiated and differentiated BM-MSCs directly, the differentiated cells secrete greater amounts of neurotrophic factors, which can enhance regeneration (Dezawa *et al.*, 2001). Additionally, using differentiated/more mature cells may ensure a more precise and complete therapeutic effect because the cell population will be more homogeneous than the cell population from transplanted undifferentiated cells, where their differentiation

to a particular cell type is not controlled or monitored and the long term safety is unknown.

The undifferentiated cell types tested in the *in vitro* assay, BM-MSCs and uCX, were not taken forward because they did not promote neurite outgrowth as well as the Schwann cells. The dADSC and dCX cells however were better in promoting neurite outgrowth and could be used to make EngNT which supported directed neurite outgrowth. The CX cells are equivalent to the clinical grade CTX cells, which are already being transplanted into patients, with no immunosuppression, to treat stroke. Their differentiation into glial cells is mediated through the removal of factors, which is an appealing feature from a regulatory point of view since no additional factors would need to be used to manipulate the CTX cells.

Having established that an EngNT-based device could be assembled using clinically relevant cells, the effectiveness of these devices was investigated in a long gap *in vivo* model. EngNT-dADSC or EngNT-dCX devices were implanted into a 15 mm gap in the rat sciatic nerve for 8 weeks. Data obtained using the EngNT-Schwann cell devices, empty NeuraWrap™ tubes and nerve grafts from littermates reported in chapter 4 were used as comparators, and hence were not repeated for the dADSC and dCX *in vivo* experiments.

The EngNT-dADSC devices showed equivalent regeneration to the EngNT-Schwann cell devices, in terms of the amount of neural tissue at the mid-point of the devices and the number of regenerated axons that were supported at the distal part of the device, although no statistical analysis was done because the number of animals used in the EngNT-dADSC group was n=3 only.

The regeneration across a 15 mm gap after 8 weeks using the EngNT-dCX devices was less clear because there was no regeneration present in three out of the five implanted devices, and so no quantification was carried out because of the inconsistency within the group. The regeneration observed in the two EngNT-dCX devices that did show some regeneration, was less than that observed in the other EngNT devices. This may be due to species differences and the immune response to the human cells and indeed the animals receiving immunosuppression lost up to 20 % of their weight prior to the surgery.

Interestingly, the relative gastrocnemius muscle weight ratio was similar in the EngNT-dCX repairs (n = 5), compared to EngNT-Schwann cell (n = 5) and EngNT-dADSC (n = 3) groups, even though less regeneration was observed in the mid-point of EngNT-dCX. This may be because in the EngNT-dCX repairs, the degeneration of the gastrocnemius muscle is not as rapid. The effect of cyclosporine A (CsA) on neuron regeneration is not clear from the literature. CsA has been known to promote neuro-protection and neuro-regeneration (Strittmatter *et al.*, 1992; Ibarra *et al.*, 2007). The dose of CsA used in this experiment was 15 mg/kg body weight. A study comparing different doses of CsA (2, 4, 8 and 16 mg/kg), administered daily after primary repair of the rat sciatic nerve, concluded that CsA had adverse effects on peripheral nerve regeneration (Meirer *et al.*, 2002). In this study by Meirer and colleagues, histology revealed significantly reduced numbers of myelinated axons, reduced myelin sheath thickness, and reduced diameters in all CsA treatment groups compared with the untreated control group, which seemed to be dose related for sensory neuron recovery (Meirer *et al.*, 2002). It would be essential to conduct control experiments using the same immunosuppression protocol in conjunction with the control groups

before the findings can be interpreted. However this was an initial experiment to investigate the feasibility of using the dCX cells, and while the data are not promising, they are inconclusive (without the controls) and it may be worth exploring these cells more in the future because the failure may be due to the technical challenge of testing human cells in rats. To avoid this issue, an alternative to immunosuppression would be to use nude rats or mice.

The overall aim for this part of the study was to investigate the feasibility of constructing a repair device from EngNT using clinically relevant cells and materials. It has shown that bovine collagen, which is currently used in the clinic, can be used to produce EngNT. Furthermore, autologous (dADSC) and allogeneic (dCX) cells were tested within EngNT and results from the *in vitro* assay showed that they could promote guided neurite outgrowth within EngNT. The EngNT-dADSC devices could support neuron regeneration across a long gap *in vivo*, where regeneration was equivalent to that observed using EngNT-Schwann cell devices. There was some regeneration in the EngNT-dCX devices, however this was not consistent and requires further investigation. In summary, there is evidence of the efficacy of dADSCs and dCXs in a peripheral nerve therapy within EngNT devices.

The findings of the present study suggest that the dADSCs have potential to be used for peripheral nerve repair. There are many advantages of using Schwann cell-like cells differentiated from a patient's own adipose-derived stem cells, these include: no immune reaction as it would be an autologous therapy, large amounts of adipose tissue can be collected via liposuction, eliminating the need for cell expansion and dADSCs have been reported to promote peripheral nerve regeneration in animal models. Peripheral nerve repair using the dCX cells is less clear, but that may be due to the

complications of using immunosuppression, so it is worth investigating them further. There is a clear advantage in using the dCX cells in that they are allogeneic and can be used for an off-the-shelf therapy; however allogeneic cells are potentially immunogenic and so are likely to evoke an immune response unless the patient is immunosuppressed.

In summary, this part of the study demonstrates that EngNT can be constructed using clinically relevant cells and materials. Furthermore, the *in vivo* experiments provide an indication of efficacy of dADSCs and dCXs in a peripheral nerve therapy based on EngNT, to support and guide neuronal regeneration.

## 6.0 Discussion

The overall aim for this thesis was to develop an implantable tissue-engineered device for the surgical repair of the peripheral nervous system. The primary goals were to develop an aligned cellular biomaterial that could promote guided neuronal growth and be used to form the basis of a peripheral nerve repair device, with a proof-of-principle study to demonstrate efficacy *in vivo* in a model representative of the clinical situation.

The main objectives were outlined in section 1.5:

1. To develop and optimise a robust biomaterial with highly aligned cells [Engineered Neural Tissue (EngNT)] that could potentially form the basis of a peripheral nerve repair device.
2. To engineer an 'endoneurium' using EngNT that supported the re-growth of axons across the gap in injured nerves.
3. To investigate the feasibility of constructing a repair device from EngNT using clinically relevant cells and materials.

As described in chapter 3, the alignment of cells in tethered hydrogels was preserved by plastic compression (stabilisation) once the gel was removed from the tethering bars, thereby forming EngNT. The studies in this chapter showed that EngNT-Schwann cell could support and guide neurite outgrowth *in vitro* (objective 1). The next step was to investigate whether this material could be used to form the basis of a repair device. The studies described in chapter 4 assessed the different ways in which EngNT could be incorporated into a repair device, investigating different arrangements, amounts of 'surface' and material, and cell density. This allowed decisions to be made regarding the EngNT arrangement within a conduit and indicated an arrangement based on ease of assembly and amount of regeneration in a short gap model (objective 2). A proof-of-

principle study using EngNT-Schwann cell in a long gap model, representative of the clinical situation where an autograft would be indicated, showed that the EngNT-Schwann cell devices supported regeneration across the gap (15 mm) at the injury site better than the empty conduit group (objective 2).

The next step was to assess the feasibility of constructing an EngNT device from clinically relevant cells and materials (chapter 5). In these studies, a bovine source of native collagen was used to construct EngNT-Schwann cell, which was equivalent to the rat collagen EngNT-Schwann cell, in terms of gel contraction and cellular alignment (objective 3). A comprehensive literature search was conducted to identify cells that might be suitable for this approach. Potential therapeutic cells were tested within EngNT; EngNT-dADSC devices showed promising preliminary results in the long gap (15 mm) *in vivo* model, indicating their potential for use in an autologous therapy (objective 3). An allogeneic source of cells was also used within EngNT (EngNT-dCX) and tested in the same model; results showed evidence of regeneration, however further investigation into their use is required (objective 3).

This thesis began with the hypothesis that combining two techniques (cellular self-alignment in tethered gels and plastic compression) could produce a robust material (EngNT) that could support guided neuronal growth. The combination of these two techniques had been attempted before (East *et al.*, 2010); however established protocols for the procedure, and a quantitative assessment of the efficacy of this approach, were lacking. This project has developed protocols to identify some of the parameters required to construct aligned gels (e.g. contraction profiles to establish the required cell density), and an *in vitro* assay to assess the ability of EngNT to support and direct neurite outgrowth (i.e. amount and guidance) using 3D image analyses. The



combination of alignment and compression is now being developed for commercial use by TAP Biosystems (UK) in collaboration with Dr James Phillips at The Open University, building on existing RAFT<sup>®</sup> technology.

The EngNT material constructed in this present study was used to form a repair device, demonstrating regeneration across a repair gap in a relevant model and showing it could be used with clinically relevant cells and materials. This study has moved this project significantly forward to a point where it is being developed further to construct a translational peripheral nerve repair device using therapeutic cells, in collaboration with two companies with the relevant expertise.

There are limitations to the experimental models used in this study. For example, the *in vitro* model used to assay different cell types within EngNT used neurons from dissociated dorsal root ganglia, which comprised only the sensory neuronal bodies, therefore it does not permit the model to predict the ability of the cells to promote motor neuron regeneration. There are differences between motor and sensory neuron regeneration (Madorsky *et al.*, 1998). In that study, Madorsky and colleagues showed that in the repair of 10 mm gap in rat sciatic nerve using collagen conduits, only 6.2 % of motor neurons regenerated and 63 % of sensory neurons regenerated, compared to primary (end-to-end) repair where 65 % of motor neurons and 79 % of sensory neurons had regenerated (Madorsky *et al.*, 1998). This could be because of a difference in the rate of neuron regeneration. It has been reported that motor neurons regenerate at a slower rate (1.7 mm/day) than sensory neurons (5 mm/day) after primary repair in patients following a 2 year follow up (Dolenk and Janko, 1976).

The *in vivo* rat sciatic nerve model also has limitations in that rat nerve microstructure, composition, inflammatory response, fibrosis and capacity for nerve regeneration are not the same as they are in humans. The rat sciatic nerve used in the *in vivo* model has one fascicle at the level of the hips, whereas human sciatic nerve has multiple fascicles, which would potentially make the repair of human sciatic nerve different. Additionally, peripheral nerve regeneration is reported to be slower in humans than it is in rats (Buchthal and Kuhl, 1979). Furthermore, the proximal stump in humans is less able to respond to regenerative cues with time (Fu and Gordon, 1997); and fibrosis occurs after PNI in humans, which is inhibitory to the repair process, and so complete recovery is less likely to occur after PNI in humans, compared to rat. There is also a key difference in the critical sized gap length for rats (15 mm) and humans (30 mm). Despite these differences, there are advantages to using the rat sciatic model, these include: rats are easy to handle and care for, resistant to surgical infections, economical and can be investigated in large groups, which is why it is the most widely used animal model of peripheral nerve repair (Angius *et al.*, 2012).

For the rat sciatic nerve model, it is considered to be important to use a gap size that is at least 15 mm in length and to include an autograft control (Bellamkonda, 2006). The autograft control data can be used to define the success criteria of the peripheral nerve repair device. Anatomical and histological analyses were used in this study, which are adequate to address the experimental questions, to assess the amount of axon regeneration at different points along the repair site. A limitation could be the sample size of five animals per group was used could be considered too low for reliable statistical analysis. However, this is a typical group size for these kinds of experiments and represents a compromise between statistical power and the principles of the 3Rs. There is currently no consensus on which models should be used to assess nerve

regeneration, but it is suggested that a rodent model could be used for initial experiments, before progressing to a larger animal for the repair of longer nerve gaps, for example in sheep or primate models (Angius *et al.*, 2012).

Whilst this project has made good progress in addressing the objectives outlined in section 1.5, there is scope for considerable additional future work to develop and fully characterise EngNT as a nerve repair material. The mechanisms of alignment of cells within collagen gels, and longer term effects of stability of EngNT, in terms of cellular alignment and guidance were not investigated. The mechanisms of alignment could be investigated by looking at how the cells attach to the collagen, by for example, blocking integrin attachments and assessing the extent of cell attachment by measuring the differences in gel contraction profiles. This could be useful for identifying desirable or undesirable cell-matrix interactions, which could identify ways to speed up cellular alignment and/or retain cellular alignment. It is important that cellular alignment persists *in vivo* for the duration required to support regeneration, and also alignment duration has implications for storage and transport of devices. It would be useful to assess whether the cells survive the freeze-thaw process within EngNT and also if the alignment is retained after thawing. Future work could investigate these and also some features such as cell differentiation or de-differentiation within the material. The phenotype and purity of the cells within EngNT should be characterised and monitored throughout the process of making EngNT devices, for example, after stabilisation and rolling to form rods. The EngNT could be characterised by immunostaining for antibodies to detect desirable or undesirable cell markers.

Further investigation into using fibrin to construct EngNT is required, as there was an indication that fibrin could be used to generate EngNT that can promote guided neurite

outgrowth, however the cellular alignment in fibrin EngNT was inconsistent. Fibrin was not pursued in this study; however future work could investigate, for example, different concentrations and proportions of the constituents used to make fibrin EngNT to achieve reliable alignment, ability to support regeneration, stability and feasibility.

The *in vivo* pilot work to assess the ability of differentiated human neural (CX) cells within EngNT to guide neurite regeneration across a 15 mm gap in rat sciatic nerve gave inconsistent results. There was some evidence of regeneration and some animals with no regeneration. The animals became unresponsive, lost weight and were eating much less than usual, as a result of immunosuppression with CsA, which may have also had an effect on regeneration. Future work could investigate the dose required for the immunosuppression and also the length of time the animal needs to be immunosuppressed for. The clinical grade ReNeuron CTX cells (undifferentiated) have been used in various species without immunosuppression (personal communication with ReNeuron), suggesting that immunosuppression may not be required at all. Alternatively, other methods of testing human cells *in vivo* could be employed such as using mutant strains of animal that are immunosuppressed, e.g. nude rats; or other immunosuppressive drugs, such as FK506.

In the future, it would be interesting to understand the mechanisms by which cells in EngNT promote regeneration. Two areas to explore would be growth factor release and surface proteins. This could be investigated using *in vitro* models. For example, ELISAs to measure factors in the media, co-cultures using transwells to distinguish between contact-mediated and diffusible factors. Surface proteins could be identified by immunostaining co-cultures of neurons and glia. This would help determine optimal cell choice and differentiation state. Beneficial factors could be over-expressed or inhibitory

factors could be inhibited. This would also help to optimise the device design; for contact-mediated factors the cells would need to be on the surface of the material, or if the beneficial factors are diffusible then they could be distributed throughout the material.

The *in vivo* experiments showed that the EngNT devices could support regeneration across the gap; however the growth into the repair device was significantly less than that observed in the graft groups. Further work to optimise the rod design is required, for example investigating the effect of altering the shape (for example expanded or tapered ends) or other physical/chemical properties (for example using depots of immobilised neurotrophic factors) of the EngNT rods at the proximal part of the device to promote axonal ingrowth. The incorporation of neurotrophic factors or gradients of factors along the length of the device could also enhance regeneration into the device, as well as the incorporation of ECM components such as laminin (Dodla and Bellamkonda, 2008).

Future work could also explore alternative approaches for the construction of EngNT, such as using blends of materials, for example collagen and fibrin in order to exploit beneficial aspects of each. Combinations of materials could even be used to construct different sections within one rod, for example building EngNT rods with one end enriched in fibrin and the other enriched in collagen. The fibrin end of the rod could be positioned near the proximal stump, providing a fibrin bridge for rapid initial regeneration (Liu, 1992), with the potentially more stable collagen elements persisting for a longer duration to support sustained repair. Another approach could be to explore the potential of composite devices containing collagen rods and fibrin rods in various proportions within the repair conduit to promote regeneration.

The ultimate aim of this research is to develop a peripheral nerve repair device that can be implanted into patients. This will require further studies like the ones mentioned above, and also efficacy data for EngNT constructed with clinically relevant cells and materials, to obtain regulatory approval to begin clinical trials. An allogeneic device would be simpler to produce and administer because the device could be made and stored until it is required for use. This is in contrast to an autologous device, which would need to be prepared after the patient has sustained an injury, thereby adding a time delay to the treatment whilst the patient's cells are expanded and used to construct EngNT. A hypothetical scenario would be a patient with a forearm injury that includes extensive damage to the median nerve resulting in a gap. An EngNT device would be indicated as an alternative to the nerve autograft treatment. The EngNT rods with allogeneic cells, for example, dCTX (clinical grade differentiated human neural cells from ReNeuron), would be prepared from frozen and the required number of rods (corresponding to the size of the injured nerve) placed within an adjustable sheath, and then used to bridge the gap at the injury site.

The field of regenerative medicine is progressing rapidly, particularly in terms of stem cell technology (for example iPS cells), and so in a few years there might be a totally different environment for tissue engineering technology. The technology reported here offers a simple, rapid and effective method for the manufacture of an aligned cellular biomaterial and can be made using various therapeutic cells. The most advanced cell therapies being used at the moment tend to be injections of cells. This project was centred on the next generation of tissue-engineered constructs that go a step further and organise the cells into tissues.

It is difficult to predict what the future holds in this dynamic field; perhaps off-the-shelf cells that require no immunosuppression and can be adapted to over-express neurotrophic factors and contract collagen to form EngNT in a matter of minutes? Or perhaps constructs with a functional neuronal element that can be connected to the proximal and distal stumps of the injured nerve to restore patients' function immediately? This work may be quite an early step along the road to a useful therapy, but it provides an exciting new alternative to the 'seeding cells into scaffolds' paradigm.

In summary, this project demonstrated that there is potential for EngNT to be used within a nerve repair conduit in order to promote neuronal regeneration across a critical sized defect *in vivo*.

## 7.0 References

A.M.A. (1998) American Medical Association: Physician's Current Procedural Terminology, Aspen Publishers Inc.

Abrams RA, Butler JM, Bodine-Fowler S, Botte MJ (1998). Tensile properties of neurorraphy site in the rat sciatic nerve. *Journal of Hand Surgery (American volume)*; 23:465-70.

Ahmed Z, Brown RA (1999). Adhesion, alignment and migration of cultured Schwann cells on ultrathin fibronectin fibres. *Cell Motility and the Cytoskeleton*; 42:331-43.

Adalbert R, Gillingwater TH, Haley JE, Bridge K, Beirowski B, Berek L, Wagner D, Grumme D, Thomson D, Celik A, Addicks K, Ribchester RR, Coleman MP (2005). A rat model of slow Wallerian degeneration (Wlds) with improved preservation of neuromuscular synapses. *European Journal of Neuroscience*; 21:271–277.

Allodi, I., M. S. Guzman-Lenis, et al. (2011). In vitro comparison of motor and sensory neuron outgrowth in a 3D collagen matrix. *Journal of Neuroscience Methods*; 198(1): 53-61.

Alovskaya A, Alekseeva T, Phillips JB, King V and Brown R (2007). Fibronectin, collagen, fibrin – components of extracellular matrix for nerve regeneration. Topics in Tissue Engineering. Chapter 12, Volume 2. Eds. N Ashammakhi, R Reis and E Chiellini.



Anani RAA, El-Sadek AN (2009). Fibrin Glue Versus Microsurgical Sutures in Peripheral Nerve Repair: Experimental and Clinical Study. *Journal of Plastic and Reconstructive Surgery*; 33:69-74.

Angius D, Wang H, Spinner RJ, Gutierrez-Cotto Y, Yaszemski MJ, Windebank AJ (2012). A systematic review of animal models used to study nerve regeneration in tissue-engineered scaffolds. *Biomaterials*; 33:8034-8039.

Anselin, A D, Fink T, *et al.* (1997). Peripheral nerve regeneration through nerve guides seeded with adult Schwann cells. *Neuropathology and Applied Neurobiology*; 23(5): 387-398.

Anton ES, Sandrock AW Jr, Matthew WD (1994). Merosin promotes neurite growth and Schwann cell migration in vitro and nerve regeneration in vivo: evidence using an antibody to merosin, ARM-1. *Developmental Biology*; 164(1):133-46.

Aquino J, Hjerling-Leffler J, Koltzenburg M, Villar M, Ernfors P (2006). In vitro and in vivo differentiation of boundary cap neural crest stem cells into mature Schwann cells. *Experimental Neurology*; 198:438-449.

Apel PJ, Garrett JP, Sierpinski P, Ma J and Atala A *et al.* (2008). Peripheral nerve regeneration using a keratin-based scaffold: Long-term functional and histological outcomes in a mouse model. *Journal of Hand Surgery (American volume)*; 33:1541-1547.

Babington EJ, Vatanparast J, Verrall J, Blackshaw SE (2005). Three-dimensional culture of leech and snail ganglia for studies of neural repair. *Invertebrate Neuroscience*; 5:173–182.

Badylak SF, Record R, Lindberg K, Hodde J and Park K (1998). Small intestine submucosa: a substrate for in vitro cell growth. *Journal of Biomaterials Science, Polymer Edition*; 9:863-878.

Barnes CP, Pemble IV CW, Brand DD, Simpson DG, Bowlin GL (2007). Cross-linking electrospun type II collagen tissue engineering scaffolds with carbodiimide in ethanol. *Tissue Engineering*; 13:1593-605.

Battiston B, Tos P, Cushway R, Geuna S (2000). Nerve repair by means of vein filled with muscle grafts: Clinical results. *Microsurgery*; 20:32-36.

Behonick DJ, Werb Z (2003). A bit of give and take: the relationship between the extracellular matrix and the developing chondrocyte. *Mechanisms of Development*; 120, 1327-1336.

Belkas JS, Shoichet MS, Midha R (2004). Peripheral nerve regeneration through guidance tubes. *Neurological Research*; 26.

Bell JHA and Haycock JW (2012). Next generation nerve guides: materials, fabrication, growth factors, and cell delivery. *Tissue Engineering*; 18:116-128.

Bellamkonda RV (2006). Peripheral nerve regeneration: An opinion on channels, scaffolds and anisotropy. *Biomaterials*; 27:3515-18.

Bertleff MJOE, Meek MF, Nicolai JPA (2005). A prospective clinical evaluation of biodegradable neurolac nerve guides for sensory nerve repair in the hand. *Journal of Hand Surgery (American volume)*; 30:513.

Bhandari PS, Sadhotra LP, Bhargava P, Bath AS, Mukherjee MK, Bavdekar RD (2007). What is new in peripheral nerve repair? *Indian Journal of Neurotrauma*; 4(1):21- 23.

Bitar M, Brown RA, Salih V, Kidane AG, Knowles JC, Nazhat SN (2008). Effect of cell density on osteoblastic differentiation and matrix degradation of biomimetic dense collagen scaffolds. *Biomacromolecules*; 9(1):129-35.

Bloch J, Fine EG, Bouche N, Zurn AD, Aebischer P (2001). Nerve growth factor and neurotrophin-3 releasing guidance channels promote regeneration of the transected rat dorsal root. *Experimental Neurology*; 172:425–432.

Bott K, Upton Z, *et al.* (2010). The effect of matrix characteristics on fibroblast proliferation in 3D gels. *Biomaterials*; 31(32):8454-8464.

Boudou T, Legant WR, Mu A, Borochin MA, Thavandiran N, Radisic M, Zandstra PW, Epstein JA, Margulies KB, Chen CS (2012). A Microfabricated Platform to Measure and Manipulate the Mechanics of Engineered Cardiac Microtissues. *Tissue Engineering Part A*; 18(9-10):910–919.

Bozkurt A, Deumens R, *et al.* (2009). In vitro cell alignment obtained with a Schwann cell enriched microstructured nerve guide with longitudinal guidance channels.

*Biomaterials*; 30(2):169-179.

Brännvall K, Corell M, Forsberg-Nilsson K, Fex-Svenningsen Å, (2008).

Environmental cues from CNS, PNS and ENS cells regulate CNS progenitor differentiation. *Neuroreport*; 19:1283-1289.

Braun S, Croizat B, Lagrange MC, Warter JM, Poindron P (1996). Neurotrophins increase motoneurons' ability to innervate skeletal muscle fibers in rat spinal cord-human muscle cocultures. *Journal of Neurological Sciences*; 136(1-2):17-23.

Bremer M, Fröb F, Kichko T, Reeh P, Tamm ER, Suter U, Wegner M (2011). Sox10 is required for Schwann-cell homeostasis and myelin maintenance in the adult peripheral nerve. *Glia*; 59(7):1022-32.

Britsch S, Goerich DE, Riethmacher D, Peirano RI, Rossner M, Nave KA, Birchmeier C, Wegner M (2001). The transcription factor Sox10 is a key regulator of peripheral glial development. *Genes and Development*; 15(1):66-78.

Brooks DN, Weber RV, Chao JD, Rinker BD, Zoldos J, Robichaux MR, Ruggeri SB, Anderson KA, Bonatz EE, Wisotsky SM, Cho MS, Wilson C, Cooper EO, Ingari JV, Safa B, Parrett BM, Buncke GM (2012). Processed nerve allografts for peripheral nerve reconstruction: a multicenter study of utilization and outcomes in sensory, mixed, and motor nerve reconstructions. *Microsurgery*; 32(1):1-14.

Brown RA, Phillips JB (2004). Self-aligning tissue growth guide. Patent.

Brown RA, Phillips JB (2007). Cell responses to biomimetic protein scaffolds used in tissue repair and engineering. *International Review of Cytology*; 262:75-150.

Brown RA and Phillips JB (2011). Micro-structured materials and mechanical cues in 3D collagen gels. in J W Haycock (Ed) 3D Cell Culture, Methods in Molecular Biology, Humana Press, pp183-196.

Brown RA, Wiseman M, Chuo CB, Cheema U, Nazhat SN (2005). Ultrarapid Engineering of Biomimetic Materials and Tissues: Fabrication of Nano- and Microstructures by Plastic Compression. *Advanced Functional Materials*; 15:1762-1770.

Bryan DJ, Holway AH, Wang KK, et al. (2000). Influence of glial growth factor and Schwann cells in a bioresorbable guidance channel on peripheral nerve regeneration. *Tissue Engineering*; 6:129–138.

Buchthal F, Kuhl V (1979). Nerve conduction, tactile sensibility, and the electromyogram after suture or compression of peripheral nerve: a longitudinal study in man. *Journal of Neurology, Neurosurgery and Psychiatry*; 42:436–451.

Bunge RP (1994). The role of the Schwann cell in trophic support and regeneration. *Journal of Neurology*; 242:S19-S21.

Ceballos D, Navarro X, Dubey N, Wendelschafer-Crabb G, Kennedy WR, et al., (1999). Magnetically aligned collagen gel filling a collagen nerve guide improves peripheral nerve regeneration. *Experimental Neurology*; 158:290-300.

Cen L, Liu W, Cui L, Zhang W, Cao Y (2008). Collagen tissue engineering: development of novel biomaterials and applications. *Pediatric Research*; 63, 492-496.

Chamberlain LJ, Yannas IV, Arrizabalaga A, Hsu HP, Norregaard TV, Spector M (1998). Early peripheral nerve healing in collagen and silicone tube implants: myofibroblasts and the cellular response. *Biomaterials*; 19(15):1393-403.

Chang CJ, Hsu SH (2004). The effects of low-intensity ultrasound on peripheral nerve regeneration in poly(DL-lactic acid-co-glycolic acid) conduits seeded with Schwann cells. *Ultrasound in Medicine and Biology*; 30(8):1079-84.

Charriere G, Bejot M, Schnitzler L, Ville G, Hartmann DJ (1989). Reactions to a bovine collagen implant. Clinical and immunologic study in 705 patients. *Journal of the American Academy of Dermatology*; 21:1203-8.

Cheema, U., H. Zuijdendorp, *et al.* (2005). Collagen Conduits for Neural Repair. *European Cells and Materials*; 10:3.

Cheema U, Nazhat S, Alp BA, Foroughi F, Anandagoda N, Mudera V, Brown R (2007). Fabricating tissues: Analysis of farming versus engineering strategies. *Biotechnology and Bioprocess Engineering*; 12:9-14.

Chen ZL, Strickland S (2003). Laminin gamma1 is critical for Schwann cell differentiation, axon myelination, and regeneration in the peripheral nerve. *Journal of Cell Biology*; 163(4):889-99.

Chen CJ, Ou YC, Liao SL, Chen WY, Chen SY, Wu CW, Wang CC, Wang WY, Huang YS, Hsu SH (2007). Transplantation of bone marrow stromal cells for peripheral nerve repair. *Experimental Neurology*; 204:443-53.

Chiu, D (1995) Special article: the development of autogenous venous nerve conduit as a clinical entity. *P&S Medical Review*; 3.

Choi BH, Han SG, Kim SH, Zhu SJ, Huh JY, Jung JH, Lee SH, Kim BY (2005) Autologous fibrin glue in peripheral nerve regeneration in vivo. *Microsurgery*; 21:495-499.

Clark WL, Trumble TE, Swiontkowski MF, Tencer AF (1992). Nerve tension and blood flow in a rat model of immediate and delayed repairs. *Journal of Hand Surgery (American volume)*; 17(4):677-87.

Clark P, Connolly P, *et al.* (1990). Topographical control of cell behaviour: II. Multiple grooved substrata. *Development*; 108(4): 635-644.

Cohen J, Johnson AR (1991). Differential effects of laminin and merosin on neurite outgrowth by developing retinal ganglion cells. *Journal of Cell Science, Supplement*; 15:1-7.

Cukierman E.R.P.D.R.S.a.K.M.Y (2001). Taking cell-matrix adhesions to the third dimension. *Science*; 294:1708.

Currie LJ, Sharpe JR, Martin R (2001). The use of fibrin glue in skin grafts and tissue-engineered skin replacements: a review. *Plastic and Reconstructive Surgery*; 108:1713-26.

D'Ippolito G, Schiller PC, Ricordi C, Roos BA, Howard GA (1999). Age-related osteogenic potential of mesenchymal stromal stem cells from human vertebral bone marrow. *Journal of Bone and Mineral Research*; 14:1115–1122.

Dahlin LB (2008). Techniques of peripheral nerve repair. *Scandinavian Journal of Surgery*; 4: 310-316.

Dahlin LB and Brandt J (2004). Basic Science of Peripheral Nerve Repair: Wallerian degeneration/Growth Cones. *Operative Techniques in Orthopaedics*; 14(3):138-145.

Dailey AT, Avellino AM, Benthem L, Silver J, Kliot M (1998). Complement depletion reduces macrophage infiltration and activation during wallerian degeneration and axonal regeneration. *Journal of Neuroscience*; 18:6713–22.

Daly WT, Yao L, Abu-rub MT, O'Connell C, Zeugolis DI, Windebank AJ, Pandit AS (2012). The effect of intraluminal contact mediated guidance signals on axonal mismatch during peripheral nerve repair. *Biomaterials*; 33(28):6660-71.



Daly WT, Yao L, Zeugolis D, Windebank A, Pandit A (2012). A biomaterials approach to peripheral nerve regeneration: bridging the peripheral nerve gap and enhancing functional recovery. *Journal of the Royal Society Interface*; 9:202-221.

Danielsen N, Dahlin LB, Thomsen P (1993). Inflammatory cells and mediators in the silicone chamber model for nerve regeneration. *Biomaterials*; 14:1180–1185.

Davis JB, Stroobant P (1990). Platelet-derived growth factors and fibroblast growth factors are mitogens for rat Schwann cells. *Journal of Cell Biology*; 110(4),1353–1360.

Desai TA (2000). Micro- and nanoscale structures for tissue engineering constructs. *Medical Engineering and Physics*; 22(9): 595-606.

Deumens R, Bozkurt A, Meek MF, Marcus MA, Joosten EA, Weis J, Brook GA (2010). Repairing injured peripheral nerves: Bridging the gap. *Progress in Neurobiology*; 92:245-276.

Dewitt D, Kaszuba S, *et al.* (2009). Collagen I-Matrigel scaffolds for enhanced schwann cell survival and control of three-dimensional cell morphology. *Tissue Engineering*; 15(10): 2785-2793.

Dezawa M, Takahashi I, Esaki M, Takano M, Sawada H (2001). Sciatic nerve regeneration in rats induced by transplantation of in vitro differentiated bone-marrow stromal cells. *European Journal of Neuroscience*; 14:1771–1776.

di Summa PG, Kingham PJ, Raffoul W, Wiberg M, Terenghi G, Kalbermatten DF (2010). Adipose-derived stem cells enhance peripheral nerve regeneration. *Journal of Plastic, Reconstructive and Aesthetic Surgery*; 63:1544–1552.

di Summa PG, Kalbermatten DF, Pralong E, Raffoul W, Kingham PJ, Terenghi G (2011). Long-term in vivo regeneration of peripheral nerved through bioengineered nerve grafts. *Neuroscience*; 181:278-91.

Dodla MC, Bellamkonda RV (2008). Differences between the effect of anisotropic and isotropic laminin and nerve growth factor presenting scaffolds on nerve regeneration across long peripheral nerve gaps. *Biomaterials*; 29(1):33-46.

Dolenc V, Janko M (1976). Nerve regeneration following primary repair. *Acta Neurochirurgica*; 34:223–234.

Dubey N, Letourneau PC, Tranquillo RT (1999). Guided neurite elongation and Schwann cell invasion into magnetically aligned collagen in simulated peripheral nerve regeneration. *Experimental Neurology*; 158:338-50.

Dubey N, Letourneau PC, Tranquillo RT (2001). Neuronal contact guidance in magnetically aligned fibrin gels: effect of variation in gel mechano-structural properties. *Biomaterials*; 22:1065-75.

Duncan ID, Aguayo AJ, Bunge RP, Wood PM (1981). Transplantation of rat Schwann cells grown in tissue culture into the mouse spinal cord. *Journal of Neuroscience*; 49:241-252.

Durbeej M (2010). Laminins. *Cell and Tissue Research*; 339 (1), 259–268.

Dutta RC and Dutta AK (2009). Cell-interactive 3D-scaffold; advances and applications. *Biotechnology Advances*; 27, 334-339.

East E, de Oliveira DB, Golding JP, Phillips JB (2010). Alignment of astrocytes increases neuronal growth in three-dimensional collagen gels and is maintained following plastic compression to form a spinal cord repair conduit. *Tissue Engineering Part A*; 16:3173-3184.

Eastwood M, Mudera VC, McGrouther DA, Brown RA (1998). Effect of Precise Mechanical Loading on Fibroblast Populated Collagen Lattices: Morphological Changes. *Cell Motility and the Cytoskeleton*; 40:13–21.

Edwina SL, Claire MA and Gerald GF (2011). Designing a tubular matrix of oriented collagen fibrils for tissue engineering, *Acta Biomaterialia*; 7(6):2448-2456.

Ellis P, Fagan BM, Magness ST, Hutton S, Taranova O, Hayashi S, McMahon A, Rao M, Pevny L (2004). SOX2, a persistent marker for multipotential neural stem cells derived from embryonic stem cells, the embryo or the adult. *Developmental Neuroscience*; 26(2-4):148-65.

Evans GR, Brandt K, Niederbichler AD, Chauvin P, Herrman S *et al.* (2000). Clinical long-term in vivo evaluation of poly(l-lactic acid) porous conduits for peripheral nerve regeneration. *Journal of Biomaterials Science, Polymer Edition*; 11:869-878.

Evans GR (2001). Peripheral nerve injury: a review and approach to tissue engineered constructs. *Anatomical Record*; 263(4):396-404.

Evans GR, Brandt K, Katz S, Chauvin P, Otto L, *et al.* (2002). Bioactive poly(l-lactic acid) conduits seeded with Schwann cells for peripheral nerve regeneration. *Biomaterials*; 23:841-48.

Fawcett JW. and Keynes RJ (1990). The role of Schwann cells in the regeneration of peripheral nerve axons through muscle basal lamina grafts. *Annual Review of Neuroscience*; 13:43-60.

Fox MA (2008). Novel roles for collagens in wiring the vertebrate nervous system. *Current Opinion in Cell Biology*; 20 (5):508–513.

Fraser JK, Wulur I, Alfonso Z, Hedrick MH (2006). Fat tissue: an underappreciated source of stem cells for biotechnology. *Trends Biotechnology*; 24:150-4.

Fried K, Sime W, Lillesaar C, Virtanen I, Tryggvasson K, Patarroyo M (2005). Laminins 2 (alpha2beta1gamma1, Lm-211) and 8 (alpha4beta1gamma1, Lm-411) are synthesized and secreted by tooth pulp fibroblasts and differentially promote neurite outgrowth from trigeminal ganglion sensory neurons. *Experimental Cell Research*; 307 (2):329–341.

Frostick SP, Yin Q, Kemp GJ (1998). Schwann cells, neurotrophic factors, and peripheral nerve regeneration. *Microsurgery*; 18:397.

Fu SY, Gordon T (1997). The cellular and molecular basis of peripheral nerve regeneration. *Molecular Neurobiology*; 14:67–116.

Funakoshi H, Frisén J, Barbany G, Timmusk T, Zachrisson O, Verge VM, Persson H (1993). Differential expression of mRNAs for neurotrophins and their receptors after axotomy of the sciatic nerve. *Journal of Cell Biology*; 123(2), 455–465.

Gardiner NJ, Moffatt S, Fernyhough P, Humphries MJ, Streuli CH, Tomlinson DR (2007). Preconditioning injury-induced neurite outgrowth of adult rat sensory neurons on fibronectin is mediated by mobilisation of axonal alpha5 integrin. *Molecular and Cellular Neuroscience*; 35 (2):249–260.

Genetic Engineering and Biotechnology News (2012). TAP, UCL Receive Additional Funding to Take Biomimetic Cornea into Human Safety Study.

<http://www.genengnews.com/gen-news-highlights/tap-ucl-receive-additional-funding-to-take-biomimetic-cornea-into-human-safety-study/81246687/?kwrtd=TAP%20Biosystems>.

Georgeu GA, Walbeehm ET, Tillett R, Afoke A, Brown RA, Phillips JB (2005). Investigating the mechanical shear-plane between core and sheath elements of peripheral nerves. *Cell and Tissue Research*; 320(2):229-34.

Ghaznavi AM, Kokai LE, Marra KG *et al.* (2011). Silk Fibroin Conduits: A Cellular and Functional Assessment of Peripheral Nerve Repair. *Annals of Plastic Surgery*; 66(3): 273-279.

Giannini C and Dyck PJ (1990). The fate of Schwann cell basement membranes in permanently transected nerves. *Journal of Neuropathology and Experimental Neurology* ; 49(6): 550-563.

Gillen C, Korfhage C, Muller HW (1997). Gene expression in nerve regeneration. *Neuroscientist*; 3 (2), 112–122.

Glass JD (2004). Wallerian degeneration as a window to peripheral neuropathy. *Journal of the Neurological Science*; 220, 123–124.

Gloster A, Diamond J (1992). Sympathetic nerves in adult rats regenerate normally and restore pilomotor function during an anti-NGF treatment that prevents their collateral sprouting. *Journal of Comparative Neurology*; 326(3), 363–374.

Glowacki J, Mizuno S (2008). Collagen scaffolds for tissue engineering. *Biopolymers*; 89(5):338-44.

Gold B (1997). Axonal regeneration of sensory nerves is delayed by continuous intrathecal infusion of nerve growth factor. *Neuroscience*; 76 (4):1153–1158.

Gomez TM, Letourneau PC (1994) Filopodia initiate choices made by sensory neuron growth cones at laminin/fibronectin borders in vitro. *Neuroscience*; 14(10):5959-72.

Gordon MK, Hahn RA (2010). Collagens. *Cell and Tissue Research*; 339 (1), 247–257.

Goto E, Mukozawa, *et al.* (2010). A rolled sheet of collagen gel with cultured Schwann cells: model of nerve conduit to enhance neurite growth. *Journal of Bioscience and Bioengineering*; 109(5): 512-518.

Grimpe B and Silver J (2002). The extracellular matrix in axon regeneration. *Progress in Brain Research*; 137:333-349.

Grinnell F (2003). Fibroblast biology in three-dimensional collagen matrices. *Trends Cell Biology*; 13(5):264-9.

Gronthos S, Mankani M, Brahim J, Robey PG, and Shi S (2000). Postnatal human dental pulp stem cells (DPSCs) in vitro and in vivo. *Proceedings of the National Academy of Sciences of the United States of America*; 97(25):13625–13630.

Gronthos S, Brahim J, Li W *et al.* (2002). Stem cell properties of human dental pulp stem cells. *Journal of Dental Research*; 81(8):531–535.

Grothe C, Nikkhah G (2001). The role of basic fibroblast growth factor in peripheral nerve regeneration. *Anatomy and Embryology (Berlin)*; 204 (3):171–177.

Gu X, Ding F, Yang Y and Liu J (2011). Construction of tissue engineered nerve grafts and their application in peripheral nerve regeneration. *Progress in Neurobiology*; 93(2): 204-230.

Gu JH, Ji YH, Dhong ES, Kim DH, Yoon ES (2012). Transplantation of adipose derived stem cells for peripheral nerve regeneration in sciatic nerve defects of the rat. *Current Stem Cell Research and Therapy*; 7:347-55.

Guenard V, Kleitman N, Morrissey TK, Bunge RP, Aebischer P (1992). Syngeneic Schwann cells derived from adult nerves seeded in semipermeable guidance channels enhance peripheral nerve regeneration. *Neuroscience*; 12:3310–3320.

Guest JD, Rao A, Olson L, Bunge MB, Bunge RP (1997). The ability of human Schwann cell grafts to promote regeneration in the transected nude rat spinal cord. *Experimental Neurology*; 148:502-522.

Guido S, Tranquillo RT (1993). A methodology for the systematic and quantitative study of cell contact guidance in oriented collagen gels. *Journal of Cell Science*; 105:317-31.

Gupta D, Venugopal J, Prabhakaran MP, Dev VRG, Low S, Choon AT, Ramakrishna S (2009). Aligned and random nanofibrous substrate for the in vitro culture of Schwann cells for neural tissue engineering. *Biomaterials*; 5:2560.

Hadjipanayi E, Cheema U, Mudera V, Deng D, Liu W, Brown RA (2010). First implantable device for hypoxia-induced angiogenic engineering. *British Journal of Surgery*; 97, S37.



Hadlock T, Sundback C, Hunter D, Cheney M, Vacanti JP (2000) A polymer foam conduit seeded with Schwann cells promotes guided peripheral nerve regeneration. *Tissue Engineering*; 6:119-27.

Hall SM (1986). Regeneration in cellular and acellular autografts in the peripheral nervous system. *Neuropathology and Applied Neurobiology*; 12:27-46.

Hall S (2005). The response to injury in the peripheral nervous system. *Journal of Bone and Joint Surgery*; 87B:1309-19.

Haugh MG, Thorpe SD, Vinardell T, Buckley CT, Kelly DJ (2012). The application of plastic compression to modulate fibrin hydrogel mechanical properties. *Journal of the Mechanical Behaviour of Biomedical Materials*; 16:66-72.

Hayani A, Lampeter E, Viswanatha D, Morgan D, and Salvi SN (2007). First report of autologous cord blood transplantation in the treatment of a child with leukemia. *Pediatrics*; 119(1):e296–e300.

Haynes LW, Rushton JA, Perrins MF, Dyer JK, Jones R, Howell R (1994). Diploid and hyperdiploid rat Schwann cell strains displaying negative autoregulation of growth in vitro and myelin sheath-formation in vivo. *Journal of Neuroscience Methods*; 52(2):119-27.

Hayes AG, Jobin CM, Akelina Y, Rosenwasser MP (2007). Collagen Nerve Protectors in Rat Sciatic Nerve Repair: A Functional and Mechanical Analysis. The American Society for Peripheral Nerve. Conference Abstract.

Henderson CE, Phillips HS, Pollock RA, Davies AM, Lemeulle C, Armanini M, Simmons L, Moffet B, Vandlen RA, Simpson LC (1994). GDNF: a potent survival factor for motoneurons present in peripheral nerve and muscle. *Science*; 266 (5187), 1062–1064.

Hill PS, Apel PJ, Barnwell J, Smith T, Koman LA, Atala A, and Dyke MV (2011). Repair of Peripheral Nerve Defects in Rabbits Using Keratin Hydrogel Scaffolds. *Tissue Engineering Part A*; 17(11-12): 1499-1505.

Hirono, T., K. Torimitsu, *et al.* (1988). Recognition of artificial microstructures by sensory nerve fibers in culture. *Brain Research*; 446(1): 189-194.

Hoke A, Cheng C, Zochodne DW (2000). Expression of glial cell line-derived neurotrophic factor family of growth factors in peripheral nerve injury in rats. *Neuroreport*; 11 (8), 1651–1654.

Hu J, Zhu QT, Liu XL, Xu YB, and Zhu JK (2007). Repair of extended peripheral nerve lesions in rhesus monkeys using acellular allogenic nerve grafts implanted with autologous mesenchymal stem cells. *Experimental Neurology*; 204:658–666.

Huang W, Begum R, Barber T, Ibba V, Tee NCH, Hussain M, Arastoo M, Yang Q, Robson LG, Lesage S, Gheysens T, Skaer NJV, Knight DP, Priestley JV (2012). Regenerative potential of silk conduits in repair of peripheral nerve injury in adult rats. *Biomaterials*; 33(1):59–71.

Ibarra A, Hernandez E, Lomeli J, Pineda D, Buenrostro M, Martinon S, Garcia E, Flores N, Guizar-Sahagun G, Correa D, Madrazo I (2007). Cyclosporin-A enhances non-functional axonal growing after complete spinal cord transection. *Brain Research*; 1149:200–209.

Ichihara S, Inada Y, Nakamura T (2008). Artificial nerve tubes and their application for repair of peripheral nerve injury: an update of current concepts. *Injury*; 4:29-39.

Ide C (1996). Peripheral nerve regeneration. *Neuroscience Research*; 25:101-125.

Ikeda M and Oka Y (2012). The relationship between nerve conduction velocity and fiber morphology during peripheral nerve regeneration. *Brain Behaviour*; 2:382-90.

Jacobson S, Guth L (1965). An electrophysiological study of the early stages of peripheral nerve regeneration. *Experimental Neurology*; 11, 48-60.

Janebodin K, Horst OV, Ieronimakis N, et al. (2011). Isolation and characterization of neural crest-derived stem cells from dental pulp of neonatal mice. *Public Library of Science*; 6(11), article e27526.

Jessen KR, Mirsky R (1997). Embryonic Schwann cell development: the biology of Schwann cell precursors and early Schwann cells. *Journal of Anatomy*; 191, 501-505.

Jungnickel J, Haase K, Konitzer J, Timmer M, Grothe C (2006). Faster nerve regeneration after sciatic nerve injury in mice over-expressing basic fibroblast growth factor. *Journal of Neurobiology*; 66 (9), 940–948.

Kalbermatten DF, Pettersson J, Kingham PJ, Pierer G, Wiberg M, Terenghi G (2009). New Fibrin Conduit for Peripheral Nerve Repair. *Journal of Reconstructive Microsurgery*; 25(1): 027-033.

Karabekmez FE, Duymaz A, Moran SL (2009). Early clinical outcomes with the use of decellularized nerve allograft for repair of sensory defects within the hand. *Hand (New York)*; 4(3):245-9.

Karamichos D, Brown RA, Mudera V (2006). Complex dependence of substrate stiffness and serum concentration on cell-force generation. *Journal of Biomedical Materials Research Part A*; 78A, 407-415.

Keeley, R., T. Atagi, et al. (1993). Synthetic nerve graft containing collagen and synthetic Schwann cells improves functional, electrophysiological, and histological parameters of peripheral nerve regeneration. *Restorative Neurology and Neuroscience*; 5(5): 353-366.

Kehoe S, Zhang XF, Boyd D (2012) FDA approved guidance conduits and wraps for peripheral nerve injury: A review of materials and efficacy. *Injury*; 43:553–572.

Kingham PJ, Kalbermatten DF, Mahay D, Armstrong SJ, Wiberg M, Terenghi G (2007). Adipose-derived stem cells differentiate into a Schwann cell Phenotype and promote neurite outgrowth in vitro. *Experimental Neurology*; 207:267-274.

Kim K, Yu M, Zong X, Chiu J, Fang D, Seo YS, Hsiao BS, Chu B, Hadjiargyrou M (2003). Control of degradation rate and hydrophilicity in electrospun non-woven poly(D,L-lactide) nanofiber scaffolds for biomedical applications. *Biomaterials*; 24(27):4977-85.

Kim YT, Haftel VK, Kumar S, Bellamkonda RV (2008). The role of aligned polymer fiber-based constructs in the bridging of long peripheral nerve gaps. *Biomaterials*; 29(21):3117-27.

Kirsch M, Terheggen U, Hofmann HD (2003). Ciliary neurotrophic factor is an early lesion-induced retrograde signal for axotomized facial motoneurons. *Molecular and Cellular Neuroscience*; 24 (1), 130–138.

Kitahara, A., Y. Suzuki, et al. (1998). Evaluation of collagen nerve guide in facial nerve regeneration. *Journal of Artificial Organs*; 1(1): 22-27.

Kirsch M, Terheggen U, Hofmann HD (2003). Ciliary neurotrophic factor is an early lesion-induced retrograde signal for axotomized facial motoneurons. *Molecular and Cellular Neuroscience*; 24 (1), 130–138.

Klimaschewski L, Nindl W, Feurle J, Kavakebi P, Kostron H (2004). Basic fibroblast growth factor isoforms promote axonal elongation and branching of adult sensory neurons in vitro. *Neuroscience*; 126 (2), 347–353.

- Koh HS, Yong T, Teo WE, Chan CK, Puhaindran ME, Tan TC, Lim A, Lim BH, Ramakrishna S (2010). In vivo study of novel nanofibrous intra-luminal guidance channels to promote nerve regeneration. *Journal of Neural Engineering*; 7(4):046003.
- Koshima I, Okabe, Harri K (1981). Comparative study of free and vascularized nerve grafts transplanted in the scar tissue in rats. *Journal of Microsurgery*; 3: 126-132.
- Kuappila T, Jyvasjarvi E, Huopaniemi T, Hujanen E, Liesi P (1993). A laminin graft replaces neurorrhaphy in the restorative surgery of the rat sciatic nerve. *Experimental Neurology*; 123:181-91.
- Labrador RO, Buti M, Navarro X (1998). Influence of collagen and laminin gels concentration on nerve regeneration after resection and tube repair. *Experimental Neurology*; 149 (1), 243–252.
- Ladak A, Olson J, Tredget EE, Gordon T (2011). Differentiation of mesenchymal stem cells to support peripheral nerve regeneration in a rat model. *Experimental Neurology*; 228:242–252.
- Langer R, Vacanti JP (1993). Tissue engineering. *Science*; 260, 920-926.
- Laurens N, Koolwijk P, de Maat MP (2006). Fibrin structure and wound healing. *Journal of Thrombosis and Haemostasis*; 4(5):932-9.
- Le Douarin NM and Dupin E (2003) Multipotentiality of the neural crest. *Current Opinion in Genetics and Development*; 13:529 -536.

Leah JD, Herdegen T, Bravo R (1991). Selective expression of Jun proteins following axotomy and axonal transport block in peripheral nerves in the rat: evidence for a role in the regeneration process? *Brain Research*; 566(561–562), 198–207.

Lee P, Lin R, Moon J, Lee LP (2006). Microfluidic alignment of collagen fibers for in vitro cell culture. *Biomedical Microdevices*; 8:35-41.

Leong KF, Cheah CM, Chua CK (2003). Solid freeform fabrication of three-dimensional scaffolds for engineering replacement tissues and organs. *Biomaterials*; 24, 2363-2378.

Levi-Montalcini R (1987). The nerve growth factor: thirty-five years later. *Bioscience Reports*; 7 (9), 681–699.

Levis HJ, Brown RA, Daniels JT (2010). Plastic compressed collagen as a biomimetic substrate for human limbal epithelial cell culture. *Biomaterials*; 31:7726-37.

Levis HJ, Peh GSL, Toh K-P, Poh R, Shortt AJ, et al. (2012). Plastic Compressed Collagen as a Novel Carrier for Expanded Human Corneal Endothelial Cells for Transplantation. *Public Library of Science*; 7(11): e50993.

Lewin GR, Barde YA (1996). Physiology of the neurotrophins. *Annual Review of Neuroscience*; 19, 289–317.

Li, R.-H., M. X. Sliwowski, et al. (1996). Establishment of Schwann cell lines from normal adult and embryonic rat dorsal root ganglia. *The Journal of Neuroscience Methods*; 67: 57-69.

Lietz M, Dreesmann L, Hoss M, Oberhoffner S, Schlosshauer B (2006). Neuro tissue engineering of glial nerve guides and the impact of different cell types. *Biomaterials*; 27:1425–1436.

Lin YC, Ramadan M, Van Dyke M, Kokai LE, Philips BJ, Rubin JP, Marra KG (2012). Keratin gel filler for peripheral nerve repair in a rodent sciatic nerve injury model. *Plastic and Reconstructive Surgery*; 129(1):67-78.

Liu HM (1992). The role of extracellular matrix in peripheral nerve regeneration: a wound chamber study. *Acta Neuropathologica*; 83 (5), 469–474.

Lundborg G, Dahlin LB, Danielsen N, Gelberman RH, Longo FM, Powell HC, Varon S (1982). Nerve regeneration in silicone chambers: influence of gap length and of distal stump components. *Experimental Neurology*; 76(2):361-75.

Lundborg G, Dahlin L, Dohi D, Kanje M, Terada N (1997). A new type of “bioartificial” nerve graft for bridging extended defects in nerves. *Journal of Hand Surgery*; 22:299-303.

Lundborg G, Rosen B, Dahlin L, Holmberg J and Roden I (2004). Tubular Repair of the Median or Ulnar Nerve in the Human Forearm: A 5-Year Follow-Up. *Journal of Hand Surgery*; 29:100-107.



Mackinnon SE, Doolabh VB, Novak CB and Trulock EP (2001). Clinical outcome following nerve allograft transplantation. *Plastic and Reconstructive Surgery*; 107:1419.

Madduri S, Gander B (2010). Schwann cell delivery of neurotrophic factors for peripheral nerve regeneration. *Journal of the Peripheral Nervous System*; 15:93.

Madorsky SJ, Swett JE, Crumley RL (1998). Motor versus sensory neuron regeneration through collagen tubules. *Plastic and Reconstructive Surgery*; 102(2):430-6.

Maeda E, Robinson HPC, Kuroda Y, Kawana A (1993). Synaptic potentiation in cultured cortical neurons: long-lasting modification of spontaneous synchronized periodic firing by patterned electrical stimulation. *Society for Neuroscience Abstract* 19:1323.

Mafi P, Hindocha S, Mafi R, Griffin M, Khan WS (2011). Adult Mesenchymal Stem Cells and Cell Surface Characterization - A Systematic Review of the Literature. *Open Orthopaedics Journal*; 5(Suppl 2):253-60.

Marenzana M, Wilson-Jones N, Mudera V, Brown RA (2006). The origins and regulation of tissue tension: Identification of collagen tension-fixation process in vitro. *Experimental Cell Research*; 312:423-433.

Marchesi C, Pluderi M, Colleoni F, et al. (2007) Skin-derived stem cells transplanted into resorbable guides provide functional nerve regeneration after sciatic nerve resection. *Glia*; 55(4):425–438.

Mason S, Phillips JB (2011). An ultrastructural and biochemical analysis of collagen in rat peripheral nerves: the relationship between fibril diameter and mechanical properties. *Journal of the Peripheral Nervous System*; 16, 261-269.

Matejcik V (2002). Peripheral nerve reconstruction by autograft. *Injury*; 33(7):627-631.

Mathieu L, Adam C, Legagneux J, Bruneval P, Masméjean E (2012). Reduction of neural scarring after peripheral nerve suture: an experimental study about collagen membrane and autologous vein wrapping. *Chirurgie de la Main*; 31(6):311-7.

Matsumoto K, Ohnishi K, Kiyotani T, Sekine T, Ueda H, Nakamura T, Endo K, Shimizu Y (2000). Peripheral nerve regeneration across an 80-mm gap bridged by a polyglycolic acid (PGA)-collagen tube filled with laminin-coated collagen fibers: a histological and electrophysiological evaluation of regenerated nerves. *Brain Research*; 868(2):315-28.

McKenzie IA, Biernaskie J, Toma JG, et al. (2006) Skin-derived precursors generate myelinating Schwann cells for the injured and dysmyelinated nervous system. *Neuroscience*; 26:6651–6660.

Meek MF, Coert JH (2008). US Food and Drug Administration /Conformit Europe-approved absorbable nerve conduits for clinical repair of peripheral and cranial nerves. *Annals Plast Surgery*; 60(4):466-72.

Meirer R, Babuccu O, Unsal M, Nair DR, Gurunluoglu R, Skugor B, Meirer B, Siemionow M (2002). Effect of chronic cyclosporine administration on peripheral nerve regeneration: a dose-response study. *Annals Plast Surgery*; 49(1):96-103.

Meisinger C, Zeschnigk C, Grothe C (1996). In vivo and in vitro effect of glucocorticoids on fibroblast growth factor (FGF)-2 and FGF receptor 1 expression. *Journal of Biological Chemistry*; 271 (28), 16520–16525.

Merle M, Dellon AL, Campbell JN, Chang PS (1989). Complications from silicone polymer intubulation of nerves. *Microsurgery*; 10:130-133.

Michael-Titus A, Revest P, Shortland P (2010). The Nervous System. Elsevier Health Sciences.

Micol LA, Ananta M, Engelhardt EM, Mudera VC, Brown RA, Hubbell JA (2011). High-density collagen gel tubes as a matrix for primary human bladder smooth muscle cells. *Biomaterials*; 32:1543-8.

Miller, C., S. Jefinija, et al. (2001). Micropatterned Schwann cell-seeded biodegradable polymer substrates significantly enhance neurite alignment and outgrowth. *Tissue Engineering*; 7(6): 705-715.

Millesi H (1973) Microsurgery of peripheral nerves. *Hand*. 5:157-60.

Miner JH (2008). Laminins and their roles in mammals. *Microscopy Research and Technique*; 71 (5), 349–356.

Mosahebi A, Fuller P, Wiberg M, Terenghi G (2002). Effect on allogeneic Schwann cell transplantation on peripheral nerve regeneration. *Experimental Neurobiology*; 173:213-23.

Mumenthaler M, Mattle H (2001). *Fundamentals in Neurology*. Georg Thieme Verlag.

Murakami T, Fujimoto Y, Yasunaga Y, *et al.* (2003). Transplanted neuronal progenitor cells in a peripheral nerve gap promote nerve repair. *Brain Research*; 974:17–24.

Murugan R, Ramakrishna S (2007). Design strategies of tissue engineering scaffolds with controlled fiber orientation. *Tissue Engineering*; 13, 1845-1866.

Nadim, W., P. N. Anderson, *et al.* (1990). The role of Schwann cells and basal lamina tubes in the regeneration of axons through long lengths of freeze-killed nerve grafts. *Neuropathology and Applied Neurobiology*; 16(5): 411-421.

Navarro X, Rodriguez FJ, Labrador RO, Buti M, Ceballos D, Gomez N, Cuadras J, Perego G (1996). Peripheral nerve regeneration through bioresorbable and durable nerve guides. *Journal of the Peripheral Nervous System*; 1 (1), 53–64.

Nectow, A.R., Marra, K.G. & Kaplan, D.L. Biomaterials for the development of peripheral nerve guidance conduits. *Tissue Engineering Part B*; 18, 40-50 (2012).

NeuraWrap™ FDA approval number K041620, 2004;

[http://www.accessdata.fda.gov/cdrh\\_docs/pdf4/k041620.pdf](http://www.accessdata.fda.gov/cdrh_docs/pdf4/k041620.pdf) Accessed May 2013.

Ngo TT, Waggoner PJ, Romero AA, Nelson KD, Eberhart RC, Smith GM (2003).

Poly(L-Lactide) microfilaments enhance peripheral nerve regeneration across extended nerve lesions. *Journal of Neuroscience Research*; 72(2):227-38.

Nisbet DR, Forsythe JS, Shen W, Finkelstein DI, Horne MK (2009). Review paper: a review of the cellular response on electrospun nanofibers for tissue engineering. *Journal of Biomaterials Applications*; 24, 7-29.

Noble J, Munro CA, Prasad VS, Midha R (1998) Analysis of upper and lower extremity peripheral nerve injuries in a population of patients with multiple injuries. *Journal of Trauma*; 45: 116–122.

Oakley C and Brunette DM (1993). The sequence of alignment of microtubules, focal contacts and actin filaments in fibroblasts spreading on smooth and grooved titanium substrata. *Journal of Cell Science*; 106 ( Pt 1), 343-354.

Ozgenel GY (2003). Effects of hyaluronic acid on peripheral nerve scarring and regeneration in rats. *Microsurgery*; 23(6):575-81.

Park D, Xiang AP, Mao FF, Zhang L, Di CG, Liu XM, Shao Y, Ma BF, Lee JH, Ha KS, Walton N, Lahn BT. (2010). Nestin is required for the proper self-renewal of neural stem cells. *Stem Cells*; 28(12):2162-71.

Philipeaux JM, Vulpian A. (1870). Note sur des essais de greffe d'un tronçon du nerf lingual entre les deux bouts du nerf hypoglosse, après excision d'un segment de ce dernier nerf. *Arch de Physiol Norm et Path*; 8: 618–620.

Phillips JB, Smit X, DeZoysa N, Afoke A, Brown RA (2004). Peripheral nerves in the rat exhibited localized heterogeneity of tensile properties during limb movement. *Journal of Physiology*; 3:879-887.

Phillips JB, Bunting SC, Hall SM, Brown RA (2005). Neural tissue engineering: a self-organizing collagen guidance conduit. *Tissue Engineering*; 11:1611-1617.

Raivich G, Hellweg R, Kreutzberg GW (1991). NGF receptor-mediated reduction in axonal NGF uptake and retrograde transport following sciatic nerve injury and during regeneration. *Neuron*; 7 (1), 151–164.

Raivich G, Makwana M (2007). The making of successful axonal regeneration: genes, molecules and signal transduction pathways. *Brain Research Reviews*; 53(2), 287–311.

Rama P, Matuska S, Paganoni G, Spinelli A, De Luca M, and Pellegrini G (2010). Limbal stem-cell therapy and long-term corneal regeneration. *The New England Journal of Medicine*; 363(2):147–155.

Rappaport WD, Valente J, Hunter GC, Rance NE, Lick S, Lewis T, Neal D (1993). Clinical utilization and complications of sural nerve biopsy. *American Journal of Surgery*; 166(3):252-6.

Reid AJ, Sun M, Wiberg M, Downes S, Terenghi G, Kingham PJ (2011). Nerve repair with adipose-derived stem cells protects dorsal root ganglia neurons from apoptosis. *Neuroscience*; 199:515-22.

Resch MD, Schlotzer-Schrehardt U, Hofmann-Rummelt C, Sauer R, Cursiefen C, Kruse FE, Beckmann MW, Seitz B (2006). Adhesion structures of amniotic membranes integrated into human corneas. *Investigative Ophthalmology & Visual Science*; 47, 1853-1861.

Restrepo Y, Merle M, Michon J, Folliguet B, Barrat E (1985) Free vascularized nerve grafts. *Microsurgery*; 6:78–84

Ricard-Blum S (2010). The collagen family. *Cold Spring Harb Perspect Biol*, 3.

Rich KM, Disch SP, Eichler ME (1989). The influence of regeneration and nerve growth factor on the neuronal cell body reaction to injury. *Journal of Neurocytology*; 18(5):569–576.

Richardson JA, Rementer CW, Bruder JM, Hoffman-Kim D. Guidance of dorsal root ganglion neurites and Schwann cells by isolated Schwann cell topography on

poly(dimethyl siloxane) conduits and films. *Journal of Neural Engineering*; 2011;8: 046015.

Risitano G, Cavallaro G, Merrino T, Coppolono S and Ruggeri F (2002). Clinical results and thoughts on sensory nerve repair by autologous vein graft in emergency hand reconstruction. *Chirurgica Main*; 21:194-97.

Rodrigues MC, Rodrigues AA Jr, Glover LE, Voltarelli J, Borlongan CV (2012). Peripheral nerve repair with cultured Schwann cells: Getting closer to the clinics. *The Scientific World Journal*; Article ID 413091, 10 pages.

Rosberg HE, Carlsson KS, Hojgard S, Lindgren B, Lundborg G, Dahlin LB (2005). Injury to the human median and ulnar nerves in the forearm analysis of costs for treatment and rehabilitation of 69 patients in southern Sweden. *Journal of Hand Surgery*; 30: 35-39.

Ruijs AC, Jaquet JB, Kalmijn S, Giele H, Hovius SE (2005). Median and ulnar nerve injuries: a meta-analysis of predictors of motor and sensory recovery after modern microsurgical nerve repair. *Plastic and Reconstructive Surgery*; 116:484-494.

Rush RA, Mayo R, Zettler C (1995). The regulation of nerve growth factor synthesis and delivery to peripheral neurons. *Pharmacology and Therapeutics*; 65(1):93–123.

Rustemeyer J and Dicke U (2010). Allografting combined with systemic FK506 produces greater functional recovery than conduit implantation in a rat model of sciatic nerve injury. *Journal of Reconstructive Microsurgery*; 26:123.



Sabelman EE, Hentz VR (1999). Clinical Trial of Peripheral Nerve Graft, ClinicalTrials.gov.

Schmidt CE, Leach JB (2003). Neural tissue engineering: strategies for repair and regeneration. *Annual Reviews of Biomedical Engineering*; 5:293-347.

Schnell E, Klinkhammer K, Balzer S, Brook G, Klee D, Dalton P, Mey J (2007). Guidance of glial cell migration and axonal growth on electrospun nanofibers of poly-[epsilon]-caprolactone and a collagen/poly-[epsilon]-caprolactone blend. *Biomaterials*; 30:5251.

Seckel, B., D. Jones, K. Hekimian, K. Wang, D. Chakalis, and P. Costas. (1995). Hyaluronic acid through a new injectable nerve guide delivery system enhances peripheral nerve regeneration in the rat. *Journal of Neuroscience Research*; 40(3):318-24.

Seddon HJ (1943). Three types of nerve injury. *Brain*; 66:237-288.

Seggio AM, Narayanaswamy A, Roysam B, Thompson DM (2010). Self-aligned Schwann cell monolayers demonstrate an inherent ability to direct neurite outgrowth. *Journal of Neural Engineering*; 7:046001.

Shimizu S, Kitada M, Ishikawa H, Itokazu Y, Wakao S, Dezawa M (2007). Peripheral nerve regeneration by the in vitro differentiated-human bone marrow stromal cells with

Schwann cell property. *Biochemical and Biophysical Research Communications*; 359:915-20

Shin RH, Friedrich PF, Crum BA, Bishop AT, Shin AY (2009) Treatment of a segmental nerve defect in the rat with use of bioabsorbable synthetic nerve conduits: a comparison of commercially available conduits. *The Journal of Bone and Joint Surgery*; 91:2194.

Sieber-Blum M, Grim M, Hu YF, Szeder V (2004). Pluripotent neural crest stem cells in the adult hair follicle. *Development of Dynamics*; 231:258-69

Snow DM, Brown EM, Letourneau PC (1996). Growth cone behaviour in the presence of soluble chondroitin sulphate proteoglycan (CSPG), compared to behaviour on CSPG bound to laminin or fibronectin. *International Journal of Developmental Neuroscience*; 14(3):331-49.

Soderhall C, Marenholz I, Kerscher T, et al. (2007). Variants in a novel epidermal collagen gene (COL29A1) are associated with atopic dermatitis. *Public Library of Science*; 5, e242.

Sorenson, E. J. and A. J. Windebank (1993). Relative importance of basement membrane and soluble growth factors in delayed and immediate regeneration of rat sciatic nerve. *Journal of Neuropathology and Experimental Neurology* ; 52(3): 216-222.

Spilker MH (2000). Peripheral nerve regeneration through tubular devices: A comparison of assays and device effectiveness. Ph.D. Massachusetts Institute of Technology, Department of Mechanical Engineering.

Spreca A, Rambotti MG, Rende M, Saccardi C, Aisa MC, Giambanco I, Donato R (1989). Immunocytochemical localization of S-100b protein in degenerating and regenerating rat sciatic nerves. *Journal of Histochemistry and Cytochemistry*; 37(4):441-446.

Staniforth P, Fisher TR (1978). The effects of sural nerve excision in autogenous nerve grafting. *Hand*; 10(2):187-90.

Sterne GD, Brown RA, Green CJ, Terenghi G (1997). Neurotrophin-3 delivered locally via fibronectin mats enhances peripheral nerve regeneration. *European Journal of Neuroscience*; 9(7):1388–1396.

Stevens MM, George JH (2005). Exploring and engineering the cell surface interface. *Science*; 310:1135-1138.

Strittmatter SM, Vartanian T, Fishman MC (1992). GAP-43 as a plasticity protein in neuronal form and repair. *Journal of Neurobiology*; 23:507–520.

Stroncek, J. D. and W. M. Reichert (2008). Overview of Wound Healing in Different Tissue Types. *Indwelling Neural Implants: Strategies for Contending with the in Vivo Environment*. W. M. Reichert. Boca Raton (FL), Taylor & Francis Group, LLC.

Sulaiman OAR, Gordon T (2000). Effects of short- and long-term Schwann cell denervation on peripheral nerve regeneration, myelination, and size. *Glia*; 32 (3), 234–246.

Sun, M., M. McGowan, et al. (2010). Novel thin-walled nerve conduit with microgrooved surface patterns for enhanced peripheral nerve repair. *Journal of Material Science: Materials in Medicine*; 21(10): 2765-2774.

Sun F, Zhou K, Mi W-J, Qiu J-H (2011) Repair of facial nerve defects with decellularized artery allografts containing autologous adipose-derived stem cells in a rat model. *Neuroscience Letters*; 499:104–108.

Sundback C, Hadlock T, Cheney M, Vacanti J (2003). Manufacture of porous polymer nerve conduits by a novel low-pressure injection molding process. *Biomaterials*; 24:819-30.

Sunderland IR, Brenner MJ, Singham J, Rickman SR, Hunter DA, Mackinnon SE. (2004). Effect of tension on nerve regeneration in rat sciatic nerve transection model. *Annals of Plastic Surgery*; 53:382–7.

Szynkaruk M, Kemp SW, Wood MD, Gordon T, Borschel GH (2012). Experimental and clinical evidence for use of decellularized nerve allografts in peripheral nerve gap reconstruction. *Tissue Engineering Part B Rev*.

Taniuchi M, Clark HB, Schweitzer JB, Johnson Jr EM (1988). Expression of nerve growth factor receptors by Schwann cells of axotomized peripheral nerves:

ultrastructural location, suppression by axonal contact, and binding properties. *Journal of Neuroscience*; 8 (2), 664–681.

Techatanawata S, Suraritb R, Suddhasthirac T, Khovidhunkit SP (2011). Type I collagen extracted from rat-tail and bovine Achilles tendon for dental application: a comparative study. *Asian Biomedicine*; 787-798.

Terenghi G (1999). Peripheral nerve regeneration and neurotrophic factors. *Journal of Anatomy*; 194:1-14.

Thompson DM, Buettner HM (2006). Neurite outgrowth is directed by schwann cell alignment in the absence of other guidance cues. *Annals of Biomedical Engineering*; 34:161-168.

Toba, T, Nakamura T, Shimizu Y, Matsumoto K, Ohnishi K, et al. (2001) Regeneration of canine peroneal nerve with the use of polyglycolic acid-collagen tube filled with laminin-soaked collagen sponge: a comparative study of collagen sponge and collagen fibers as filling materials for nerve conduits. *Journal of Biomedical Materials Research*; 58:622-30.

Toba T, Nakamura T, Lynn AK, Matsumoto K, Fukuda S et al., (2002) Evaluation of peripheral nerve regeneration across an 80mm gap using a polyglycolic acid (PGA)-collagen nerve conduit filled with laminin-soaked collagen sponge in dogs. *International Journal of Artificial Organs*; 25:230-37.

Tohill M, Terenghi G (2004). Stem-cell plasticity and therapy for injuries of the peripheral nervous system. *Biotechnology and Applied Biochemistry*; 40:17–24.

Tomasek JJ, Gabbiani G, Hinz B, Chaponnier C, Brown RA (2002). Myofibroblasts and mechano-regulation of connective tissue remodelling. *Nature Reviews: Molecular Cell Biology*; 3(5):349-63.

Tomita K, Madura T, Mantovani C, Terenghi G (2012). Differentiated adipose-derived stem cells promote myelination and enhance functional recovery in a rat model of chronic denervation. *Journal of Neuroscience Research*; 90:1392–1402.

Tong XJ, Hirai K, Shimada H, Mizutani Y, Izumi T et al., (1994). Sciatic nerve regeneration navigated by laminin-fibronectin double coated biodegradable collagen grafts in rats. *Brain Research*; 663:155-62.

Topp K S and Boyd B S (2006). Structure and Biomechanics of Peripheral Nerves: Nerve Responses to Physical Stresses and Implications for Physical Therapist Practice. *Physical Therapy*; 86:92-109.

Trupp M, Ryden M, Jornvall H, Funakoshi H, Timmusk T, Arenas E, Ibanez CF (1995). Peripheral expression and biological activities of GDNF, a new neurotrophic factor for avian and mammalian peripheral neurons. *Journal of Cell Biology*; 130 (1), 137–148.

Ulrich, T. A., A. Jain, et al. (2010). Probing cellular mechanobiology in three-dimensional culture with collagen-agarose matrices. *Biomaterials*; 31(7): 1875-1884.

Valentini RF, Aebischer P, Winn SR, Galletti PM (1987). Collagen- and laminin-containing gels impede peripheral nerve regeneration through semi-permeable nerve guidance channels. *Experimental Neurology*; 98:350.

Verhandlungen AE, des Naturwissenschaftlichen und Medizinischen Vereins in Innsbruck. 9(97).

Wakao S, Hayashi T, Kitada M, Kohama M, Matsue D, Teramoto N, Ose T, Itokazu Y, Koshino K, Watabe H, Iida H, Takamoto T, Tabata Y, Dezawa M (2010). Long-term observation of auto-cell transplantation in non-human primate reveals safety and efficiency of bone marrow stromal cell-derived Schwann cells in peripheral nerve regeneration. *Experimental Neurology*; 223:537-47.

Waller A (1850). Experiments on the sections of glossopharyngeal and hypoglossal nerves of the frog and observations of the alterations produced thereby in the structure of their primitive fibers. *Philosophical Transactions of the Royal Society, London*; 140:423-429.

Wallquist W, Zelano J, Plantman S, Kaufman SJ, Cullheim S, Hammarberg H (2004). Dorsal root ganglion neurons up-regulate the expression of laminin-associated integrins after peripheral but not central axotomy. *Journal of Comparative Neurology*; 480 (2), 162–169.

Walsh S, Midha R (2009). Use of stem cells to augment nerve injury repair. *Neurosurgery*; 65:A80-6.

Walton R L, Brown R E, Matory Jr W E, Borah G L and Dolph J L (1989).

Autogeneous vein graft repair of digital nerve defects in the finger: a retrospective clinical study. *Plastic Surgery*; 89:944-49.

Wang KK, Nemeth IR, Seckel BR, Chakalis-Haley DP, Swan DA, Kuo JW et al. (1998) Hyaluronic acid enhances peripheral nerve regeneration in vivo. *Microsurgery*; 18, 270-275.

Wang X, Hu W, Cao Y, Yao J, Wu J and Gu X (2005). Dog sciatic nerve regeneration across a 30-mm defect bridged by a chitosan/PGA artificial nerve graft. *Brain*; 128, 1897–1910.

Wang CY, Zhang KH, Fan CY, Mo XM, Ruan HJ, Li FF (2011). Aligned natural-synthetic polyblend nanofibers for peripheral nerve regeneration. *Biomaterials*; 7:634.

Wang X, Luo E, Li Y, Hu J (2011). Schwann-like mesenchymal stem cells within vein graft facilitate facial nerve regeneration and remyelination. *Brain Research*; 1383:71–80.

Wang G, Lai JCK, and Leung SW (2012). Functional enhancement of chitosan and nanoparticles in cell culture, tissue engineering, and pharmaceutical applications. *Frontiers in Physiology*; 3: 321.

Wangenstein KJ, Kallianen LK (2010). Collagen Tube Conduits in Peripheral Nerve Repair: A Retrospective Analysis. *Hand (New York)*; 5(3): 273–277.



Weinstein DE (1999). The role of Schwann cells in neural regeneration. *Neuroscientist*; 5:208–216

Weiss, P (1934). In vitro experiments on the factors determining the course of the outgrowing nerve fiber. *Journal of Experimental Zoology*; 69:393–448.

Weiss, P (1945). Experiments on cell and axon orientation in vitro: the role of colloidal exudates in tissue organisation. *Journal of Experimental Zoology*; 100:353-86.

Whitworth IH, Brown RA, Dore C, Green CJ, Terenghi G (1995). Orientated mats of fibronectin as a conduit material for use in peripheral nerve repair. *Journal of Hand Surgery*; 20:429-36.

Whitworth IH, Brown RA, Doré CJ, Anand P, Green CJ, Terenghi G (1996). Nerve growth factor enhances nerve regeneration through fibronectin grafts. *Journal of Hand Surgery*; 21(4):514–522.

Wiberg M, Terenghi G (2003). Will it be possible to produce peripheral nerves? *Surgical Technology International*; 11:303-310.

Williams LR, Longo FM, Powell HC, Lundborg G, Varon S (1983). Spatialtemporal progress of peripheral nerve regeneration within a silicone chamber. Parameters for a bioassay. *Journal of Comparative Neurology*; 218 (4), 160–170.

Witzel C, Rohde C, Brushart TM (2005). Pathway sampling by regenerating peripheral axons. *Journal of Comparative Neurology*; 485 (3), 183–190.

Wojciak-Stothard B, Curtis AS, Monaghan W, McGrath M, Sommer I, Wilkinson CD (1995). Role of the cytoskeleton in the reaction of fibroblasts to multiple grooved substrata. *Cell Motility and the Cytoskeleton*; 31, 147-158.

Wolford LM and Stevao ELL (2003). Considerations in nerve repair. *Baylor University Medical Centre Proceedings*; 16(2): 152–156.

Woodhoo A, Sommer L (2008). Development of the Schwann cell lineage: from the neural crest to the myelinated nerve. *Glia*; 56:1481–1490.

Wu P, Spinner RJ, Gu Y, Yaszemski MJ, Windebank AJ, Wang H (2013). Delayed repair of the peripheral nerve: A novel model in the rat sciatic nerve. *Journal of Neuroscience Methods*; 214:37-44.

Yang Y, Chen X, Ding F, Zhang P, Liu J, Gu X (2007). Biocompatibility evaluation of silk fibroin with peripheral nerve tissues and cells in vitro. *Biomaterials*; 28:1643–1652.

Yao, L., G. C. de Ruitter, et al. (2010). Controlling dispersion of axonal regeneration using a multichannel collagen nerve conduit. *Biomaterials*; 31(22): 5789-5797.

Yi C, Dahlin LB (2010). Impaired nerve regeneration and Schwann cell activation after repair with tension. *Neuroreport*; 21(14):958-962.

Yoshii, S. and M. Oka (2001). Peripheral nerve regeneration along collagen filaments. *Brain Research*; 888:158-162.

Yoshimura H, Muneta T, Nimura A, Yokoyama A, Koga H, Sekiya I (2007).

Comparison of rat mesenchymal stem cells derived from bone marrow, synovium, periosteum, adipose tissue, and muscle. *Cell and Tissue Research*; 327:449-462.

Young RC, Terenghi G, Wiberg M (2002). Poly-2-hydroxybutyrate (PHB): a resorbable conduit for long-gap repair in peripheral nerves. *British Journal of Plastic Surgery*; 55:235.

Zhang F, Inserra M, Richards I, et al. (2001). Quantification of nerve tension after nerve repair: correlations with nerve defects and nerve regeneration. *Journal of Reconstructive Microsurgery*; 17(6):445–51.

Zhang P, He X, Liu K, Zhao F, Fu Z, Zhang D, Zhang Q, Jiang B (2004). Bone marrow stromal cells differentiated into functional Schwann cells in injured rats sciatic nerve. *Artificial Cells, Blood Substitute, Immobilization Biotechnology*; 32:509–518.

Zhao Z, Alam S, Oppenheim RW, Prevette DM, Evenson A, Parsadanian A (2004). Overexpression of glial cell line-derived neurotrophic factor in the CNS rescues motoneurons from programmed cell death and promotes their longterm survival following axotomy. *Experimental Neurology*; 190 (2), 356–372.